Neural Network-Based Controller Designs for Active Vehicle Suspension Systems

---

Olurotimi Akintunde Dahunsi (318224)

A thesis submitted to the Faculty of Engineering and the Built Environment, University of the Witwatersrand, Johannesburg, in fulfilment of the requirements for the degree of Doctor of Philosophy.

Johannesburg, July 2013

Declaration

I declare that this thesis is my own, unaided work, except where otherwise acknowledged. It is being submitted for the degree of Doctor of Philosophy in the University of the Witwatersrand, Johannesburg. It has not been submitted before for any degree or examination at any other university.

Signed this ___ day of _____ 20___

_____

Olurotimi Akintunde Dahunsi (318224).

Acknowledgements

I am greatly indebted to all individuals who assisted and encouraged me throughout the course of my research. Firstly, I would like to thank my supervisor, Professor Jimoh Pedro, for the discussions, critique and advice throughout this research.

I also want to thank Prof. Laurent Dala , Dr. A. A. Ilemobade, Prof. Montaz Ali, Dr. Otis Nyandoro, Prof. J. A. Afolayan, Prof. John Ade-Ajayi and Prof. Taigbenu though not my supervisors they assisted in various ways through inspiring ideas, discussions and encouragement.

Friends and colleagues at the University of Witwatersrand; Jianchang Huang, Horacio Ernesto, Milan Beharie and Nyiko Baloyi. Akindahunsi Akindehinde, James Adewumi, Julius and Isaac Popoola, for the after hours encouragement along the way. Special thanks to Awopetu Olayinka, Abadariki Samson, Shola Oni-Buraimoh and Saka Abdulkareem.

A special thanks to my wife, Folasade Mojisola, our daughters Ayomikuoluwa Titilianifeoluwa, Oluwafeyikemi Ibukunoluwa and Temitopeoluwa Abisolaoluwa. They are a constant encouragement and a reason to be focussed. To My parents, father and mother in-law, also my siblings on both sides, thanks for been outstanding, I deeply appreciate your prayers, encouragement and love.

Friends are important wherever a man is and my friends in South Africa have indeed made my stay memorable. Some of these outstanding persons and families include; the Ilemobades, Olanrewajus, Abes, Olubambis, Akindahunsis, Popoolas, Adelekes, Adewumis, Adams, Ikotuns, Olasehindes, Ronos, and so many more.

Finally, I want to thank my home University, Federal University of Technology, Akure (FUTA) for granting me the opportunity and also my colleagues at the Mechanical Engineering Department, FUTA.

Abstract

Vehicle suspension design necessitates achieving complex compromise between various performance objectives. Active vehicle suspension systems (AVSS) outperforms all the other suspension types in this regard but at the cost of higher bandwidth and power consumption as well as, physical space constraint. This limitations have however not hindered research on AVSS as some of the automobile manufacturers have started introducing AVSS in their products thereby prompting improvement of its current level of performance.

The challenges of AVSS design centres around the inherent nonlinearities and uncertainties. This explains the recent interests in the introduction of intelligent control techniques to AVSS design. Neuro-adaptive controllers designed in this work are able to leverage on the combination of the strengths in chosen nonlinear techniques (that is, feedback linearisation and model predictive control) and model-based neural networks, thus avoiding the traditional need for linearisation.

The design of an indirect adaptive, neural network-based model predictive control (NNMPC) for a 7DOF nonlinear full-vehicle suspension design has been presented in this thesis. Its performance was benchmarked against that of PID controller in the presence of both random and deterministic road disturbance inputs. Improved system control was achieved by stabilising the actuator dynamics using PID control sub-loops. The performance of the NNMPC was superior, though the control process was slower because of the internal optimisation routine of the NNMPC.

Control voltage, actuator force and actuator spool-valve displacement are bounded within the specified limits. They are also well regulated (except at the instance of disturbance, however steady state was restored within about $0.5s$) without chattering. The result presented improved ride comfort, handling and road holding without violating the suspension travel limits. The weighted RMS body acceleration values for the vehicle sprung mass were evaluated based on international standards. Frequency domain analysis also showed that the AVSS was relatively insensitive to changes in the physical parameters between $7 - 80Hz$.

Scope and Contribution

The contributions resulting from this research work are as follows:

1. A neural network-based adaptive controller for real-time control (based on model predictive control) of an active suspension system have been developed for a nonlinear full-car AVSS.

2. The superior disturbance rejection-based performance and suitability of the developed controller for time-varying operating conditions and uncertainties have been demonstrated.

3. Four controllers have been studied in this work: a linear controller (PID), a direct adaptive neuro-controller (DANN), and two indirect adaptive neuro-controllers (NNFBL and NNMPC). Each controller is employed with an internal PID feedback loop to stabilize the actuator dynamics. These contributions are in widely circulated international journals and conference proceedings [Dahunsi et al. (2009, 2010); Ekoru et al. (2011); Pedro and Dahunsi (2011); Pedro et al. (2011)].

Published Work

Aspects of this thesis have been published in the following references:

1. Journal Articles

1. O. A. Dahunsi, J. O. Pedro and O. T. Nyandoro, System Identification and Neural Network-Based PID Control of Servo - Hydraulic Vehicle Suspension System, *Africa Research Journal, Transactions of the South African Institute of Electrical Engineers*, Vol. 101, No. 3, pp. 93-105, September 2010.

2. O. A. Dahunsi and J. O. Pedro, Neural Network-Based Identification and Approximate Predictive Control of a Servo-Hydraulic Vehicle Suspension System, *Engineering Letters*, Vol. 18, No. 4, pp. 357-368, November 2010.

3. J. O. Pedro and O. A. Dahunsi, Neural Network-Based Feedback Linearization Control of a Servo-Hydraulic Vehicle Suspension System, *International Journal of Applied Mathematics and Computer Science*, Vol. 21, No. 1, pp. 137-147, March 2011.

4. J. O. Pedro, O. A. Dahunsi and O. T. Nyandoro, Direct Adaptive Neural Control of Antilock Braking Systems Incorporated with Passive Suspension Dynamics, *Journal of Mechanical Science and Technology*, Vol. 26, No. 12, pp. 4115-4130, December 2012.

5. J. O. Pedro, M. Dangor and O. A. Dahunsi and M. M. Ali, Differntial Evolution-based PID Control of Nonlinear Full-Car Electrohydraulic Suspensions, *Mathematical Problems in Engineering*, (Status: Accepted for publication)

2. Conference Papers

1. O. A. Dahunsi, J. O. Pedro and O. T. Nyandoro, Neural Network-Based Model Predictive Control of Servo - Hydraulic Vehicle Suspension System, *Proceedings of IEEE AFRICON Conference (AFRICON2009)*, 23 - 25 September, 2009 at Safari Park Hotel, Nairobi, Kenya, pp. 1-6.

2. O. A. Dahunsi and J. O. Pedro, Multidisciplinary Design Optimization Framework for Active Vehicle Suspension - A Mechatronic Approach, presented at the *New Generation University Conference*, 17 - 19 November, 2009 at Emerald Casino, Vanderbijlpark, Gauteng, South Africa.

3. O. A. Dahunsi, J. O. Pedro and O. T. Nyandoro, Neural Network-Based PID Control of Servo - Hydraulic Vehicle Suspension System, presented at the *7th South African Conference on Computational and Applied Mechanics (SACAM10)*, 10 - 13 January, 2010 at University of Pretoria, South Africa.

4. O. T. Nyandoro, J. O. Pedro, B. Dwolatzky and O. Dahunsi, Control-Scheduling Codesign of Real-Time Optimal Braking of Antiock Braking Systems, presented at the *2nd African Conference on Computational Mechanics*, 5 - 8 January, 2011, Cape Town, South Africa.

5. O. T. Nyandoro, J. O. Pedro, B. Dwolatzky and O. A. Dahunsi, State Feedback based Linear Slip Control Formulation for Vehicular Antilock Braking System, *Lecture Notes in Engineering and Computer Science: Proceedings of the World Congress on Engineering 2011, WCE 2011*, 6-8 July, 2011, London, U.K., pp. 33-38.

6. O. T. Nyandoro, J. O. Pedro, O. A. Dahunsi and B. Dwolatzky, Linear Slip Control Formulation for Vehicular Antilock Braking System with Suspension Effects, *Proceedings of the 18th IFAC World Congress, Milano 2011*, August 28 - 2 September, 2011, Milano, Italy, pp.4779-4784.

7. J. E. D. Ekoru, O. A. Dahunsi and J. O. Pedro, PID Control of a Nonlinear Half-Car Active Suspension System via Force Feedback, *Proceedings of IEEE AFRICON Conference (AFRICON2011)*, 13 - 15 September 2011, Livingstone, Zambia, pp. 1-6.

8. J. O. Pedro, O. A. Dahunsi and N. Baloyi, Direct Adaptive Neural Control of a Quarter-Car Active Suspension System, *Proceedings of IEEE AFRICON Conference (AFRICON2011)*, 13 - 15 September 2011, Livingstone, Zambia, pp. 1-6.

9. J. O. Pedro, M. Dangor, O. A. Dahunsi and M. Ali, CRS and PS-Optimised PID Controller for Nonlinear, Electrohydraulic Suspension Systems, submitted to *9th IEEE Asian Control Conference (ASCC2013)*, 23 -26 June 2013, Istanbul, Turkey.

10. J. O. Pedro, M. Dangor, O. A. Dahunsi and M. Ali, DE-based PID Controller for Nonlinear, Servo-Hydraulic Suspension Systems, submitted to *9th IEEE*

Africon Conference (AFRICON2013), 9 - 12 September 2013, Pointe aux Piments, Mauritius. (Status: Accepted)

3. Submitted Journal Papers

1. O. A. Dahunsi and J. O. Pedro, $\mathcal{H}_2/\mathcal{H}_\infty$ Control of an Active Vehicle Suspension System, submitted to *Mathematical Problems in Engineering*
2. M. Dangor, O. A. Dahunsi, J. O. Pedro and M. Ali, Evolutionary Algorithm Enhanced PID Control of Nonlinear Servo-Hydraulic Active Vehicle Suspension System, submitted to *Asian Journal of Control*.
3. O. A. Dahunsi, M. Dangor, J. O. Pedro and M. Ali, Active Vehicle Suspension Systems Using CRS and PS Control Optimization Algorithms, submitted to *Expert Systems with Applications*.
4. J. O. Pedro, M. Dangor, O. A. Dahunsi and M. Ali, Intelligent Feedback Linearisation Control of Nonlinear Electrohydraulic Suspension Systems Using Particle Swarm , submitted to *Applied Soft Computing*.

3. Submitted Conference Papers

1. O. A. Dahunsi, J. O. Pedro and M. Ali, On PID Control for Nonlinear Active Vehicle Suspension Systems, submitted to *Proceedings of the Mathematics in Industry Study Group 2013*.

Contents

List of Figures

List of Tables

List of Symbols

Acronyms

AF	Actuator Force
$ARMAX$	AutoRegressive Moving Average eXogenous input
ARX	AutoRegressive eXogenous input
$AVSS$	Active Vehicle Suspension System
BA	Body Acceleration
$BIBO$	Bounded-Input-Bounded-Output
CAN	Controller Area Network
CI	Computational Intelligence
CLF	Control Lyapunov Function
$COMPENDEX$	COMPuterized ENgineering InDEX
CV	Control Voltage
$DANN$	Direct Adaptive Neural Network
DFT	Discrete Fourier Transform
DOF	Degree-of-Freedom
EA	Evolutionary Algorithm
EAV	Exposure Action Value
ELV	Exposure Limit Value

$FASS$	Fully-Active Suspension System
FBL	Feedback Linearisation
FFT	Fast Fourier Transform
FL	Fuzzy Logic
FPE	Final Prediction Error
GA	Genetic Algorithm
$HBAS$	High-Bandwidth Active Suspension
HFV	High Frequency Vibration
$LBAS$	Low-Bandwidth Active Suspension
LFT	Linear Fractional Transform
LFV	Low Frequency Vibration
LMI	Linear Matrix Inequalities
LPV	Linear Parameter Varying
LQG	Linear Quadratic Guassian
LQR	Linear Quadratic Regulator
$LVDT$	Linear Variable Differential Transformer
$MIMO$	Multi-Input-Multi-Output
MLP	Multi-Layer Perceptron
MPC	Model Predictive Control
MSE	Mean-Squared Error
$NARMA$	Nonlinear AutoRegressive Moving Average
NN	Neural Network

$NNARX$	Neural Network AutoRegressive eXogenous input
$NNFBL$	Neural Network-Based Feedback linearisation
$NWDL$	Normalized Wheel Dynamic Load
$NNMPC$	Neural Network-Based Model Predictive Control
PAA	Pitch Angular Acceleration
$PASS$	Parallel Active Suspension System
PID	Proportional-Integral-Derivative Control
PSD	Power Spectral Density
$PVSS$	Passive Vehicle Suspension System
RAA	Roll Angular Acceleration
RBF	Radial Basis Function
RDI	Road Disturbance Input
RMS	Root-Mean Square
$SASS$	Semi-Active Suspension System
$SISO$	Single-Single-Single-Output
ST	Suspension Travel
SVD	Spool-Valve Displacement
TDL	Tapped Delay Line
WDL	Whole Body Vibration

Latin Alphabets - Upper Case

A	Area of piston, m^2
C_d	Discharge coefficient
C_{tp}	Total leakage coefficient of the piston
F	Actuator force, N
F_{b_s}	Damping force acting on the body, N
F_{k_s}	Spring force acting on the body, N
F_{k_t}	Spring force acting on the wheel, N
K	Servo valve gain, m/V
K_D	PID derivative gain
K_I	PID integral gain
K_P	PID proportional gain
K_v	Positive design parameter (a positive definite diagonal matrix)
P_r	Return pressure, N/m^2
P_s	Supply pressure, N/m^2
Q	Hydraulic load flow through the piston, m^3/s
S	Spool-valve area gradient
V	Lyapunov candidate function, or Vehicle forward velocity, m/s
V_t	Total actuator volume, m^3

Latin Alphabets - Lower Case

b_s^l	Linear component of the damping coefficient, Ns/m
b_s^{nl}	Nonlinear component of the damping coefficient, Ns/m

b_s^{sym}	Damping coefficient component with asymmetry, Ns/m
e	Error signal (that is, difference between y and y_d), m
k_s^l	Linear component of the spring constant, N/m
k_s^{nl}	Nonlinear component of the spring constant, N/m
k_t	Wheel spring constant, N/m
m_s	Sprung mass, kg
m_u	Unsprung mass, kg
r	Filtered tracking error
t	Time, s
u	Control input, $Volt$
w	Road disturbance displacement, m
x_1	Vehicle body vertical displacement, m
x_2	Vehicle wheel vertical displacement, m
x_v	Spool-valve displacement, m
x_p	Pressure drop across the piston, N/m^2
y	Controlled output (suspension travel), m
y_d	Desired controlled output, m

Greek Alphabets - Upper case

Λ	Positive design parameters, or half-wavelength of road undulation, m
Φ	Hydraulic load flow

Greek Alphabets - Lower case

β_e	Effective bulk modulus of the system
ν	Virtual control input
ρ	Density, kg/m^3
σ	Wheel dynamic load, N
τ	Time constant, s

Vectors and Matrices

f	A matrix of nonlinear functions used in system approximation
g	A matrix of nonlinear functions used in system approximation
$\hat{W}$	Neural network weight vector
$\phi(x)$	Column vector of RBF units in a network

Subscripts

f	Front
l	Left
r	Rear, Right
u	Unsprung
s	Sprung, suspension
t	Tyre

Superscripts

l	Linear
nl	Nonlinear
sym	Symmetrical

1 Introduction

1.1 General Background

Apart from the aesthetic values that buyers seek for in vehicle products today, the other factors determining their choice include ride comfort, safety and stability [Cao et al. (2010); Kaddissi et al. (2009); Kim et al. (2012)]. The role of vehicle suspension system in meeting these demands is shown by the volume of research in the area in the past five decades [Cao et al. (2011); Chantranuwathana and Peng (2004); Fialho and Balas (2002); Guglielmino and Edge (2004); Kim et al. (2012); Lin and Lian (2011); Shi et al. (2010)].

Vehicle suspension units consist of springs, dampers (shock absorbers), link members and actuators (in active suspension systems). They are located between the wheels and the body of the vehicle in such a way that they carry the weight of the vehicle directly. Figure 1.1 shows the location of the suspension systems (shown as the MacPherson Struts) in a car.

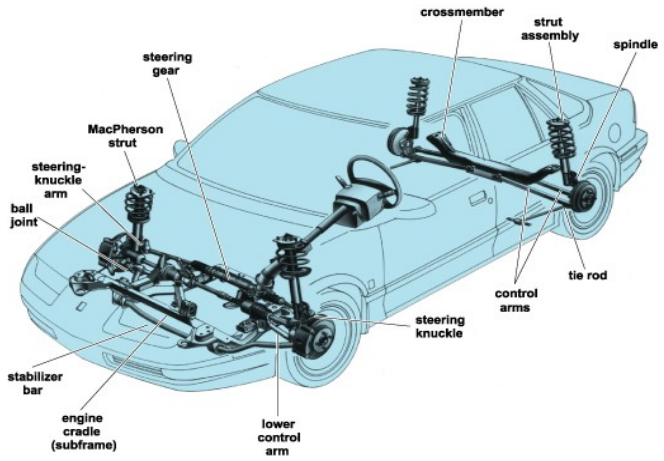

Figure 1.1: Location of suspension systems in a car
Source:http://www.webmaxmachine.com/schemamecanique/Direction%20-%20Suspension/slides/CE064600FG0010.html

Quality of the suspension system influences the *driving safety* of the vehicle, and this is related to effective braking and steering of the vehicle [Fischer and Isermann (2004); Kaddissi et al. (2009); Montazeri-GH and Soleymani (2008); Turkay and Akcay (2008)]. Good vehicle suspension ensures *ride comfort*, which is associated with the ability to isolate the vehicle from road induced vibrations [Du and Zhang (2008*b*); Fischer and Isermann (2004); Hrovat (1997); Turnip et al. (2010)].

It is also responsible for ensuring adequate contact between the wheel and the road surface (this is associated with the term, *road holding*) [Du and Zhang (2008*b*); ElMadany and Qarmoush (2011)]. Poor road holding indicates that the engine torque generated is not effectively translated into traction force on the road [Gillespie (1992); Turnip et al. (2010)]. It is desirable that the vehicle suspension should be able to enhance the stability and directional control of the vehicle during steering, maneuvering or cornering (this is associated with the term, *vehicle handling*) [Biglarbegian et al. (2008); Chen and Guo (2005); Yagiz and Sakman (2005)].

A good suspension helps to control the vehicle body motion (that is, *pitch*, *bounce* and *roll*) which are caused by acceleration, deceleration or steering of the vehicle [Biglarbegian et al. (2008); Cao et al. (2007); ElMadany and Qarmoush (2011); Smith et al. (2011)]. It also helps to maintain the vehicle suspension travel (that is, keeping vertical displacement of the vehicle within the allowable *suspension packaging space*) [Akbari et al. (2010); Du and Zhang (2008*b*); Huang and Lin (2002); Okumura et al. (2010)]; and minimizing road damage, improvement of braking and ensuring good static deflection [Cole (2001)].

Vehicle suspension systems are available with configuration and classification shown in Figure 1.2:

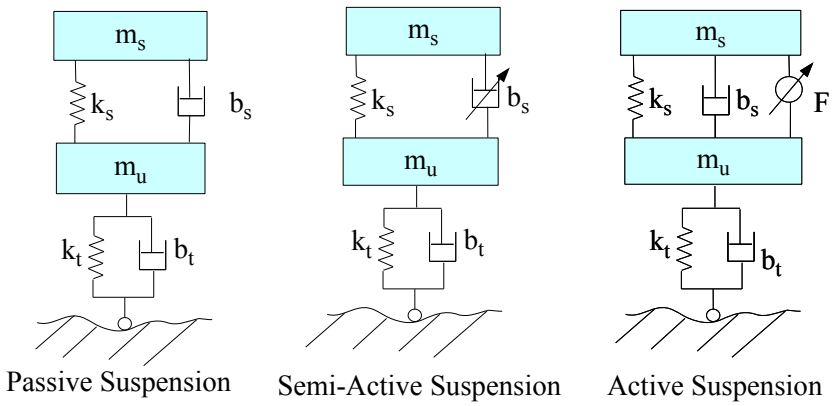

Figure 1.2: Types of Vehicle Suspension Systems

1. Passive suspension (PVSS), which consists of spring and damper, and are connected in parallel to each other,

2. Semi-active suspension (SASS), which has adjustable damper in place of the usual damper in the PVSS, and

3. Active suspension system (AVSS), which has an actuator in addition to the spring and damper (i.e., passive elements).

Figure 1.3 shows the major components of each class of vehicle suspension system. Active and semi-active suspension systems require controllers for their actuators or variable damper. The fixed design parameters or settings of passive suspensions result in their poorer performance in terms of robustness and ability to handle system non-linearities in contrast with the semi-active and active suspension systems.

Semi-active and active suspension systems are controlled suspension systems, this makes them flexible, thus becoming adaptive to varying operational conditions. Active suspension dynamically alters the energy flow to and from the system, thereby widening the scope of the trade-off between the various conflicting design objectives [ElMadany and Qarmoush (2011)].

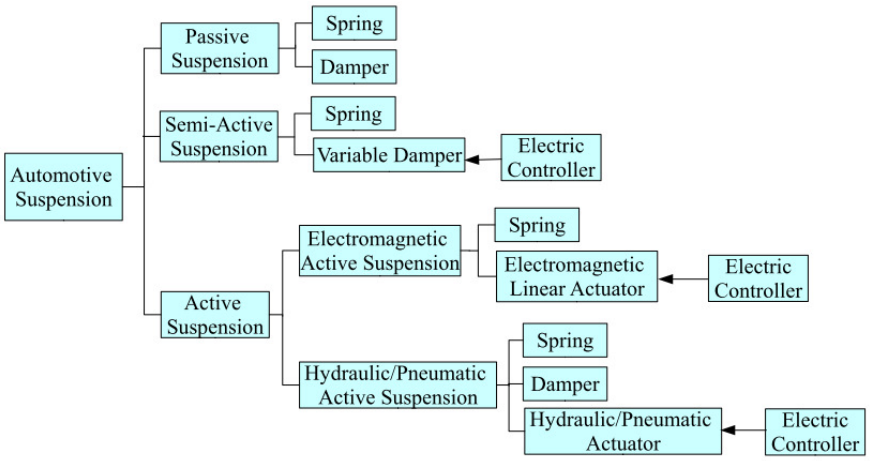

Figure 1.3: Schematic Classification of Vehicle Suspension Systems [Xue et al. (2011)]

Table 1.1 presents a qualitative comparison between the various classes of vehicle suspension systems showing their relative strengths in terms of some performance parameters.

Table 1.1: Qualitative Comparison Between Vehicle Suspension Categories [Xue et al. (2011)]

Parameters	Passive suspensions	Semi-active suspensions	Hydraulic/Pneumatic active suspensions	Electromagnetic active suspensions
Structure	Simplest	Complex	Most complex	Simple
Weight or Volume	Lowest	Low	High	Highest
Cost	Lowest	Low	Highest	High
Ride comfort	Fair	Medium	Good	Best
Handling performance	Fair	Medium	Good	Best
Reliability	Highest	High	Medium	High
Dynamic performance	Passive	Passive	Medium	Good
Energy regeneration	No	No	No	Yes
Commercial maturity	Yes	Yes	Yes	No

1.2 Active Vehicle Suspension System (AVSS)

Active suspension system is a closed-loop control system consisting of a controller linked to the controlled actuator and feedback signals through sensors to determine the control input signal to the system. AVSS responds dynamically to road disturbance inputs by inducing relative motion between the body and the wheel through the actuator supplied energy [Hrovat (1997); Joo et al. (2000); Lin and Lian (2011); Pedro (2007)].

Figure 1.4 presents the generic active vehicle suspension system (AVSS) feedback control loop. The system consists of a controller issuing the command input to the actuator to generate a manipulating signal. Optimal trade-off between the design objectives is achieved in the process, thereby making the suspension system adaptive to the road and other operating conditions.

AVSS holds great prospect as controlled suspension. Detail classification and characteristics of active suspension systems are available in the literature [Fijalkowski

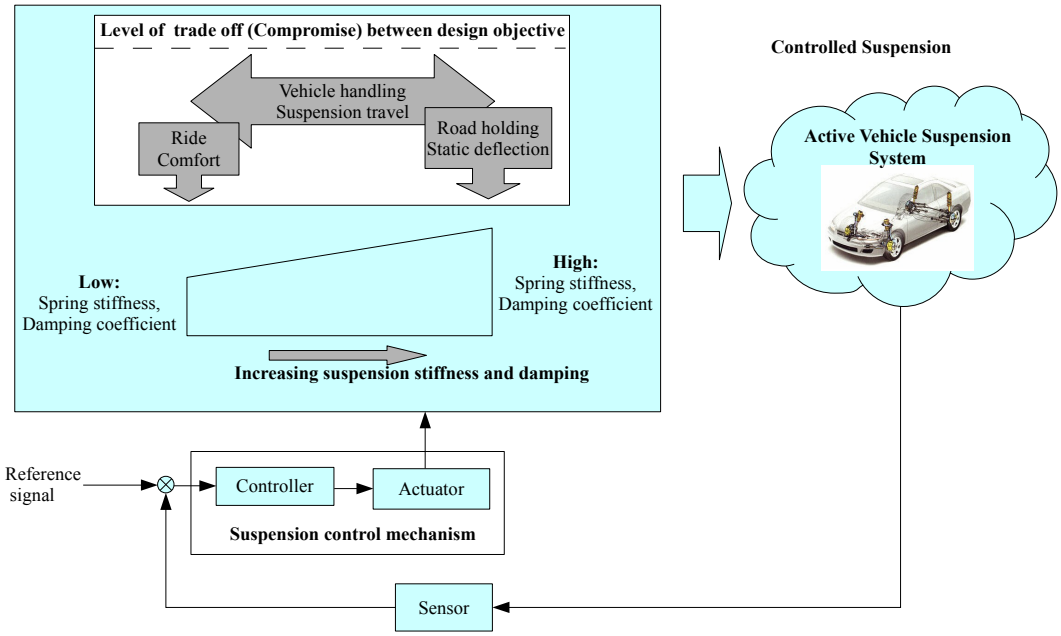

Figure 1.4: AVSS Feedback Control Loop

(2011); Fischer and Isermann (2004); Hrovat (1997); Koch et al. (2008); Leighton and Pullen (1994); Williams (1997*b*)]. Figure 1.5 shows the broad classification of active suspension systems on the basis of system bandwidth level.

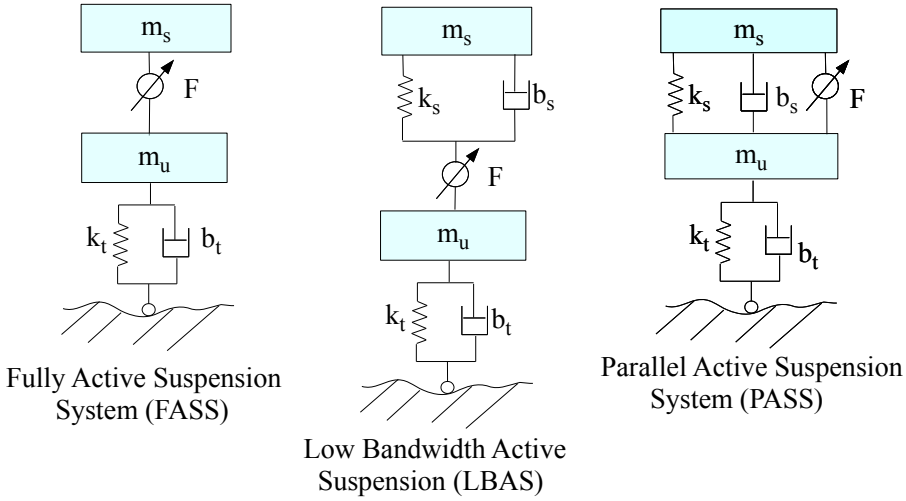

Figure 1.5: Types of Active Vehicle Suspension Systems

1. *Fully Active Suspension System* (FASS), is made up of hydraulic or electromagnetic actuators alone. These actuators are individually controlled by servo valves and an engine-driven pump. They have a frequency bandwidth ranging from 20 to $40Hz$, therefore this class of AVSS belongs to the *high bandwidth active suspension system* (HBAS) range. This class of AVSS is characterised by very high power consumption $(5 - 10kW)$ [Fischer and Isermann (2004);

Leighton and Pullen (1994); Xue et al. (2011)].

2. Parallel Active Suspension System (PASS), in this case, the actuator is positioned in parallel with the normal conventional passive suspension elements. This class of AVSS also belong to the *high bandwidth active suspension system (HBAS)* range and is the more popular form of AVSS in the literature because of its broad bandwidth range (that is, 0.1 to about $40Hz$ with a cut-off frequency of $25Hz$). It is thus positioned for both low and high frequency applications. It is also used as benchmark when designing for the low bandwidth active suspensions [Koch et al. (2008); Leighton and Pullen (1994)].

3. Low Bandwidth Active Suspension (LBAS), in this case, the actuator is positioned in series with the spring and damper, thus making its power requirement relatively lower. It is therefore a cheaper alternative though with small bandwidth range $(3-5Hz)$ [ElMadany and Qarmoush (2011); Koch et al. (2008); Leighton and Pullen (1994)].

   The HBAS frequency response must at least cover the following frequency ranges which are regarded as resonant frequencies) [Fijalkowski (2011); Fischer and Isermann (2004); Gillespie (1992); Hrovat (1997); Williams (1997*a*)]:

   (a) *rattle-space* frequency $(10-12Hz)$,

   (b) *wheel-hop* frequency $(10-15Hz)$,

   (c) *roll* frequency $(0.5-1Hz)$,

   (d) *pitch* frequency $(2.5-3Hz)$,

   (e) Low frequency sprung mass motion,(*body heave*) frequency $(1-3Hz)$,

AVSS is an example of a complex control application with multiple variable and nonlinear coupling. The basic sources of its nonlinearities and uncertainties are:

1. System nonlinearities

   (a) *Dampers and springs of the suspension systems*: these elements normally have nonlinear properties that are time varying;

   (b) *Hydraulic / pneumatic actuator dynamics*;

   (c) *Topping* and *bottoming* when the rattle space limits are reached.

2. Uncertainties

   (a) *Unstable operating conditions*: these are irregularities due to excitation inputs caused by road surface roughness and varying vehicle speed;

(b) *Varying vehicle mass and payload*;

(c) *Component wear and deterioration.*

AVSS requires that sensors be positioned at different locations in order to provide signals which the controller can act on in order to drive the actuator. The necessity for sensors, actuators and controllers has been partly responsible for the high cost of active suspension implementation, but the current growth in electronics engineering is gradually making active suspension implementation in commercial vehicles feasible [Cao et al. (2007); ElMadany and Qarmoush (2011); Hyvarinen (2004)].

Moreover in the last decade, active suspension has begun to find implementation, on commercial scale, in passenger cars, as well as construction and military vehicles [Eski and Yildrim (2009); Fischer and Isermann (2004); Gysen et al. (2010); Koch (2011); Priyandoko et al. (2009); Shi et al. (2010); Smoker et al. (2009)]. This development is facilitated by the rapid advances in electronic technology and intelligent control system [Hada et al. (2007); Hyvarinen (2004)].

Evidence from the literature, some of which include Fischer and Isermann (2004); Hrovat (1997); Pedro (2007); Yagiz and Sakman (2005), confirms the benefits of the active suspension to include:

1. Ability to adapt to different road conditions and flexibility in the choice of desired dynamic characteristics.
2. Capability to engage the full suspension working space in ensuring a good compromise between performance requirements like ride comfort, road holding and vehicle handling, and
3. Better system static ability and performance at low frequencies. For example, it is able to remove the resonance frequencies due to chassis dynamics, which is around $1Hz$.
4. With an improvement in ride quality due to the active suspension, comes reduction in driver fatigue. This results in better safety and vehicle control.

The listed benefits of AVSS must however be achieved in spite of the following challenges:

1. External power requirement,

2. Hardware complications in terms of the actuator fitting the available packaging space,
3. Sensors and measurement complications,
4. System nonlinearities and uncertainties,
5. Actuator dynamics complications,
6. Degradation in performance due to chattering in hydraulic actuators,
7. High bandwidth requirement, and
8. High manufacturing cost.

1.3 Current Trend in AVSS Controller Design

Controller design is central to active suspension design. Several control methods ranging from optimal to adaptive, robust and nonlinear control methods have been proposed. Detail and chronological review of this applications are available in the literature [Chen and Guo (2005); ElMadany and Qarmoush (2011); Hrovat (1997); Pedro (2007); Shi et al. (2010)].

Research interest in AVSS took the form of an exponential growth in the last three decades but has risen to an unprecedented level in the contemporary time. This is evident from Figure 1.6, which is based on a random internet search through the COMPENDEX database.

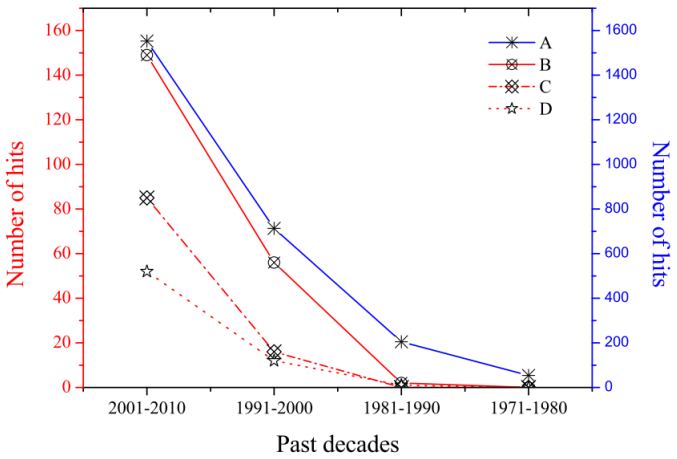

Figure 1.6: Number of hits resulting from a random search for AVSS related terms in the COMPENDEX database

In the figure, graph A - represents the plot for the number of hits returned using the search term "active vehicle suspension system", graph B - represents the plot when the search term "active vehicle suspension system with adaptive control" was used, graph C - represents the plot when the search term "active vehicle suspension system with fuzzy logic" was used, and graph D - represents the plot when the search term "active vehicle suspension system with neural networks" was used.

In the decade that ended in 2010, about 150 research publications were based on AVSS control using adaptive control methods. About 90 of this publications were based on application of fuzzy control and about 50 were based on the application of neural networks. The total number of publications on AVSS within the same period was almost 1600. Increase in the application of intelligent control method like neural networks was low but growing fast.

It also be inferred from Figure 1.6 that AVSS controllers whose design was based on linear control methods were ten times more available in the literature than those based on adaptive or intelligent control methods. The figure also showed increase in AVSS controller design documented works in a geometric pattern. AVSS controller design works based on nonlinear and intelligence control techniques followed this pattern too.

The complexity of the AVSS makes it necessary to broadly classify its controller design into linear and nonlinear control groups. Figure 1.7 demonstrates this classification using some of the control methods as illustration.

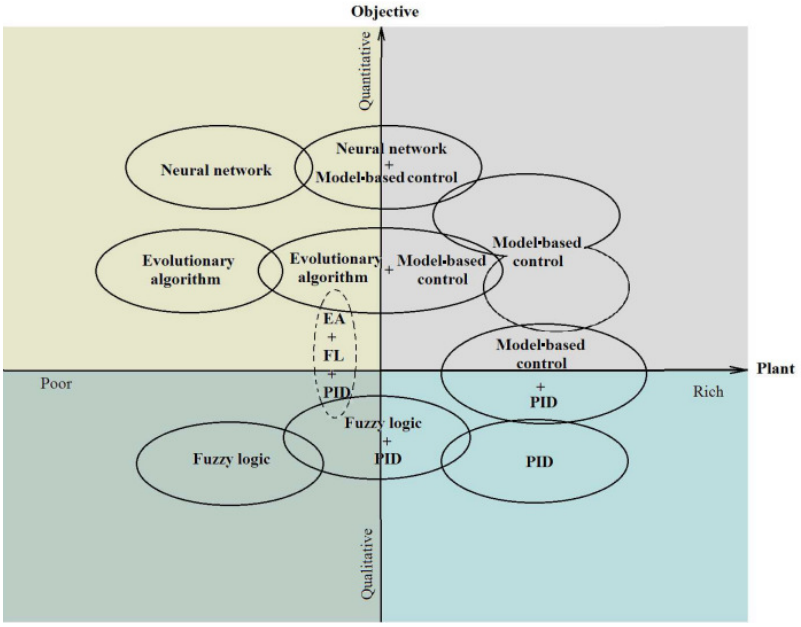

Figure 1.7: Properties of Control Methodologies

The figure positions the various methods in various quadrants based on their suitability for different control problems. The quadrants are partitioned using axes with scales graduated for the richness of the plant information available, and nature of the plant's performance objectives.

Several documented works like, [Ge and Lee (1997); Kim and Ro (1998); Lin and Lian (2011); Wang and Shih (2011)] have demonstrated the weakness of the conventional linear feedback control methods at handling the complex nonlinear dynamical systems and uncertainties associated with AVSS operation.

Nonlinear control methods hold good prospect in terms of AVSS design because they are more readily applicable to the AVSS time varying and nonlinear nature. They also combine with the computational intelligence (CI) - based control methods for performance enhancement.

Computational intelligence techniques includes several *adaptive mechanisms* which are mostly inspired by biological systems or nature. They are employed in modelling or controlling systems for which mathematically-based modelling have been ineffective. Examples of computational intelligence techniques includes: neural networks, fuzzy systems, evolutionary computing, swarm intelligence, probabilistic methods and learning theory [Chen and Chiang (2003); Juuso (2004)]. Inter-disciplinary application of CI techniques with control systems yields intelligent control, whose application in AVSS design holds great prospect. The combination is also becoming more commercially available for smaller luxury cars and off-road vehicles [Becker et al. (1996); Cao et al. (2011, 2008)].

Other documented works in the literature like, [Chen and Guo (2005); Fialho and Balas (2002); Kim and Ro (1998)] have also made strong cases for *adaptive suspension*. These are vehicle suspensions that are able to adjust the controller performance in response to the time-varying interaction between the road and the vehicle. In spite of the enormous prospect of the classical adaptive control methods employed, there have been severe limitations due to AVSS nonlinearity [Cao et al. (2008)]. This deficiency is responsible for the increase in the application of intelligent control methods in AVSS.

Table 1.2 presents some examples of works in the literature which are classified according to the general categories of the control methods. The first three categories, classical, optimal and robust control methods, make up the conventional control

method group. These methods are well developed in terms of application to AVSS design. Current research efforts are now being directed towards the application of intelligent control and its combination with other control methods to yield robust and adaptive controller.

Table 1.2: Classes and Examples of Control Methods Applied to AVSS Design in the Literature in the Past Two Decades

General classification	Control method	Some references in literature	Combined with Intelligent Control
Classical control	PID	Ekoru et al. (2011); Kumar (2008); Chen and Xiao (2011); Guclu (2004); Nusantoro and Priyandoko (2011)	Aldair and Wang (2010); Dahunsi et al. (2010); Kuo and Li (1999); Shen et al. (2010); Chiou et al. (2012); Xinjie and Shengjin (2009)
Optimal control	LQR	Koch et al. (2008); Pedro and Mgwenya (2004); Gopala Rao and Narayanan (2009); Smoker et al. (2009); ElMadany et al. (2011); Kumar and Vijayarangan (2006); ElMadany and Al-Majed (2001); Gavriloski et al. (2007); Palkovics et al. (1993)	
	LQG	Hrovat (1997); Turkay and Akcay (2008); Chai and Sun (2010); ElMadany and Abduljabbar (1999) He and McPhee (2005); Li et al. (2008); Zhong et al. (2010) Chen et al. (2011); Crivellaro and Donha (2011a)	Fateh and Alavi (2005) Younesian and Nankali (2009)
Robust control	H_∞	Akbari et al. (2010); Du and Zhang (2007) Ryu et al. (2008); Yamashita et al. (1994) Chen and Guo (2005); Fallah et al. (2009) Hayakawa et al. (1999); Wang et al. (2001) Orvnaas et al. (2011); Zuscikova and Belavy (2011)	
	H_2	Miaomiao and Chen (2006); Zuo and Nayfeh (2003b);	

General classification	Control method	Some references in literature	Combined with Intelligent Control
Robust control	H_2/H_∞	Aghaie and Amirifar (2007)	Du and Zhang (2008*a*)
	LPV	Fialho and Balas (2002); Gaspar et al. (2003); Gaspar et al. (2011); Onat et al. (2007);	
	Multiobjective Control Methods	Du and Zhang (2008*b*) Loyer et al. (2008); Poussot-Vassal et al. (2006)	
Nonlinear control	Feedback linearisation	Chien et al. (2009); Shi et al. (2010)	Buckner et al. (2000); Huang et al. (2009); Pedro and Dahunsi (2011)
	Sliding Mode	Sam et al. (2004); Sam and S.Osman (2005) Chamseddine and Noura (2008); Chen and Guo (2005) Koshkouei and Burnham (2008)	Al-Holou et al. (2002); Huang and Lin (2002)
	Backstepping	Huang et al. (2010); Kaddissi et al. (2009) Hu and Lin (2008); Lin and Huang (2004)	
Intelligent control	Neural Network Based	Renn and Wu (2007); Zhao et al. (2011) Dahunsi et al. (2009); Eski and Yildrim (2009)	Crivellaro and Donha (2011*a*) Huang and Lin (2002)
	Fuzzy Logic Based	Cao et al. (2010); Lin and Lian (2011) Sharkawy (2005); Yoshimura and Teramura (2005) Du and Zhang (2009); Huang and Chao (2000)	Montazeri-GH and Soleymani (2008) Chiou and Liu (2009) Chen et al. (2010)
	Evolution Algorithm Based	Baumal et al. (1998); Hada et al. (2007) He and McPhee (2005); Shirahatt et al. (2008) Alfi and Fateh (2011); Fateh and Zirkohi (2011)	Wang and Shih (2011)

1.3.1 Linear control schemes

Linear controllers range from PID to optimal control schemes and the multivariable-multiobjective controllers. In the linear control schemes, approximations of AVSS are obtained by ignoring the second- and higher-order terms of the Taylor series expansion of the AVSS mathematical model around an equilibrium point. Thus, the behaviour of the linear models are different from those of the nonlinear models because some of the system's dynamics have been ignored. Moreover, it is desirable in the course of AVSS controller design to consider the system model as completely as possible [Gaspar et al. (2003); Hrovat (1997); Joo et al. (2000); Nagai et al. (1997)].

Larger proportion of the control schemes that has been employed in AVSS design in the literature are the linear control schemes. Examples of these schemes include; LQR, LQG, H_2 and H_∞. The theoretical basis for these control methods are relatively well developed [Baumal et al. (1998); Wang et al. (2006)]. These methods are based on obtaining an optimal feedback gain to minimise the chosen performance objectives like; ride comfort, suspension deflection, road holding and vehicle handling [Cao et al. (2007); Dahunsi et al. (2010)].

Linear optimal control schemes are attractive because they are stable and robust. Moreover, the robustness becomes quite limited in the face of typical AVSS system uncertainties due to inaccessibility and variation in parameters, and inaccurate measurements. The parametric uncertainties in AVSS have more impact on the vehicle mass and payload, as well as, spring stiffness and damping coefficient of the suspension system. Meanwhile, most AVSS applications of linear optimal control schemes presume time-invariant situation. The controllers are well suited for random disturbance inputs and frequency response related analysis.

In practice, linear optimal control schemes require the availability and accessibility of all the *states* for implementation. This is a source of major challenge because of the cost and difficulty involved in measuring some of the states. Designing *observers* for estimating the unavailable states is the typical solution to this problem, however, a state like tyre deflection could be challenging to estimate. Solving AVSS control problem by the use of linear control schemes is based on the assumption of a broad bandwidth actuator, whose response is fast enough and its parameters can be linearised (the Jacobian way) within some operating regions [Cao et al. (2008)].

Although these optimal control schemes are able to guarantee system stability and robustness within a reasonable operation region about the equilibrium position, they

yield complex higher-order systems. Multiobjective combinations of various optimal control methods have been proposed with improved performance results and robustness. Moreover, the multiobjective control problem yields a non-convex optimisation problem that could be difficult to solve. Also, the fixed optimal gains cannot be adjusted in the face of varying operating condition like changing road disturbance input [Du and Zhang (2008*b*); Lu and DePoyster (2002)].

PID control method is the most widely used control method, it accounts for over 90% of all the industrial control loops [Ang et al. (2005); Gao (2002); Goncalves et al. (2008)]. It is simple and easy to apply, but it lacks robustness to parameter variation and could be challenging to implement physically because of its high loop gains. For these reasons, PID applications with AVSS is limited except for the purpose of performance benchmarking during controller designs for other control methods. It however, holds great prospect when combined with an appropriate intelligent control technique [James et al. (1999); Kaddissi et al. (2009)].

Model predictive control (MPC) is regarded as the most successful advanced control technique in terms of academic and industrial application. It controls the plant's future behaviour by online computation of control inputs in an iterative optimisation process. MPC readily handles states and input constraints, multivariable interactions and time-delays [Bequette (2007); Jazayeri et al. (2008); Qin and Badgwell (2000)].

Moreover, successful application of MPC depends on the availability of an explicit dynamic model of the plant and its operation is based on linear model with a quadratic objective thatoften leads to non-convex multi-modal optimisation problem, that is not readily solved. A likely problem could also arise in the absence of a universal optimisation procedure to resolve this problem [Jazayeri et al. (2008); Lawrynczuk (2007); Yan and Wang (2011)].

These challenges are being handled by the introduction of nonlinear model predictive control methods, especially by the neural network-based model predictive methods. These methods utilise the universal approximator capacity of neural networks in developing nonlinear dynamic models of the systems to be controlled. Its setbacks could however include its unsuitability for systems with unstable inverses [Akesson and Toivonen (2006); Chen and Yea (2002); Dahunsi et al. (2009); Lawrynczuk (2007)].

Linear parameter varying (LPV) design is a fixed gain strategy that is designed

to be optimal for a nominal parameter set and specific operating conditions. It has been demonstrated to be useful in tackling measurable and bounded nonlinearities. It employs parameterized linear systems to describe the nonlinear system dynamics over the operating range, the controller is constructed from the solutions of LMI generated over the parameter set [Bars et al. (2008); Fialho and Balas (2002); Gaspar et al. (2003); Poussot-Vassal et al. (2006)].

There has however been indications that in the last decade more attention is being paid to intelligent control-based applications to vehicle suspension control. This is because of the system nonlinearities and uncertainties that characterise the system (for example, precise parameters may not be readily obtained for the mathematical model). Another common source of uncertainty is continual variation in inertial properties [Cao et al. (2010); Du et al. (2011); Lin and Lian (2011)].

1.3.2 Nonlinear control schemes

Vehicle systems have complex dynamics characterised by nonlinearities, varying parameters, unknown friction and high amplitude disturbances. These nonlinearities are also manifested in operating conditions like, the varying vehicle speed and the irregular road excitations due to the road surface roughness [Feng et al. (2003); Gao et al. (2006); Ikenaga et al. (1999)].The complexities make linear approximations in the analysis of the AVSS impractical. This situation calls for good performance of the AVSS controller in terms of the design objectives, good level of robustness to uncertainties as well as, disturbance rejection [Feng et al. (2003); Spentzas and Kanarachos (2002)].

An active suspension system is naturally a nonlinear system, which is characterised by uncertainties that can not be fully addressed by most design methods. Real plants are usually time-varying system, therefore linear control method fails when applied to such case. For example, total vehicle mass varies as the passenger load changes in the vehicle. This is why AVSS controller must not only be designed based on optimal control laws alone, it must be designed with robust characteristics suitable for the uncertainties and nonlinearities peculiar to active suspension operation [Du and Zhang (2008*b*); Pedro (2007)].

Nonlinear control schemes should be more suitable for AVSS since it is a nonlinear system. An additional reason is the complex nonlinear behaviour of the AVSS actuator dynamics, especially when it is hydraulic or pneumatic [Chantranuwathana

and Peng (2004); Du and Zhang (2009); Feng et al. (2003); Nusantoro and Priyandoko (2011)]. Examples of nonlinear control schemes that have been applied in AVSS are; sliding mode, backstepping and feedback linearisation.

The sliding mode control method is attractive because it has good level of robustness. Sliding mode control has been proposed for actuator force control in the inner loop control of AVSS. Moreover, while it holds good prospect, being adaptive, the presence of *chattering* is a setback that could degrade the system performance, especially by exciting unmodelled high frequency dynamics due to the switching control signal [Du and Zhang (2009); Kaynak et al. (2001)].

Successful application of sliding mode control is dependent on the availability of good system dynamic model since it uses the function approximation technique [Huang and Lin (2002); Koshkouei and Burnham (2008)]. Sliding mode control is also susceptible to measurement noise and require large control signals [Kaynak et al. (2001)].

Backstepping control method is well known as an adaptive nonlinear control scheme because of its flexibility. This advantage was utilized by Lin and Huang (2004) in resolving the compromise between ride quality and suspension travel. It is usually desirable to achieve the best ride comfort possible within the constraint of the available rattle space. In backstepping control, there is additional nonlinearity because of the inclusion of a filter. The bandwidth of the filter is determined based on the magnitude of the available rattle space. With backstepping control, the AVSS can be dynamically adjusted during operation to be soft when the suspension travel is small, or stiff when the suspension travel is large.

An additional advantage is that backstepping control method is based on successful application of the Lyapunov's stability theory (that is, it involves the finding of the control Lyapunov function (CLF) and the control law simultaneously) therefore, it readily guarantees asymptotic tracking and global stability when an appropriate candidate Lyapunov function is obtained [Seo et al. (2007); Yu et al. (2004)]. In spite of the adaptive control potential of this method, it has a setback in form of repeated differentiation of the system nonlinear function, and this may lead to increase in complexity of the nonlinear functions [Chien et al. (2009); Huang et al. (2009)].

In feedback linearisation (FBL), the nonlinear problem is transformed into an equivalent linear one. This is achieved by algebraically transforming the nonlinear system

dynamics into linear ones by using state feedback and nonlinear coordinate transformation. Thus, system nonlinearities are cancelled so that a conventional linear control method could be applied to solve the control problem. FBL is also attractive for multivariable nonlinear problems because of its decoupling advantage [Garces et al. (2003); Seo et al. (2007)].

FBL is a nonlinear control technique that has been used effectively for regulation and tracking control problems. Although its setback includes requirement of full-state measurement and robustness (due to cancellation of model nonlinearities whose dynamics may be vital to system performance), its application does not lead to a computationally demanding controller (due to the high order) like some other nonlinear control methods and it is more readily combined with CI techniques like neural networks and fuzzy logic to enhance the controller performance. Accurate knowledge of the system model and zero dynamics stability are also essential for effective application of FBL [Goodwin et al. (2001); Shi et al. (2010)].

Input-output FBL is often preferable to exact FBL because it is less restrictive. Exact FBL is not always possible because full knowledge of the nonlinear system model is always required. Input-output FBL however, requires an elaborate internal stability analysis. This is because input-output FBL creates hidden states as consequence of its linearisation process. Therefore, a successful implementation of input-output FBL requires a guarantee of stable zero dynamics in the system [Behera and Kar (2009); Yesildirek and Lewis (2001)].

Intelligent control methods are nonlinear control methods with good prospect for AVSS application. This is because they do not require detail information of the plant and can tolerate both qualitative and quantitative design objectives as shown in Figure 1.7.

1.3.3 Intelligent Control Schemes

Intelligent control techniques are control schemes which employ the CI techniques in tackling control problems. They are readily applicable to nonlinear control problems with the need for Jacobian linearisation, through which some vital nonlinear system dynamics is lost. The suitability of any intelligent control method depends on the characteristics of the CI technique it uses. CI techniques can also be combined with other control methods to enhance the system control. The major categories under intelligent control are:

1. Neural network-based control schemes,

2. Fuzzy logic-based control schemes, and

3. Evolutionary algorithm-based control schemes.

Neural network (NN) and fuzzy logic are the two most applied computational intelligence techniques to control problems. Whereas, fuzzy logic has been employed in many nonlinear control problems successfully, its challenges lie in the selection of the appropriate if-then rules and membership functions, as well as the process of tuning to achieve desired performance. As shown in Figure 1.7, fuzzy logic is most suited for control problems whose performance objectives are relatively qualitative and available plant information is poor [Lufty et al. (2009)].

Neural networks can be readily implemented as components in feedback systems, where its universal approximation capability can be employed in the design of identifiers and controllers. Some conditions must be met for FBL-based adaptive control techniques to be applied. Introduction of NN helps in relaxing these conditions. Efficient neural network-based system identification algorithms are now available, these ensure successful implementation of neural network-based model predictive control algorithms. Moreover, it has been widely accepted that control problems where information about the plant is little but the objectives are well laid out, are best treated with neural networks and genetic algorithm-based strategies [Goodwin et al. (2001); Kawaji et al. (1999); Lawrynczuk (2007)].

Neural network-based controller is more suitable for vehicle suspension control because it can be readily applied in the *adaptive control* mode (that is, through on-line learning ability and adjustment of weights). Moreover, it is very suitable for nonlinear and multivariable application and can be combined with other control methods for better performance [Al-Duwaish and Rizvi (2011); Hunt et al. (1992); Kar and Behera (2009); Pedro and Dahunsi (2011); Wang et al. (2009)]. The required controller must be adaptive to the various uncertainties and yet be robust enough to cater for the system nonlinearities. Although robust control techniques are well developed for linear control problems they have suffered setbacks when used for nonlinear problems.

1.3.4 Adaptive Neural Network-Based Control Schemes

Robust controllers are required to be able to cope with little differences between the nominal model used for its design and the true system. To achieve this, some system variables are unknown but assumed to be bounded. Adaptive control schemes achieve or maintain a set of performance goals by adjusting the control weights in response to measured variations [Jha and He (2004)]. This is done based on its ability for online estimation of uncertain parameters. Therefore, adaptive controllers are useful for time varying control problems. Neural network-based control schemes are able to work within the framework of adaptive control to guarantee the required robustness to uncertainties [Cao et al. (2008); Chen and Guo (2005); Guglielmino et al. (2008); Slotine and Li (1991); Spooner et al. (2002)].

Artificial neural network presents alternative adaptive (otherwise known as, *indirect adaptive*) control schemes based on their ability to approximate arbitrary linear and nonlinear mapping through *learning*. Once, a proper past input and output data are obtained, and suitable NN structures and training methods are chosen, the NN can be trained to learn the system forward dynamics, such that it can predict and model control [Al-Duwaish and Rizvi (2011); Ge and Lee (1997); Hunt et al. (1992)].

Adjustments are done in indirect adaptive control method on the basis of the identified model of the plant. System identification is a function approximation stage where the dynamic model of the system is established based on observed input-output data. The objective of the identification process is to adjust the NN parameters until the training data satisfies the mean-squared-error (MSE) performance criteria [Dahunsi et al. (2010); Hunt et al. (1992); Norgaard et al. (1996)].

In the FBL-based direct adaptive neuro-controller design, the nonlinear model of the system is approximated by two separate functions using the NN. The resulting controller could be trained off-line to make it less computationally challenging. Although the direct adaptive neural control method is less popular, it is more effective in some cases, for example when one or both of the approximated functions are unknown [Kar and Behera (2009); Pedro and Dahunsi (2011); Spooner et al. (2002); Yesildirek and Lewis (1995)].

Other distinguishing features and benefits of the NN-based direct adaptive controllers over the indirect adaptive control schemes are:

1. In direct adaptive neuro-controllers, the adjusted weights belong to the NN

that serves as the controller. The indirect adaptive neuro-controller requires a NN approximator that generates a dynamic model of the plant. Weights of the NN approximator is adjusted till the predicted model is a good representation of the plant model [Norgaard et al. (1996); Spooner et al. (2002)].

2. Direct adaptive neuro-controllers present less design and computational challenges compared to the indirect adaptive neuro-controllers, since it does not require system identification.

3. With direct adaptive neuro-controllers, closed-loop stability, where the tracking error converges to zero, is more readily achieved and maintained than the indirect adaptive neuro-controllers where ensuring stability is more challenging [Kar and Behera (2009); Pedro et al. (2011)].

4. Direct adaptive neuro-control is tuned online with NN weights that are updated dynamically thereby ensuring closed-loop robustness to bounded unknown disturbances [Yesildirek and Lewis (1995)].

Figure 1.8 presents the general classification of neural network models and architectures employed in adaptive neuro-control schemes. NN is classified broadly into, static and dynamic NN. Static NN model is represented by algebraic relationship while dynamic NN model is represented by difference or differential equations. Dynamic NN models are also characterised by feedback between neurons of different or the same layers, thus it is described as being *recursive*. The feedforward pattern in the static NN model makes it to respond instantaneously to inputs and to be conditionally stable [Haykin (2009); Hunt et al. (1992); Yesildirek and Lewis (2001)].

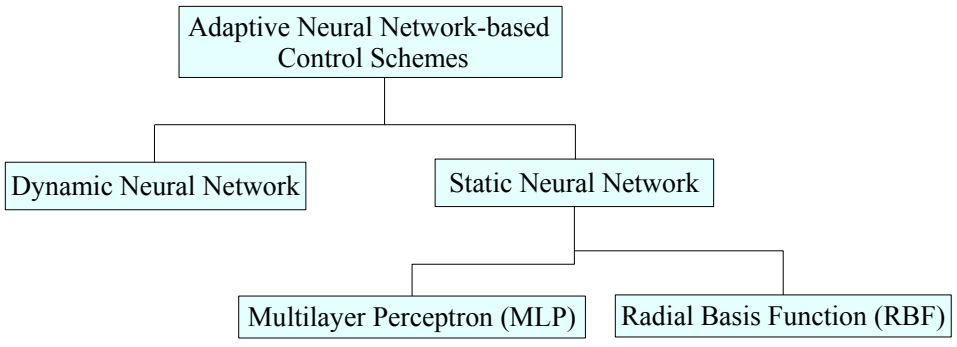

Figure 1.8: General Classification of Adaptive Neuro-Control Schemes

MLP and RBF are the most popular of the NN architectures. Both of them are similar in the sense that, they both use feedforward network architectures to generate nonlinear mappings and they are both proven universal approximators. Therefore,

both are good candidates for adaptive neuro-control applications.

RBF networks use a single hidden layer with several nodes, thereby constructing *local* approximations based on the different activation functions at each node. In the RBF feedforward structure, the neurons in the hidden layer all receives data simultaneously from the input layer and transforms them on the basis of the Gaussian function, before combining the function responses to construct data for the output layer [Haykin (2009); Lin and Lian (2011)].

MLP networks on the contrary, can use multiple hidden layers, but it constructs *global* approximations because the nodes in each hidden layer use the same activation function. RBF networks are also trained faster than MLP networks of comparable size. [Hunt et al. (1992); Norgaard et al. (2000); Spooner et al. (2002)].

1.4 Identified Gaps in the Literature

The volume of documented research works in the last five decades on AVSS does not correspond to its level of commercial application in the society. This, with regard to controller design, is because the class of control method applied in most cases is not the most suitable considering the inherent characteristics of the system. Other challenges are hardware related. The present level of technological development indicates that the known setbacks to commercial application of AVSS is giving way, however observed gaps in the documented AVSS research works include:

1. A large proportion of AVSS controller designs are based on linear models or Jacobian linearisation of nonlinear models [Gao et al. (2006); Hrovat (1997); Joo et al. (2000); Kim and Ro (1998); Nagai et al. (1997); Sharp and Peng (2011)]. Linear optimal control based solutions are well developed in the literature for linearised models of AVSS but nonlinear control methods are more suitable[Al-Holou et al. (2002); Cao et al. (2010); Sharp and Peng (2011); Shi et al. (2010)].

2. Most AVSS control designs were limited because they were based on linear optimal control theories in which a defined quadratic function is minimised. In most cases, these quadratic functions are limited to ride comfort alone or sometimes in addition to road holding.

3. The complexity of AVSS modelling makes the usual assumption of stable zero dynamics in the implementation of FBL and backstepping control methods

insufficient for AVSS control design [Isidori (1995); Kristic et al. (1995); Park et al. (2009); Shi et al. (2010)].

4. The contemporary nonlinear control techniques; feedback linearisation, backstepping and sliding mode control are relatively robust but plagued with implementation related challenges like chattering, requirement of full-state measurements and inadequate support in handling actuator redundancy [Du and Zhang (2009); Huang et al. (2009)].

5. Development of adaptive suspensions based on uncertain operating conditions.

6. Application of intelligent-based control to AVSS control design is limited in spite of its system complexity and coupled dynamics. Moreover, intelligent based control methods are able to yield improved performance in spite of modelling inadequacies and uncertainties [Guo and Zhang (2012)].

7. Actuator dynamics is often erroneously assumed negligible in many works [Chantranuwathana and Peng (2004); Nusantoro and Priyandoko (2011)].

8. Both the spring and the damper are known to have nonlinear characteristics which are often ignored to allow for easy linearisation of the model.

1.5 Rationale and Motivation

Until recently, vehicle suspension designs (that is, PVSS) had been based on fixed-gain strategies. They are designed to be optimal around some pre-set nominal parameters and operating conditions, and used extensively for the purpose of vibration isolation because of their lower cost and simplicity.

Gradually, introduction of the controlled suspension systems became inevitable because of the challenge of achieving trade-off between the suspension design requirements. With the advent of controlled suspensions, focus shifted to optimal design for disturbance rejection (that is, optimal ride comfort in spite of uneven road profile) [Hrovat (1997); Pedro (2007); Shirahatt et al. (2008)]. Vehicle suspension control problem in this work is approached as an *adaptive-nonlinear control* problem.

Adaptive control methods are suitable for controlled suspension systems because of the varying operating conditions and model uncertainties faced in the operation of vehicle suspension systems. More so, these uncertainties are related to the complexity of the system, so they are often difficult to determine from first principles.

Adaptive control methods achieve robustness by adjusting the controller online to reduce the effects of parametric variations in the system [Astrom and Wittenmark (1989); Spooner et al. (2002)]. Neural network-based control methods fit into adaptive control classification based on the weights update process during its training.

1.6 Research Objectives

The overall goal in AVSS controller design is the achievement of optimal performance through good robustness to parameter variations and disturbance rejection. The main objective of this research work is to develop a neuro-adaptive controller to improve the performance of active vehicle suspension system. This can be further broken down into the following:

1. To design and evaluate the performance of direct and indirect (that is, neural network-based feedback linearisation and model predictive control) adaptive neuro-controllers for the quarter-car model.
2. To select and develop a neuro-adaptive controller to achieve multiple performance objectives for the nonlinear AVSS full-car model.
3. To evaluate the dynamic performance of the neuro-adaptive controller against selected benchmark control methods and PVSS under varying operating conditions.
4. To evaluate the sensitivity of the PVSS and AVSS designs to variation in physical parameters and properties.

1.7 Research Scope, Strategy and Methodology

The entire scope of work and the methodology for the research is illustrated with Figure 1.9. This entails the design of an AVSS controller with good capacity for random and deterministic road disturbance inputs for nonlinear SISO and MIMO vehicle systems.

The focus of this study is the design of a neuro-adaptive controller using the feedback linearisation and model predictive control techniques. Figure 1.10 is a layout of the outlined activities involved in the design process.

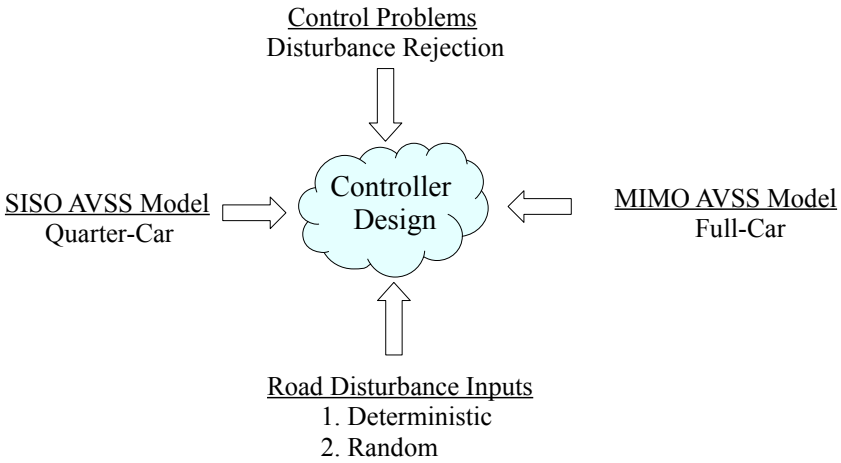

Figure 1.9: Summary of Research Scope and Methodology

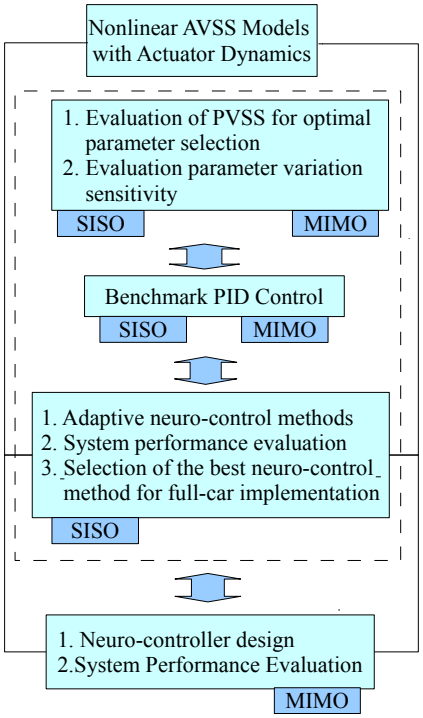

Figure 1.10: Layout of Research Methodology

The performance of the controller designed will be analyzed in the following dimensions:

1. Analysis will be carried out using the SISO, 2DOF quarter-car model, and later extended to the MIMO, 7DOF full-car model.

2. Deterministic and random road disturbance inputs will be used to excite the system for low and high frequency vibrations.

3. Designs will be based on nonlinear mathematical models.
4. Performance of the designed controllers will be benchmarked against PID control.
5. Design of direct and indirect adaptive neuro-controllers for the SISO and MIMO models of the AVSS.

1.8 Research Contributions

The contributions resulting from this research work are as follows:

1. A neural network-based adaptive controller for real-time control (based on model predictive control) of an active suspension system have been developed for a nonlinear full-car AVSS, .
2. The superior disturbance rejection-based performance and suitability of the developed controller for time-varying operating conditions and uncertainties have been demonstrated.
3. Four controllers have been studied in this work: a linear controller (PID), a direct adaptive neuro-controller (DANN), and two indirect adaptive neuro-controllers (NNFBL and NNMPC). Each controller is employed with internal PID feedback loops to stabilize the actuator dynamics and enhance performance. These contributions are in widely circulated in international journals and conference proceedings [Dahunsi et al. (2009, 2010); Ekoru et al. (2011); Pedro and Dahunsi (2011); Pedro et al. (2011)]

1.9 Organization of Thesis

The thesis is divided into six chapters. The structure is illustrated with Figure 1.11. The first chapter, tagged introduction provides a background description of active vehicle suspension system (AVSS) and an exhaustive review of control schemes applied to vehicle suspension control design. It also identified gaps in literature based on controller design method applied and highlights the objectives of the study.

Chapter two presents a detailed analysis that resulted in the nonlinear quarter and full-car mathematical models, taking into consideration the actuator dynamics, wheel damping and wheel dynamic load. The chapter also presents the models

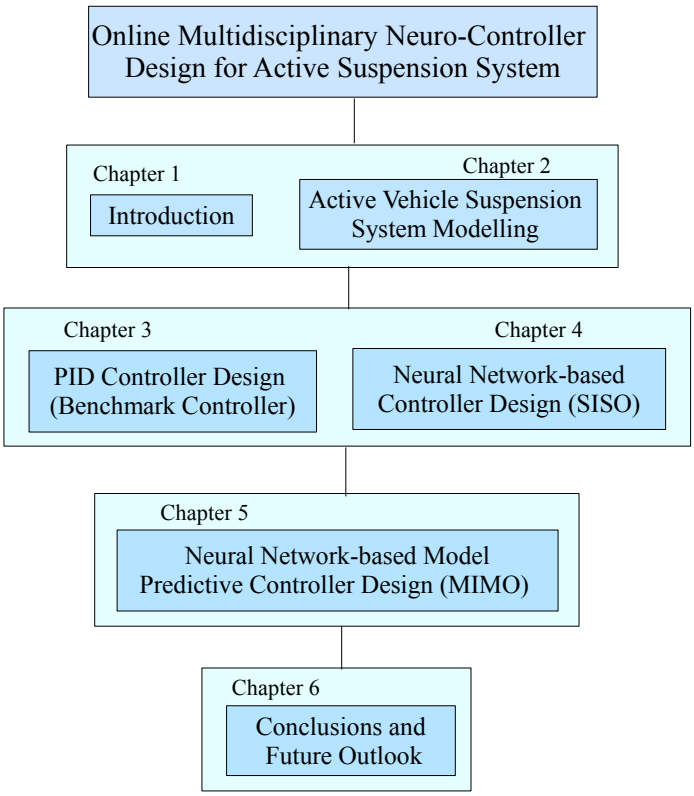

Figure 1.11: Structure of the Thesis

of multiple hump and random road disturbance inputs used in the design analysis. Parameter sensitivity analysis to assess the optimal selection of the passive suspension parameters is also covered. Lastly the chapter also outlines the various performance specifications for evaluating all the designed controllers.

Chapter three presents PID controller design for quarter and full-car AVSS models. Chapter four presents the design and evaluation of the performances of the three neuro-controllers. Their performances were benchmarked against that of the PID and the performance specifications in chapter two. The focus of this chapter is to evaluate and select the best controller for the full-car AVSS controller design.

In Chapter five, the design and evaluation of the neural network-based model predictive controller (NNMPC) for the full-car AVSS is presented. Its performance is compared with the performance of the PID controlled AVSS in the time and frequency domain analysis. The sensitivity of the designed AVSS to changes in physical parameters related to the suspension is also analysed.

Chapter six presents a general overview and discussion of the results obtained, as well as the concluding comments for future outlook of the research.

2 Active Vehicle Suspension System (AVSS) Modelling

2.1 Introduction

The AVSS is modelled as a dynamic system of lumped masses interconnected by nonlinear springs, dampers, electrohydraulic actuators and tyre (which is modelled as spring constant due to its compressibility). In this Chapter, physical and mathematical models are presented for: the two degree-of-freedom (2DOF), quarter-car model and the seven degree-of-freedom (7DOF), full-car model. Also covered are, the system dynamics of the AVSS electrohydraulic actuator as well as the road disturbance input models.

Tyre damping is often ignored in vehicle suspension modelling because it is difficult to estimate and it introduces couplings that adds to model complexity. Its impact, especially as regards wheel-hop vibration, is little since this mode is damped by the shock absorber, it is however added in this work for completeness [Akcay and Turkay (2009); Maher and Young (2011)].

Actuator dynamics modelling is an important component of AVSS models in this study. AVSS controller designs will be inadequate without consideration for the actuator dynamics since its presence distinguishes AVSS from the other suspension types. [Chantranuwathana and Peng (2004); Du and Zhang (2009); Feng et al. (2003)].

2.2 Actuator Dynamics

The types of actuators used in AVSS include hydraulic, pneumatic, and electromagnetic actuators. The use of electromagnetic actuators has good prospect for

FASS applications but the technology is relatively new and still evolving. Rotational electromagnetic actuators require gears or ball-screw designs to convert the rotary motion and this adds to the complication of the system.

The biggest set-backs for electromagnetic actuators include its cost, the increase in moving parts as well as, additional masses. The system also requires between $12 - 14V$ to provide continuous excitation force, whereas electrohydraulic actuators require about $10V$. The benefits of the electromagnetic actuator include increased efficiency, mechanically stiffer, improved stability and dynamic behaviour, and more accurate force control [Fijalkowski (2011); Gysen et al. (2010); Lee and Kim (2010)].

Pneumatic actuators' wide usage in the industry is because of its advantages like their lower specific weight to higher power rate, clean and dry environment and operation. Moreover, their application in AVSS is limited because the bandwidth requirement for AVSS is higher. They are also characterised by nonlinearities due to compressibility of air and gas flow related complications in pneumatic components [Junyi and Binggang (2011); Richer and Hurmuzlu (2000)].

The few commercially available AVSS in the society employs the hydraulic or pneumatic actuators. This popularity is because of their superior power-to-weight ratio, good stiffness characteristics, high load capability, fast and relatively smooth response to change in speed and direction, relative ease of control, availability of parts, lower cost, low wear rate and lower possibility of overheating after working for long time [Guan and Pan (2008); Seo et al. (2007)].

The operation of electrohydraulic actuators is characterised by highly nonlinear dynamics that has been neglected in many AVSS publications for the sake of simplicity. For example, parameter variations due to load, valve and hydraulic oil used are time varying and difficult to estimate. Moreover, handling uncertainties is required in all AVSS types because of their actuators, but this problem is more significant with hydraulic systems. Control of the actuator dynamics is important for good performance, stability and effective force control in the actuator [Chantranuwathana and Peng (2004); Du and Zhang (2009); Gysen et al. (2010)].

The inadequacy of linear control methods for electrohydraulic control design, the problems associated with its model linearisation about an operating point and the successes of the nonlinear control methods are well documented in the literature [Alleyne and Lui (2000); Guan and Pan (2008); Karpenko and Sepehri (2012); Rahmat et al. (2011); Seo et al. (2007)].

2.2.1 Mathematical Modelling of Electrohydraulic Systems

Figure 2.1 describes the physical representation of the three land four-way hydraulic actuator mounted in between the sprung and unsprung masses. The actuator is made up of the primary spool-valve and the double-acting piston. The dynamics of the actuator is based on the change in force being proportional to the spool position with respect to the center, velocity of the piston and leakage through the piston seals.

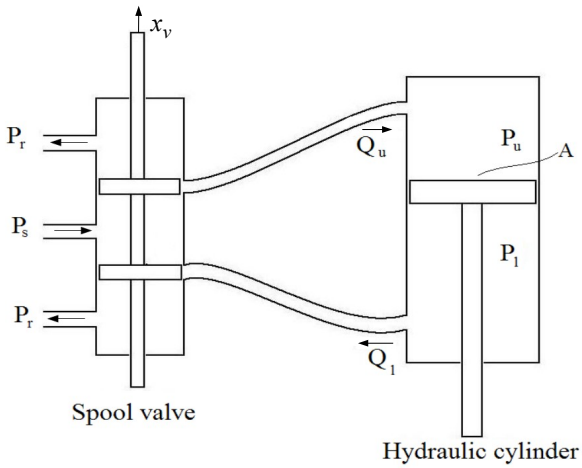

Figure 2.1: Schematic of the Double Acting Hydraulic Strut

A is the area of the piston, P_s is the supply pressure into the hydraulic cylinder, P_r is the return pressure from the hydraulic cylinder, P_u and P_l are the oil pressure in the upper and lower portion of the cylinder.

The actuator is controlled by means of electrohydraulic servo-valves in a three land four-way spool-valve system. The maximum control input (voltage) of $10V$ was applied to the servo-valves to achieve a maximum suspension travel of $10cm$. The servo valve displacement is caused by the actuation of the solenoid by the control voltage. The following assumptions are necessary for the mathematical modelling of the electrohydraulic systems [Mailah and Priyandoko (2007); Rahmat et al. (2011); Renn and Wu (2007); Seo et al. (2007)]:

Assumption 2.1: The servo-valves are matched and symmetric.

Assumption 2.2: Internal leakage in the servo-valve is negligible.

Assumption 2.3: The valve dynamics is sufficiently fast.

Assumption 2.4: The sign convention describing the spool position determines

the direction of oil flow.

Assumption 2.5: The supply pressure is high enough to prevent reverse flow.

The actuator spool-valve displacement is controlled based on its upstream oil pressure P_u being controlled via the changse in the downstream oil pressure P_l. To achieve this dynamics of the servo-valve can be approximated as a gain, K, such that the spool-valve position is given by $x_v = Ku$, where u is the input control voltage. The dynamics of the servo-valve can be approximated as a first order system based on Taylor series linearisation [Fialho and Balas (2002); Gaspar et al. (2003); Seo et al. (2007)]:

$$\dot{x}_v = \frac{1}{\tau}(-x_v + Ku) \tag{2.1}$$

which corresponds to a first order system representation, and

$$\frac{V_t}{4\beta_e}\dot{x}_p = Q - C_{tp}x_p - A(\dot{x}_1 - \dot{x}_2) \tag{2.2}$$

The spool-valve displacement x_v and total flow Q are related by the equation for hydraulic fluid flow through an orifice that is given by

$$Q = sgn[P_s - sgn(x_v)x_p]C_d S x_v \sqrt{\frac{1}{\rho}|P_s - sgn(x_v)x_p|} \tag{2.3}$$

x_p is the pressure drop across the piston, V_t is the total actuator volume, β_e is the effective bulk modulus of the system, Φ is the hydraulic load flow, C_{tp} is the total leakage coefficient of the piston, C_d is the discharge coefficient, S is the spool-valve area gradient and ρ is the hydraulic fluid density.

2.3 General Design Assumptions

The following assumptions, related to active suspension design, are adopted to simplify the analysis in the work:

Assumption 2.6: Road irregularities (roughness) are the only source of disturbance input (vibrations); engine vibrations and elastic deformation of the vehicle are ignored.

Assumption 2.7: The payload is kept constant for the sake of simplicity.

Assumption 2.8: The link members, tie-rod and control arm provide static support only.

Assumption 2.9: All member components are connected by ideal joints.

Assumption 2.10: Any unbalance effect of the wheel and non-uniformity due to the tyre are also ignored.

Assumption 2.11: Primary motions of the vehicle are: vertical, pitching and rolling modes. Rocking and yawing motions of the centre of mass about nominal travel path are neglected.

Assumption 2.12: The unsprung masses are uniform.

Assumption 2.13: The centre of mass of the sprung mass always lies along the longitudinal axis of the vehicle body.

Assumption 2.14: Given that the vehicle is assumed to be travelling at constant velocity on a straight path, effects of cornering and other horizontal forces are regarded negligible [Cole (2001)].

2.4 AVSS Mathematical Model for Quarter-Car

Quarter-car analysis remains the most popular model for vehicle suspension analysis. It is simpler and has fewer design parameters. Although it is unable to provide information related to the vehicle excitations in the roll and pitch motion modes; it provides effective model that is suitable for wheel load variation, body heave and suspension travel control [Maher and Young (2011)].

Figure 2.2 represents a physical model of a 2DOF quarter-car active suspension. The hydraulic actuator force, F is applied between the sprung and unsprung masses thereby causing a relative displacement between the vehicle body and the wheel. This displacement is also known as the suspension travel, $(x_2 - x_1)$. There is also a relative displacement between the wheel and the road, $(x_2 - w)$, this characterises the road holding quality.

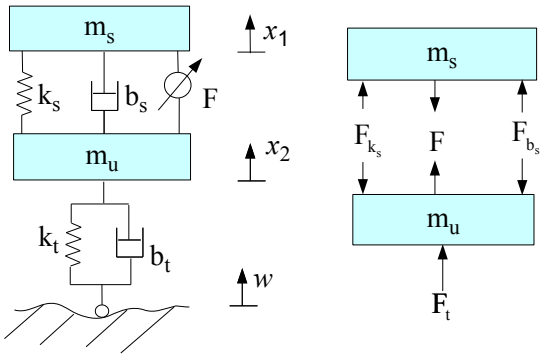

Figure 2.2: AVSS Quarter-Car Model

The governing equations of motion of the quarter car model are obtained using Newton's laws [Fialho and Balas (2002); Gaspar et al. (2003)].

$$\begin{aligned} F_{m_s} =& m_s\ddot{x}_1 \\ F_{m_u} =& m_u\ddot{x}_2 \\ F_{k_s} =& k_s^l(x_2 - x_1) + k_s^{nl}(x_2 - x_1)^3 \end{aligned}$$

$$\begin{aligned} F_{k_t} =& k_t(x_2 - w) \\ F_{b_t} =& b_t(\dot{x}_2 - \dot{w}) \\ F_t =& F_{k_t} + F_{b_t} \\ F_{b_s} =& b_s^l(\dot{x}_2 - \dot{x}_1) - b_s^{sym}|\dot{x}_2 - \dot{x}_1| + b_s^{nl}\sqrt{|\dot{x}_2 - \dot{x}_1|}sgn(\dot{x}_2 - \dot{x}_1) \\ F =& Ax_p \end{aligned}$$

therefore

$$\begin{aligned} F_{m_s} &= F_{k_s} + F_{b_s} - F \\ m_s\ddot{x}_1 &= k_s^l(x_2 - x_1) + k_s^{nl}(x_2 - x_1)^3 + b_s^l(\dot{x}_2 - \dot{x}_1) - b_s^{sym}|\dot{x}_2 - \dot{x}_1| \\ &\quad + b_s^{nl}\sqrt{|\dot{x}_2 - \dot{x}_1|}sgn(\dot{x}_2 - \dot{x}_1) - Ax_p \end{aligned} \tag{2.4}$$

and

$$\begin{aligned} F_{m_u} &= -F_{k_s} - F_{b_s} + F_{k_t} + F_{b_t} + F \\ m_u\ddot{x}_2 &= -k_s^l(x_2 - x_1) - k_s^{nl}(x_2 - x_1)^3 - b_s^l(\dot{x}_2 - \dot{x}_1) + b_s^{sym}|\dot{x}_2 - \dot{x}_1| \\ &\quad - b_s^{nl}\sqrt{|\dot{x}_2 - \dot{x}_1|}sgn(\dot{x}_2 - \dot{x}_1) + k_t(x_2 - w) + b_t(\dot{x}_2 - \dot{w}) + Ax_p \end{aligned} \tag{2.5}$$

also

$$\begin{aligned} \frac{V_t}{4\beta_e}\dot{x}_p &= Q - C_{tp}x_p - A(\dot{x}_1 - \dot{x}_2) \\ \dot{x}_p &= \alpha Q - \beta x_p - \alpha A(\dot{x}_1 - \dot{x}_2) \end{aligned} \tag{2.6}$$

where $\alpha = \dfrac{4\beta_e}{V_t}$, $\beta = \alpha C_{tp}$ and

$Q = sgn[P_s - sgn(x_v)x_p]C_d S x_v \sqrt{\dfrac{1}{\rho}|P_s - sgn(x_v)x_p|}$

and

$$\dot{x}_v = \frac{1}{\tau}(-x_v + Ku) \tag{2.7}$$

Using the state-space representation, the system governing equations can be presented as

$$\dot{\mathbf{x}} = \mathbf{f(x)} + \mathbf{g(x)}u + \mathbf{p(w)} \tag{2.8}$$

$$y = h(x) = x_2 - x_1 \tag{2.9}$$

where the state vector $\mathbf{x} = [x_1 \ x_2 \ x_3 \ x_4 \ x_5 \ x_6]^T$, the output variable $y = x_2 - x_1$, and the control input $\mathbf{u}$. The system matrices $\mathbf{f}$ and $\mathbf{g}$ are:

$$\mathbf{f}(\mathbf{x}) = \begin{bmatrix} f_1(x) & f_2(x) & f_3(x) & f_4(x) & f_5(x) & f_6(x) \end{bmatrix}^T, \tag{2.10}$$

$$\mathbf{g}(\mathbf{x}) = \begin{bmatrix} 0 & 0 & 0 & 0 & 0 & \frac{1}{\tau} \end{bmatrix}^T \tag{2.11}$$

$$\mathbf{p}(\mathbf{w}) = \begin{bmatrix} 0 & 0 & 0 & -(\frac{k_t}{m_u}w + \frac{b_t}{m_u}\dot{w}) & 0 & 0 \end{bmatrix}^T \tag{2.12}$$

$$f_1(x) = x_3 \tag{2.13}$$

$$f_2(x) = x_4 \tag{2.14}$$

$$f_3(x) = \frac{1}{m_s}\Big[k_s^l(x_2 - x_1) + k_s^{nl}(x_2 - x_1)^3 + b_s^l(x_4 - x_3) - b_s^{sym}|x_4 - x_3| + b_s^{nl}\sqrt{|x_4 - x_3|}sgn(x_4 - x_3) - Ax_5\Big] \tag{2.15}$$

$$f_4(x) = \frac{1}{m_u}\Big[-k_s^l(x_2 - x_1) - k_s^{nl}(x_2 - x_1)^3 - b_s^l(x_4 - x_3) + b_s^{sym}|x_4 - x_3| - b_s^{nl}\sqrt{|x_4 - x_3|}sgn(x_4 - x_3) + k_t x_2 + b_t\dot{x}_2 + Ax_5\Big] \tag{2.16}$$

$$f_5(x) = \gamma\Phi x_6 - \beta x_5 - \alpha A(x_3 - x_4) \tag{2.17}$$

$$f_6(x) = \frac{-x_6}{\tau} \tag{2.18}$$

where x_3 and x_4 are vertical velocities of the sprung and unsprung masses respectively, x_5 is the pressure drop across the piston and x_6 is the servo-valve displacement.

2.5 AVSS Mathematical Model for Full-Car

The full-car AVSS model is illustrated by Figure 2.3. It comprises of a rigid lumped mass m_s, representing the entire vehicle body (that is, the sprung mass). This has four lumped masses connected to its four corners representing the unsprung masses of the suspension.

Each suspension system consists of a spring, damper and the actuator. The tyre is represented by a spring and a damper. The sprung mass has vertical displacement, x_1 at the center of gravity, pitch motion mode through an angular displacement, θ and roll motion angular displacement, ϕ. Each unsprung mass has a degree-of-freedom of motion at the respective corners of the model as shown in the cross-sectional view in Figure 2.4. The vertical displacements of these unsprung masses

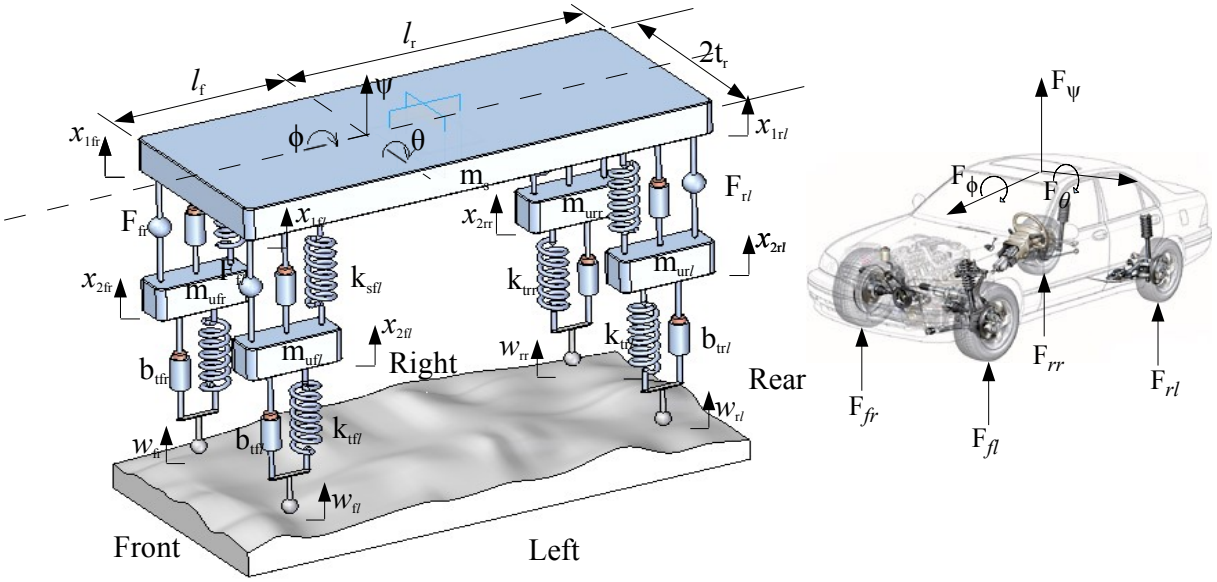

Figure 2.3: AVSS Full-Car Model

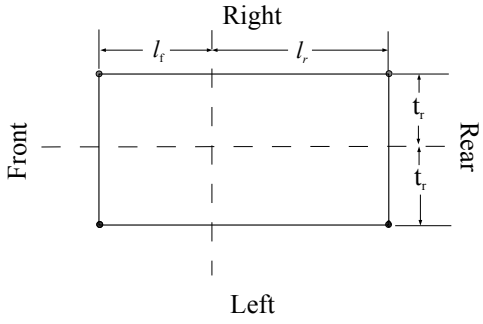

Figure 2.4: Plan View of the Full-Car Model

are given by x_{2fl}, x_{2fr}, x_{2rl} and x_{2rr} respectively.

The suspension spring forces, damping forces and tyre forces are given in general form as follows [Dong et al. (2009); Gaspar et al. (2009)]:

$$F_{kij} = k_s^l(x_{2ij} - x_{1ij}) + k_s^{nl}(x_{2ij} - x_{1ij})^3 \tag{2.19}$$

$$F_{bij} = b_s^l(\dot{x}_{2ij} - \dot{x}_{1ij}) - b_s^{sym}|\dot{x}_{2ij} - \dot{x}_{1ij}| + b_s^{nl}\sqrt{|\dot{x}_{2ij} - \dot{x}_{1ij}|}sgn(\dot{x}_{2ij} - \dot{x}_{1ij}) \tag{2.20}$$

$$F_{tij} = k_t(x_{2ij} - w_{ij}) + b_t(\dot{x}_{2ij} - \dot{w}_{ij}) \tag{2.21}$$

Therefore the governing equations in terms of the heave, pitch and roll of the vehicle body, as well as the motion at the four wheels are given by:

$$\begin{aligned} m_s\ddot{x}_1 &= F_{kfl} + F_{kfr} + F_{krl} + F_{krr} + F_{bfl} + F_{bfr} + F_{brl} + F_{brr} \\ &\quad -F_{fl} - F_{fr} - F_{rl} - F_{rr} \qquad (2.22) \\ I_\theta\ddot{\theta} &= l_f F_{kfl} + l_f F_{kfr} - l_r F_{krl} - l_r F_{krr} + l_f F_{bfl} + l_f F_{bfr} \\ &\quad -l_r F_{brl} - l_r F_{brr} - l_f F_{fl} - l_f F_{fr} + l_r F_{rl} + l_r F_{rr} \qquad (2.23) \\ I_\phi\ddot{\phi} &= t_f F_{kfl} - t_f F_{kfr} + t_r F_{krl} - t_r F_{krr} + t_f F_{bfl} - t_f F_{bfr} \\ &\quad +t_r F_{brl} - t_r F_{brr} - t_f F_{fl} + t_f F_{fr} - t_r F_{rl} + l_r F_{rr} \qquad (2.24) \\ m_{ufl}\ddot{x}_{2fl} &= -F_{kfl} - F_{bfl} - F_{tfl} + F_{fl} \qquad (2.25) \\ m_{ufr}\ddot{x}_{2fr} &= -F_{kfr} - F_{bfr} - F_{tfr} + F_{fr} \qquad (2.26) \\ m_{url}\ddot{x}_{2rl} &= -F_{krl} - F_{brl} - F_{trl} + F_{rl} \qquad (2.27) \\ m_{urr}\ddot{x}_{2rr} &= -F_{krr} - F_{brr} - F_{trr} + F_{rr} \qquad (2.28) \end{aligned}$$

Figure 2.5 presents the pitch and roll angular displacements used to estimate the sprung mass displacements at the corners of the rigid mass, m_s representing the vehicle body.

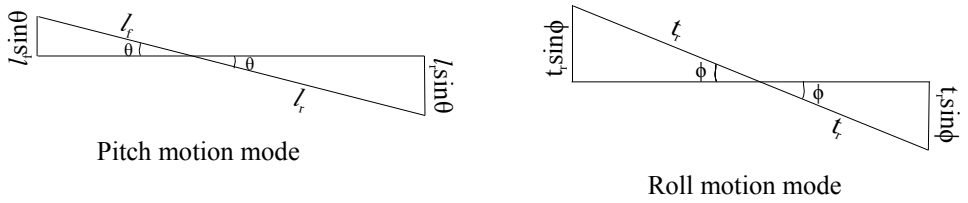

Figure 2.5: Schematics of the Pitch and Roll Angular Displacements

$$x_{1fl} = x_1 + l_f\sin\theta + t_f\sin\phi \qquad x_{1fr} = x_1 + l_f\sin\theta - t_f\sin\phi$$
$$x_{1rl} = x_1 - l_r\sin\theta + t_r\sin\phi \qquad x_{1rr} = x_1 - l_r\sin\theta - t_r\sin\phi$$

moreover, $t_r = t_f$, F_{ij} are the actuator forces, F_{kij} are the spring forces, F_{bij} are the damping forces and F_{tij} are the tyre spring forces, where $ij \in \{fl, fr, rl, rr\}$.

Using the state-space representation, the system governing equations for the full-car model can be written as

$$\dot{\mathbf{x}} = \mathbf{f(x)} + \mathbf{g(x)u} + \mathbf{p(w)} \qquad (2.29)$$
$$\mathbf{y} = \mathbf{h(x)} \qquad (2.30)$$

where the state vector $\mathbf{x} = [x_1 \quad x_2 \quad x_3 \quad \dots \quad x_{22}]^T$, the output vector $\mathbf{y} = [s_{fl} \quad s_{fr} \quad s_{rl} \quad s_{rr}]^T$, the road disturbance vector $\mathbf{w} = [w_{fl} \quad w_{fr} \quad w_{rl} \quad w_{rr}]^T$, the control input vector $\mathbf{u} = [u_{fl} \quad u_{fr} \quad u_{rl} \quad u_{rr}]^T$, and output variables, which are

the suspension travels at the corners of the vehicle, $s_{ij} = x_{2ij} - x_{1ij}$. The system matrices $\mathbf{f}$ and $\mathbf{g}$ are:

$$\mathbf{f}(\mathbf{x}) = \begin{bmatrix} f_1(x) & f_2(x) & \dots & \dots & f_{21}(x) & f_{22}(x) \end{bmatrix}^T, \tag{2.31}$$

$$\mathbf{g}(\mathbf{x}) = \begin{bmatrix} g_1(x) & \dots & g_{15}(x) & \frac{1}{\tau_{fl}} & g_{17}(x) & \frac{1}{\tau_{fr}} & g_{19}(x) & \frac{1}{\tau_{rl}} & g_{21}(x) & \frac{1}{\tau_{rr}} \end{bmatrix}^T \tag{2.32}$$

$$\mathbf{p}(\mathbf{w}) = \Big[p_1(w) \quad \dots \quad p_{10}(w) \quad \frac{k_{tfl}}{m_{1fl}} w_{fl} \quad \frac{k_{tfr}}{m_{1fr}} w_{fr} \quad \frac{k_{trl}}{m_{1rl}} w_{rl} \quad \frac{k_{trr}}{m_{1rr}} w_{rr} \quad p_{15}(w) \quad \dots \quad p_{22}(w)\Big]^T \tag{2.33}$$

$$f_1(x) = \dot{n}_1 = \dot{x}_1 = n_8 \tag{2.34}$$

$$f_2(x) = \dot{n}_2 = \dot{\phi} = n_9 \tag{2.35}$$

$$f_3(x) = \dot{n}_3 = \dot{\varphi} = n_{10} \tag{2.36}$$

$$f_4(x) = \dot{n}_4 = \dot{x}_{2fl} = n_{11} \tag{2.37}$$

$$f_5(x) = \dot{n}_5 = \dot{x}_{2fr} = n_{12} \tag{2.38}$$

$$f_6(x) = \dot{n}_6 = \dot{x}_{2rl} = n_{13} \tag{2.39}$$

$$f_7(x) = \dot{n}_7 = \dot{x}_{2rr} = n_{14} \tag{2.40}$$

$$f_8(x) = \dot{n}_8 = \ddot{x}_1 \tag{2.41}$$

$$f_9(x) = \dot{n}_9 = \ddot{\phi} \tag{2.42}$$

$$f_{10}(x) = \dot{n}_{10} = \ddot{\varphi} \tag{2.43}$$

$$f_{11}(x) = \dot{n}_{11} = \ddot{x}_{2fl} \tag{2.44}$$

$$f_{12}(x) = \dot{n}_{12} = \ddot{x}_{2fr} \tag{2.45}$$

$$f_{13}(x) = \dot{n}_{13} = \ddot{x}_{2rl} \tag{2.46}$$

$$f_{14}(x) = \dot{n}_{14} = \ddot{x}_{2rr} \tag{2.47}$$

$$f_{15}(x) = \dot{n}_{15} = \gamma\Phi x_{vfl} - \beta x_{pfl} - \alpha A(\dot{x}_{1fl} - \dot{x}_{2fl}) \tag{2.48}$$

$$f_{16}(x) = \dot{n}_{16} = \frac{-x_{vfl}}{\tau_{fl}} \tag{2.49}$$

$$f_{17}(x) = \dot{n}_{17} = \gamma\Phi x_{vfr} - \beta x_{pfr} - \alpha A(\dot{x}_{1fr} - \dot{x}_{2fr}) \tag{2.50}$$

$$f_{18}(x) = \dot{n}_{18} = \frac{-x_{vfr}}{\tau_{fr}} \tag{2.51}$$

$$f_{19}(x) = \dot{n}_{19} = \gamma\Phi x_{vrl} - \beta x_{prl} - \alpha A(\dot{x}_{1rl} - \dot{x}_{2rl}) \tag{2.52}$$

$$f_{20}(x) = \dot{n}_{20} = \frac{-x_{vrl}}{\tau_{rl}} \tag{2.53}$$

$$f_{21}(x) = \dot{n}_{21} = \gamma\Phi x_{vrr} - \beta x_{prr} - \alpha A(\dot{x}_{1rr} - \dot{x}_{2rr}) \tag{2.54}$$

$$f_{22}(x) = \dot{n}_{22} = \frac{-x_{vrr}}{\tau_{rr}} \tag{2.55}$$

All the other elements of function $\mathbf{g}(\mathbf{x})$ are equal to zero except for the following elements

$$g_{16}(x) = \frac{1}{\tau_{fl}} \qquad g_{18}(x) = \frac{1}{\tau_{fr}} \qquad g_{20}(x) = \frac{1}{\tau_{rl}} \qquad g_{22}(x) = \frac{1}{\tau_{rr}},$$

similarly, all the other elements of function $\mathbf{p}(\mathbf{w})$ are equal to zero except for the following elements

$$p_{11}(w) = \frac{k_{tfl}}{m_{1fl}} w_{fl} \qquad p_{12}(w) = \frac{k_{tfr}}{m_{1fr}} w_{fr} \qquad p_{13}(w) = \frac{k_{trl}}{m_{1rl}} w_{rl} \qquad p_{14}(w) = \frac{k_{trr}}{m_{1rr}} w_{rr}$$

The position of the elements of $\mathbf{g}(\mathbf{x})$ and $\mathbf{g}(\mathbf{x})$ are shown in Equation 2.56 and 2.57. The models for the road disturbance are presented in Section 2.6.

$$\mathbf{g}(\mathbf{x}) = \begin{bmatrix} 0 & 0 & 0 & 0 & 0 & 0 & 0 & 0 & 0 & 0 & 0 & 0 & 0 & 0 & 0 & \frac{1}{\tau_{fl}} & 0 & 0 & 0 & 0 & 0 & 0 \\ 0 & 0 & 0 & 0 & 0 & 0 & 0 & 0 & 0 & 0 & 0 & 0 & 0 & 0 & 0 & 0 & 0 & \frac{1}{\tau_{fr}} & 0 & 0 & 0 & 0 \\ 0 & 0 & 0 & 0 & 0 & 0 & 0 & 0 & 0 & 0 & 0 & 0 & 0 & 0 & 0 & 0 & 0 & 0 & 0 & \frac{1}{\tau_{rl}} & 0 & 0 \\ 0 & 0 & 0 & 0 & 0 & 0 & 0 & 0 & 0 & 0 & 0 & 0 & 0 & 0 & 0 & 0 & 0 & 0 & 0 & 0 & 0 & \frac{1}{\tau_{rr}} \end{bmatrix}^T \tag{2.56}$$

$$\mathbf{p}(\mathbf{w}) = \begin{bmatrix} 0 & 0 & 0 & 0 & 0 & 0 & 0 & 0 & 0 & 0 & \left(\frac{k_{tfl}}{m_{1fl}} w_{fl} + \frac{b_{tfl}}{m_{1fl}} \dot{w}_{fl}\right) & 0 & 0 & 0 & 0 & 0 & 0 & 0 & 0 & 0 & 0 & 0 \\ 0 & 0 & 0 & 0 & 0 & 0 & 0 & 0 & 0 & 0 & 0 & \left(\frac{k_{tfr}}{m_{1fr}} w_{fr} + \frac{b_{tfr}}{m_{1fr}} \dot{w}_{fr}\right) & 0 & 0 & 0 & 0 & 0 & 0 & 0 & 0 & 0 \\ 0 & 0 & 0 & 0 & 0 & 0 & 0 & 0 & 0 & 0 & 0 & 0 & \left(\frac{k_{trl}}{m_{1rl}} w_{rl} + \frac{b_{trl}}{m_{1rl}} \dot{w}_{rl}\right) & 0 & 0 & 0 & 0 & 0 & 0 & 0 & 0 \\ 0 & 0 & 0 & 0 & 0 & 0 & 0 & 0 & 0 & 0 & 0 & 0 & 0 & \left(\frac{k_{trr}}{m_{1rr}} w_{rr} + \frac{b_{trr}}{m_{1rr}} \dot{w}_{rr}\right) & 0 & 0 & 0 & 0 & 0 & 0 & 0 & 0 \end{bmatrix}^T \tag{2.57}$$

2.6 Road Disturbance Input Models

Road surface irregularities are a major factor influencing vehicle dynamic performance and durability. It is associated with the deterioration of *ride comfort* due to the inducement of mechanical vibrations within a frequency range of 0 to $80Hz$. Moreover, the resonance peaks of the vehicle body and the wheels occur at about $1Hz$ and $10Hz$ respectively.

It is required of the AVSS to have a bandwidth that will accommodate this frequencies and yet separate or distinguish them for effective control [Du and Zhang (2009); Fischer and Isermann (2004)]. Road surface irregularities can contribute significantly to system noise, and are of greater concern in the design of passive suspensions since they are the only input to the system.

The vibration induced is also associated with damage to the road because of the increased dynamic load applied at the wheels [Kropac and Mucka (2008); Verros et al. (2005); Zhang et al. (2002)]. Road irregularities are modelled in vehicle dynamics as large isolated irregularities such as potholes or humps, or as continuously distributed profile irregularities. Although the forward vehicle velocity is time-varying in real life, for the scope of this study, it can be safely assumed to be constant because of the limited length of the irregularity.

2.6.1 Deterministic Road Disturbance Model

Deterministic road disturbances are made up of discrete events of elevation or depression on an otherwise smooth road. Examples include; humps, bumps and pot-holes. While pot-holes are usually defects on the road, humps and bumps are employed as *speed calming devices* but their dimensions and configurations vary from country to country.

Detail studies about the design of hump profile for optimal speed control have been reported [Baslamisli and Unlusoy (2009); Khorshid et al. (2007); Kropac and Mucka (2008)]. A list of some types of humps used in experimental analysis is presented in Table 2.1. Critical comfort, CC is the maximum magnitude of the shock transmitted to the driver seat when the vehicle crosses the hump. Critical speed, CS is defined as the set speed limit for the hump. Hump Type 5 will be used in this study. It has been reported to be in use in many European countries.

Table 2.1: Typical Speed Control Humps [Khorshid et al. (2007)]

Name	Description of Geometry	Height (cm)	Width (cm)	Comfort Criteria, CC (g)	Critical Speed, CS (km/h)
1	Short bump, circular	10	90	0.6	≤ 35
2	Long hump-circular	10	4	0.6	$45 \leq CS \leq 60$
3	Long hump-circular and large height	15	4	1.3	$35 \leq CS \leq 60$
4	Sinusoidal hump	6.7	4	0.6	$35 \leq CS \leq 60$
5	Optimal sinusoidal, cycloidal hump	7.3	3.9	0.6	35
6	Optimal polynomial hump of degree-7	8.9	8	0.6	60

Humps are also called *pavement undulations*. They are expected to cause a gentle rocking motion and/or minimal driver discomfort that ensures that the vehicle slows down. The expected speed range is usually $25km/h - 40km/h$. Humps however acts like bumps, jolting both vehicle suspension and occupants, when vehicles goes over it at high speed. Table 2.1 shows that the configuration for a hump varies between $6.7cm$ and $15cm$ height, and $3.9m$ and $8m$ width. Humps should also be visible and far from the nearest intersection by about $60m$ and are mostly used in urban areas [ITE Technical Council Task Force on Speed Humps (1993); Khorshid et al. (2007); Zaidel et al. (1992)].

Bumps are designed to induce stronger discomfort to the driver because it is meant to slow the vehicle to $8km/h - 16km/h$. The discomfort experienced by the drivers causes them to completely or almost completely stop before going over a bump. They are suitable for private roadways and parking lots [ITE Technical Council Task Force on Speed Humps (1993); Khorshid et al. (2007)].

The profile of the deterministic road disturbance inputs used in this study for quarter-car model are given by Equation 2.58 and Figures 2.6 and 2.7 . The profile

is made up of two humps of heights $6.7cm$ and $5cm$ respectively. The amplitudes of the humps are given by a_1 and a_2, while V, vehicle forward velocity is, $40km/h$ and λ is the half-wavelength of the sinusoidal road undulation which is $4m$.

$$w(t) = \begin{cases} \frac{a_1}{2}(1 - cos\frac{2\pi Vt}{\lambda}) & 1 \leq t \leq 1.25 \\ \\ \frac{a_2}{2}(1 - cos\frac{2\pi Vt}{\lambda}) & 3 \leq t \leq 3.25 \\ \\ 0 & \text{otherwise} \end{cases} \tag{2.58}$$

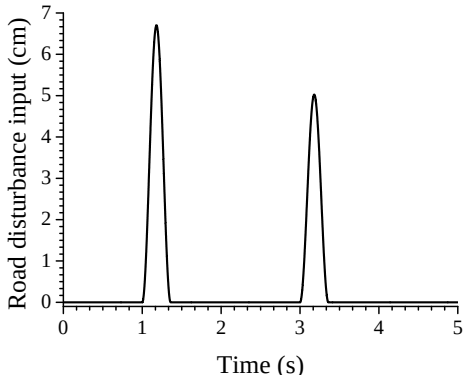

Figure 2.6: Deterministic Road Disturbance Input Profile - Quarter-Car Model

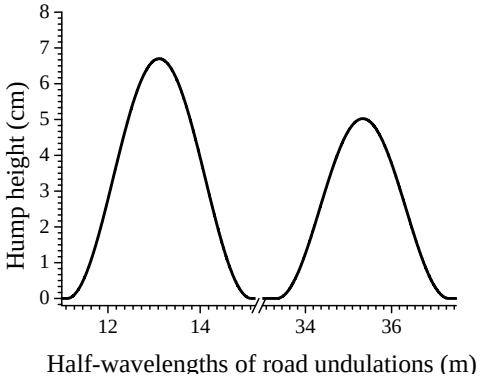

Figure 2.7: Lateral View of the Deterministic Road Disturbance Input Profile - Quarter-Car Model

The profile for the deterministic road disturbance inputs for the full-car model are given by Equations 2.59 and 2.60 and Figure 2.8.

$$w_{fl}(t) = w_{fr}(t) = \begin{cases} \frac{a_1}{2}(1 - cos\frac{2\pi Vt_f}{\lambda}) & 1 \leq t_f \leq \left(1 + \frac{\lambda}{V}\right) \\ \\ \frac{a_2}{2}(1 - cos\frac{2\pi Vt}{\lambda}) & 3 \leq t_f \leq \left(3 + \frac{\lambda}{V}\right) \\ \\ 0 & \text{otherwise} \end{cases} \tag{2.59}$$

$$w_{rl}(t) = w_{rr}(t) = \begin{cases} \frac{a_1}{2}(1 - cos\frac{2\pi Vt_r}{\lambda}) & (1 + t_d) \leq t_r \leq \left(1 + t_d + \frac{\lambda}{V}\right) \\ \\ \frac{a_2}{2}(1 - cos\frac{2\pi Vt_r}{\lambda}) & (3 + t_d) \leq t_r \leq \left(3 + t_d + \frac{\lambda}{V}\right) \\ \\ 0 & \text{otherwise} \end{cases} \tag{2.60}$$

note that the heights of the humps are the same, thus rolling motion is not induced. t_f and t_r are simulation times for the front and rear wheels, l_f and l_r are the distances from the wheel bases to the center of the car and V is the forward velocity of the vehicle and the time delay between the motion of the front and rear wheels is given by

$$t_d = \frac{l_f + l_r}{V} \tag{2.61}$$

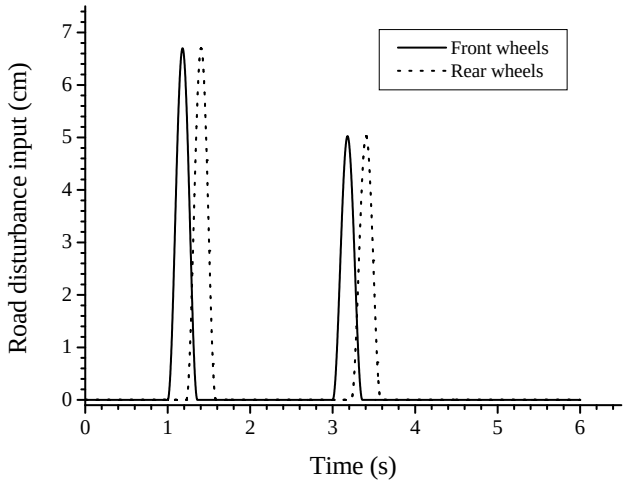

Figure 2.8: Deterministic Road Disturbance Input Profile for Full-Car Model

2.6.2 Stochastic Road Disturbance Model

The stochastic road disturbance input is expected to typify the uncertainty nature of the terrain in terms of roughness. These are road surfaces with continuously occurring random excitations. It is normally modelled using pseudo-random road profile, power spectral density (PSD). The characteristics of a typical non-deformable terrain is defined by the frequency and amplitude or the degree of roughness of the road. This random road disturbance inputs excites high frequency vibrations in the vehicle [Bogsjo et al. (2012); Cao et al. (2008); Gillespie (1992); Wang and Shih (2011)].

The road condition classification according to ISO 8608 (1995) used in this work is listed in Table 2.2 (where, $G(n_0) \times (10^{-6} m^2/(cycle/m))$ at $n_0 = 0.1 cycle/m$). It uses Fourier analysis to estimate the PSD function of the surface. The PSD function,

$G(n)$ can be expressed as

$$G(n) = \begin{cases} G(n) = G(n_0)\left(\dfrac{n}{n_0}\right)^{-\varepsilon_1} & \dfrac{n}{n_0} \leq 1 \\ G(n) = G(n_0)\left(\dfrac{n}{n_0}\right)^{-\varepsilon_2} & \dfrac{n}{n_0} > 1 \\ 0 & \text{otherwise} \end{cases} \tag{2.62}$$

where n_0 is the reference spatial frequency, n is the spatial frequency, $G(n_0)$ is the

Table 2.2: ISO Classification of Road Surface Roughness [Dixon (2007); ISO 8608 (1995)]

Road class	Spectral Density	
	Range l $\times(10^{-6}m^2/(cycle/m))$	Geometric mean $\times(10^{-6}m^2/(cycle/m))$
A (very good)	< 8	4
B (good)	$8 - 32$	16
C (Average)	$32 - 128$	64
D (Poor)	$128 - 512$	256
E (very poor)	$512 - 2048$	1024
F	$2048 - 8192$	4096
G	$8192 - 32768$	16384
H	$32768 <$	

road surface roughness coefficient or displacement PSD. It is the PSD at the specified reference spatial frequency. ε is the linear fitting coefficient, which indicates the waviness of the road.

It is customary and convenient to set the value of ε to 2, being the mean value of the range $1.75 \leq \varepsilon \leq 2.25$. This setting is for the grade C roads with road surface roughness PSD $G(n)$ geometric mean value $256 \times 10^{-6}m^2/(cycle/m)$ and a vehicle forward velocity, V range $20 \leq V \leq 80km/h$ [Ngwangwa et al. (2010); Verros et al. (2005); Zhang et al. (2002)].

The road surface input model can then be built using the Gaussian white noise:

$$\dot{w}_i = -2\pi n_0 w_i + \sqrt{G_0 V} W_0(t) \tag{2.63}$$

where W_0 is a zero variance Gaussian white noise, w_i represents the wheel vertical displacement, $\dot{w}_i$ represents the vertical velocity of the wheel and G_0 is the road

roughness coefficient. Figure 2.9 shows the road surface model for the quarter-car model. The random intensity of the disturbance vary between approximately $-3.6cm$ and $4.4cm$.

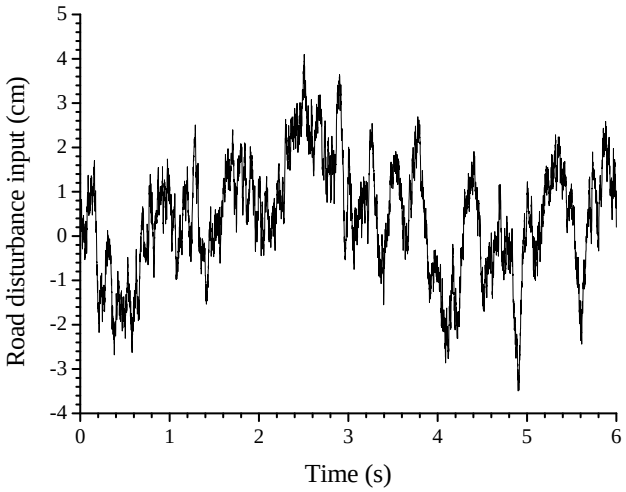

Figure 2.9: Random Road Disturbance Input Profile for Quarter-Car Model

Figures 2.10 and 2.11 represent the road surface model for the full-car model. The front and rear wheels are expected to be excited by the same stochastic excitation, $w(t)$ which is characterised by a time delay, t_d.

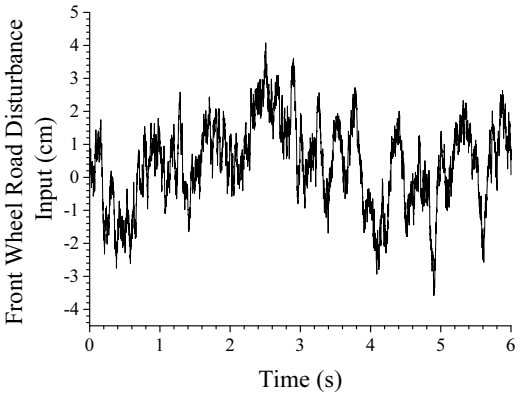

Figure 2.10: Random Road Disturbance Input Profile for the Front Wheels of the Full-Car Model

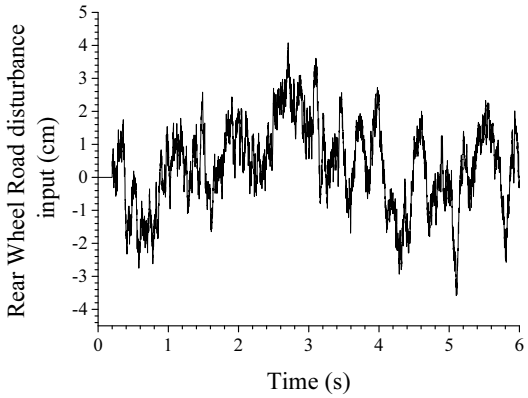

Figure 2.11: Random Road Disturbance Input Profile for the Rear Wheels of the Full-Car Model

2.7 Actuator Feedback Sub-Loops

It is customary in control design to use feedback loop in stabilising unstable systems and cut down the influence of the disturbance inputs, model inaccuracies and nonlinear actuator dynamics [Chantranuwathana and Peng (2004); Fateh and Alavi (2005); Nusantoro and Priyandoko (2011)]. In this work, multi-loop feedback control loops are used. Inner loops are used for force and spool-valve displacement feedback control while the outer loops are used for the suspension travel feedback control.

The outer loop is used for disturbance rejection control; it attenuates the unwanted disturbances from the uneven road surface. This loop arrangement is illustrated in Figure 2.12. Suspension travel is the controlled output of the system because it is readily measurable [Du and Zhang (2009)].

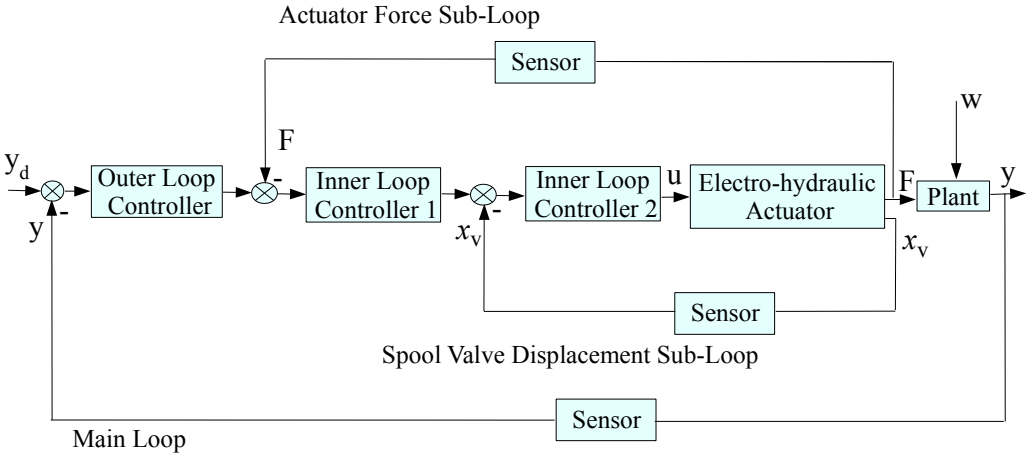

Figure 2.12: Schematic of the AVSS Multi-Loop Configuration

2.7.1 Actuator Force Control Inner-Loop

Electrohydraulic systems have numerous industrial applications because of their effective position control, appropriate force control design is however essential in applications like robotics and active suspension systems. To ascertain the suitability of the actuator for use in these systems, it must first demonstrate a good level of robustness to the parametric uncertainties associated with the electrohydraulic systems [He (2009); Karpenko and Sepehri (2012); Nusantoro and Priyandoko (2011)].

This test was carried out on the AVSS model using sinusoidal, saw-tooth and square wave set-point trajectories. Figure 2.13 shows good trajectory following for the different trajectories used.

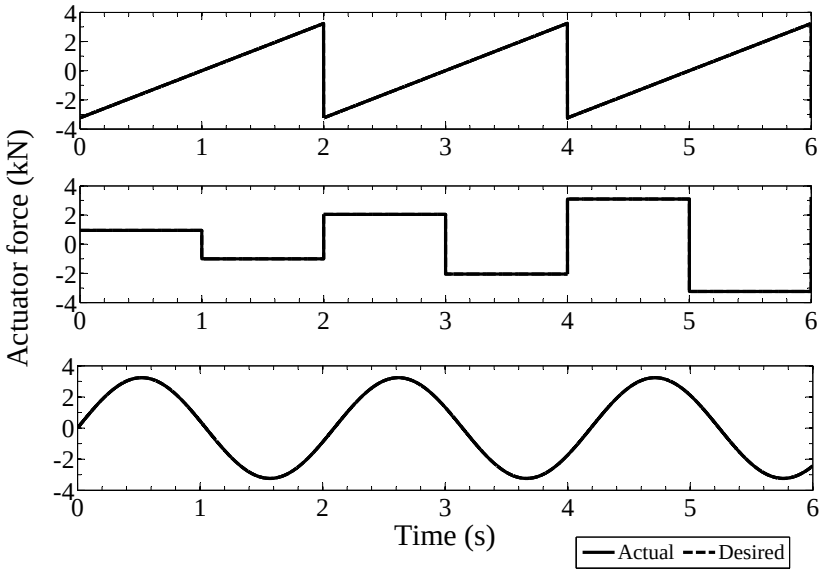

Figure 2.13: Actuator Force Set-Point Tracking

2.7.2 Position Control Inner-Loop

High performance position and force control of electrohydraulic systems requires the use of spool-valve displacement feedback. The effectiveness of an electrohydraulic actuator is related to accurate positioning of its spool-valve and piston. spool-valve displacement control is often ignored and classified as an unmeasurable state in AVSS and electrohydraulic design analysis. This is because its order of magnitude is commonly millimetres, thereby posing instrumentation challenges.

This challenge has been solved through the advent of the servo-valves assemblies with embedded or mounted miniaturised Linear Variable Differential Transformer (LVDT). An instantaneous relative position of the spool-valve is sensed in the LVDT feedback path and converted to a calibrated voltage signal [Ayalew and Kulakowski (2005); Chamseddine and Noura (2008); Fialho and Balas (2002); Li and Yuan (2005); Nakata and Zhao (2011)].

Introduction of the spool-valve feedback loop enhances the frequency response of the system and can be implemented with a PID controller for better performance. The controller performance at the high frequencies (that is, above 15Hz), however tends to be inaccurate especially for the higher order derivatives of the displacement [Nakata and Zhao (2011)]. Although spool-valve displacement measurement increases the general cost because of the sensitivity requirement for the LVDT instrument, the overall improvement and system stability is enhanced [Ayalew and Kulakowski (2005); Li and Yuan (2005)].

2.8 Passive Suspension System Sensitivity to Parameter Variations

The main design focus of vehicle suspension system is the achievement of an appropriate trade-off between the various performance objectives. For the PVSS, this trade-off is limited and associated with the fixed properties of the passive suspension elements [Williams (1997*a*); Zhong et al. (2010)]. It is however desirable that the optimal performance of the PVSS should not be localized about a fixed point defined by the PVSS elements.

Meanwhile, if the road excitation is uniform and the vehicle mass is constant, then an appropriate optimal combination of spring stiffness and damping rate can be obtained [Slaski (2011)]. Therefore, the process of AVSS design starts with an optimal design analysis of the PVSS. This provides a *nominal* suspension action on which the actuator could improve upon [Breytenbach and Els (2011); Raj and Padmanabhan (2009)].

In the course of service, the suspension properties (that is, suspension spring constant and damper coefficient) tend to vary due to deterioration in the physical properties of the elements [Zhong et al. (2010)]. Also, there could be variation in the operating conditions. For example, the sprung mass could vary due to changes in number of passengers in a vehicle [Gao et al. (2006); Herrnberger et al. (2008)]. The suspension design is expected to be insensitive to these changes in spite of varying road conditions and vehicle speed [Dong et al. (2011); Sekulic and Dedovic (2011); Slaski (2011)].

Sensitivity analysis on the passive suspension system helps to assess if the system parameters are well chosen. This is visible in the nominal performance of the passive suspension system. It is also useful in assessing which component of the suspension system is more readily affected by the type of road disturbance under consideration as well as, assess how this impact progresses.

In this section, the performance of the passive suspension system, on which the active suspension system to be considered is built, will be examined. This is to ascertain that the parametric properties of the suspension elements were optimally chosen and to check the level of robustness achievable from the PVSS [Mirza et al. (2005); Sekulic and Dedovic (2011)]. The performance is to be evaluated in terms of ride comfort, suspension travel and normalized wheel dynamic load.

2.8.1 Passive Vehicle Suspension System (PVSS) Nonlinear Quarter-Car Model

Figure 2.14 represents the physical model of 2DOF quarter-car passive suspension, and the nonlinear mathematical model can be extracted from Equations 2.4 and 2.5. This mathematical model is also derived based on the assumptions in Section 2.3.

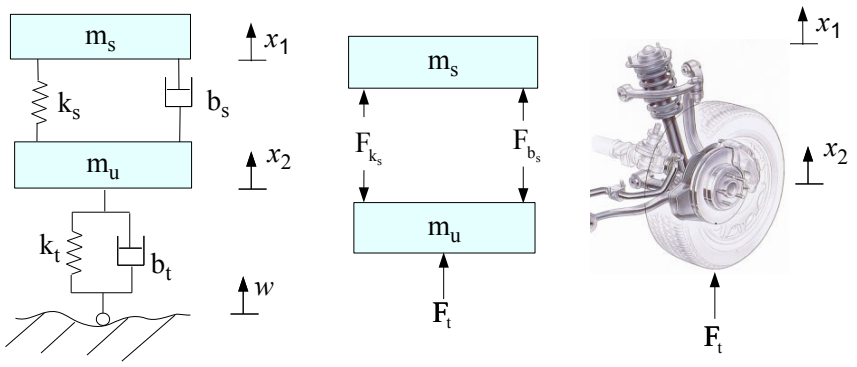

Figure 2.14: PVSS Quarter-Car Model

$$\begin{aligned} F_{m_s} &= F_{k_s} + F_{b_s} \\ m_s\ddot{x}_1 &= k_s^l(x_2 - x_1) + k_s^{nl}(x_2 - x_1)^3 + b_s^l(\dot{x}_2 - \dot{x}_1) - b_s^{sym}|\dot{x}_2 - \dot{x}_1| \\ &\quad + b_s^{nl}\sqrt{|\dot{x}_2 - \dot{x}_1|}sgn(\dot{x}_2 - \dot{x}_1) \end{aligned} \tag{2.64}$$

and

$$\begin{aligned} F_{m_u} &= -F_{k_s} - F_{b_s} + F_{k_t} + F_{b_t} \\ m_u\ddot{x}_2 &= -k_s^l(x_2 - x_1) - k_s^{nl}(x_2 - x_1)^3 - b_s^l(\dot{x}_2 - \dot{x}_1) + b_s^{sym}|\dot{x}_2 - \dot{x}_1| \\ &\quad - b_s^{nl}\sqrt{|\dot{x}_2 - \dot{x}_1|}sgn(\dot{x}_2 - \dot{x}_1) + k_t(x_2 - w) + b_t(\dot{x}_2 - \dot{w}) \end{aligned} \tag{2.65}$$

where $F_t = F_{k_t} + F_{b_t}$

Sensitivity of Quarter-Car PVSS to Parameters' Variations and Deterministic Road Excitations

Sensitivity of the PVSS to variation in suspension properties and sprung mass within the allowable limits (that is, $\pm\Delta 30\%$), can be assessed using Equations 2.64 and 2.65. This is done in the presence of the twin hump road deterministic input and vehicle forward velocity of $40km/h$.

Numerical experiments and documented results in some literature however, showed

that suspension characteristics tend to differ with little margin outside this range (especially between ±30% and ±50% range of parameter variation) [Dong et al. (2011); Sun and Cui (2011); Thoresson et al. (2009)].

Figures 2.15 and 2.16 shows the responses of the PVSS in terms of the vehicle body acceleration, suspension travel and the normalized wheel dynamic load as the sprung mass and suspension properties were varied. The trend in all the cases was similar. Both figures show that the PVSS is sensitive to the parametric variations and increase in settling time is also prominent in all the cases. Table 2.3 presents the full meanings of acronyms used in the figures.

Table 2.3: Parameters Plotted in the Figures 2.15 to 2.20

Abbreviation	Full meaning	Abbreviation	Full meaning
ST	Suspension travel	BA	Body acceleration
NWDL	Normalized wheel displacement	RDI	Road disturbance input

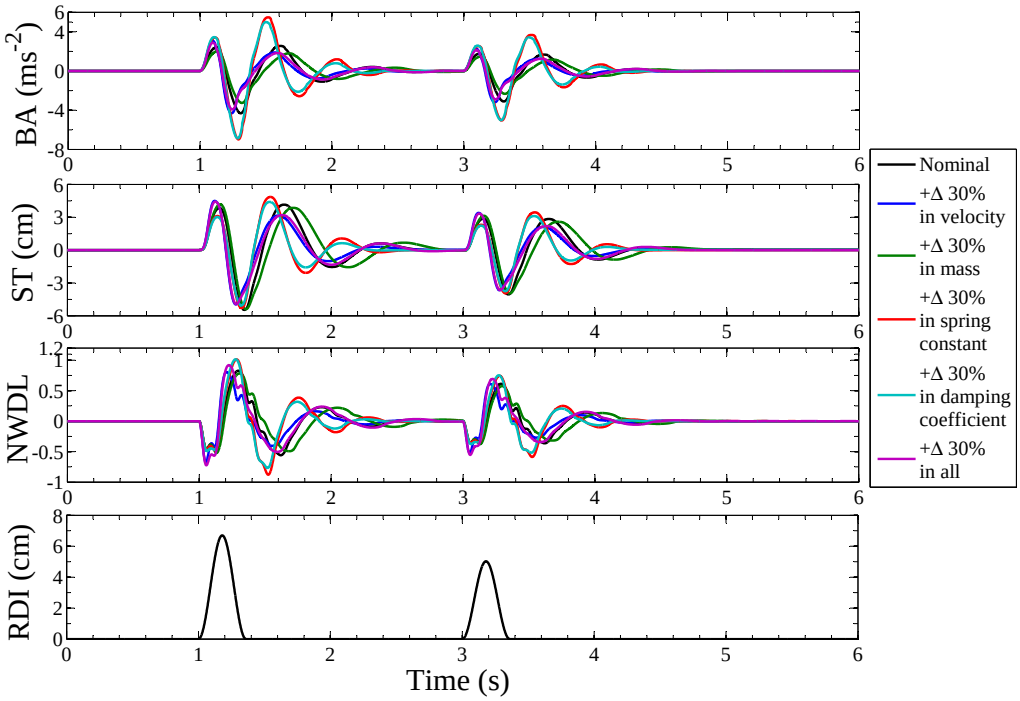

Figure 2.15: Sensitivity of the PVSS to 30% Increase in the PVSS Parameters

The sensitivity to PVSS parameter variation in Figures 2.15 and 2.16 can also be presented in the form of bar chart distributions for the PVSS parameters as shown in Figures 2.17, 2.18 and 2.19. Each bar in the plot represents a percentage deviation

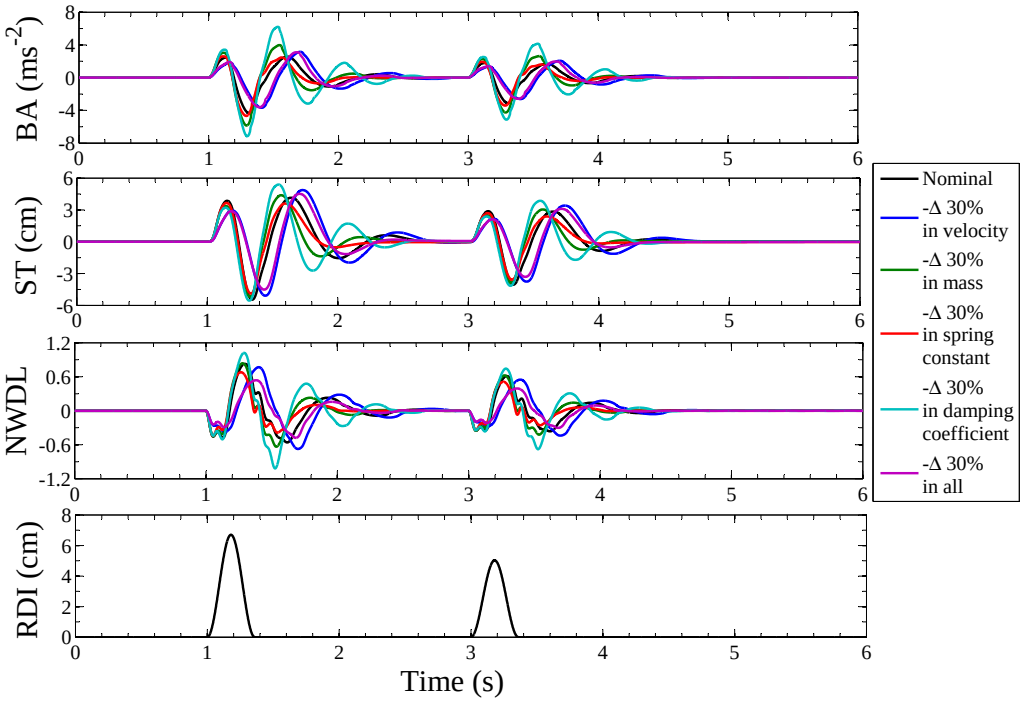

Figure 2.16: Sensitivity of the PVSS to 30% Decrease in the PVSS Parameters

of the respective suspension performance objective from the corresponding nominal values.

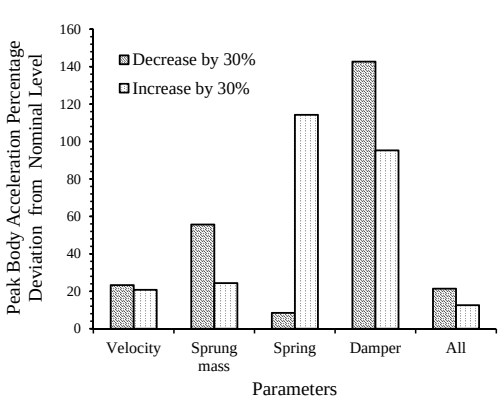

Figure 2.17: Evaluation of the PVSS Sensitivity to Parameter Variation using Relative Peak Body Acceleration

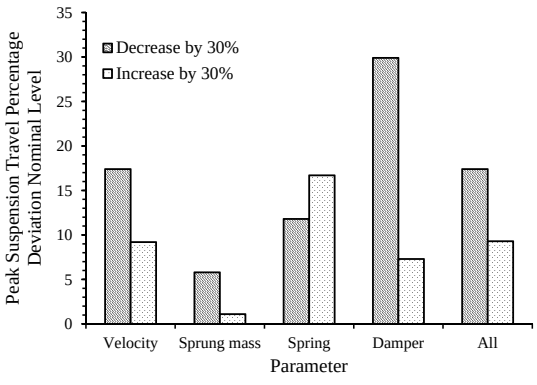

Figure 2.18: Evaluation of the PVSS Sensitivity to Parameter Variation using Relative Peak Suspension Travel

It could be inferred from Figures 2.17, 2.18 and 2.19 that the percentage deviation of the peak values were more prominent for the spring rate and damping coefficient but the damping coefficient was more consistent. Therefore, the PVSS was more

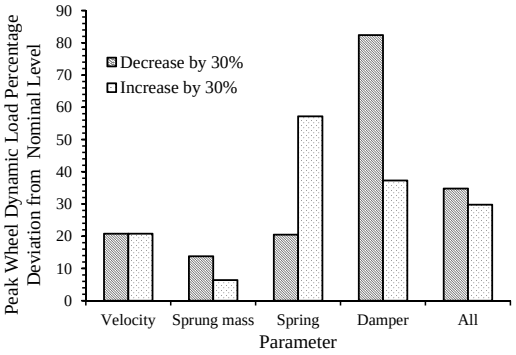

Figure 2.19: Evaluation of the PVSS Sensitivity to Parameter Variation using Relative Peak Wheel Dynamic Load

sensitive to damping coefficient reduction. This observation underscores the significance of damping in relation to road vibrations transmitted to the vehicle [Dixon (2007)].

The magnitude of the damping coefficient of a suspension system is influential to the vehicle stability and ride comfort. High damping characteristics enhance road holding but minimises suspension travel; force transmissibility is however increased making the road excitations to be transmitted to the vehicle occupants [Nguyen et al. (2012); Slaski (2011)].

The variation in the sprung mass and the spring rate both result in the variation of the system natural frequency. At nominal (that is, optimal) damping rate, the PVSS can be expected to exhibit two distinct modes of vibration (that is, body heave and wheel hop modes). These modes are still available when the damping rates is reduced but their peak magnitudes are higher. Moreover, the modes tend to merge as the damping rate is increased [Dong et al. (2011); Williams (1997*a*)].

Therefore, the objective of PVSS design is the attainment of the optimal damping coefficient and natural frequency of the system. Natural frequency cannot however be expected to remain constant within each span of operation of the vehicle because of sprung mass variation. Achieving this objective is part of the motivation for the AVSS design [Cole (2001); Dong et al. (2011)].

Sensitivity of Quarter-Car PVSS to Parameters' Variations and Random Road Excitations

When the PVSS was subjected to random road disturbance, as shown in Figure 2.20, the sensitivity to change in damping coefficient was found to be marginal. This confirms that the suspension properties have been optimally selected for random road excitation situations.

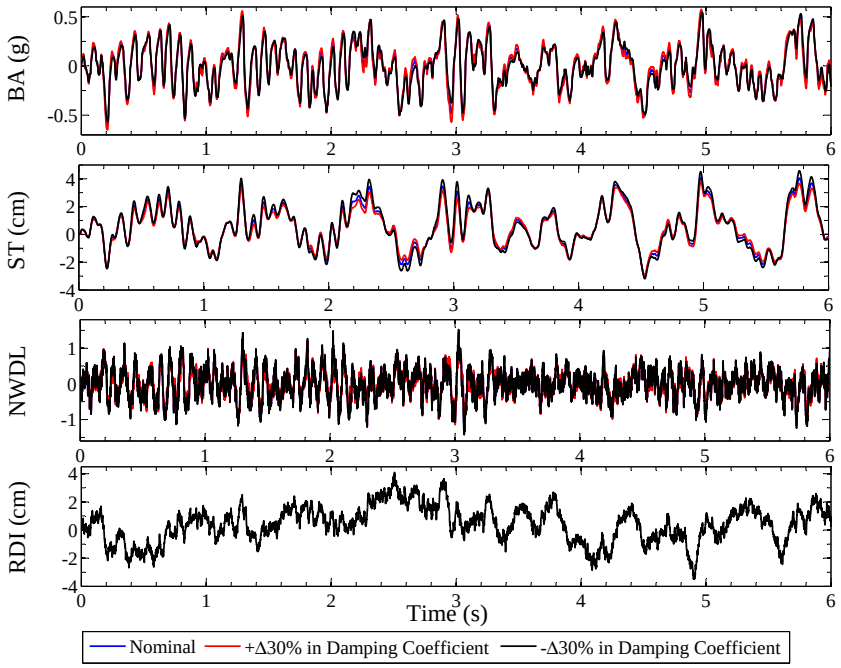

Figure 2.20: Sensitivity of the PVSS to Variation in Damping Coefficient

2.8.2 Passive Vehicle Suspension System (PVSS) Nonlinear Full-Car Model

The 7DOF nonlinear full-car passive vehicle suspension system model shown in Figure 2.21 is extracted from the AVSS model in Figure 2.3. The nonlinear mathematical model for the PVSS can also be extracted from Equations 2.19 to 2.28, based on the assumptions in Section 2.3.

The suspension spring forces, damping forces and tyre forces are given in general

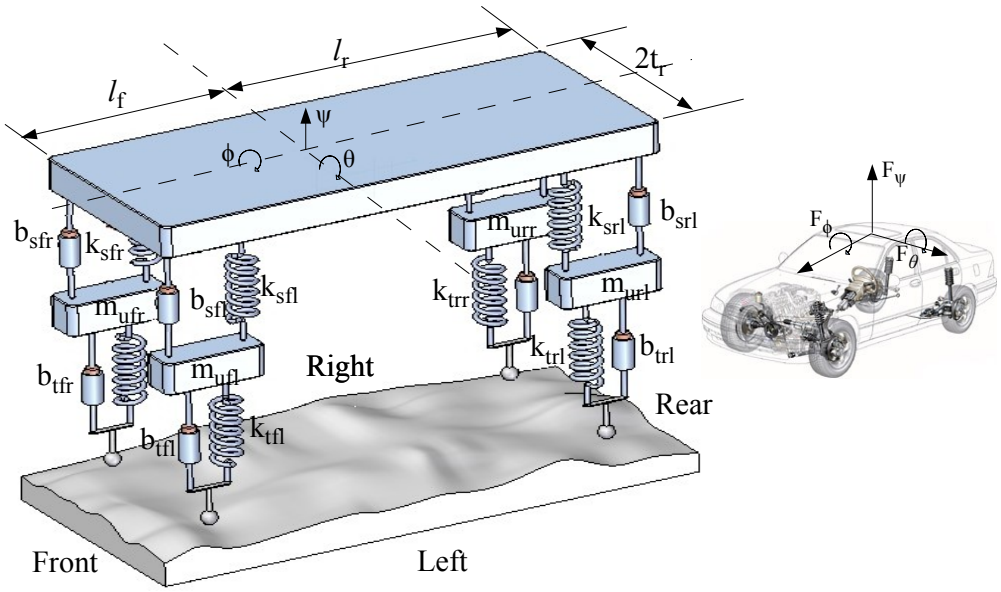

Figure 2.21: PVSS Nonlinear Full-Car Model

form as follows[Gaspar et al. (2009); Marzbanrad et al. (2002); Pedro (2007)]:

$$F_{kij} = k_s^l(x_{2ij} - x_{1ij}) + k_s^{nl}(x_{2ij} - x_{1ij})^3 \tag{2.66}$$

$$\begin{aligned} F_{bij} &= b_s^l(\dot{x}_{2ij} - \dot{x}_{1ij}) - b_s^{sym}|\dot{x}_{2ij} - \dot{x}_{1ij}| \\ &\quad + b_s^{nl}\sqrt{|\dot{x}_{2ij} - \dot{x}_{1ij}|}sgn(\dot{x}_{2ij} - \dot{x}_{1ij}) \end{aligned} \tag{2.67}$$

$$F_{tij} = k_t(x_{2ij} - w_{ij}) + b_t(\dot{x}_{2ij} - \dot{w}_{ij}) \tag{2.68}$$

Therefore the governing equations in terms of the heave, pitch and roll of the vehicle body, as well as the motion at the four wheels are given by:

$$m_s\ddot{x}_1 = F_{kfl} + F_{kfr} + F_{krl} + F_{krr} + F_{bfl} + F_{bfr} + F_{brl} + F_{brr} \tag{2.69}$$

$$\begin{aligned} I_\theta\ddot{\theta} &= l_fF_{kfl} + l_fF_{kfr} - l_rF_{krl} - l_rF_{krr} + l_fF_{bfl} + l_fF_{bfr} \\ &\quad - l_rF_{brl} - l_rF_{brr} \end{aligned} \tag{2.70}$$

$$\begin{aligned} I_\phi\ddot{\phi} &= t_fF_{kfl} - t_fF_{kfr} + t_rF_{krl} - t_rF_{krr} + t_fF_{bfl} - t_fF_{bfr} \\ &\quad + t_rF_{brl} - t_rF_{brr} \end{aligned} \tag{2.71}$$

$$m_{ufl}\ddot{x}_{2fl} = -F_{kfl} - F_{bfl} - F_{tfl} \tag{2.72}$$

$$m_{ufr}\ddot{x}_{2fr} = -F_{kfr} - F_{bfr} - F_{tfr} \tag{2.73}$$

$$m_{url}\ddot{x}_{2rl} = -F_{krl} - F_{brl} - F_{trl} \tag{2.74}$$

$$m_{urr}\ddot{x}_{2rr} = -F_{krr} - F_{brr} - F_{trr} \tag{2.75}$$

Sensitivity of Full-Car PVSS to Parameters' Variations and Deterministic Road Excitations

Figures 2.22 through 2.34 presents the PVSS response to 30% reduction and increase in the suspension parameters. This is evaluated using the system models given by Equations 2.66 to 2.68 and subjected to a twin hump road disturbance input when the vehicle is travelling with a forward velocity of $40km/h$. Table 2.4 presents the key to the acronyms used the plots.

Table 2.4: Parameters Plotted in the Figures 2.22 to 2.41

Abbreviation	Full meaning	Abbreviation	Full meaning
ST	Suspension travel	BA	Body acceleration
PAA	Pitch angular acceleration	RAA	Roll angular acceleration
NWDL	Normalized wheel displacement	RDI	Road disturbance input

The plot showed some similarities in trend for the different cases though distortions due to couplings in the different motions of the wheels is evident tended to disturb quick return to steady-state situations after humps. Figures 2.22 and 2.23 presents the PVSS response to 30% reduction and increase in the suspension parameters.

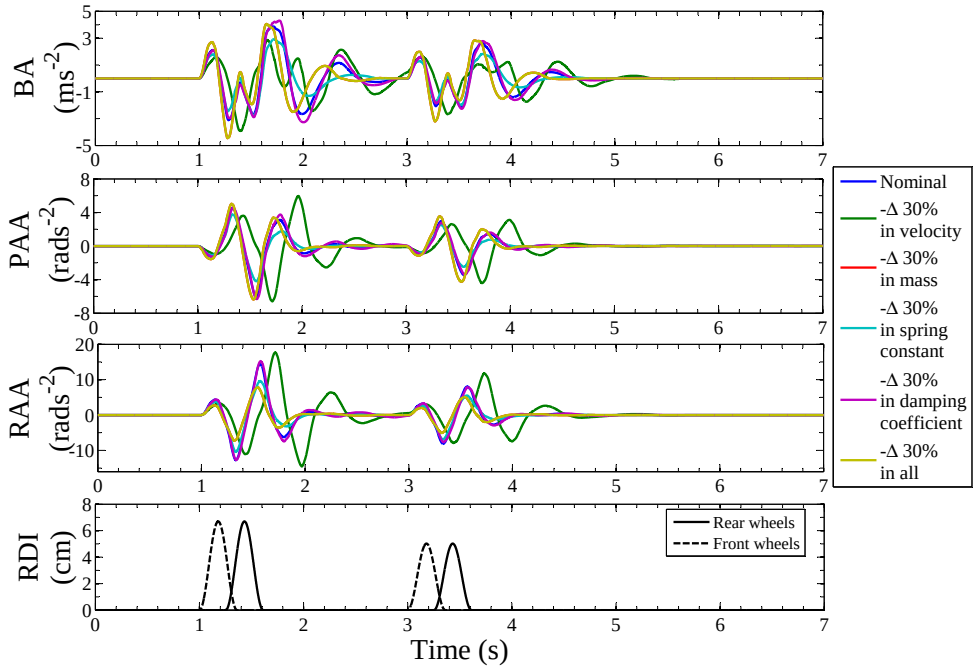

Figure 2.22: Sensitivity to 30% Reduction in the PVSS Parameters Using Body Heave and Vehicle Handling Plots

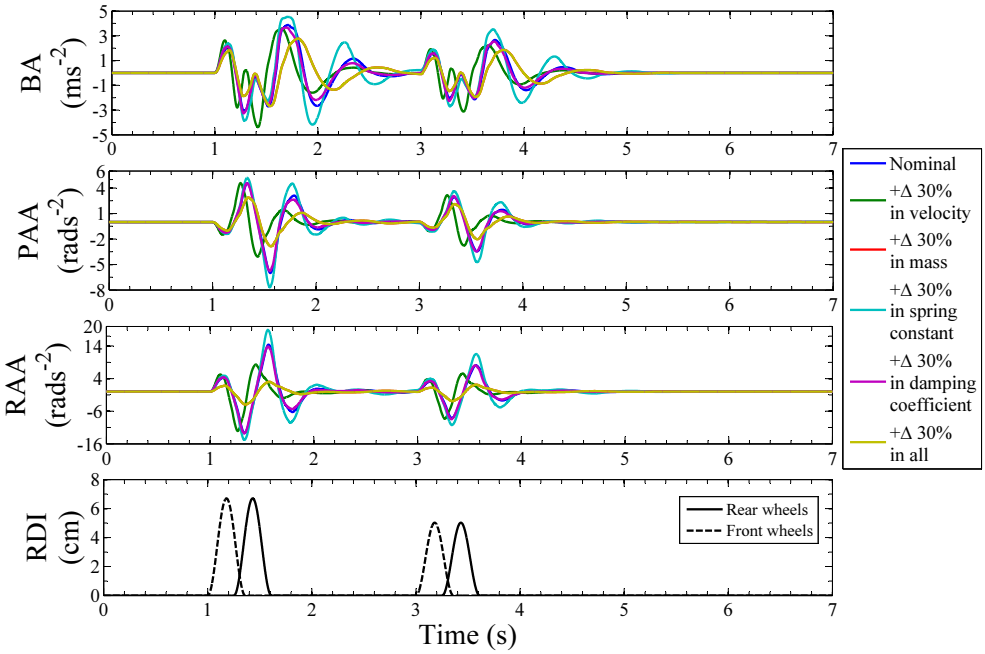

Figure 2.23: Sensitivity to 30% Increase in the PVSS Parameters Using Body Heave and Vehicle Handling Plots

The variation in the parameters resulted in increasing instability of the PVSS. This is evident in the suspension travel and normalized wheel dynamic load plots in Figures 2.27 to 2.34. The response signals were progressively veering away from the steady-state value after the second hump indicating depreciation in stability.

Figures 2.24 to 2.26 present the peak percentage deviations for the body acceleration, pitch and roll angular accelerations for the PVSS. It shows the sensitivity of the suspension parameters to these performance criteria.

Body, pitch and roll angular accelerations are most affected by variation in sprung mass of the suspension, especially when the variation is in the positive sense. This implies that the vehicle suspension's performance is affected easily by payload variation in terms of these performance criteria.

Figures 2.27 and 2.28 show the suspension travel response for the four wheels of the car in response to variation in the physical parameters of the suspension system and the vehicle speed.

The suspension travel response measured at the different wheels are each affected in unique patterns, although the impact of the coupling of their motion modes visible. The signals are also diverging from the steady state as the variation values for the parameters increase signalling the onset and increase in instablility.

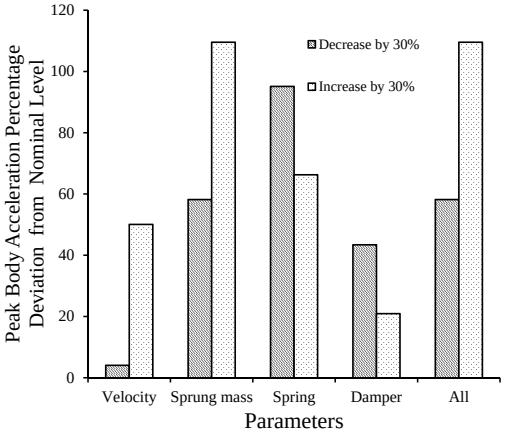

Figure 2.24: Evaluation of the PVSS Sensitivity to Parameter Variation using Relative Peak Body Acceleration

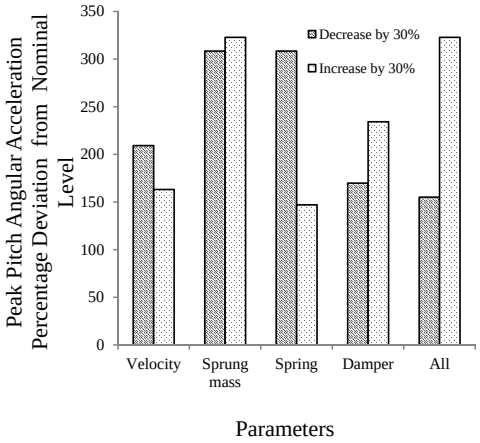

Figure 2.25: Evaluation of the PVSS Sensitivity to Parameter Variation using Relative Peak pitch Angular Acceleration

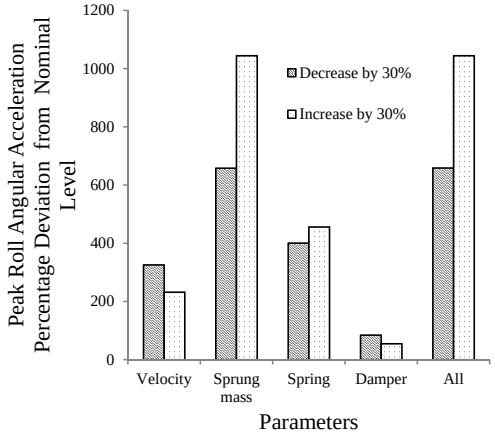

Figure 2.26: Evaluation of the PVSS Sensitivity to Parameter Variation using Relative Peak Wheel Dynamic Load

Suspension travel sensitivity to variation in suspension parameters for the four wheels are shown in Figures 2.29 to 2.32. The suspension travel values plotted in these graphs have been plotted relative to the nominal suspension travel values.

Suspension travel sensitivity to the variation in the parameters is less pronounced when the magnitudes is reduced in the "Front right" and "Rear left" wheels. On the whole, sensitivity due to variation in sprung mass (especially increase in sprung mass) is more prominent.

Figures 2.33 and 2.34 present the sensitivity of the wheel dynamic loads (WDL)

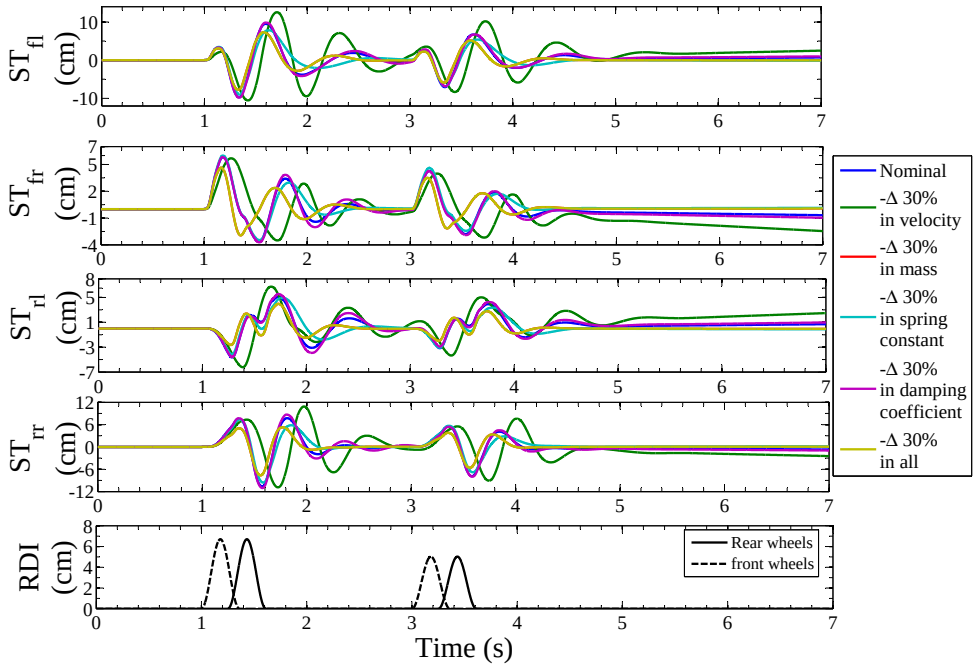

Figure 2.27: Sensitivity of the PVSS to 30% reduction in the PVSS Parameters Using the Suspension Travel Plots

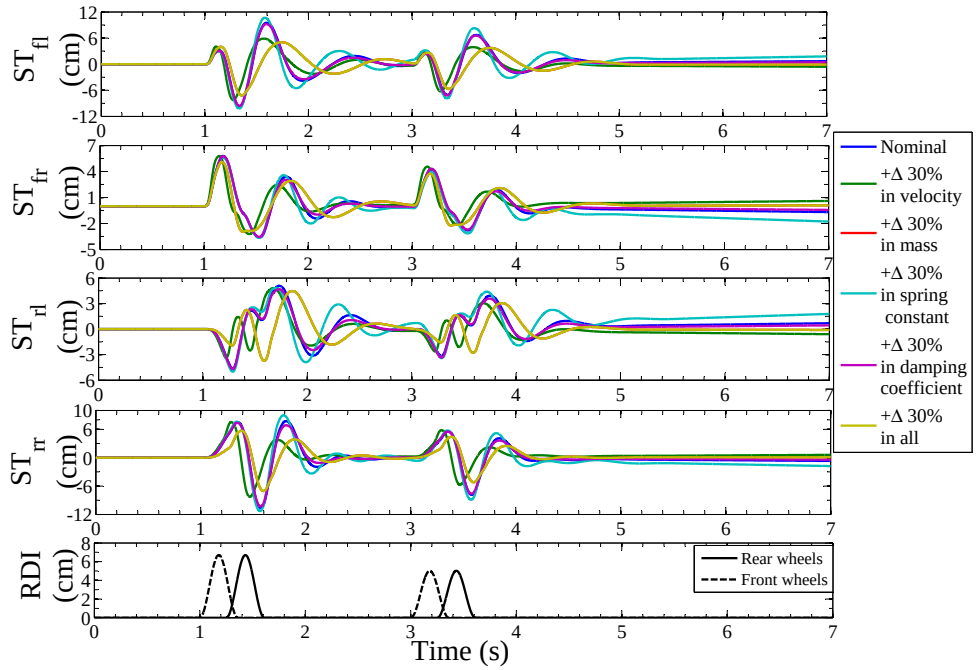

Figure 2.28: Sensitivity to 30% increase in the PVSS Parameters Using the Suspension Travel Plots

at the four wheels to variation in the suspension parameters and the vehicle forward velocity. The WDL signals are also found to be diverging from the steady-state value after the second hump.

Sensitivity to variation in vehicle speed and suspension parameters in terms of peak

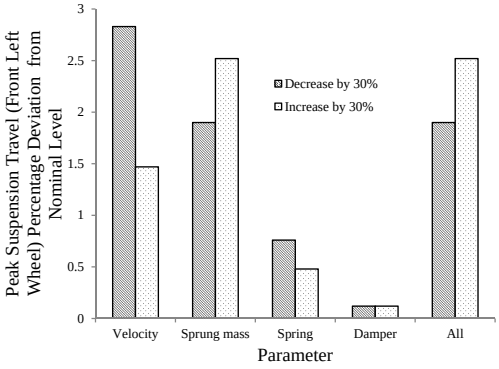

Figure 2.29: Evaluation of the PVSS Sensitivity to Parameter Variation using Relative Peak Body Acceleration

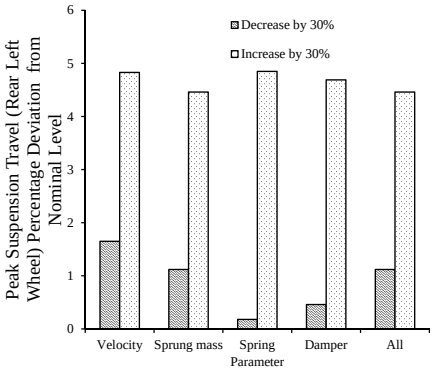

Figure 2.30: Evaluation of the PVSS Sensitivity to Parameter Variation using Relative Peak Pitch Angular Acceleration

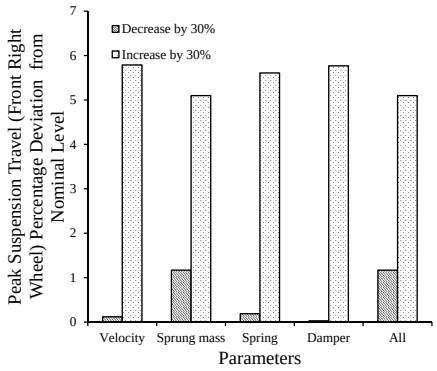

Figure 2.31: Evaluation of the PVSS Sensitivity to Parameter Variation using Relative Peak Body Acceleration

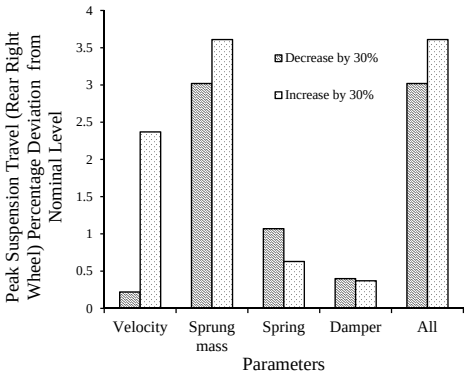

Figure 2.32: Evaluation of the PVSS Sensitivity to Parameter Variation using Relative Peak Pitch Angular Acceleration

percentage deviation of the wheel dynamic loads to nominal values are presented in Figures 2.35 and 2.38.

Wheel dynamic load sensitivity to vehicle forward velocity is the most prominent when considering decrease in the values of the parameters in the front wheels. On the whole, the sensitivity based on sprung mass property variation consistently and could be said to have the most impact on the performance of the vehicle suspension.

The parameter whose variation affects the suspension performance most (in the most consistent manner) is therefore the sprung mass or the vehicle payload. The sensitivity based on the other parameters does not follow a pattern that could be identified.

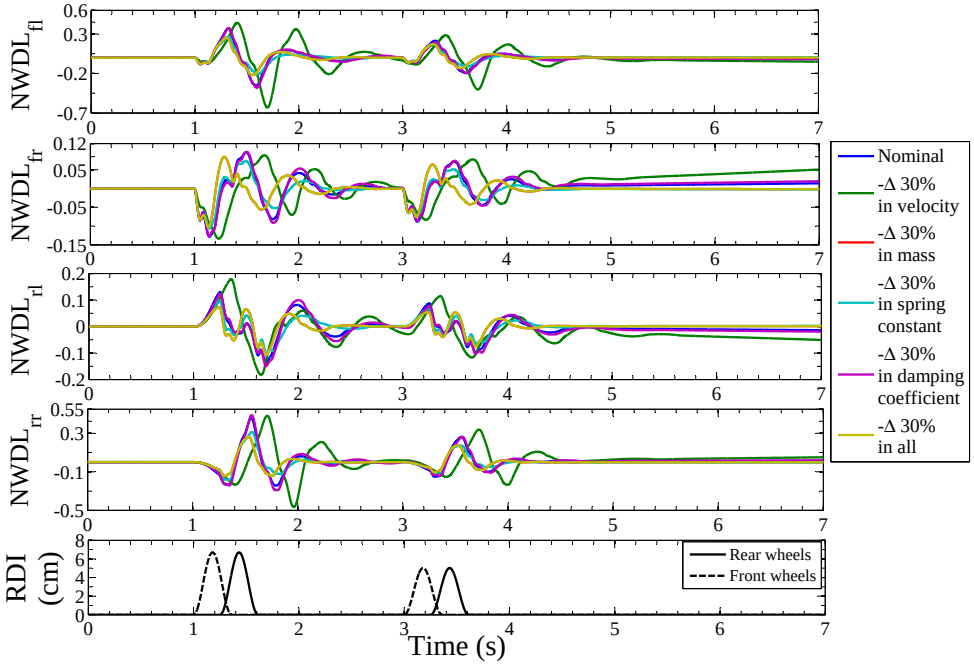

Figure 2.33: Sensitivity to 30% increase in the PVSS wheel dynamic load

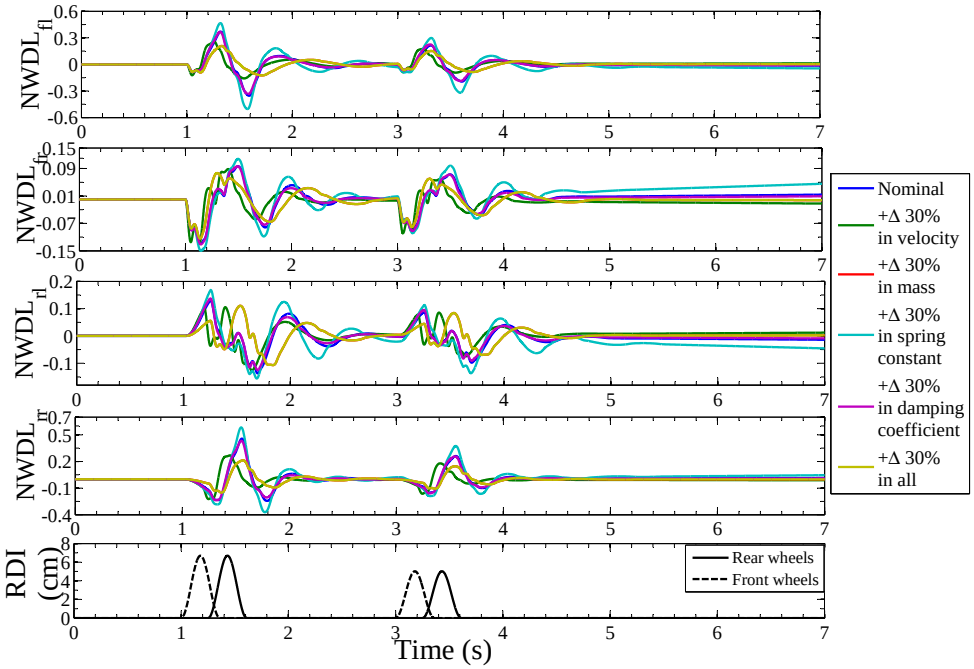

Figure 2.34: Sensitivity to 30% increase in the PVSS wheel dynamic load

The prominence of payload variation (in the full-car analysis) is a contrast to the situation for full-car in Section 2.8.1, where damping is the most influential parameter. This different situation is expected because of the higher level of complexity of full-car compared to the quarter-car model.

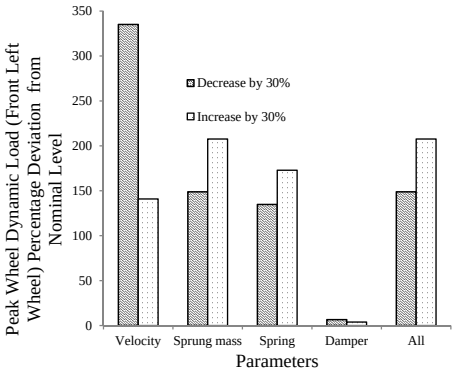

Figure 2.35: Evaluation of the PVSS Sensitivity to Parameter Variation using Relative Peak Body Acceleration

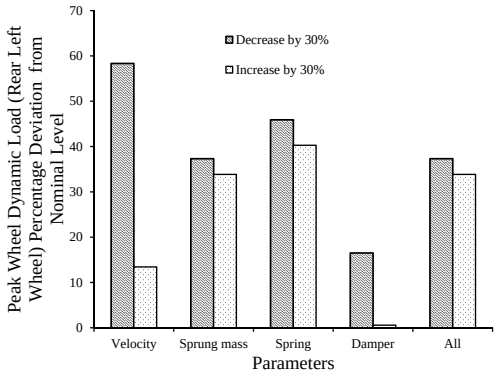

Figure 2.36: Evaluation of the PVSS Sensitivity to Parameter Variation using Relative Peak Pitch Angular Acceleration

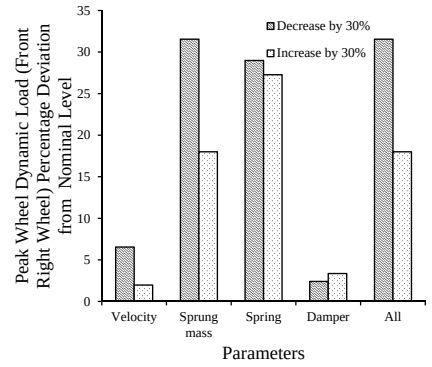

Figure 2.37: Evaluation of the PVSS Sensitivity to Parameter Variation using Relative Peak Body Acceleration

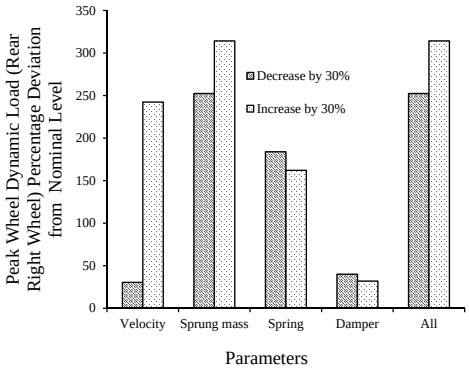

Figure 2.38: Evaluation of the PVSS Sensitivity to Parameter Variation using Relative Peak Pitch Angular Acceleration

Sensitivity of Full-Car PVSS to Parameters' Variations and Random Road Excitations

Figures 2.39 to 2.41 show the sensitivity of the PVSS to sprung mass variation with respect to body acceleration, pitch and roll angular acceleration, suspension travel and wheel dynamic load when travelling over random input disturbance road.

In Figure 2.39, there is only a marginal difference between the graph for nominal body acceleration, pitch and roll angular acceleration, and the ones for $\pm\Delta 30\%$ increase in the sprung mass magnitude. A similar pattern could be found in Figure 2.41 for the normalized wheel dynamic load plots for each wheel.

Figure 2.40 presents a different trend in the suspension travel plots. Here, there is a

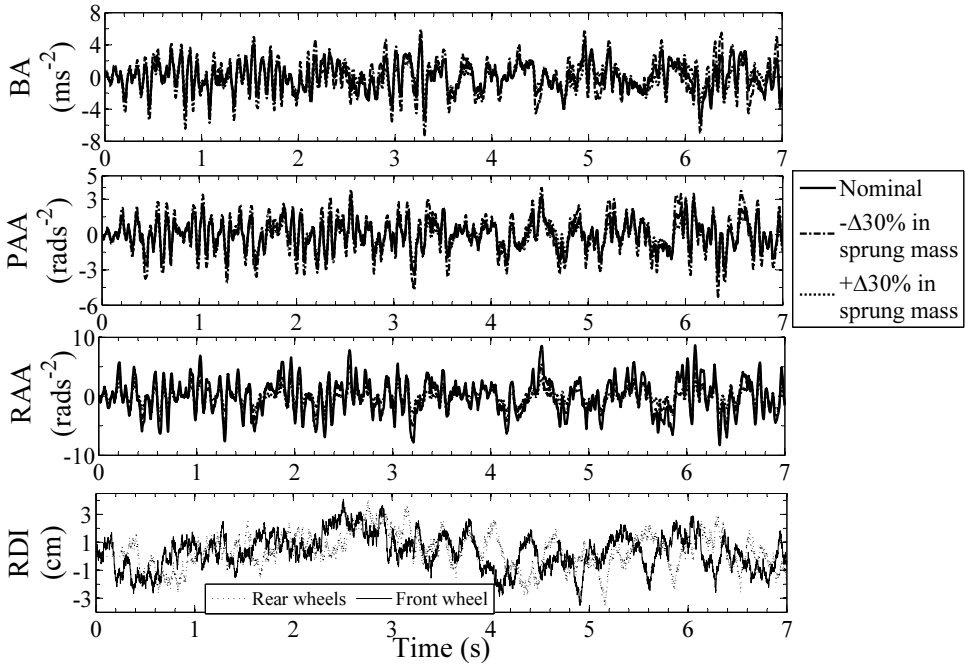

Figure 2.39: Sensitivity of the PVSS to Variation in Sprung mass When Suspension is Exposed to Random Excitations-Body Heave Acceleration and Handling Plots

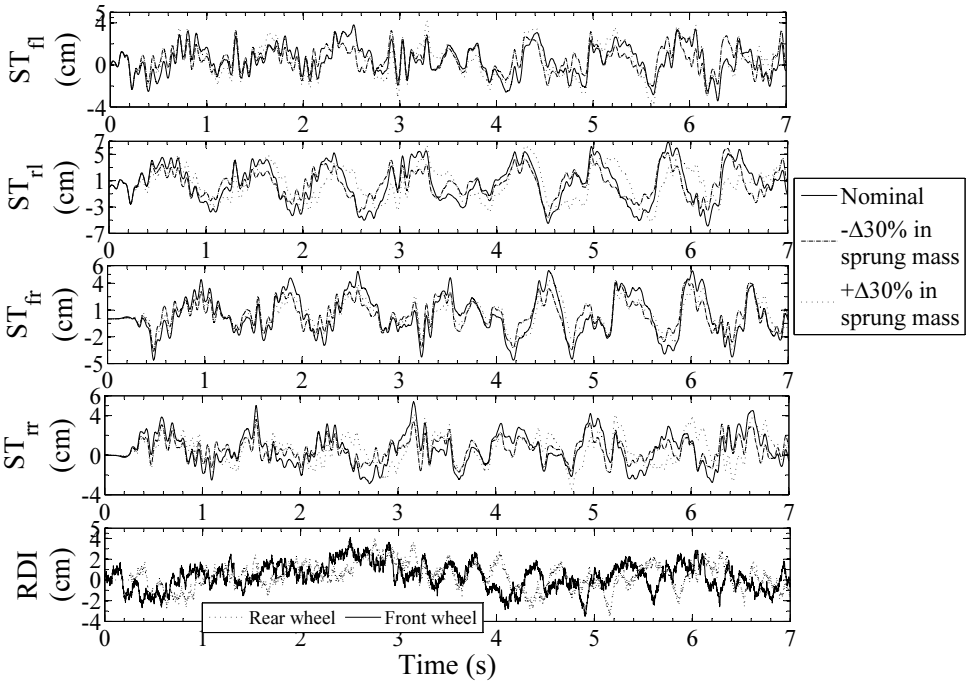

Figure 2.40: Sensitivity of the PVSS to Variation in Sprung Mass When Suspension is Exposed to Random Excitations-Suspension Travel Plots

clear difference between the graph for the nominal response and those for $\pm\Delta 30\%$. This further demonstrates that the PVSS parameters that yielded the "nominal" graphs have been optimally selected and sensitivity to variation in payload will only

affect the suspension travel performance of the PVSS within $\pm\Delta 30\%$ sprung mass variation range.

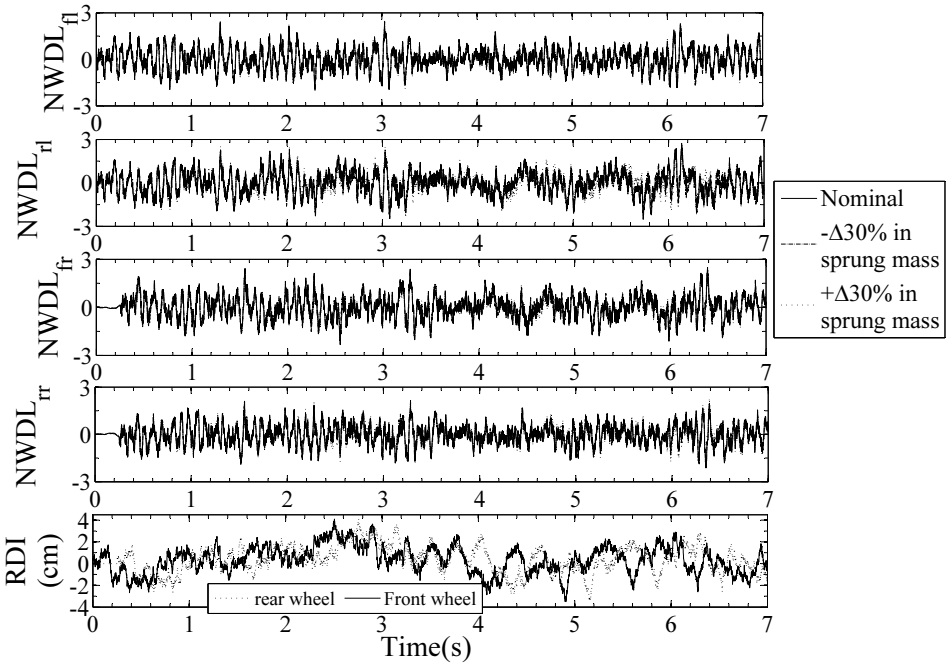

Figure 2.41: Sensitivity of the PVSS to Variation in Sprung Mass When Suspension is Exposed to Random Excitations-Wheel Dynamic Load Plots

2.9 AVSS Performance Specifications

Evaluation of the dynamic characteristics of vehicle suspension systems is carried out using criteria like ride comfort, suspension working space (that is, suspension travel), vehicle handling, energy consumption, infrastructure damage, roll-over stability, yaw stability, and braking and traction [Cole (2001); Evers et al. (2011); Gillespie (1992)]. In this work, only the first four criteria will be used due to the scope of the work.

The performance assessment of the designed AVSS controller was carried out for straight-line and constant velocity travel. The road conditions considered were, one with occasional shocks (that is, humps) and another with randomly distributed intensity of roughness. Also, the controller performances were evaluated for disturbance rejection.

Time domain analysis makes it possible to visualize the impact of the nonlinearity in the model and its effect on the vehicle's kinematics as well as, other suspension

parameters. A performance index that combines the RMS evaluation for all these parameters in the time domain will be computed to allow for a comparative evaluation of the controller performances quantitatively. The frequency domain analysis makes it possible to visualize the different vibration modes thus revealing transmissibilities and resonances [Cossalter et al. (2006)].

Vehicle ride comfort is related to the heaving, pitching and rolling motion of the vehicle. It is usually the most prominent of the suspension performance parameters because the primary role of suspension is isolation of passengers from the excitations due to road disturbances [Dixon (2007)]. The other performance characteristics will be evaluated in the time domain.

2.9.1 Basic Performance Criteria

The following basic characteristics are required of the AVSS controller in a bid to meet the set performance objectives:

1. **Nominal stability**: The closed-loops should be nominally stable. Stability in the inner loop is enhanced through a force feedback loop. The enhanced stability of the actuator dynamics should improve the overall system stability.
2. **Disturbance rejection**: The controller should demonstrate good low frequency disturbance attenuation.
3. **Good command following**: The suspension travel response of the AVSS is examined in the presence of the stochastic and deterministic road inputs shown in Figures 2.6 and 2.9. The controller should be able to keep the steady-state error as close to zero as possible.
4. **Sensor noise rejection**: For the controller to be able to attenuate high frequency noise and handle unmodelled dynamics; and have less than $-20dB$ gain above $32Hz$ [Pedro (2007)].
5. **Bandwidth**: The bandwidth should enable the actuator to cater for both high and low frequency disturbances and system resonance frequencies, therefore

   $$0 \leq Bandwidth \leq 20rad/s \qquad 0 \leq \zeta \leq 1$$

   It is desired that the controller be conformable with a second order control system whose damping ratio is 0.7071 and the $-3dB$ bandwidth equals the system (that is, sprung mass frequency) natural frequency [Fijalkowski (2011); Pedro (2007); Shahian and Hassul (1993)].

2.9.2 Time-Domain Performance Criteria

Quantitative assessment of the controller performance is achieved by the computation of aggregated mean-integrated-squared performance index that is based on selected normalized parameters. This formulated criteria is similar to the performance index used in optimal control design [Duarte-Mermoud and Prieto (2004); Tavazoei (2010)].

The selected parameters include, the body motion modes (that is, body heave, as well as roll and pitch angular accelerations), suspension travels, wheel dynamic loads and control inputs [Cao et al. (2007); Fallah et al. (2009); Turkay and Akcay (2011)]. Therefore, the objective of the controller is to minimise the performance index given by:

$$\begin{aligned} J \;=\; & \frac{1}{T}\int_0^T \left[\left(\frac{\ddot{x}_1(t)}{\ddot{x}_{1\,max}(t)}\right)^2 + \left(\frac{\ddot{\theta}(t)}{\ddot{\theta}_{\,max}(t)}\right)^2 + \left(\frac{\ddot{\phi}(t)}{\ddot{\phi}_{\,max}(t)}\right)^2 \right. \\ & \left(\frac{y_{i,j}(t)}{y_{i,j\,max}(t)}\right)^2 + \left(\frac{\sigma_{i,j}(t)}{\sigma_{i,j\,max}(t)}\right)^2 + \left(\frac{F_{i,j}(t)}{F_{i,j\,max}(t)}\right)^2 \\ & \left.\left(\frac{u_{i,j}(t)}{u_{i,j\,max}(t)}\right)^2\right] dt \end{aligned} \tag{2.76}$$

where $ij \in (fl, fr, rl, rr)$, u represents the control voltage, y represents controlled output (suspension travel), σ represents the wheel dynamic load, F represents the actuator force, $\ddot{x}_1$ represents the vertical acceleration of the vehicle body, $\ddot{\theta}$ represents the pitch angular acceleration and $\ddot{\phi}$ represents the roll angular acceleration.

Each of the performance criteria is also to satisfy the following requirements:

1. **Suspension travel**: is constrained to physical limits to avoid damages due to topping and bottoming [Cole (2001); Li et al. (2012)]. Maximum allowable suspension travel is given by [Du and Zhang (2008*a*); Fateh and Zirkohi (2011)]

   $$y_{max}(t) \leq \pm 0.1m$$

   where $ij \in (fl, fr, rl, rr)$ [Gaspar et al. (2003); Turkay and Akcay (2011)]. Moreover, the controller gain must be limited to 0 to $3dB$ in the frequencies lower than $0.5Hz$ to ensure that the rattle space is not exceeded [Crivellaro and Donha (2011*b*)].

2. **Ride comfort**: This is quantified using the vehicle body acceleration in the vertical direction. The vertical acceleration of the vehicle body needs to be

minimal for good ride comfort, especially within the low frequency band of 0.1 to $10Hz$. Its general frequency range of evaluation is however 0 to $20Hz$ [European Commission (2002); Gysen et al. (2010); Savaresi et al. (2010)],

$$-\ddot{x}_{1\,max} \leq \ddot{x}_1(t) \leq \ddot{x}_{1\,max}$$

This vertical body acceleration represents the response to the road disturbance and the vertical acceleration percieved by the driver body acceleration evaluated in this work is normalized with acceleration due to gravity constant, g [Fischer and Isermann (2004); Griffin (2007); Koch et al. (2008)].

Although it is generally recommended that the response gain must be on the decrease within the low frequency band, maximum gain in the frequency domain must not exceed $1.8m/s^2$ within the frequency range of 0 and $5Hz$ [Do et al. (2006); Poussot-Vassal et al. (2008)].

3. **Handling Quality**: It is desirable to keep the vehicle wheel in good contact and perpendicular position to the road surface even while braking, accelerating or cornering. Handling capability of the vehicle influences its stopping distance during braking and its tractive force while moving. Pitch, $\theta(t)$ and roll, $\phi(t)$ refer to the angular displacement of the vehicle body about its transverse and longitudinal axes respectively [Cao et al. (2011); Cole (2001)].

   While estimation of qualitative handling characteristics of a vehicle remains subjective, it is necessary to minimise the pitch and roll acceleration to obtain good handling. This is expressed mathematically as

$$-\ddot{\theta}_{max} \leq \ddot{\theta}(t) \leq \ddot{\theta}_{max} \qquad ; \qquad -\ddot{\phi}_{max} \leq \ddot{\phi}(t) \leq \ddot{\phi}_{max}$$

4. **Control input**: to the actuator is in the form of voltage to the solenoid of the spool-valve. This determines the hydraulic flow in and out of the actuator cylinder [Li et al. (2012)]. The control limits are given by:

$$-u_{max)} \leq u_{ij}(t) \leq u_{max)}$$

   Maximum allowable control voltage

$$u_{max} = 10V$$

5. **Actuator force**: is limited by the available control voltage to actuator and the maximum allowable controlled force is given by [Fateh and Zirkohi (2011)]

$$-F_{max)} \leq F_{ij}(t) \leq F_{max)} \qquad ; \qquad F_{max)} = m_s g$$

   where, $F_{max} = 3.24kN$ (for quarter-car model), and $F_{max} = 11.6kN$ (for full-car model).

6. **Wheel dynamic load Variation** is the criterion used to evaluate the road holding performance. It is normalized with static load at the wheels for good road holding. It is also a way of ascertaining the vehicle stability through the maintenance of good contact force between the wheel and the road [Cao et al. (2011); Fallah et al. (2009); Fischer and Isermann (2004); Li et al. (2012); Raj and Padmanabhan (2009)]. The wheel dynamic load variation is also influential in the generation of longitudinal forces related to braking and traction [Cole (2001)].

   The wheel dynamic load variation criterion can be expressed as,

$$\begin{aligned} \sigma_{ij} &= k_{(t\,ij)}(x_{(2\,ij)} - w_{ij}) + b_{(t\,ij)}(\dot{x}_{2\,ij} - \dot{w}_{ij}) \\ &\leq 9.81\Big(m_s + \sum_{ij}^{4} m_{(u\,ij)}\Big) \\ \Rightarrow\ 0 &\leq \sigma_{ij} \leq 3237.3N \end{aligned}$$

   the normalized wheel dynamic load NWDL must therefore be greater than 1 and must be maximised for good road holding.

7. **spool-valve displacement** is limited to $\pm 1cm$ due to physical constraint [Fateh and Zirkohi (2011); Fialho and Balas (2002)], therefore

$$-x_{v\,max} \leq x_v \leq x_{v\,max}$$

2.9.3 Frequency-Domain Performance Criteria - Vehicle Ride Performance Evaluation Based on Human Sensitivity

Epidemiological studies related the various health risks associated with whole-body vibration associated with road-induced vehicle vibration is well documented. The low-frequency vibration induced also leads to fatigue, motion sickness and loss of concentration [Griffin (2007); Milosavljevic et al. (2011)].

The spectrum of the vehicle vibrations excited by the road roughness covers the three frequency ranges enumerated in Table 2.5. Whole-body vibration (WBV) includes all the macroscopic movements which arise when a person is subjected to vibration by virtue of his standing, sitting or lying on a vibrating surface. The basic assumptions for biodynamics of seated human subjects exposed to vertical vibrations enumerated in Liang and Chiang (2006).

Although WBV in vehicles, on platform and in buildings is within the range 0.5

Table 2.5: Classification of Vehicle Vibration Induced by Road Roughness

Class	Range	Description
Quasi-static	$\nu < 0.5Hz$	Corresponds to passage through slopes and hills.
Ride	$0.5Hz < \nu < 20Hz$	Corresponds to traverse across typical road undulations.
Acoustic	$20Hz < \nu < 20kHz$	Generate audible noise

to $80Hz$ and the critical frequency range for human occupants of the vehicle in the vertical and horizontal directions are 4 to $8Hz$ and 1 to $2Hz$ respectively [Crivellaro and Donha (2011*b*); ISO 2631 (2003); Milosavljevic et al. (2011)].

Whole-body vibration perception in moving vehicle is a well studied area of research, especially for seated vehicle occupants. Moreover, most vibration isolation achievements in the AVSS design has been for frequency ranges near the natural frequency of the vehicle sprung mass (that is, approximately $1Hz$). Only marginal improvement has been achieved for the human sensitive frequency range [Cossalter et al. (2006); Lee and Salman (1989)].

While evaluation of human sensitivity to whole-body vibration in road vehicles is not within the scope of this work, ride comfort assessment in terms vehicle body accelerations (that is, vertical acceleration, pitch angular acceleration and roll angular acceleration) must be evaluated on the basis of the international standards. Moreover, evaluation of ride comfort in this standards are linked with human vibration perception, therefore one of the focus of AVSS design is to minimise vibration transmitted to the vehicle seats and occupants. [Ahlin and Granlund (2002); Bonin et al. (2007); Guglielmino et al. (2008); Wang et al. (2005)].

The ride frequency range is of more concern in vehicles because it accommodates the resonance frequencies of several human body parts [Griffin (2007); Shivakumara (2010)] as shown in Figure 2.42 as well as, some vehicle body parts [Cole (2001); Cossalter et al. (2006); Karen et al. (2012)].

Frequency-Weighted Vertical RMS Acceleration

Vehicle ride comfort is commonly associated with the level of vibrations perceived by the occupants of the vehicle, therefore its evaluation remains subjective. In spite

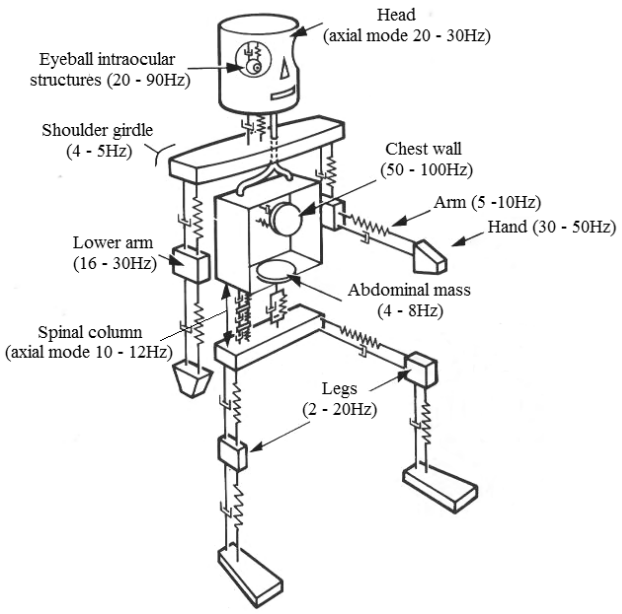

Figure 2.42: Mechanical Model of the Human Body Showing the Resonance Frequency Ranges for Various Part
Source: http://www.powerstandards.com/HumanResonance.php
Credit: Sven-Olof Emanuelsson, SKF, Goteborg, Sweden, 1998

of the various whole-body vibration investigations being carried out, a common ride comfort criterion that links the subjective and the objective assessment variables is not available for road vehicles the way *Sperling index* is for railway vehicles.

The available techniques are Statistical and RMS methods. These are used to estimate frequency-weighted RMS acceleration values that is compared with standard stipulated comfort levels [Kim et al. (2003); Zhou et al. (2009)]. ISO 2631 (2003) and BS 6841 (1987) specifications for human comfort evaluation based on frequency-weighted vertical accelerations are presented in Table 2.6. Figure 2.43 shows the basicentric axes used for the WBV evaluations.

Using the ISO 2631 (2003), the vehicle ride comfort in terms of RMS frequency weighted vibration acceleration emanating from the vehicle floor is estimated using

$$a_v = \sqrt{\left(k_\Psi^2 a_\Psi^2 + k_\theta^2 a_\theta^2 + k_\phi^2 a_\phi^2\right)} \tag{2.77}$$

where a_i represent the individual RMS frequency weighted accelerations given by

$$a_i = \sqrt{\frac{1}{T}\int_0^T a_i^2(t)dt}$$

and $i \in [\Psi, \phi, \theta]$ for the vertical acceleration, roll angular acceleration and pitch angular accelerations respectively. $a_i(t)$ represents the instantaneous frequency-weighted

Table 2.6: International Standards' Scale of Discomfort [BS 6841 (1987); ISO 2631 (2003)]

Intervals of the frequency-weighted vertical acceleration (m/s^2)	Comfort level
< 0.315	not uncomfortable
0.315 to 0.63	a little uncomfortable
0.5 to 1	fairly uncomfortable
0.8 to 1.6	uncomfortable
1.25 to 2.5	very uncomfortable
> 2	extremely uncomfortable

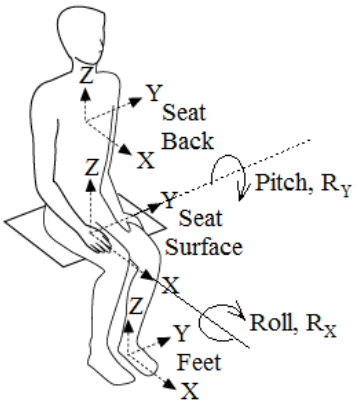

Figure 2.43: Basicentric Axes for Human Body Vibration Evaluation

acceleration measured at the floor of the vehicle, T is total time period and k represents the respective multiplying factor for weighting. These weightings are essential in capturing the spectral sensitivity of human body to vibration frequency ranges.

To compare the frequency-weighted accelerations obtained with the ISO comfort levels, the multiplying factors used are the ones corresponding to weighted-frequency values at the feet of seated passengers in ISO 2631 (2003). These values are given as, $k_\Psi = 0.4$ in the vertical direction, and $k_\theta = k_\phi = 0.25$ for the pitch and roll modes. This way, the vibration transmitted directly to the passengers (that is, excluding the seat) is estimated for direct comparison with standard comfort levels listed in Table 2.6 [Evers et al. (2011); Karen et al. (2012); Kim et al. (2011)].

To use the ISO 2631 (2003) ride comfort evaluation method, perception filters corresponding to the multiplying factors must be designed. They are necessary to make good approximation of the vibration sensitivity curves. A fifth and fourth-order

transfer function approximation for the filter design in the magnitude plot is shown in Figure 2.44, as given by Equations 2.78 and 2.78. [Evers et al. (2011); Karen et al. (2012); Kim et al. (2011); Zuo and Nayfeh (2003*a*)]. W_k is only applicable to the vehicle heave motion mode, while W_d is applicable to the pitch and roll angular acceleration modes.

$$W_k(s) = \frac{87.72s^4 + 1138s^3 + 11336s^2 + 5453s + 5509}{s^5 + 92.6854s^4 + 2549.83s^3 + 25969s^2 + 81057s + 79783} \tag{2.78}$$

$$W_d(s) = \frac{12.66s^3 + 163.7s^2 + 60.64s + 12.79}{s^4 + 23.77s^3 + 236.1s^2 + 692.8s + 983.4} \tag{2.79}$$

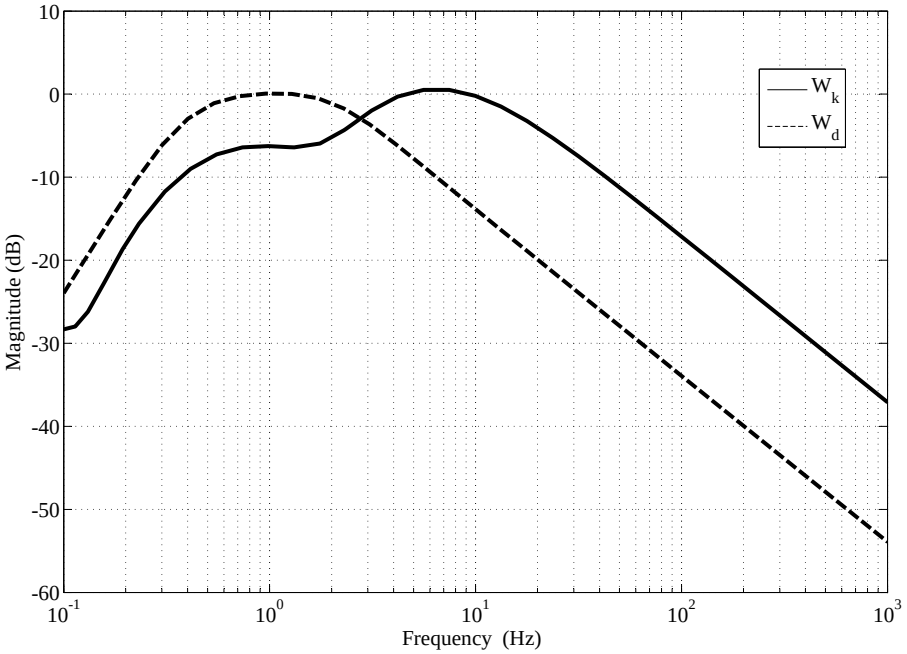

Figure 2.44: ISO 2631 Frequency-Weighting (W_k) and (W_d) Curve for Vertical and Horizontal Accelerations at the Feet

The directive of the Parliament and of the Council of the European Union stipulates that in preventing occupational health risk due to WBV, the limit values given in Table 2.7 must not be exceeded: The legislation stipulates the maximum allowable

Table 2.7: European Communities' Whole-Body Vibration Limit Values [European Commission (2002)]

	Exposure Action Value, EAV (m/s^2)	Exposure Limit Value, ELV (m/s^2)
WBV Acceleration	0.5	1.15

daily vibration exposure levels in terms of exposure action value (EAV) and exposure

limit value (ELV) in terms of frequency weighted root mean square acceleration values over an eight hour period.

2.9.4 Actuator Power Consumption

This is useful in evaluating the economic viability of the actuator since power requirement of the actuator will influence the fuel consumption rate of the vehicle [Cole (2001); Crolla and Nour (1992); Marzbanrad et al. (2002); Williams (1997*b*)]. Therefore actuator power consumption criterion can be expressed as

$$min \qquad H_{ij} = F_{ij}(v_{1ij} - v_{2ij})$$

where $ij \in (fl, fr, rl, rr)$. Also F_{ij} and v_{ij} are the actuator forces and relative velocities between the sprung and unsprung masses respectively.

2.10 Summary of Chapter Two

This chapter presents the physical description and mathematical models of the AVSS, elctrohydraulic actuators and the road disturbance inputs.

1. AVSS models: The SISO (quarter-car) and MIMO (full-car) models are presented. The mathematical model highlights nonlinear properties of the springs, dampers and electrohydraulic actuators that make up the system. The control inputs to the system, **u** is made up of the voltage to the actuator while the system controlled signals consist of the suspension travel variable at each suspension units.

2. Electrohydraulic actuator model: The dynamics of the actuator is presented mathematically. Force and position feedback sub-loops that help in stabilising the actuator dynamics are also presented.

3. Road disturbance input models: Models of the random and deterministic road excitations used are also presented in this chapter. The deterministic road disturbance input consists of two humps with $6.5cm$ and $5cm$ elevation, and separated by about $19m$. The twin hump situation enhances better analysis transient response of the system. The random road disturbance is modelled after the grade C whose surface roughness is ranked average.

4. Sensitivity to parameter variation by passive suspension system was evaluated to ascertain that they are optimally chosen.

5. The process of assessing the controller performances, which has been presented in this chapter is summarized and illustrated in Figure 2.45. The performance quality of the designed controllers are evaluated based on the four categories controller performance objectives shown.

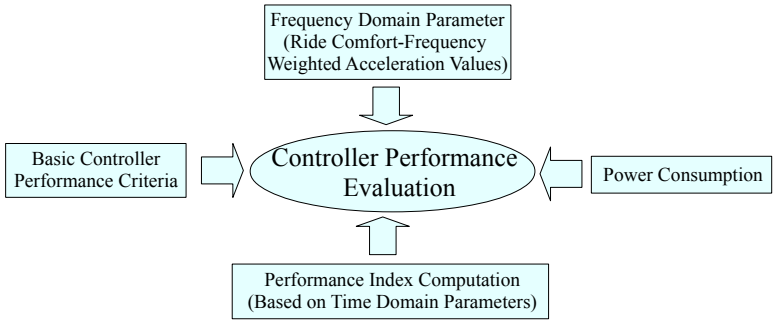

Figure 2.45: Schematic for Controller Performance Evaluation Process

3 PID Controller Design (Benchmark Controller Design)

3.1 Introduction

The PID control is the most popular and versatile feedback control loop applied in the industry, it exists in many variants that are inspired by the simplicity of the generic PID. It is widely accepted to benchmark the performance of other controllers against PID when designing controllers, this is because of its simple structure and relative ease of tuning either intuitively or with several tuning methods available [Astrom and Hagglund (2001); Giovanni (2009); O'Dwyer (2006)].

It is also popular because it is effective in the adjustment of system parameters of controllers like overshoot, rise and settling time. It however lacks robustness to parameter variation and requires high loop gains. Alternative control methods often have to sacrifice their better performance in this areas for simplicity and computational ease [Cetin and Akkaya (2010); Giovanni (2009)].

3.2 PID Control and Tuning

The control signal of a generic classical PID controller is the sum of three terms: K_P term, which is proportional to the error signal, K_I term, which is proportional to the integral of the error signal, and the K_D term, which is proportional to the derivative of the error signal [Gao (2002)].

$$u_{(ij)} = K_P e_{(ij)}(t) + K_I \int e_{(ij)} dt + K_D \frac{de_{(ij)}}{dt} \tag{3.1}$$

$$e_{(ij)} = y_{d\,(ij)} - y_(ij) \tag{3.2}$$

where $ij \in (fl, fr, rl, rr)$ and e_{ij} is the error signal. For the system to be set up as a regulatory control problem, the reference signals $y_{d\,(ij)}$ was set to zero. It is therefore

desired that a control law $u_{(ij)}$ be designed such that $e_{(ij)}(t) \rightarrow 0$, as $t \rightarrow \infty$.

The optimal gains of the PID controllers were determined through the use of the Ziegler-Nichols tuning criterion Astrom and Hagglund (2001); O'Dwyer (2006). Based on the understanding of the system characteristics, the first step in fine tuning the PID controller is to adjust the proportional gain in such a way that the rise time is minimised. Then the integral gain is adjusted to reduce overshoot and settling time. Lastly, the derivative gain is adjusted to avoid steady-state error.

The optimal gains of the PID controllers were determined through the use of the Ziegler-Nichols tuning criterion. The tuning rule is used with a decay ratio of 0.25 to obtain the PID controller gains. This method often requires careful fine tuning manually because PID controllers can easily generate too high control inputs which can lead to saturation [Astrom and Hagglund (2001); O'Dwyer (2006)].

While the rigorous tuning rules applied could assist in achieving the required performance, like disturbance rejection. It does not guarantee robustness to model uncertainties. Ziegler-Nichols' tuning method has become the first choice tuning technique because it is relatively easy to apply [Ang et al. (2005); Gao (2002)].

3.3 SISO : Quarter-Car Analysis

The control problem in this chapter is set-up as disturbance rejection problem. The model was subjected to both deterministic (described in Section 2.6.1) and random road excitations (described in 2.6.2). The vehicle velocity used for the analysis involving the deterministic road excitation was $40km/h$, while those for the random road excitations was $72km/h$. The deterministic road disturbance elements (that is, hump) in this study, serves the purpose of regulating the vehicle speed in designated areas.

Spool-valve displacement and actuator force outputs of the actuator are both fed back in the inner sub-loops shown in Figure 3.1. The system responses based on both formats are influenced by the presence of the inner feedback loops. The regulatory control problem is set-up to assess the degree of deviation of the controlled output of a system from a fixed desired value as a result of the presence of a disturbance input. The numerical simulations for the PID controlled system with a sampling frequency of $1kHz$ were carried out in the $MATLAB^{®}/SIMULINK^{®}$.

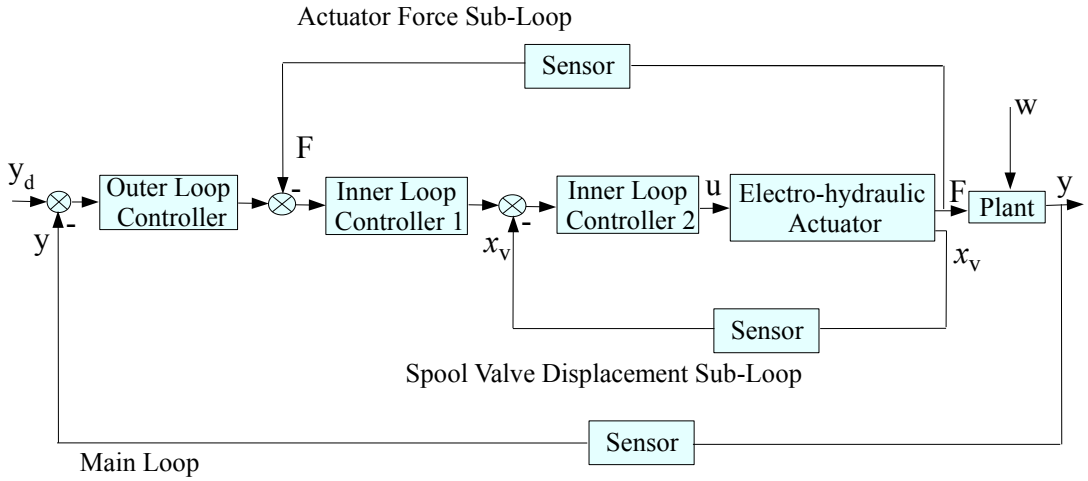

Figure 3.1: Schematic of the AVSS Multi-Loop Configuration

The desired controlled output value in this case is zero suspension travel.

Responses for Deterministic Road Excitation

Table 3.1 presents the various PID tuning parameters for the main feedback loop controller and the two sub-loop controllers for deterministic and random road excitation situations and zero reference input (that is, for regulatory control problem).

Table 3.1: Quarter-Car AVSS PID Tuning Parameters - Deterministic Road Disturbance Input

	PID Gains		
	K_p	K_i	K_d
Outer loop	100	1×10^{-6}	1×10^{-6}
spool-valve displacement sub-loop	7×10^{-3}	1×10^{-6}	1×10^{-6}
Actuator force sub-loop	3.87×10^{-4}	1×10^{-6}	1×10^{-8}

Figure 3.2 presents the time history trend of the system responses to the zero reference input in the presence of the twin deterministic road disturbance inputs. The range of values for the spool-valve displacement, control voltage and the suspension travel are well below the maximum allowable limits of $\pm 1cm$, $\pm 10V$ and $\pm 10cm$ respectively.

The peak body acceleration values range between $-1.41ms^{-2}$ and $1.11ms^{-2}$, the normalized wheel dynamic load ranged between -1.16 and 1.45, and the actuator

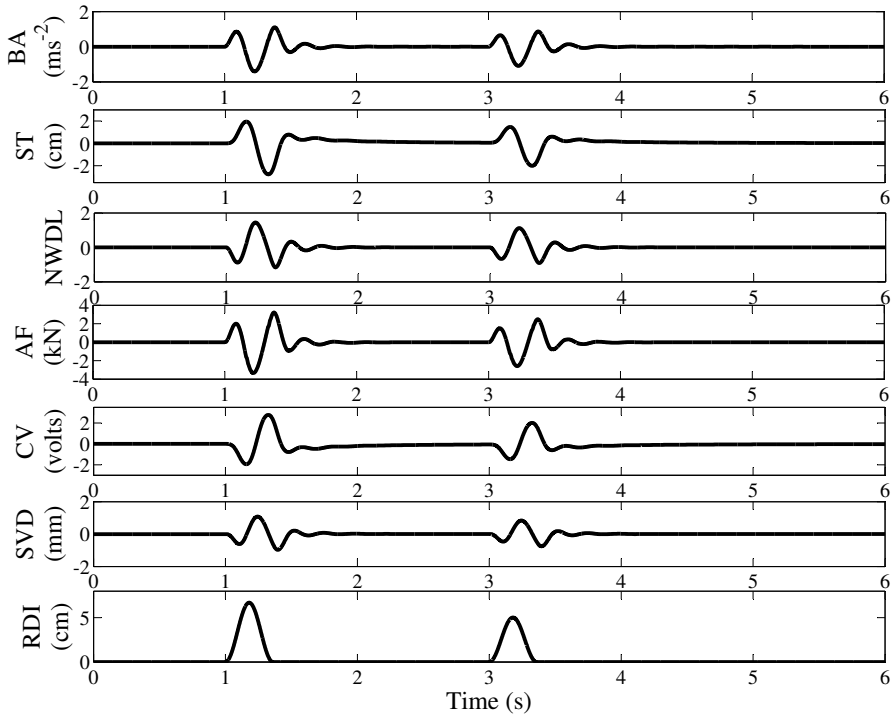

Figure 3.2: Time History of the AVSS Responses to Deterministic Road Excitations

force ranged between $-3.34kN$ (which is marginally above the maximum allowable value) and $3.23kN$ (which is marginally below the maximum allowable value).

Responses for Random Road Excitation

Table 3.2 presents the PID tuning parameters for the control loops when the system is exposed to random road excitations. The reference input to the system is zero. Similarly, the values for the PID gains in the inner loop indicates the level of influence of the inner feedback loops as regard the performance of the AVSS.

Table 3.2: Quarter-Car AVSS PID Tuning Parameters - Random Road Disturbance Input

	PID Gains		
	K_p	K_i	K_d
Outer loop	3.80×10^{-6}	2.80×10^{-6}	1×10^{-9}
spool-valve displacement sub-loop	1×10^{3}	1×10^{7}	2.50×10^{4}
Actuator force sub-loop	1×10^{-15}	0.75	1×10^{-6}

A set of time histories for the responses of the PID controlled AVSS in the presence of random road excitation is shown in Figure 3.3. The plots presents a situation that

is similar to that of the AVSS encountering series of deterministic road excitations in quick succession. The amplitudes in the plots also show that the random road excitation presented a more challenging situation.

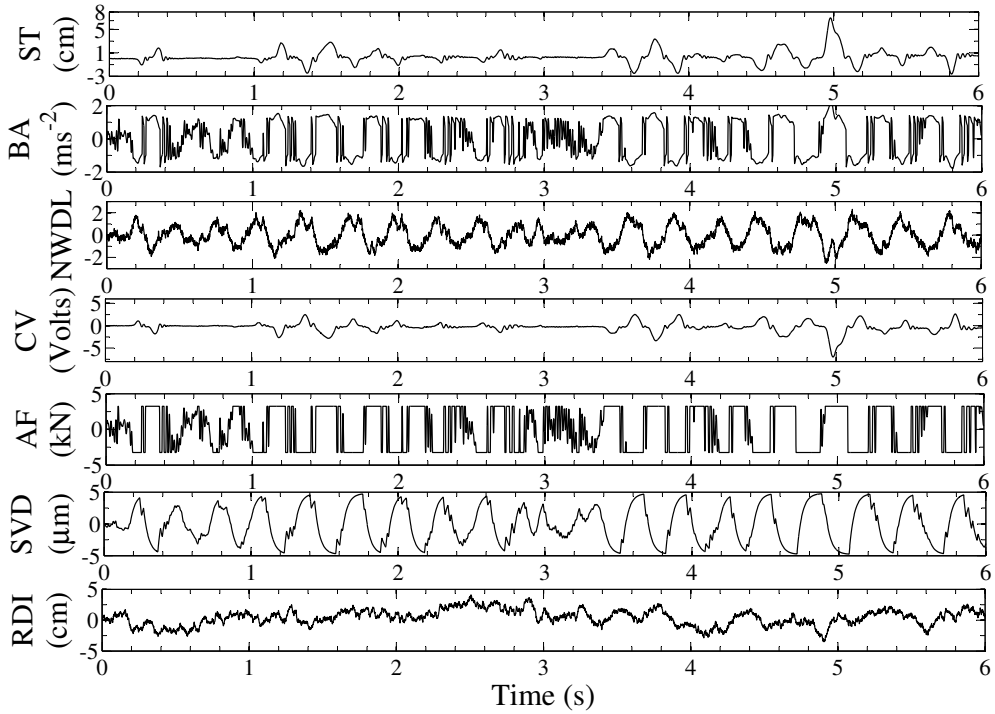

Figure 3.3: Time History of the AVSS Responses to Random Road Excitations

Other features noticeable in the figure are, relatively lower peak values for the control voltage while the peak values for all the other parameters increased. The maximum allowable limits for the actuator force was reached several times and the body acceleration value oscillated between $\pm 1.6 ms^{-2}$.

3.4 MIMO: Full-Car AVSS Analysis

This section presents the PID controller design for the full-car AVSS model. The model incorporates single PID inner loops for actuator forces at each wheel. This is to facilitate easier tuning of the controllers and also, because of the challenge associated with measuring the spool-valve displacement.

Figure 3.4 presents the schematic of the full-car control architecture. The control input is the electrical voltages supplied to each of the electrohydraulic actuators and the controlled outputs remain the various suspension travel measurements at each wheel.

The control problem here is also considered in terms of the random and deterministic road disturbances at vehicle speed of $72km/h$ and $40km/h$ respectively. Coupling of the dynamics of the wheels is expected to manifest clearly in the controller implementation results. The process of PID controllers were tuned manually using Ziegler-Nichols criterion, as explained in subsection 3.2.

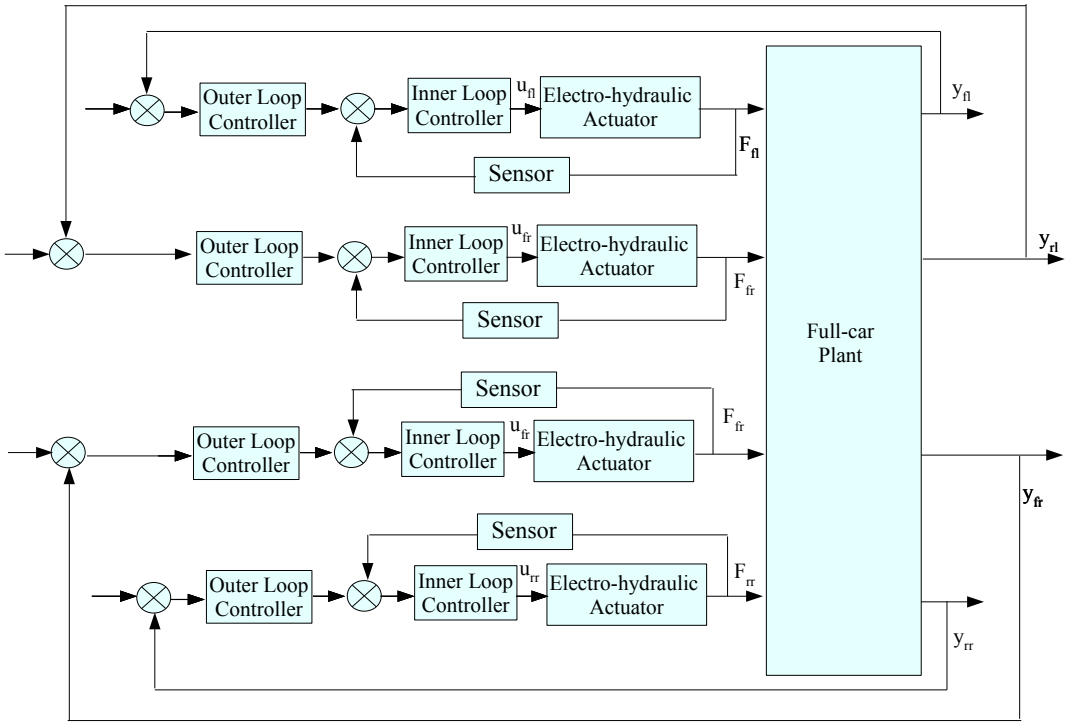

Figure 3.4: Full-Car AVSS Architecture Schematic

The control architecture in Figure 3.4 differs from the one in Figure 3.1 because it has only one inner loop (which is for the actuating force). This is necessary in order to reduce the complexity of the full-car model and enhance its tuning process, moreover the installation of a LVDT to monitor the spool-valve displacement introduces a challenge in the physical sense. Also, Ekoru et al. (2011) has shown that the use of only one inner control loop (for actuator force feedback) is sufficient in stabilising the actuator dynamics.

Responses for Deterministic Road Excitation

Table 3.3 presents the PID tuning parameters for the AVSS controllers when subjected to the twin humps, deterministic road disturbance excitations.

Table 3.3: Full-Car AVSS PID Tuning Parameters - Deterministic Road Disturbance Input

Wheel Location	Loop	PID Gains		
		K_p	K_i	K_d
Front left	Outer loop	5	1×1^{-3}	1
	Inner loop	1×10^{-3}	5×10^{-6}	1×10^{-10}
Rear left	Outer loop	1.5×10^{3}	1×10^{2}	1×10^{-3}
	Inner loop	1×10^{-3}	1×10^{-6}	1×10^{-9}
Front right	Outer loop	1×10^{3}	1×10^{2}	1×10^{-3}
	Inner loop	5×10^{-3}	1×10^{-6}	1×10^{-10}
Rear right	Outer loop	600	75	10
	Inner loop	7.513×10^{-3}	1×10^{-4}	1×10^{-10}

Table 3.4 defines the acronyms used in Figures 3.5 to 3.16. These figures presents the performance of the full-car AVSS in the presence of the deterministic and random road excitations. These performances were compared with those of the PVSS.

Attainment of the optimal trade-off based on the PID tuning becomes the challenge here. This is because originally, the response showed that suspension travel and dynamic wheel load were seriously minimised, but at the same time body acceleration had deteriorated badly, showing worse vibration attenuation to PVSS.

Table 3.4: Parameters Plotted in the Time Histories

Abbreviation	Full meaning	Abbreviation	Full meaning
ST	Suspension travel	BA	Body acceleration
PAA	Pitch angular acceleration	RAA	Roll angular acceleration
NWDL	Normalized wheel displacement	SVD	spool-valve displacement
RDI	Road disturbance input	AF	Actuator force
		CV	Control voltage

Generally there was marginal improvement in the body acceleration and pitch angular acceleration, while the roll angular acceleration followed similar trend though its plots were set out of phase at the onset of the bump.

The trend in the suspension travel and wheel dynamic load plots are similar (Please

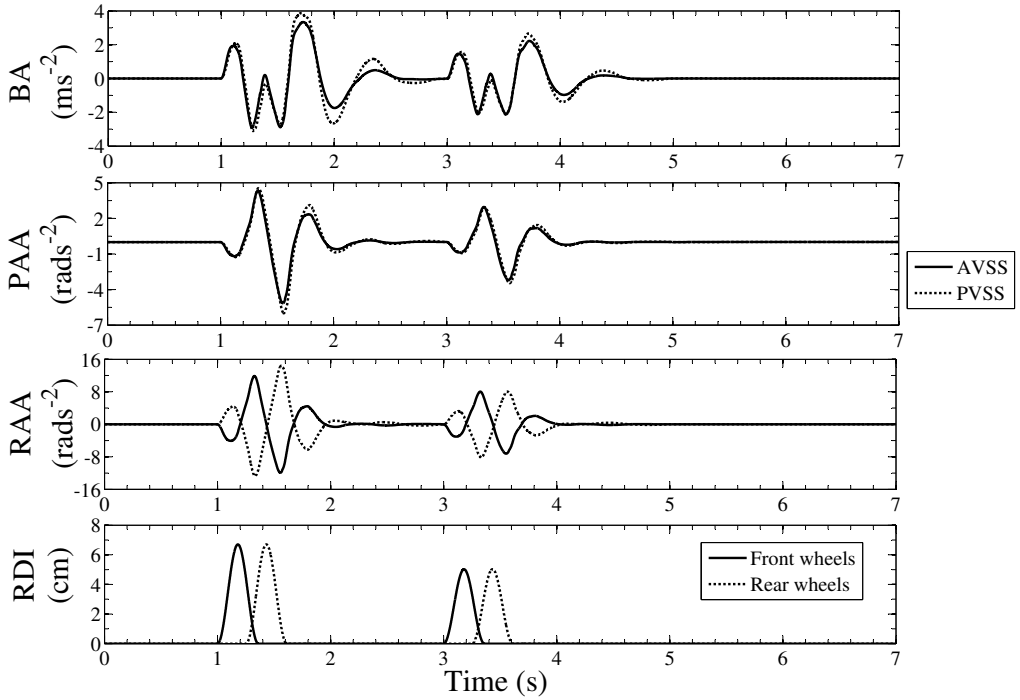

Figure 3.5: Time History of the AVSS Body Heave Acceleration and Handling Responses to Deterministic Road Excitations

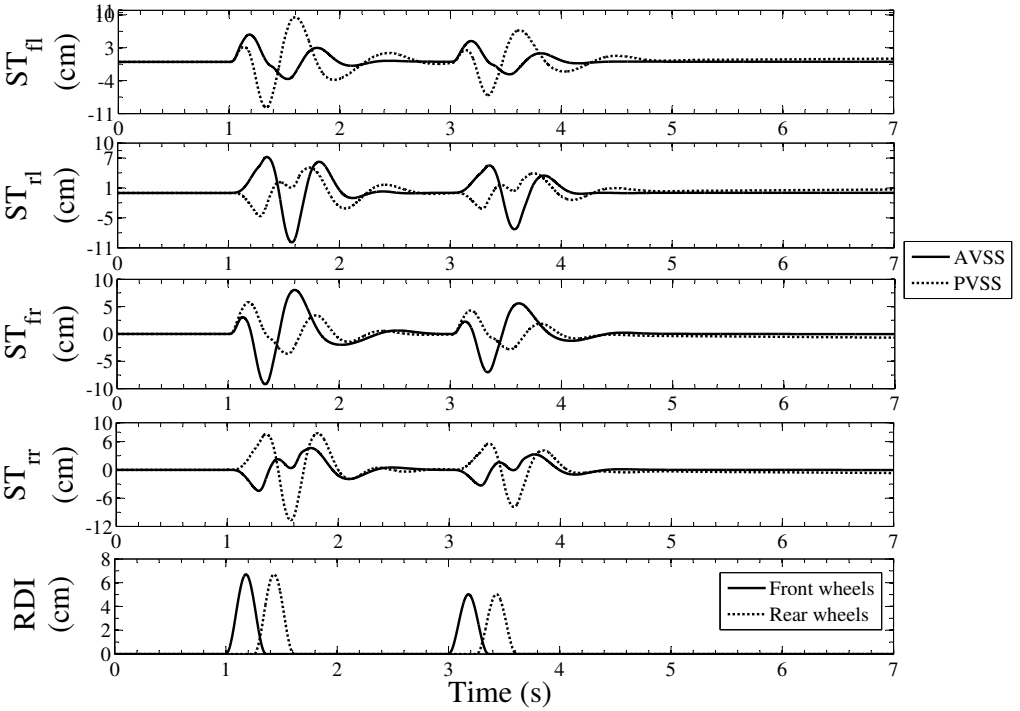

Figure 3.6: Time History of the AVSS Suspension Travel Responses to Deterministic Road Excitations

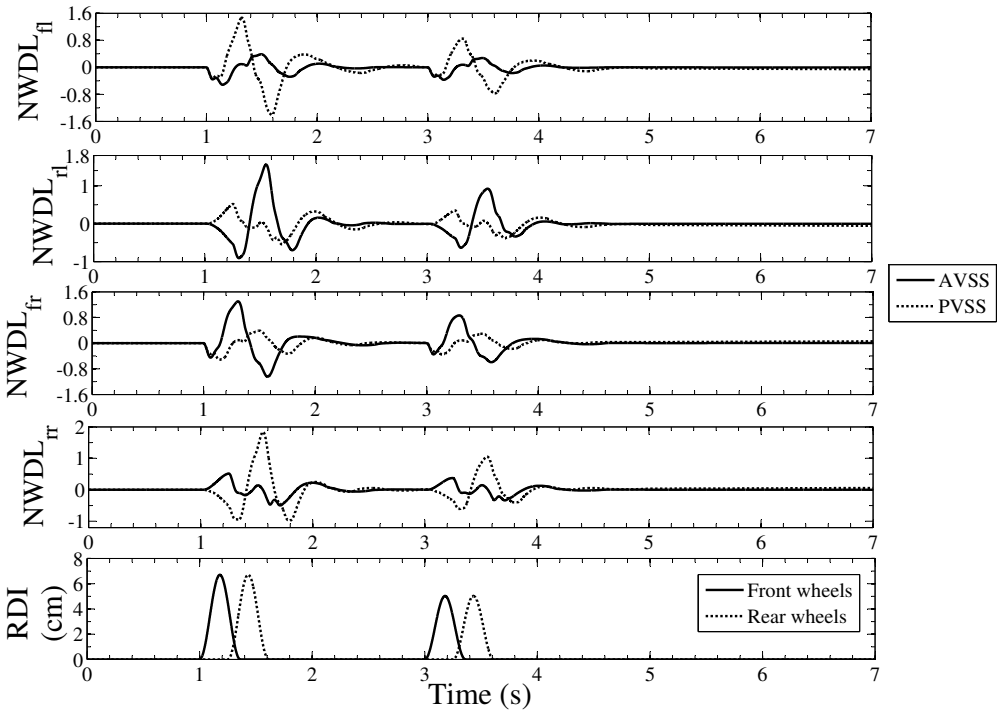

Figure 3.7: Time History of AVSS Normalized Wheel Dynamic Load Responses to Deterministic Road Excitations

see Figures 3.6 and 3.7). Both performance criteria were better minimised, as compared with PVSS for the front left and rear right suspension, but the opposite was the case for the other two suspensions.

This observation shows the impact of the coupling between the dynamics of the wheels in complicating the process of attaining optimal tuning of the controllers.

While the control voltages, actuator forces and spool-valve displacement values were all within the desired range as shown in Figures 3.8 to 3.9, the trend in their plot buttress the observations made concerning the suspension travel and wheel dynamic load responses. This is expected because these three parameters are linked to the actuators and their plots indicates the demand made of each actuator within the control process.

Responses for Random Road Excitation

The tuning parameters for the AVSS PID controllers under the influence of random road disturbance input is presented in Table 3.5.

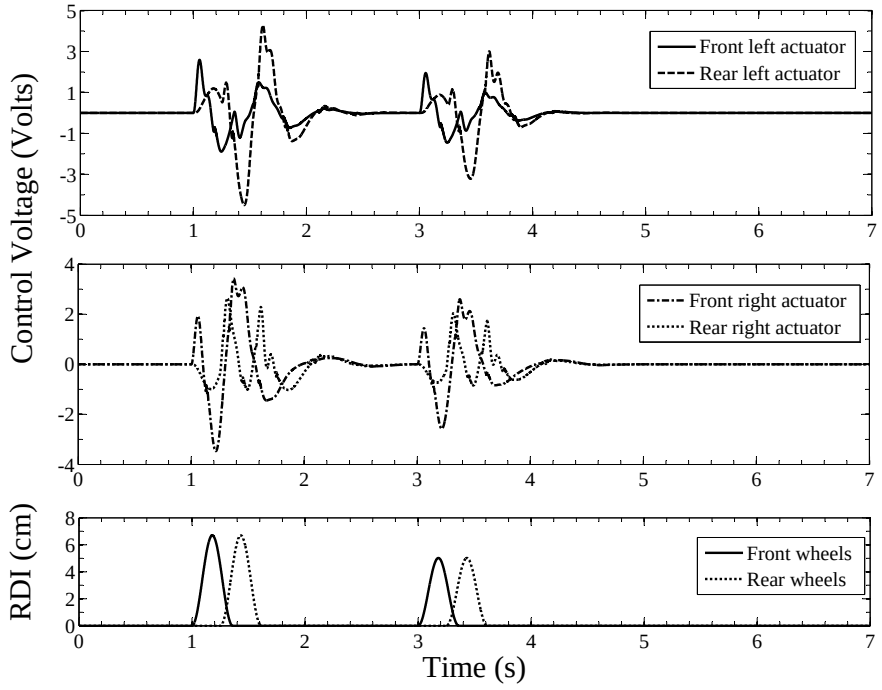

Figure 3.8: Time History of AVSS Control Voltage Responses to Deterministic Road Excitations

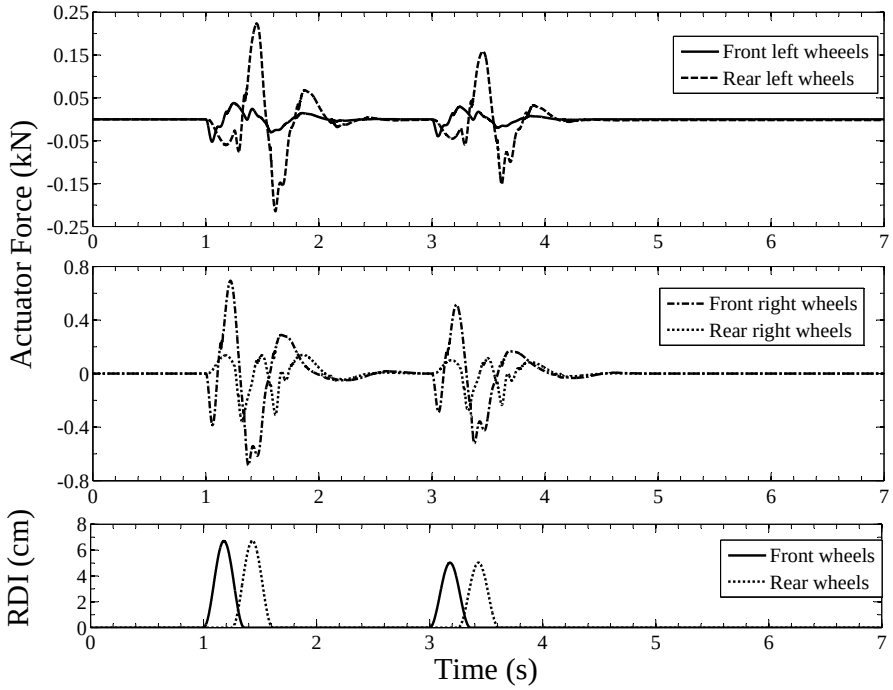

Figure 3.9: Time History of AVSS Actuator Force Responses to Deterministic Road Excitations

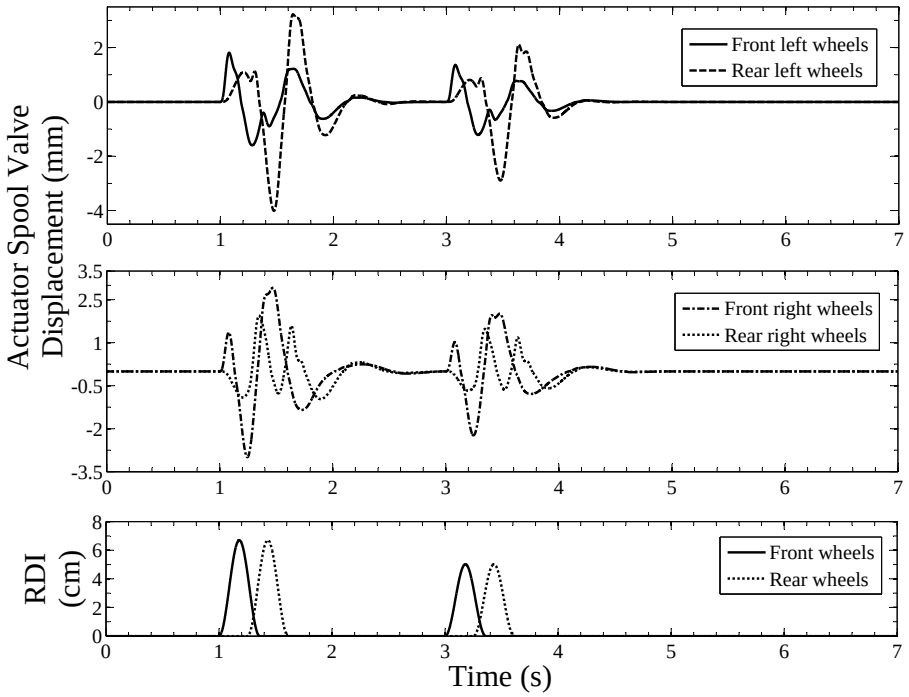

Figure 3.10: Time History of AVSS Spool-Valve Displacement Responses to Deterministic Road Excitations

Table 3.5: Full-Car AVSS PID Tuning Parameters - Random Road Disturbance Input

Wheel Location	Loop	PID Gains		
		K_p	K_i	K_d
Front left	Outer loop	4.5×10^{-2}	1×10^{-3}	1×10^{-10}
	Inner loop	5×10^{-2}	1.25×10^{-3}	1×10^{-9}
Rear left	Outer loop	2×10^{-2}	4×10^{-4}	1×10^{-9}
	Inner loop	3×10^{-2}	1.25×10^{-3}	1×10^{-12}
Front right	Outer loop	5×10^{-2}	6×10^{-3}	1×10^{-10}
	Inner loop	1×10^{-2}	1.25×10^{-3}	1×10^{-10}
Rear right	Outer loop	5×10^{-2}	3×10^{-3}	1×10^{-9}
	Inner loop	3×10^{-2}	1.25×10^{-3}	1×10^{-9}

The system responses are presented in Figures 3.11 to 3.16. Generally, the performance of the PID controlled AVSS is at par with that of the PVSS for most of the parameters considered in this case. Moreover, the peak body acceleration value over the considered road excitation spectrum was about $0.5g$.

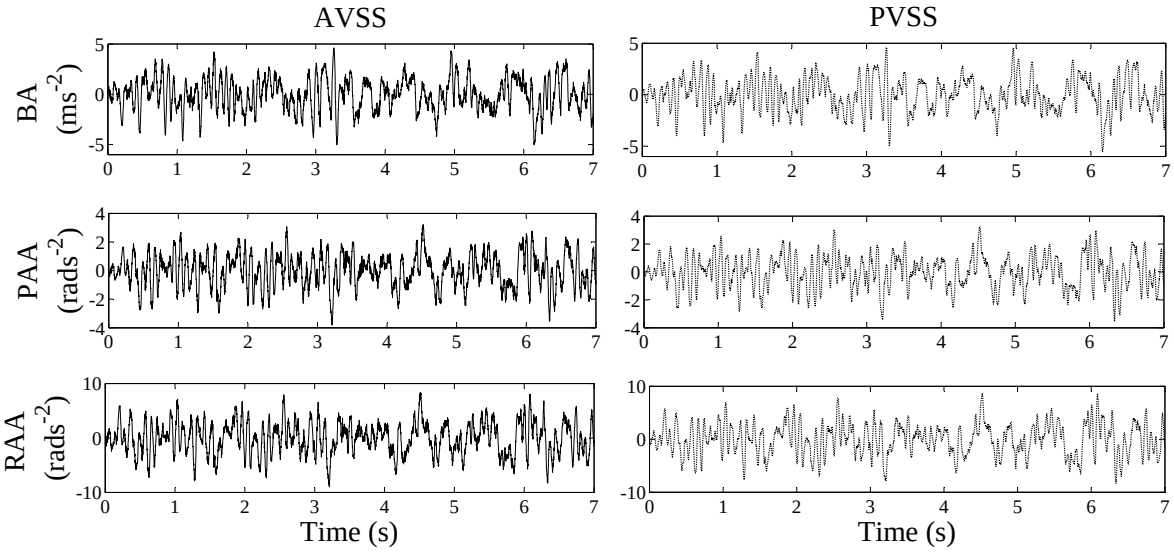

Figure 3.11: Time History of AVSS Body Heave Acceleration and Handling Responses to Random Road Excitations

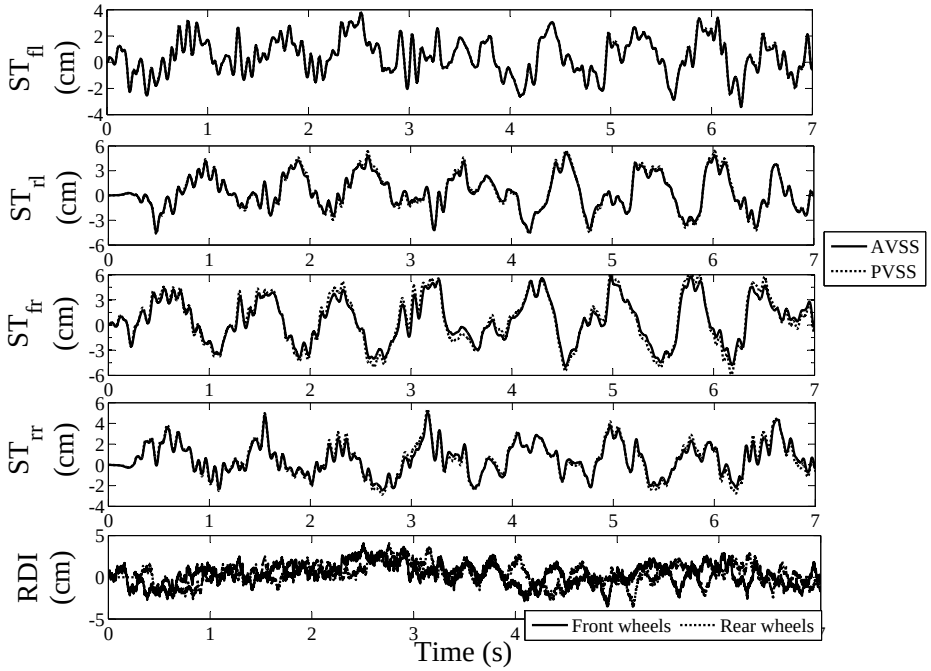

Figure 3.12: Time History of AVSS Suspension Travel Responses to Random Road Excitations

The suspension travel plots show that the peak values did not exceed $\pm 6cm$ for all

the wheels. This is less than the maximum allowable value of $\pm 10cm$. Similarly, the peak values for the normalized wheel dynamic load exceed the nominal value by about ± 0.5.

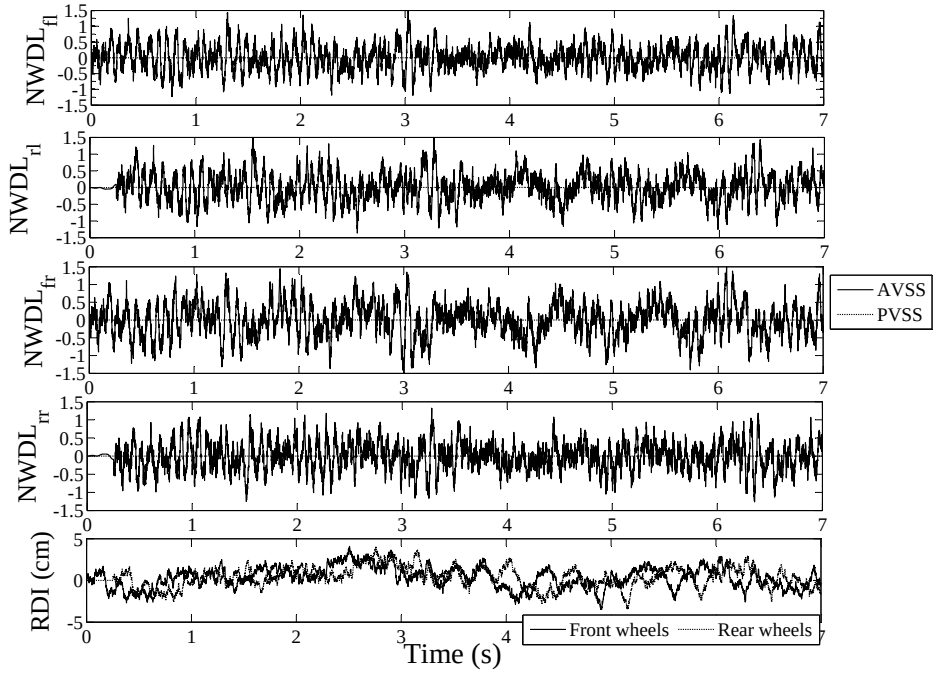

Figure 3.13: Time History of AVSS Normalized Wheel Dynamic Load Responses to Random Road Excitations

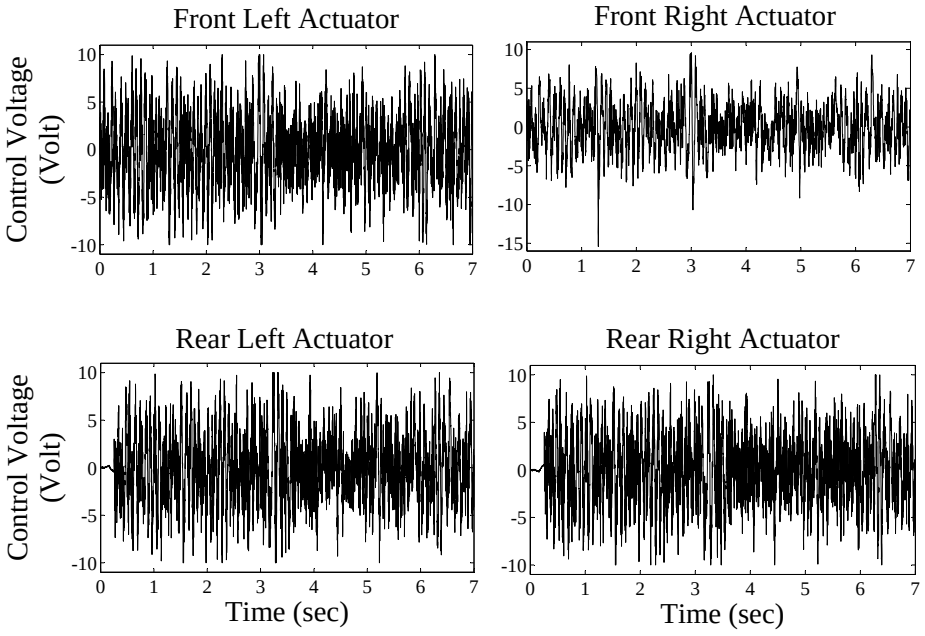

Figure 3.14: Time History of AVSS Control Voltage Responses to Random Road Excitations

Figures 3.14, 3.15 and 3.16 present the control voltage, spool-valve displacement

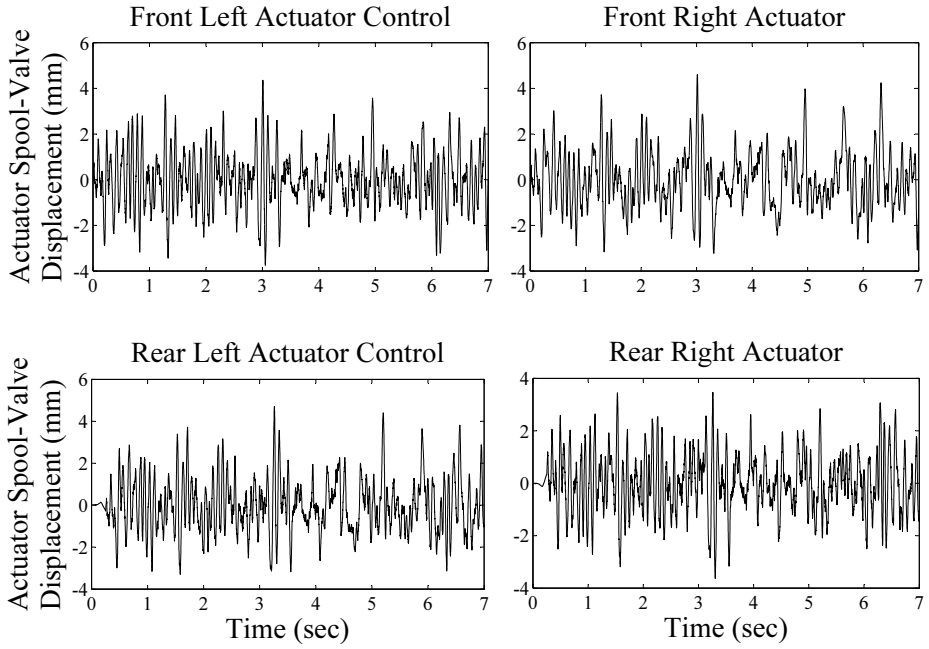

Figure 3.15: Time History of AVSS Spool-Valve Displacement Responses to Random Road Excitations

and actuator force. These are all within the maximum allowable values. The actuator force plots are however characterised by the presence of outliers. Without the outliers, the peak actuator forces are below $1kN$.

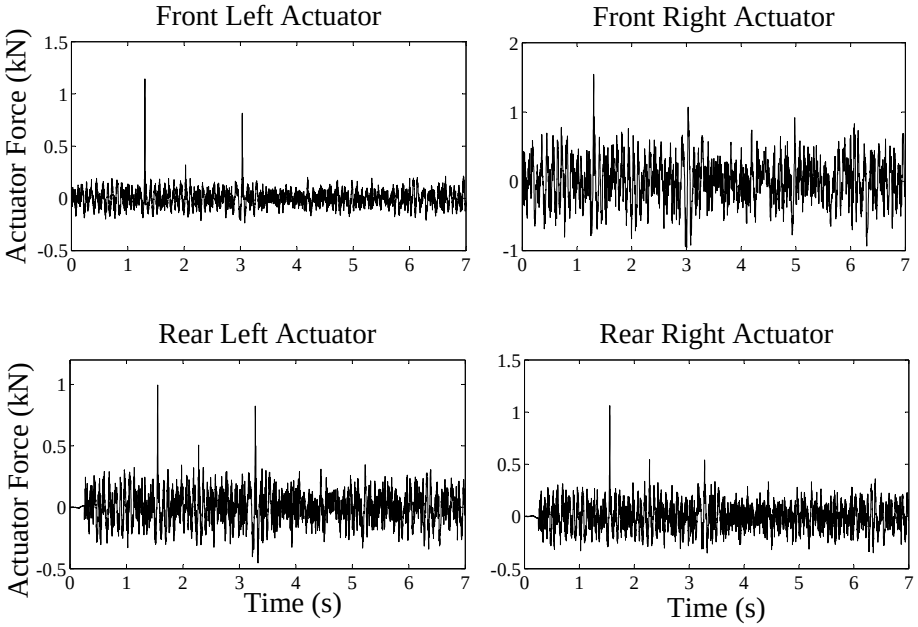

Figure 3.16: Time History of AVSS Actuator Force Responses to Random Road Excitations

3.5 Summary of Chapter Three

Design and implementation of AVSS PID control has been presented in this chapter for the quarter- and full-car models. The inner PID loop has been demonstrated to assist in stabilising the actuator dynamics thereby enabling better control by the controller in the outer loop. The performance of the PID controlled AVSS is however marginally better than the PVSS. The PID based performances will in subsequent chapter be used to benchmark the performances from the neuro-controllers designed.

4 Neural Network-Based Controller Designs for Quarter-Car AVSS

4.1 Introduction

The performance of the PID controlled AVSS exposed to random and deterministic road excitations has been evaluated in the previous chapter in terms of disturbance rejection control problem. Although the PID controllers were sensitive to disturbance input changes, they were useful in stabilising the actuator dynamics. PID controllers were therefore retained in the inner feedback loops for the neural network-based controller designs and tuned manually.

This chapter presents the design and performance analysis of two indirect adaptive neuro-controllers, namely; neural network-based feedback linearisation (also known as, NARMA-L2 or NNFBL) and neural network-based model predictive control (NNMPC). These are the most popular neural network-based indirect adaptive control schemes. In both cases, successful implementation depends on the availability of accurate dynamic models of the plant. Dynamic models to be used for the control of this plant is obtained through the system identification of the plant. Both controller employed the multilayer feedforward NN [He (2009); Jha and He (2004)].

The accuracy of the system identification process in the neural network-based indirect adaptive control methods determines its level of suitability for plant control. Direct adaptive neural network (DANN) control method avoids this requirement, and is often preferred for this reason. The indirect adaptive control method could however be a better choice where an accurate dynamic model is predictable.

Radial basis function (RBF) and multi-layered perceptron (MLP) neural network structures are employed in the neuro-controller designs. Although they are both

universal approximators with feedforward architectures, RBF is the preferred neural network structure for the direct adaptive neural network control for the following reasons:

1. Proof of stability is readily achieved using RBF NN [Behera and Kar (2009); Ge et al. (1998)].
2. Weight adjustment by backpropagation algorithm in MLP NN may not be guaranteed to converge, or could take a long while to converge thereby affecting its choice for online application [Haykin (2009); Spooner et al. (2002)].
3. RBF NN also guarantees faster learning because it constructs local mappings unlike the construction of global approximations to input-output mapping in MLP NN [Haykin (2009)].
4. RBF learning is at two levels: the centres and the weights. Only synaptic weights are involved in the MLP learning [Haykin (2009)].
5. MLP architectures are more prone to the *forgetting factor* thus, little adjustment in the weights could distort the data obtained from an initial training of the network [Azimi-Sadjadi and Liou (1992); Ge et al. (1998)].

4.2 Indirect Adaptive Neural Network-Based Controller Design

Therefore the execution of the indirect adaptive neuro-control schemes is in two stages, namely: system identification and control design. In system identification, an approximate model of the dynamic system is inferred from a set of input-output data obtained based on experiment carried out on the plant. This data is also used to *train* the neural network (NN). Training the NN involves adjusting NN parameters systematically until the training data satisfies a prescribed performance criteria (which is usually the minimization of mean squared error (MSE)). The level of accuracy of the identified model guarantees the accuracy of control operation [Dahunsi et al. (2010); Norgaard et al. (2000)].

A generalized structure describing the implementation of system identification and control is shown in Figure 4.1. Here, $y(k)$ is the controlled output, $u(k)$ is the control input, $d(k)$ makes up the disturbance signal, $\hat{y}(k)$ is the identified model's output, $\varepsilon(k) = y(k) - \hat{y}(k)$ is the model residual, θ is a vector of adjustable NN weights and

$e(k) = y_d(k) - y(k)$ is the tracking error where $y_d(k)$ is the reference trajectory.

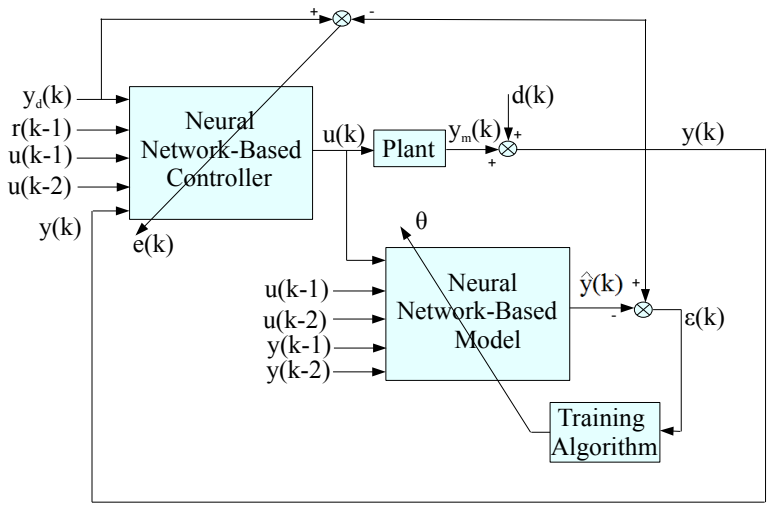

Figure 4.1: Generalized Structure for Neural Network-Based Indirect Adaptive Control

The performances of the controllers designed in this chapter were evaluated for cases under the influences of deterministic and random road disturbance inputs. They were also evaluated under constant input signal situation (that is, regulatory problem). The plant model was built in the MATLAB / SIMULINK®, all numerical experimentation were conducted using the ordinary differential equation fixed step solver (ode45) at a sampling frequency of $1kHz$.

4.2.1 System Identification

System identification consists of four processes highlighted in Figure 4.2. A positive validation of the NN plant model guarantees its suitability for use in the controller design. This is achieved when the performance criteria is met through the minimization of the MSE. This is the *prediction error criterion (PEM)*. It is an iterative process to determine the model parameters and minimise the PEM.

Experimentation

A set of input-output data pairs was collected from a numerical experiment conducted on the AVSS plant. The system was excited using a non-saturating *band-limited white noise* but *persistently exciting* (that is, random input spanning the entire operating range of the system). The use of $0.001s$ sampling interval was

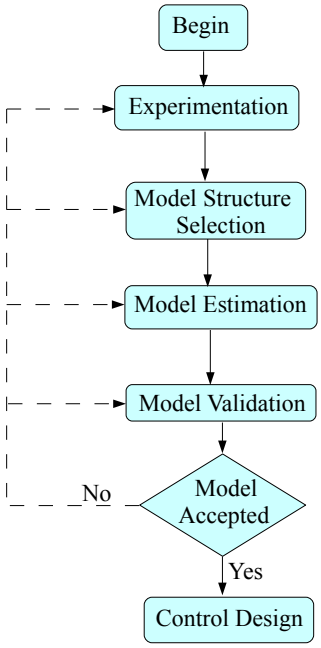

Figure 4.2: System Modelling Flowchart

based on the fastest dynamics of the system. Scaling of the collected data to zero mean and variance 1 was performed as a pre-training procedure to enable faster convergence and improve numerical stability [Jelali and Kroll (2003); Norgaard et al. (2000); Rouss et al. (2009); Yu et al. (2005)].

The generated experimental data is collected in the form:

$$Z^N = f[u(k), y(k)]; \qquad k = 1, \ldots, N \tag{4.1}$$

where Z^N is the input-output data set, $u(k) \in [\pm 10V]$ is the input signal, $y(k)$ is the output signal k is the sampling instant and N is the total number of samples. The objective of system identification is to obtain a mapping based on the input-output training data to a set of possible weights $Z^N \rightarrow \hat{\theta}$ thereby yielding $\hat{y}(k)$ predictions that are as close as possible to the true outputs, $y(k)$. This way, the training data is fitted as accurately as possible with the plant model. Figure 4.3 gives a schematic arrangement used for the numerical experimentation in Simulink®.

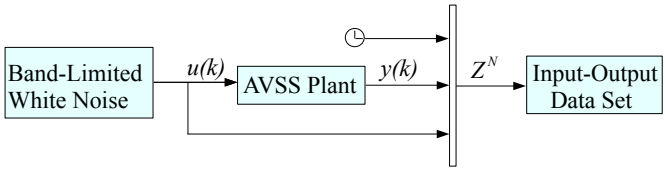

Figure 4.3: Input-Output Data Collection Arrangement

A total of 156103 input-output data samples were collected from the numerical experiment. Two $50,000$ samples sets were taken from this pool for the training

and validation data sets. At intervals in the training process, the network model is validated using the testing data set until the prediction error starts to increase indicating overfitting. The suitability of the training for online application is then checked by analysing the performance of the NN using the validation data set, this data set was not involved in the training procedure prior to this point [Demuth and Beale (2006); Haykin (2009); Lennox et al. (2001); Ljung (2006)].

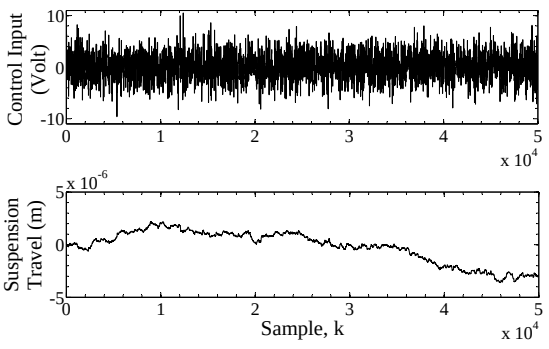

Figure 4.4: Input-Output Data Set for Neural Network Training

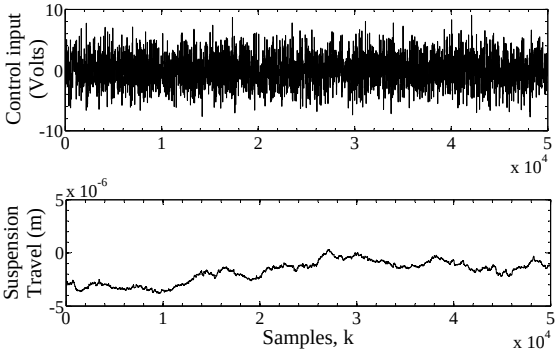

Figure 4.5: Input-Output Data Set for Neural Network Validation

Model Structure Selection

The first step in the model structure selection is to ascertain that linear models can not sufficiently represent the plant. The result of this analysis is presented in Table 4.1. The table shows the percentage fitness of the predicted output data to the measured output data.

Table 4.1: Percentage Fitness of Predicted Models

Model Type	Description	Percentage Fitness
Neuralnet	A class of NN estimators for nonlinear ARX models	99.33%
moe3	Based on output error model	38.62%
armax4	Based on autoregressive moving exogenous inputs model	43.18%
m2arx	Based on autoregressive exogenous inputs model	43.35%
m1pem	Based on prediction error estimate model	55.93%
bj5	Based on Box Jenkins polynomial model	55.68%

The superior fitness value for *neuralnet* is the justification for its adoption in modelling the system for control. Neuralnet is a class of neural network-based nonlinearity estimator. Therefore, a neural network-based model will be adequate and a single hidden layer multilayer feedforward structure is the first choice because it can readily approximate any arbitrary nonlinear function [He (2009)].

This implies that the plant can be represented by the Neural Network AutoRegressive eXogenous inputs (NNARX) or Nonlinear Autoregressive Moving Average (NARMA) model. NNARX has proven to be capable of representing any nonlinear, discrete, time-invariant system. NNARX is simpler and more stable since it is non recursive like the NARMA model [Ni et al. (1996); Rouss et al. (2009)]. NNARX is used in modelling for neural network-based model predictive control (NNMPC) while NARMA is applied in the neural network-based feedback linearisation (NNFBL) control.

The implementation of NNARX model is in two stages as illustrated in Figure 4.6. The stages involved include computation of the regressors, then linear and nonlinear mapping of the regressors in the nonlinearity estimator block.

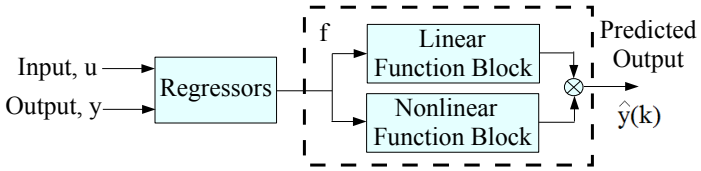

Figure 4.6: NNARX Model Structure

Therefore, the NNARX model structure representing the AVSS nonlinear system for a finite number of past inputs $u(k)$ and outputs $y(k)$ is given by [Bomberger and Seborg (1998); Jelali and Kroll (2003); Lazar and Pastravanu (2002); Norgaard et al. (2000)]:

$$y(k) = f[\phi(k), \theta] + \varepsilon(k) \tag{4.2}$$

where f is the nonlinear function that is realized by the neural network model, $\phi(k)$ represents the regressors, vector θ contains the adjustable weights and ε represents the model residual. As a result of the numerical experiment and training, the network implements an estimation of the non-linear transformation, $\hat{f}(*)$ which leads to the predicted output given by:

$$\hat{y}(k) = f[\phi(k), \theta] \tag{4.3}$$

and the regression vector is

$$\begin{aligned}\phi(k) &= [y(k-1), y(k-2), \ldots, y(k-n), u(k-d), u(k-d-1), \\ &\quad \ldots, u(k-d-m+1)] \end{aligned} \tag{4.4}$$

where d is the delay from input to the output in terms of number of samples, while n and m are the number of past outputs and inputs respectively.

The NARMA model which has been shown to be useful as exact input-output representation of nonlinear, finite-dimensional and discrete time dynamic systems in a neighbourhood of their equilibrium state. Although it has been relatively difficult to implement in control systems real time because of their nonlinearities, NN based versions, NARMA-L1 and NARMA-L2 were proposed to solve this computational challenges. NARMA-L2 remains more popular because it is relatively easier to implement practically using the MLP neural networks [Awwad et al. (2008); Demuth and Beale (2006)]. The NARMA model can be written in the following form:

$$\begin{aligned}y(k+d) &= F[y(k), y(k-1), \ldots, y(k-n+1), u(k), u(k-1), \ldots, \\ &\quad u(k-m+1)] + G[y(k), y(k-1), \ldots, y(k-n+1), \\ &\quad u(k), u(k-1), \ldots, u(k-m+1)] \cdot u(k) \end{aligned} \tag{4.5}$$

where F and G are nonlinear functions, n is the number of past outputs, m is the number of past inputs, and d is the system delay. The network is trained offline and in batch form during identification to approximate the nonlinear functions F and G. NARMA is different from NNARX in that, while both are realised in a feedforward network, the predictor in NARMA model has feedback making it recurrent [Ni et al. (1996); Rouss et al. (2009)]. Therefore Equation 4.3 can be rewritten for NARMA as

$$\begin{aligned}\phi(k) &= [y(k-1), y(k-2), \ldots, y(k-n), u(k-d), u(k-d-1), \\ &\quad \ldots, u(k-d-m+1), \varrho(k), \ldots, \varrho(k-n_\varrho+1)] \end{aligned} \tag{4.6}$$

The next step is the determination of the size of the hidden layer. This is achieved through the use of the lag space-order index plot. The theoretical basis for the determination of system order using Lipshitz algorithm is documented in the literature [Bomberger and Seborg (1998); He and Asada (1993); Jelali and Kroll (2003); Norgaard et al. (2000); Rouss et al. (2009)]. This approach is useful in estimating the number of neurons in the hidden layer of a multilayer feedforward neural network.

This method involves the plotting of the order indices based on evaluated Lipshitz quotients for the input-output data pairs against the lag space (that is, number of

past inputs and outputs), the occurrence of a prominent *knee-point* on the graph suggests the required lag space size (that is, number of past inputs and outputs) and the sum of the past inputs and output equals the number of neurons in the hidden layer.

Figures 4.7 and 4.8 presents the plots of the order of index against the number of past inputs and outputs for the data set. The number of past inputs and outputs is 3 since the knee-point occurred at 3. The adopted multilayer feedforward neural network structure is shown in Figure 4.9.

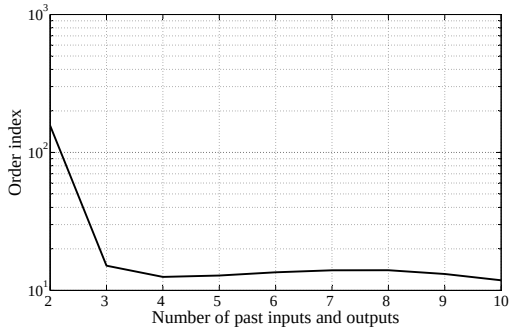

Figure 4.7: Two-Dimensional View of the Order of Index Versus Lag Space Plot

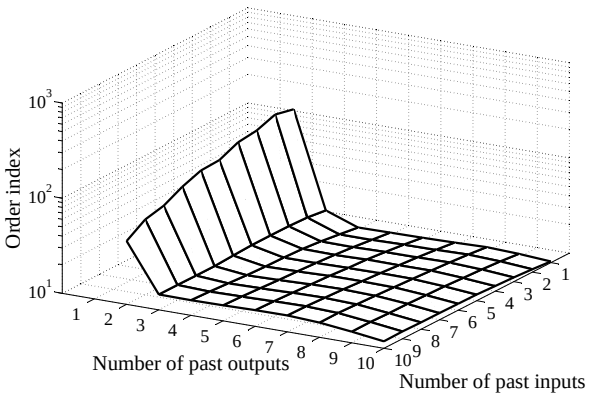

Figure 4.8: Three-Dimensional View of the Order of Index Versus Lag Space Plot

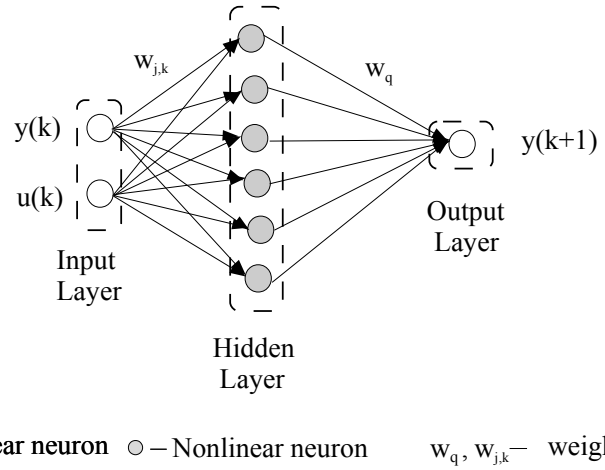

Figure 4.9: Multilayer Feedforward Neural Network Structure

Model Estimation

Feedforward multilayer perceptron neural network (MLP NN) is the selected NN structure for training the model, it is simpler when compared with other structures.

The hidden layer activation function is the tangent hyperbolic function:

$$f(x) = tanh(x) = \frac{e^x - e^{-x}}{e^x + e^{-x}} \tag{4.7}$$

while the output layer contains one neuron with a linear activation function.

Levenberg-Marquardt minimization algorithm is usually the preferred training algorithm. It converges relatively faster and it is a robust algorithm. Moreover, Levenberg-Marquardt algorithm has been known to improve over training time in comparison with other algorithms. It is a compromise between the gradient descent and the Newton optimisation methods [Dahunsi et al. (2010); Demuth and Beale (2006); Haykin (2009); Lin and Lian (2011); Norgaard et al. (2000)].

The parameters used for the system identification process are listed in Table 4.2.

Table 4.2: Parameters for the Neural Network System Identification

Parameters	Value
Total number of samples	156103
Maximum number of epochs	1000
Sampling frequency	$1KHz$
Time delay, n_k	1
Training algorithm	Levenberg-Marquandt algorithm
Number of hidden layer neurons	6
Number of past outputs, n	3
Number past inputs, m	3

Model Validation

Validation of the model is achieved based on the order of magnitude of the MSE and prediction error. After training, the validation data set is compared with the training set to ascertain a good level of fitness.

Figures 4.10 and 4.11 show the comparison of the predicted outputs against the measured outputs for the training and validation data. The level of fitness shown in both plots are acceptable while the prediction error in both cases are of the order of 10^{-8}.

Figure 4.12 also shows the performance of the NN as it was trained. Convergence was achieved with 511 epochs at a final prediction error (FPE) of 2.47×10^{-6}.

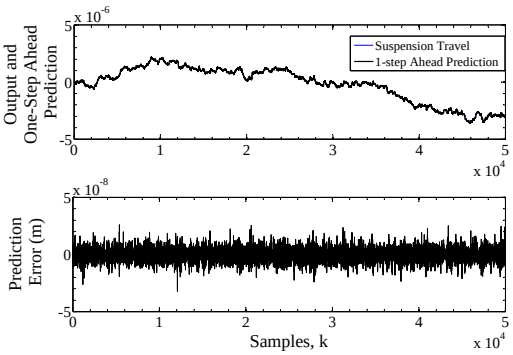

Figure 4.10: One-Step Ahead Prediction and Prediction Error for the Training Data

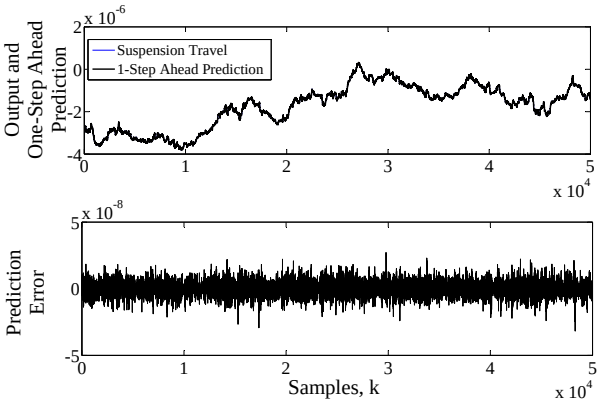

Figure 4.11: One-Step Ahead Prediction and Prediction Error for the Validation Data

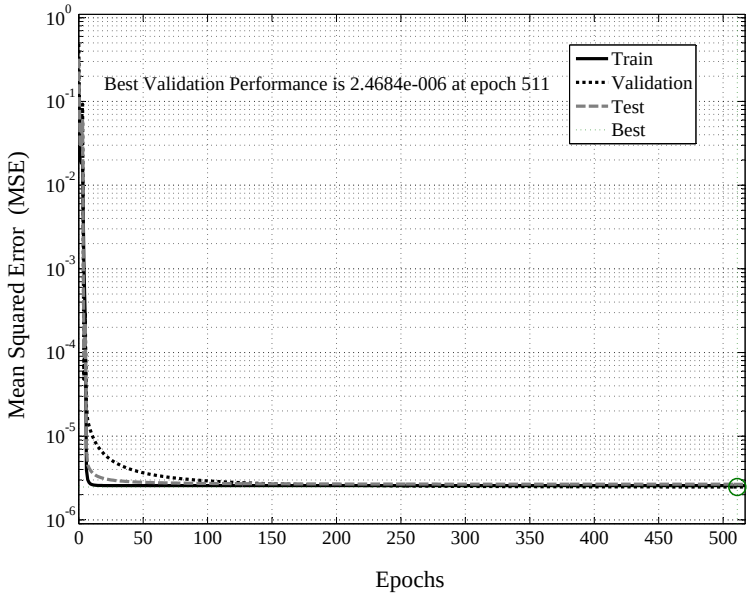

Figure 4.12: Neural Network Training Performance

4.2.2 Neuro-Controller Designs

Two different 50,000 sets of input-output data pairs shown in Figures 4.13 and 4.14 were used for the NNFBL and NNMPC controller designs. The data sets were divided into three for: training, testing and validation with the ratio 2 : 1 : 1 respectively.

Both controllers are associated with well known drawbacks, for example, NNFBL is less demanding than NNMPC computationally but has a tendency to generate chattering in the control input signal. NNMPC control involves a significant amount of online computation, it performs computation of the optimisation algorithm at each sample time for optimal control input. A successful implementation of the system

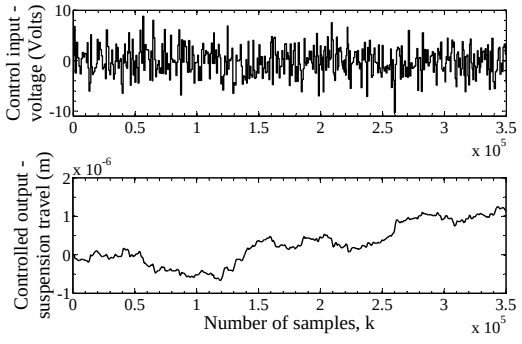

Figure 4.13: Input-Output Data Set for NNFBL (NARMA-L2) System Identification

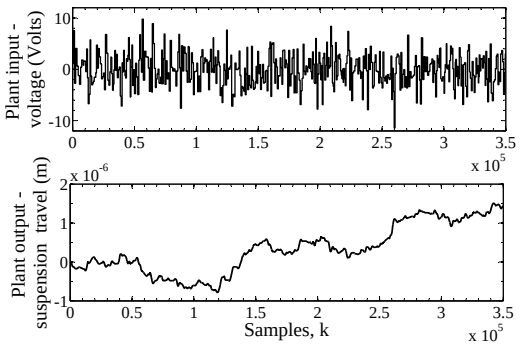

Figure 4.14: Input-Output Data Set for NNMPC

identification process is however required for the availability of an accurate dynamic model for the controller designs. The parameters used for both neuro-controller design methods are listed in Table 4.3.

Table 4.3: Parameters for the Neural Network-Based Controller Design

Parameters	Value
Total number of samples	5×10^4
Maximum number of epochs	1000
Sampling frequency	$1KHz$
Time delay, n_k	1
Training algorithm	Levenberg-Marquandt algorithm
Number of hidden layer neurons	6
Number of past outputs, n	3
Number past inputs, m	3

4.2.3 Bounded Input - Bounded Output (BIBO) Stability

Consider the affine state-space representation of the AVSS

$$\dot{\mathbf{x}} = \mathbf{f}(\mathbf{x}) + \mathbf{g}(\mathbf{x})u + \mathbf{p}(\mathbf{w}) \tag{4.8}$$

$$y = h(x) = x_2 - x_1 \tag{4.9}$$

where the state vector $\mathbf{x} = [x_1 \ x_2 \ x_3 \ x_4 \ x_5 \ x_6]^T$, the output variable $y = x_2 - x_1$, and the control input u. The system matrices $\mathbf{f}$ and $\mathbf{g}$ are:

$$\mathbf{f}(\mathbf{x}) = \begin{bmatrix} f_1(x) & f_2(x) & f_3(x) & f_4(x) & f_5(x) & f_6(x) \end{bmatrix}^T, \tag{4.10}$$

$$\mathbf{g}(\mathbf{x}) = \begin{bmatrix} 0 & 0 & 0 & 0 & 0 & \frac{1}{\tau} \end{bmatrix}^T \tag{4.11}$$

$$\mathbf{p}(\mathbf{w}) = \begin{bmatrix} 0 & 0 & 0 & -(\frac{k_t}{m_u}w + \frac{b_t}{m_u}\dot{w}) & 0 & 0 \end{bmatrix}^T \tag{4.12}$$

$$f_1(x) = x_3 \tag{4.13}$$

$$f_2(x) = x_4 \tag{4.14}$$

$$f_3(x) = \frac{1}{m_s}\Big[k_s^l(x_2 - x_1) + k_s^{nl}(x_2 - x_1)^3 + b_s^l(x_4 - x_3) - b_s^{sym}|x_4 - x_3| + b_s^{nl}\sqrt{|x_4 - x_3|}sgn(x_4 - x_3) - Ax_5\Big] \tag{4.15}$$

$$f_4(x) = \frac{1}{m_u}\Big[-k_s^l(x_2 - x_1) - k_s^{nl}(x_2 - x_1)^3 - b_s^l(x_4 - x_3) + b_s^{sym}|x_4 - x_3| - b_s^{nl}\sqrt{|x_4 - x_3|}sgn(x_4 - x_3) + k_t x_2 + b_t\dot{x}_2 + Ax_5\Big] \tag{4.16}$$

$$f_5(x) = \gamma\Phi x_6 - \beta x_5 - \alpha A(x_3 - x_4) \tag{4.17}$$

$$f_6(x) = \frac{-x_6}{\tau} \tag{4.18}$$

Meanwhile, the control objective is to design an adaptive neural network based controller for the AVSS such that its closed loop system signals are ultimately and uniformly bounded. Given that, system input $u \in \mathbb{R}^n$, state variable vector $\mathbf{x} \in \mathbb{R}^n$, unknown nonlinearity functions $\mathbf{f}(\cdot) \in \mathbb{R}^n$ and $\mathbf{g}(\cdot) \in \mathbb{R}^m$ and external disturbance $\mathbf{p}(\mathbf{w})$. The following assumptions however, need to be made:

Assumption 4.1: At least one of the elements of $\mathbf{g}(x)$ is not zero.

Assumption 4.2: $\mathbf{g}(x)$ is Lipschitz, that is, $\|\mathbf{g}(x)\| \leq \|\bar{\mathbf{g}}(\mathbf{x})\|$.

Assumption 4.3: The external disturbance is also bounded, that is, $\|\mathbf{p}(\mathbf{w})\| \leq \|\bar{\mathbf{p}}(\mathbf{w})\|$

where $\bar{\mathbf{g}}(\mathbf{x})$ and $\bar{\mathbf{p}}(\mathbf{w})$ are the upper bounds of the nonlinear function $\mathbf{g}(x)$ and the external disturbance $\mathbf{p}(\mathbf{w})$.

Moreover, it has been established that linear difference equation models are inadequate in modelling the AVSS plant, and appropriate neural network-based models, in NNARX and NARMA-L2 have been adopted. It is necessary to use the input-output behaviour of the plant to establish the model's bounded-input, bounded-output (BIBO) stability.

This is a fundamental requirement as a feedforward multilayer perceptron is introduced as an online approximator. It does not however guarantee asymptotic stability or that tracking error goes to zero. By design, NARMA-L2 can only suppress the nonlinear functions f and g, it is incapable of manipulating the internal stability of the system.

Internal stability requirement involves a well defined *relative degree* and a *minimum phase system*. These issues will be treated in the next chapter. Thus BIBO stability can be defined as follow:

Definition 1. The solution of a nonlinear function given by $\dot{x} = f(t, x)$ is uniformly and ultimately bounded within B if there exists a $B > 0$ and if corresponding to any ς and $t_o \in R^+$, there exists a $T = T(\varsigma) > 0$, which is independent of t_o, such that $\|x_o\| < \varsigma$. Thus $\|x(t; t_o, x_o)\| < B$ for all $t \geq T_o + T$. [Ioannou and Sun (1995); Nardi (2000)]

Theorem 2. *If there exists a Lyapunov function $V(t, x)$ that is defined on $0 \leq t \leq \infty$, $\|x\| \geq R$, which satisfies the following conditions:*

1. *$a(\|x\|) \leq V(t, x) \leq b(\|x\|)$ and $a(r) \to \infty$ as $r \to \infty$, where $a(\cdot) \in C$ and $b(\cdot) \in C$ are monotone increasing functions.*
2. *$\dot{V}(t, x) \leq -c(\|x\|)$, where $c(r)$ is a positive and continuous function.*

these implies that the solutions of the nonlinear function, $\dot{x} = f(t, x)$ are uniformly bounded [Bacciotti and Rosier (2005); Yoshizawa (1996)].

Theorem 3. *If $V(t, x)$ is a scalar function so that all x have continuous first partial derivatives in such a way that $V(t, x) \to \infty$ as $\|x\| \to \infty$, and $\dot{V}(t, x) < 0$ for all x outside some closed and bounded set M, then the solutions of the nonlinear function $\dot{x} = f(t, x)$ are bounded [Bacciotti and Rosier (2005); La Salle and Lefschetz (1991)]*

Definition 4. A NNARX or NARMA system is bounded-input, bounded-output stable if, and only if, any bounded input results in a bounded output.

Consider a discrete-time system given by

$$\begin{aligned} z(k+1) &= g(z(k), \ldots, z(k-n+1), u(k), \ldots, u(k-m+1)), \\ z(k_0+i) &= z_i, \qquad\qquad i = 0, 1, \ldots, n-1. \end{aligned} \tag{4.19}$$

and

$$\begin{aligned} y(k+1) &= f(y(k), \ldots, y(k-n+1), u(k), \ldots, u(k-m+1)), \\ y(k_0+i) &= y_i, \qquad\qquad i = 0, 1, \ldots, n-1. \end{aligned} \tag{4.20}$$

where g in Equation 4.19 is unknown, but its approximate model is obtainable. f is known and z represents the measured output, while y represents the predicted output. An *a priori* knowledge of m and n is available, the disturbance inputs states are bounded and not divergent. The availability of model (Equation 4.20) is a requirement for indirect adaptive neuro-control design where NNARX and NARMA are applied [Castro et al. (2010); Dzielinski (2002); Ng and Kim (2004)].

Given that boundedness connotes uniform boundedness and can be defined as follows:

Definition 5. A function $x : I_{x_0} \rightarrow \mathbb{R}$ bounded if, and only if, there exists $M \in \mathbb{R}$, such that $\|x\| \leq M$.

It follows therefore that, a function constituting a bound on the modelling error, which is the difference between f and g, bounds the norm uniformly in u. Therefore, if a modelling error yields bounded error between y and z for admissible inputs, all boundedness for y in Equation 4.19 applies for z in Equation 4.20. That is, for small modelling error, the application of any control signal to the approximate model will yield a similar behaviour in the real plant.

4.3 Neural Network-Based Feedback linearisation Control (NNFBL)

In principle, neural network-based feedback linearisation controller, which is also known as NARMA-L2 controller, transforms nonlinear system dynamics into linear dynamics, by cancelling the nonlinearities. The choice of feedback linearisation for the neuro-controller imposes the following model structure [Hagan et al. (2002); Jelali and Kroll (2003); Lazar and Pastravanu (2002); Norgaard et al. (2000)]:

$$\begin{aligned} \hat{y}(k+d) &= f[y(k), y(k-1), \ldots, y(k-n+1), u(k), u(k-1), \ldots, \\ &\quad u(k-m+1)] + g[y(k), y(k-1), \ldots, y(k-n+1), \\ &\quad u(k), u(k-1), \ldots, u(k-m+1)] \cdot u(k) \end{aligned} \tag{4.21}$$

where f and g are two nonlinear functions, the next controller input $u(k)$ is not contained in the nonlinearity and $d \geq 1$. Two separate MLP neural networks are trained to approximate the nonlinear functions $f(*)$ and $g(*)$ in the NARMA-L2 controller. The controller model can now be expressed in terms of the two neural networks F and G as follows [Hagan et al. (2002); Norgaard et al. (2000)]:

$$u(k) = \frac{\hat{y}_d(k+d) - F[y, u]}{G[y, u]} \tag{4.22}$$

where $y = [y(k), \ldots, y(k-n+1)]$ and $u = [u(k), u(k-1), \ldots, u(k-n+1)]$, also $\hat{y}(k+d)$ is the estimate of $y(k+d)$ but the system is constrained to follow a reference trajectory $\hat{y}_d(k+d)$.

The block diagram of the NARMA-L2 controller is shown in Figure 4.15, where y_d is generated by the reference model and the TDL (Tapped Delay Lines) blocks are lines of fast delays that stress preceeding values of the input signals. The controller is simply a rearrangement of the neural network plant model, which is trained in the batch form.

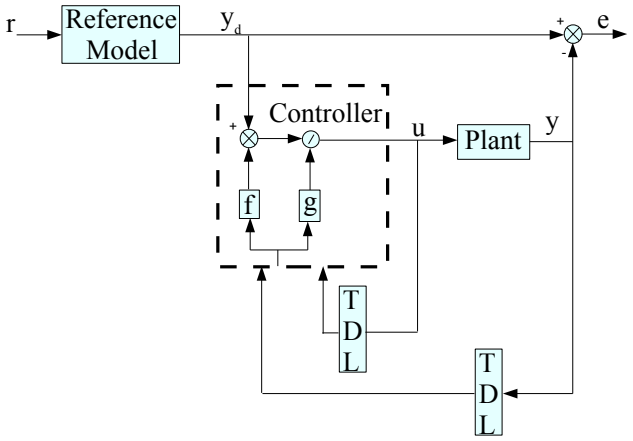

Figure 4.15: Feedback linearisation (NARMAL2) Controller

NNFBL Responses to Deterministic Road Excitations

This section presents the time response analysis for the AVSS plant to a constant reference input signal in the presence of deterministic and random road excitations whose profiles have been discussed in detail in Sections 2.6.1 and 2.6.2. Table 4.4 presents the PID tuning parameters for the actuator feedback loops.

Table 4.4: PID Tuning Parameters Used for the Inner Loops with NNFBL - Deterministic Road Disturbance Input

Sub-loop	PID Gains		
	K_p	K_i	K_d
spool-valve displacement	1×10^{-3}	1×10^{-3}	1×10^{-9}
Actuator force	1×10^{-3}	1×10^{-3}	1×10^{-9}

Figure 4.16 presents the time response for the NNFBL controller to deterministic road excitations when the reference input was constant (that is, zero). The control

input demand was maximum throughout, less than half of the rattle space was used, the spool-valve displacement and actuator force used were much lower than their maximum allowable limits.

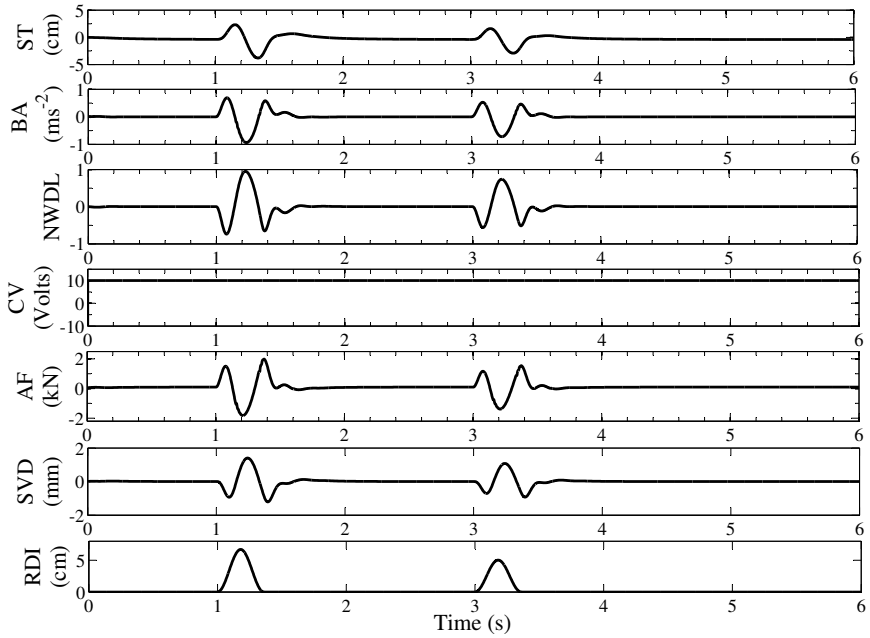

Figure 4.16: Time History of Selected System Outputs of the NNFBL-Based AVSS Responses to Deterministic Road Excitations

The peak body acceleration values oscillated between $\pm 1 ms^{-2}$ and the peak normalized wheel dynamic load also varied between $\approx \pm 1$, signifying an almost nominal road holding situation at the peak of the highest hump. The full meaning of the abbreviated parameters in the time history plots is provided in Table 4.5.

Table 4.5: Parameters Plotted in the NNFBL Graphs

Abbreviation	Full meaning	Abbreviation	Full meaning
ST	Suspension travel	BA	Body acceleration
NWDL	Normalized wheel displacement	SVD	spool-valve displacement
RDI	Road disturbance input	AF	Actuator force
		CV	Control voltage

NNFBL Responses to Random Road Excitations

The PID tuning parameters for the actuator feedback loops in the NNFBL control design with constant reference input and random road excitation are presented in

Table 4.6. Figure 4.17 presents the time response for the NNFBL controller to random road excitations when the reference input was constant (that is, zero).

Table 4.6: PID Tuning Parameters Used for the Inner Loops with NNFBL - Random Road Disturbance Input

Sub-loop	PID Gains		
	K_p	K_i	K_d
spool-valve displacement	1	1×10^{-3}	1×10^{-9}
Actuator force	1.485×10^{-5}	1×10^{-13}	1×10^{-9}

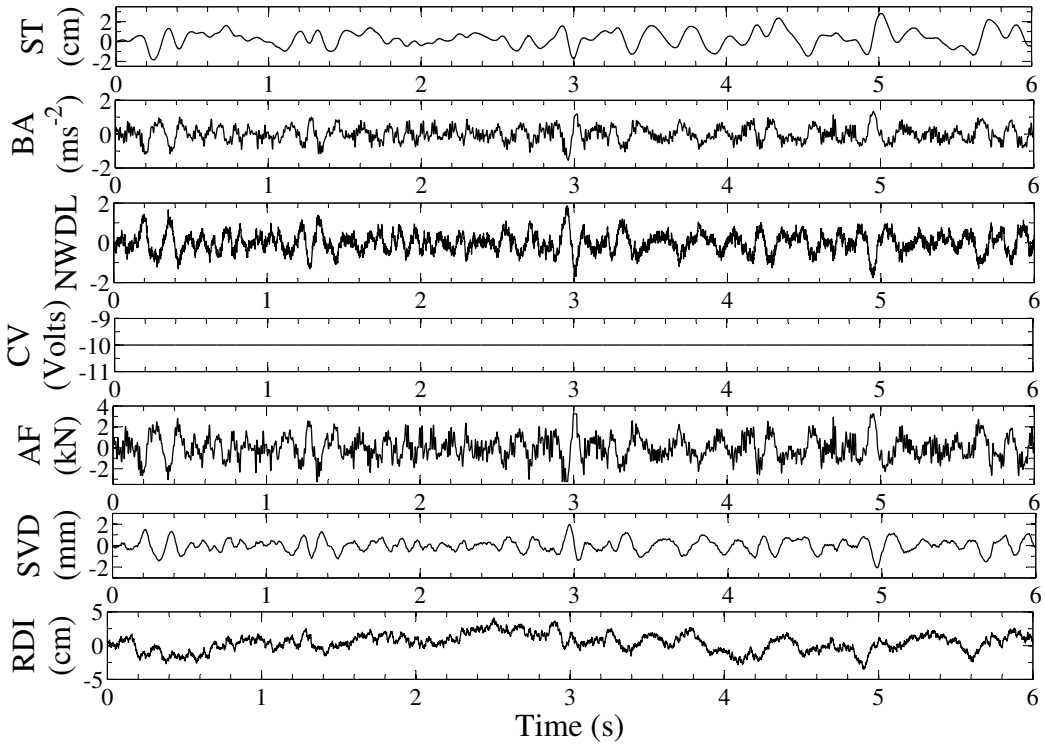

Figure 4.17: Time History of Selected System Outputs of the NNFBL-Based AVSS Responses to Random Road Excitations

In this case, the control voltage demand was also at the allowable peak value all through. While the actuator force has been cut down to about half and the spool-valve displacement, to about a quarter of the peak value for the case in which the road disturbance input was deterministic, the peak body acceleration and the normalized wheel dynamic load has been doubled. The peak suspension travel was about $2cm$.

4.4 Neural Network-Based Model Predictive Control (NNMPC)

Model predictive control is executed by solving numerical optimisation problem online. With the availability of an accurate dynamic model and measurements, it predicts future behaviour of the plant and calculates the control input required to optimise the plant performance over a specified future time horizon in the face of changing plant characteristics and constraints [Akesson and Toivonen (2006); Parlos et al. (2001)].

Its benefits lie in its suitability for online and multivariable control problems. It is also able to take into account imposed constraints on plant inputs, outputs and states. It is however prone to computational difficulties because of its iterative and dynamic optimisation approach to control problems [Akesson and Toivonen (2006); Lawrynczuk (2009)]. NARMA-L2 is relatively simpler, requires less memory, faster and less demanding computationally. However, NARMA-L2 often develops chattering in the control signal [Mokri et al. (2008); Norgaard et al. (2000)]

Tatjewski and Lawrynczuk (2006) have shown that apart from the roles NN play in system identification and predictors in NNMPC, they are also useful in reducing the computational demands by making the optimisation problem simpler (that is, convex). The typical structure for NN based model predictive control is presented in Figure 4.18.

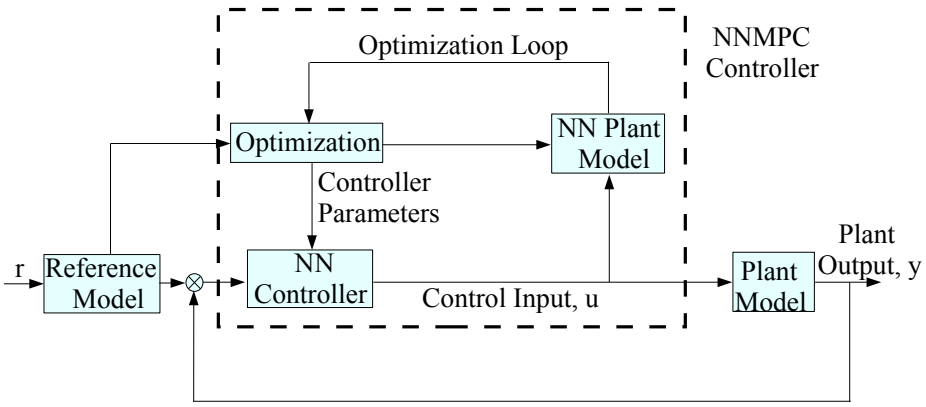

Figure 4.18: Neural Network-Based Model Predictive Control Structure

A continuous time, state-space model is given by

$$\begin{aligned} \dot{\mathbf{x}}(\mathbf{t}) &= \mathbf{f}(\mathbf{x}(\mathbf{t}), \mathbf{u}(\mathbf{t})) \\ \mathbf{y}(\mathbf{t}) &= \mathbf{h}(\mathbf{t}) \end{aligned} \tag{4.23}$$

which is subjected to state and input constraints in the form

$$u(t) \in U, \forall t \geq 0, \tag{4.24}$$

$$x(t) \in X, \forall t \geq 0, \tag{4.25}$$

where, $x(t) \in \mathbb{R}^n$ and $u(t) \in \mathbb{R}^m$ represent the vector of the states and inputs respectively. Moreover, the input constraint set U is compact, while X is connected, such that

$$U := [u \in \mathbb{R}^m \mid u_{min} \leq u \leq u_{max}] \tag{4.26}$$

$$X := [u \in \mathbb{R}^n \mid x_{min} \leq x \leq x_{max} \tag{4.27}$$

and u_{min}, u_{max}, x_{min} and x_{max} are constant vectors. In discrete time format, each consecutive sampling instant k has a set of future controls (and corresponding increments) given by:

$$\mathbf{u}(k) = \begin{bmatrix} u(k|k) \\ \vdots \\ u(k+N_u-1|k) \end{bmatrix}, \quad \mathbf{\Delta u}(k) = \begin{bmatrix} \Delta u(k|k) \\ \vdots \\ \Delta u(k+N_u-1|k) \end{bmatrix} \tag{4.28}$$

where N_u is the control horizon and $u(k+p|k) = u(k+N_u-1|k)$ for $p \geq N_u$. The MPC control variables $\mathbf{u}(k)$ are estimated at each instance to minimise differences between predicted outputs or states and the reference trajectory over the prediction horizon. Thus the control law is given by

$$u(k) = \Delta u(k) + u(k-1) = u(k|k) \tag{4.29}$$

and the measurement of the output variable is updated at the next instant k so that the prediction is moved one step forward and the whole cycle is repeated again [Akesson and Toivonen (2006); Lawrynczuk (2007)].

The optimisation process is realised through the minimization of the quadratic cost function [Lazar and Pastravanu (2002); Norgaard et al. (2000)]:

$$J(t, U(t)) = \sum_{i=N_1}^{N_2} [r(t+i) - \hat{y}(t+i)]^2 + \ \rho \sum_{i=1}^{N_u} [\Delta u(t+i-1)]^2 \tag{4.30}$$

the future controls are given by

$$U(t) = [u(t) \quad \ldots \quad u(t+N_u-1)]^T$$

and subjected to the constraint given by

$$\Delta u(t+i) = 0, \qquad N_u \leq i \leq N_2 - d$$

the tuning parameters are: N_1 - the minimum prediction horizon or minimum cost it is equal to the time delay of the system in this case; N_2 - the maximum control horizon; N_u - the control horizon; i - the order of the predictor; Δ - the differentiation operator; ρ - the weighting factor penalizing changes in the control input; and T_s - the sampling time.

The following assumptions need to be adhered to for successful implementation of the NNMPC technique and its asymptotical stability:

Assumption 4.4: The state-space model given by Equation 4.23 is sufficiently differentiable with respect to time to any order. This implies that it can readily be approximated by the use of Taylor-series expansion to required level of accuracy.

Assumption 4.5: $f(0,0) = 0$; implying that the origin is an equilibrium of the AVSS when there is no control.

Assumption 4.6: $\mathcal{D}_u \mathcal{D}_{f_x}^k h(x) = 0$, for $k = 1, \ldots, \varrho - 1$, and $\mathcal{D}_u \mathcal{D}_{f_x}^k h(x) \neq 0$, for all x and u. Given that

$$\mathcal{D}_{f_x} h(x) = \frac{\partial h(x)}{\partial (x)} f(x,u) \tag{4.31}$$

$$\mathcal{D}_{f_x}^k h(x) = \frac{\partial \mathcal{D}_{f_x}^{k-1} h(x)}{\partial (x)} f(x,u), \quad k > 1 \tag{4.32}$$

$$\mathcal{D}_u \mathcal{D}_{f_x}^k h(x) = \frac{\partial \mathcal{D}_{f_x}^k h(x)}{\partial (u)} \tag{4.33}$$

Thus, the condition for optimality is given by

$$\frac{\partial J}{\partial u} = 0 \tag{4.34}$$

Table 4.7: Parameters for the Neural Network Model Predictive Control

Parameters	Value	Parameters	Value
Control horizon, N_u	2	Cost horizon, N_2	7
Control weighting factor, ρ	0.01	Search parameter, α	0.001

NNMPC-Controlled AVSS Responses to Deterministic Road Excitations

This section presents the performances of the NNMPC controller using time-domain response plots. The assessment of the controller performance based on its responses to constant reference input in the presence of either deterministic or random road excitations. Table 4.8 presents the PID tuning parameters for the actuator feedback loops.

Table 4.8: PID Tuning Parameters - Deterministic Road Disturbance Input

Sub-loop	PID Gains		
	K_p	K_i	K_d
spool-valve displacement	10	1×10^{-3}	1×10^{-9}
Actuator force	8.5×10^{-4}	1×10^{-6}	1×10^{-9}

Figure 4.19 presents the time history plot for the responses of the NNMPC controller to the constant reference input in the presence of deterministic road excitations. Table 4.5 presents the key to the abbreviations in Figure 4.19.

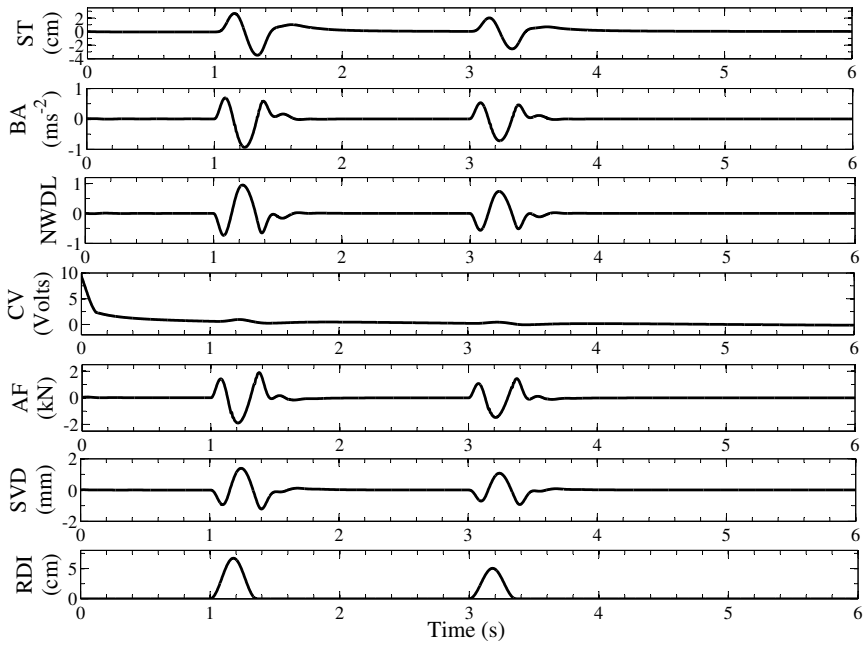

Figure 4.19: Time History of the AVSS Responses to Deterministic Road Excitations

The spool-valve displacement and actuator force were within the imposed limits based physical constraint of the system. The control voltage started to drop from $10 Volts$ to $0 Volts$ in response to constant reference input whose magnitude was zero. The trend was however marginally distorted after the first and third seconds in response to the humps.

Similarly, the suspension travel and the body acceleration are within reasonable ranges of $-4 < ST < 3cm$ and $\pm 1ms^{-2}$. The Normalized wheel dynamic load has peak values that are within the range 1.

NNMPC-Controlled AVSS Responses to Random Road Excitations

The PID tuning parameters for NNMPC controller design in the presence of random road excitations and constant reference input is presented in Table 4.9, while the time history plots for responses under the same condition are presented in Figure 4.20.

Table 4.9: PID Tuning Parameters - Random Road Disturbance Input

Sub-loop	PID Gains		
	K_p	K_i	K_d
spool-valve displacement	1	1×10^{-3}	1×10^{-9}
Actuator force	1.485×10^{-7}	1×10^{-13}	1×10^{-9}

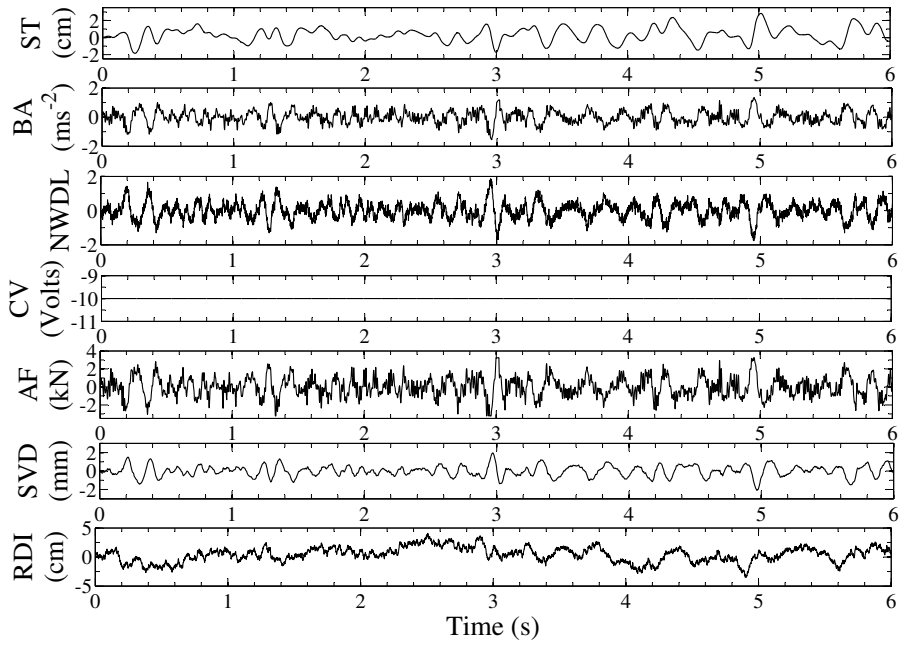

Figure 4.20: Time History of the NNMPC-Controlled AVSS Responses to Random Road Excitations

The trend in the control voltage plot is similar to the control voltage plot for the case with deterministic road excitation. The spool vale displacement values oscillated between $\pm 5mm$ but the limit values for actuator force was reached and sustained intermittently. The body acceleration and the normalized wheel dynamic load values

ranged between $\pm 2g$ and ± 2 respectively. The suspension travel was largely between $\pm 5cm$ the maximum value was approximately $10cm$.

4.5 Direct Adaptive Neural Network-Based (DANN) Controller Design

In direct adaptive neural network (DANN) control, the control law is obtained based on FBL techniques. It is expressed as a function of the nonlinearities of the system model. Approximations of the nonlinear functions can then be obtained online using a randomly initialised neural networks that is tuned based on appropriate weight update rule and a radial basis function (RBF) neural network.

The function $\mathbf{f}(\mathbf{x})$ is regarded as an unknown function in this work in order to take advantage of the universal approximation property of neural network to cater for the system uncertainties and meet the linear-in-the parameter condition for the implementation of FBL.

Direct adaptive NN-based controller implementation consists of two steps: affine system nonlinear functions approximations ($\mathbf{f}(\mathbf{x}) \approx \hat{\mathbf{f}}(\mathbf{x})$) and ($\mathbf{g}(\mathbf{x}) \approx \hat{\mathbf{g}}(\mathbf{x})$) and controller design. The nonlinear system could be expressed in the state space form:

$$\dot{\mathbf{x}} = \mathbf{f}(\mathbf{x}) + \mathbf{g}(\mathbf{x})\,\mathbf{u} + \mathbf{p}(\mathbf{w}) \tag{4.35}$$

$$\mathbf{y} = \mathbf{h}(\mathbf{x}) \tag{4.36}$$

The control law u will be required to perform an output tracking in such a way that the plant follows the desired output y_d with an acceptable level of accuracy [Chemachema and Belarbi (2011); Kar and Behera (2009); Park et al. (2009); Yesildirek and Lewis (1995)].

Given that $\mathbf{x} \in \mathbb{R}^n$ is the state vector, $\mathbf{u} \in \mathbb{R}^m$ is the vector of inputs, $\mathbf{y} \in \mathbb{R}^m$ is the vector of the outputs and $\mathbf{h} : \mathbb{R}^n \to \mathbb{R}^m$ $\mathbf{f}, \mathbf{g} : \mathbb{R}^n \to \mathbb{R}^n$ are smooth functions on the state space $\mathbb{R}^n$. The goal of the input-output linearisation is to develop a control input of the form:

$$\mathbf{u} = \mathbf{a}(\mathbf{x}) + \mathbf{b}(\mathbf{x})\,\nu \tag{4.37}$$

where

$$\mathbf{a}(x) = -\frac{\hat{\mathbf{f}}[\mathbf{x}(\mathbf{t})]}{\hat{\mathbf{g}}[\mathbf{x}(\mathbf{t})]} \quad ; \quad \mathbf{b}(x) = \frac{1}{\hat{\mathbf{g}}[\mathbf{x}(\mathbf{t})]} \tag{4.38}$$

such that there is a linear input-output mapping between the new input ν (also known as *virtual* control input) and the output $\mathbf{y}$, while the states remain bounded.

Then the function approximation is based on the application of the universal function approximation feature of the artificial neural network. This is illustrated by Figure 4.21.

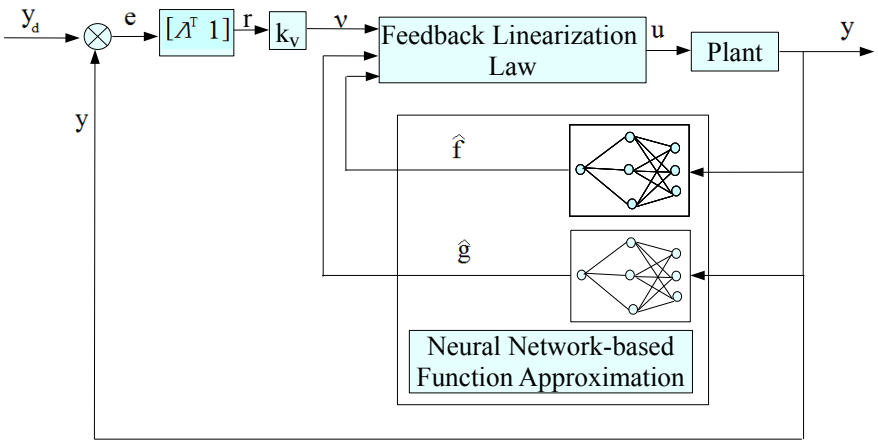

Figure 4.21: Schematic Illustration of NN-Based Feedback Linearisation

Since the nonlinear function $\mathbf{g}(x)$ is known, $\mathbf{f}(x)$ is approximated by $\hat{\mathbf{f}}(x)$ using an RBF NN structure expressed as

$$\phi_j = \sum_{i-1}^{n} exp\left[\frac{-\|x_i - c_j\|^2}{2\sigma^2}\right] \tag{4.39}$$

where ϕ_j is the output of the j^{th} RBF neuron and c_j is its centre. The spread of the RBF centres σ is taken as the standard deviation. Each unit has n inputs; x_i is the i^{th} input. Figure 4.22 shows a schematic diagram of a RBF network with four inputs and two output layer nodes.

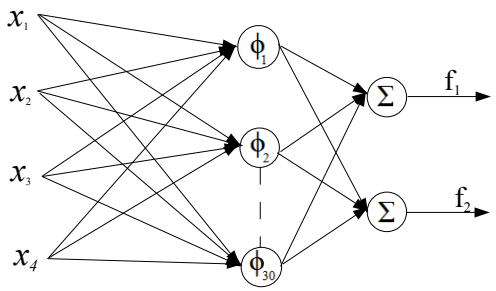

Figure 4.22: The Radial Basis Function Neural Network Structure

The hidden layer contained 30 neurons making the weight matrix W a 30×2 matrix. The neuron centres are chosen randomly between values ranging from 0 to 1. The remaining parameters are vectors whose elements are chosen to meet the required performance, that is: $F \cdot I_{30\times30}$, $K_v \cdot I_{2\times2}$ and $\Lambda_1 \cdot I_{2\times2}$, where I stands for identity matrix, F is 1×10^{-5}, K_v is 510 and Λ_1 is 1×10^{-3}.

4.5.1 Stability Analysis

The system governing equations for the AVSS quarter-car dynamics has been presented in Equations 2.4 - 2.7, and in Equations 4.40- 4.45, in state-space representation. The state-space representation shows that the system belongs to the control affine class.

Using the state-space representation, the system governing equations can be presented as

$$\dot{\mathbf{x}} = \mathbf{f(x)} + \mathbf{g(x)}u + \mathbf{p(w)} \tag{4.40}$$

$$y = h(x) = x_2 - x_1 \tag{4.41}$$

where the state vector $\mathbf{x} = [x_1 \ x_2 \ x_3 \ x_4 \ x_5 \ x_6]^T$, the output variable $y = x_2 - x_1$, and the control input u. The system matrices $\mathbf{f}$ and $\mathbf{g}$ are:

$$\mathbf{f}(\mathbf{x}) = \begin{bmatrix} f_1(x) & f_2(x) & f_3(x) & f_4(x) & f_5(x) & f_6(x) \end{bmatrix}^T, \tag{4.42}$$

$$\mathbf{g} = \begin{bmatrix} 0 & 0 & 0 & 0 & 0 & \frac{1}{\tau} \end{bmatrix}^T \tag{4.43}$$

$$\mathbf{p}(\mathbf{w}) = \begin{bmatrix} 0 & 0 & 0 & -(\frac{k_t}{m_u}w + \frac{b_t}{m_u}\dot{w}) & 0 & 0 \end{bmatrix}^T \tag{4.44}$$

$$f_1(x) = x_3 \tag{4.45}$$

$$f_2(x) = x_4 \tag{4.46}$$

$$f_3(x) = \frac{1}{m_s}\Big[k_s^l(x_2 - x_1) + k_s^{nl}(x_2 - x_1)^3 + b_s^l(x_4 - x_3) - b_s^{sym}|x_4 - x_3| + b_s^{nl}\sqrt{|x_4 - x_3|}sgn(x_4 - x_3) - Ax_5\Big] \tag{4.47}$$

$$f_4(x) = \frac{1}{m_u}\Big[-k_s^l(x_2 - x_1) - k_s^{nl}(x_2 - x_1)^3 - b_s^l(x_4 - x_3) + b_s^{sym}|x_4 - x_3| - b_s^{nl}\sqrt{|x_4 - x_3|}sgn(x_4 - x_3) + k_t x_2 + b_t\dot{x}_2 + Ax_5\Big] \tag{4.48}$$

$$f_5(x) = \gamma\Phi x_6 - \beta x_5 - \alpha A(x_3 - x_4) \tag{4.49}$$

$$f_6(x) = \frac{-x_6}{\tau} \tag{4.50}$$

4.5.2 Zero-Dynamics Analysis

Zero dynamics analysis is a necessary step in establishing that hidden states in the feedback linearisation control method is stable and will therefore not influence the stability of the linearised system negatively. The first step is by establishing the

relative order of the system, this is achieved by differentiating the output y until the control input term u appears.

The first derivative of the output is

$$\begin{aligned}\dot{\mathbf{y}} &= \frac{\partial \mathbf{h}(\mathbf{x})}{\partial \mathbf{x}} = \frac{\partial \mathbf{h}}{\partial \mathbf{x}}[\mathbf{f}(\mathbf{x}) + \mathbf{g}(\mathbf{x})\mathbf{u}] \\ &= \mathcal{L}_f\mathbf{h}(\mathbf{x}) + \mathcal{L}_g\mathbf{h}(\mathbf{x})\mathbf{u} = x_4 - x_3 \end{aligned} \tag{4.51}$$

where $\mathcal{L}_f\mathbf{h}(\mathbf{x}) = \frac{\partial \mathbf{h}}{\partial \mathbf{x}}\mathbf{f}(\mathbf{x})$, known as the Lie derivative of $\mathbf{h}$ along $\mathbf{f}$. $\mathcal{L}_g\mathbf{h}(\mathbf{x}) = \frac{\partial \mathbf{h}}{\partial \mathbf{x}}\mathbf{g}(\mathbf{x}) = 0$, implying that

$$\dot{\mathbf{y}} = \mathcal{L}_f\mathbf{h}(\mathbf{x})$$

similarly:

$$\begin{aligned}\ddot{\mathbf{y}} &= \frac{\partial(\mathcal{L}_f\mathbf{h})}{\partial x}[\mathbf{f}(\mathbf{x}) + \mathbf{g}(\mathbf{x})\mathbf{u}] = \mathcal{L}_f^2\mathbf{h}(\mathbf{x}) + \mathcal{L}_g\mathcal{L}_f\mathbf{h}(\mathbf{x})\mathbf{u} \\ &= \mathcal{L}_f^2\mathbf{h}(\mathbf{x}) = \dot{x}_4 - \dot{x}_3 \end{aligned} \tag{4.52}$$

and $\ddot{\mathbf{y}}$ is independent of $\mathbf{u}$ since $\mathcal{L}_g\mathcal{L}_f\mathbf{h}(\mathbf{x})\mathbf{u} = 0$. Also

$$\begin{aligned}\mathbf{y}^{(3)} &= \frac{\partial(\mathcal{L}_f^2\mathbf{h})}{\partial x}[\mathbf{f}(\mathbf{x}) + \mathbf{g}(\mathbf{x})\mathbf{u}] = \mathcal{L}_f^3\mathbf{h}(\mathbf{x}) + \mathcal{L}_g\mathcal{L}_f^2\mathbf{h}(\mathbf{x})\mathbf{u} \\ &= \mathcal{L}_f^3\mathbf{h}(\mathbf{x}) = \ddot{x}_4 - \ddot{x}_3 \end{aligned} \tag{4.53}$$

and $\mathbf{y}^{(3)}$ is also independent of $\mathbf{u}$ since $\mathcal{L}_g\mathcal{L}_f^2\mathbf{h}(\mathbf{x})\mathbf{u} = 0$, but

$$\begin{aligned}\mathbf{y}^{(4)} &= \frac{\partial(\mathcal{L}_f^3\mathbf{h})}{\partial x}[\mathbf{f}(\mathbf{x}) + \mathbf{g}(\mathbf{x})\mathbf{u}] \\ &= \mathcal{L}_f^4\mathbf{h}(\mathbf{x}) + \mathcal{L}_g\mathcal{L}_f^3\mathbf{h}(\mathbf{x})\mathbf{u} \end{aligned} \tag{4.54}$$

and $\mathbf{y}^{(4)}$ is dependent on $\mathbf{u}$ since $\mathcal{L}_g\mathcal{L}_f^3\mathbf{h}(\mathbf{x})\mathbf{u} \neq 0$. Therefore, the system's relative degree is 4 which is less than the system dimension of 6. Thus, it is input-output linearizable via a state feedback given by (4.37) and differential homeomorphic coordinate transformation:

$$z = \Psi(x) = [\xi \;\; \eta]^T \tag{4.55}$$

where $z_1 = y, \quad z_2 = \dot{y}, \quad z_3 = \ddot{y}, \quad z_4 = y^{(3)}$
and $z_4 = \psi_2(x) \qquad z_5 = \psi_3(x), \qquad z_6 = \psi_4(x)$
so that $\xi = [z_1 \; z_2 \; z_3 \; z_4]^T \qquad \eta = [\psi_1(x) \;\; \psi_2(x)]^T$
the linearised system in state space form is therefore given by:

$$\dot{\eta} = f_0(\eta \;\; \xi) \tag{4.56}$$

$$\begin{aligned}\dot{\xi} &= A_c\xi + B_c\nu + \tilde{p}(w) \\ &= A_c\xi + B_c\left[\frac{\mathbf{u}(t) - \mathbf{a}(x)}{\mathbf{b}(x)}\right] + \tilde{p}(w) \end{aligned} \tag{4.57}$$

$$y = C_c\xi \tag{4.58}$$

$$A_c = \begin{bmatrix} 0 & 1 & 0 & 0 \\ 0 & 0 & 1 & 0 \\ 0 & 0 & 0 & 1 \\ 0 & 0 & 0 & 0 \end{bmatrix} \tag{4.59}$$

$$\mathbf{B_c} = \begin{bmatrix} 0 & 0 & 0 & 1 \end{bmatrix}^T \tag{4.60}$$

$$\mathbf{C_c} = \begin{bmatrix} 1 & 0 & 0 & 0 \end{bmatrix}^T \tag{4.61}$$

$$\tilde{\mathbf{p}}\left(\mathbf{w}\right) = \begin{bmatrix} 0 & 0 & 0 & 1 \end{bmatrix}^T \tag{4.62}$$

$\psi(x)$ is carefully chosen to satisfy the diffeomorphism conditions, and this requires that Ψ be invertible and its derivatives be continuously differentiable. Thus satisfying [Isidori (1995); Shi et al. (2010); Slotine and Li (1991)]:

$$\mathcal{L}_g \psi_i = \frac{d\psi_i}{d\mathbf{x}} \mathbf{g}(x) = 0 \qquad r+1 \leq i \leq n \tag{4.63}$$

The unobservable states based on the controller design are the ones termed η, the zero dynamics of the system is given by $\dot{\eta} = f_0(\eta \;\; 0)$ when the origin $(\eta = 0 \;\; \xi = 0)$ is an equilibrium point, thus making the system asymptotically stable.

Equation (4.52) reduces to:

$$\mathbf{y^{(4)}} = \nu \tag{4.64}$$

implying that:

$$u = \frac{1}{\mathcal{L}_g \mathcal{L}_f^3} \left[-\mathcal{L}_f^4 \mathbf{h}(\mathbf{x}) + \nu \right] \tag{4.65}$$

when the unobservable states are set aside, the following state variables can be defined

$$x_1 = x_s \qquad\qquad x_3 = \dot{x}_1 \tag{4.66}$$

$$x_2 = x_u \qquad\qquad x_4 = \dot{x}_2 \tag{4.67}$$

such that if

$$\mathbf{q_1} = [x_1 \quad x_2]^T \qquad\qquad \mathbf{q_2} = [x_3 \quad x_4]^T \tag{4.68}$$

then

$$\dot{\mathbf{q}}_\mathbf{1} = \mathbf{q_2} \tag{4.69}$$

and

$$\dot{\mathbf{q}}_\mathbf{2} = \mathbf{f}(\mathbf{q}) + \mathbf{g}(\mathbf{q})u + \mathbf{p}(\mathbf{w}) \tag{4.70}$$

where

$$\mathbf{f}(\mathbf{q}) = [f_1 \quad f_2]^T = [f_3(x) \quad f_4(x)]^T$$
$$\mathbf{g}(\mathbf{q}) = [g_1 \quad g_2]^T = [g_3(x) \quad g_4(x)]^T$$
$$\mathbf{p}(\mathbf{w}) = [p_3(w) \quad p_4(w)]^T = \left[0 \quad -\left(\frac{k_t}{m_u}w + \frac{b_t}{m_u}\dot{w}\right)\right]^T$$
$$y = h(x) = x_2 - x_1$$

$$\dot{q}_{2d} = [\ddot{x}_{1d} \quad \ddot{x}_{2d}]^T = [0 \quad 0]^T \tag{4.71}$$

and the error matrix is given by

$$e = [y_d - (x_1 - x_2) \quad y_d]^T \tag{4.72}$$

Neural network-based direct adaptive control solution to the problem can now be pursued based on Theorem 6 for continuous time SISO affine systems. In this case, the nonlinear function $\mathbf{f}(\mathbf{x})$ is unknown while $\mathbf{g}(\mathbf{x})$ is known. This enables the NN approximations to cover all the possible sources of uncertainties.

Theorem 6. *If the nonlinear function $\mathbf{f}(\mathbf{x})$ of the system given by Equation 2.8-2.13 is unknown and the function $\mathbf{g}(\mathbf{x})$ is known. The unknown function $\mathbf{f}(x)$ can be approximated as $\hat{\mathbf{f}}(\mathbf{x}) = \hat{W}^T\phi(\mathbf{x})$ using a radial basis function neural network (RBFNN), given that there exists an ideal weight vector, $\hat{W}$ such that function $f(x)$ can be written as $\mathbf{f}(\mathbf{x}) = \hat{W}^T\phi(\mathbf{x})$. The control law*

$$u = \frac{1}{\mathbf{g}(\mathbf{x})} * \Big[-\hat{\mathbf{f}}(\mathbf{x}) + K_v + \lambda_1 e^{(n-1)} + \ldots + \lambda_{(n-1)}e + \dot{x}_{nd}\Big]$$

stabilizes the system in the sense of Lyapunov stability criterion if $\hat{W}^T$ is updated based on the update law $\dot{\hat{W}} = -F\phi(\mathbf{x})r^T$ where F is a positive definite matrix [Behera and Kar (2009)].

Proof. AVSS control problem can be formulated as a tracking problem based on filtered-error approximation-based control. The primary goal is to track the desired trajectory y_d while keeping the states and control bounded. If the error dynamics of the system is given by:

$$e = y_d - y \tag{4.73}$$

where y is the controlled output and the filtered tracking error is defined as:

$$r = \Lambda^T e$$
$$r = e^{(n-1)} + \lambda_1 e^{(n-2)} + \ldots + \lambda_{(n-1)}e \tag{4.74}$$

where, $\Lambda = [\tilde{\Lambda} \quad 1] = [\lambda_1, \ \lambda_2, \ \cdots, \ \lambda_{(n-1)}, \ 1]^T$. $e^{(n-1)}$ is the $(n-1)^{th}$ derivative of e, and so on, while $\lambda_1, \ldots, \lambda_{(n-1)}$ are appropriately chosen coefficients that enable $e(t) \rightarrow 0$ exponentially as $r(t) \rightarrow 0$, (that is, $e^{n-1} + \lambda_{n-1}e^{n-2} + \cdots + \lambda_1$ is a Hurwitz polynomial). To this end, the following assumptions must made:

Assumption 4.7: The system is feedback linearizable and all the states are bounded.

Assumption 4.8: The zero dynamics of the system is stable.

Assumption 4.9: The desired trajectory y_d is assumed to be continuous and available for measurement. Also $\| \ y_d \ \| \leq G$ where G is a known bound.

Assumption 4.10:The feedback linearizable system given by Eqs (4.35) and (4.36) has well-defined relative degree p. For example,

$$\mathbf{u} = \frac{1}{\mathcal{L}_g \mathcal{L}_f^{p-1}} \Big[-\mathcal{L}_f^p \mathbf{h}(\mathbf{x}) + \nu \Big] \tag{4.75}$$

Assumption 4.11: For controllability of the system given by Eqs (4.35) and (4.36), the sign of $g(x)$ is known to be strictly positive or negative. It is assumed throughout that $g(x) \geq \tilde{g}$, given that $\tilde{g}$ is a positive constant.

The unknown function $\mathbf{f}(x)$ is approximated as $\hat{\mathbf{f}}(\mathbf{x}) = \hat{W}^T \phi(\mathbf{x})$ using a radial basis function neural network (RBFNN), given that there exists an ideal weight vector, $\hat{W}$ such that function $f(x)$ can be written as $\mathbf{f}(\mathbf{x}) = \hat{W}^T \phi(\mathbf{x})$. The control law

$$u \ = \ \frac{1}{\mathbf{g}(\mathbf{x})} * \Big[- \hat{\mathbf{f}}(\mathbf{x}) + K_v + \lambda_1 e^{(n-1)} + \ldots + \lambda_{(n-1)} e + \dot{x}_{nd} \Big] \tag{4.76}$$

therefore

$$\begin{aligned}
\dot{\mathbf{x}}_n &= \mathbf{f}(\mathbf{x}) + \mathbf{g}(\mathbf{x}) * \frac{1}{\mathbf{g}(\mathbf{x})} * \\
&\quad \Big[-\hat{f}(x) + K_v + \lambda_1 e^{(n-1)} + \ldots + \lambda_{(n-1)} e + \dot{x}_{nd} \Big] \\
&= W^T \phi(\mathbf{x}) - \hat{W}^T \phi(\mathbf{x}) + K_v + \lambda_1 e^{(n-1)} + \ldots \\
&\quad + \lambda_{(n-1)} e + \dot{\mathbf{x}}_{nd} \\
&= \tilde{W}^T \phi(\mathbf{x}) + K_v + \lambda_1 e^{(n-1)} + \ldots + \lambda_{(n-1)} e + \dot{\mathbf{x}}_{nd} \qquad (4.77) \\
\Rightarrow e^n &= \dot{\mathbf{x}}_{nd} - \dot{x}_n \\
&= -\tilde{W}^T \phi(\mathbf{x}) - K_v - \lambda_1 e^{(n-1)} - \ldots - \lambda_{(n-1)} e \qquad (4.78)
\end{aligned}$$

meanwhile the time derivative of the filtered error yields

$$\begin{aligned}
\dot{r} &= e^n + \lambda_1 e^{(n-1)} + \ldots + \lambda_{(n-1)} e + \dot{\mathbf{x}}_{nd} \\
&= -K_v r - \tilde{W}^T \phi(\mathbf{x}) \qquad (4.79)
\end{aligned}$$

The expected tracking performance will be achieved when Equation. (4.74) is a stable system and $e(t)$ is bounded, as long as the closed-loop error dynamics

$$\dot{r} = -K_v r \tag{4.80}$$

is linear and stable, and K_v and λ's are positive design parameters.

Based on the affine form of the quarter-car AVSS mathematical model, Eqs. (9 and 15), Eq.(4.76) can be rewritten as Eq. (4.81) which is the appropriate DANN multi-input multi-output (MIMO) control law [Kar and Behera (2009)].

$$u = \mathbf{g}^T(\mathbf{g}\mathbf{g}^T)^{-1}\left[-\hat{\mathbf{f}}(\mathbf{q}) + K_v r + \Lambda_1 \dot{e} + \dot{q}_{2d}\right] \tag{4.81}$$

The unknown system nonlinearity $\mathbf{f}(\mathbf{x})$ is approximated by $\hat{\mathbf{f}}(\mathbf{x}) = \hat{W}^T\phi(\mathbf{x})$ using a radial basis function (RBF) network.

The control law (Eq. (4.81)) stabilizes the system in the sense of Lyapunov since the weight update law $\dot{\hat{W}} = -F\phi(\mathbf{q})r^T$ is used. $\phi(\mathbf{x})$ is a column vector of outputs of RBF units in a network. F is a positive definite matrix whose size is determined by the number of units in the RBF network. The closed-loop error dynamics $r = \dot{e} + \Lambda_1 e$. The error signal e is the difference between the suspension travel y and the desired output y_d. Λ_1 and K_v are design parameters defined as positive definite matrices.

4.5.3 Lyapunov Stability Analysis

Stability of the system could be established based on Lyapunov's method using the weight update law.

$$V = \frac{1}{2}r^2 + \frac{1}{2}\tilde{W}^T F^{-1}\tilde{W} \tag{4.82}$$

where F is a positive definite matrix and the derivative of V with Eq. 4.79 substituted for $\dot{r}$ gives

$$\dot{V} = -K_v r^2 - \tilde{W}^T(\phi(\mathbf{x})r + F^{-1}\dot{\tilde{W}}) \tag{4.83}$$

when $\phi(\mathbf{x})r + F^{-1}\dot{\tilde{W}} = 0$

$$\dot{\tilde{W}} = -F\phi(\mathbf{q})r \tag{4.84}$$

thus implying that

$$\dot{V} = -K_v r^2 \tag{4.85}$$

also $V > 0$ and $\dot{V} \leq 0$. This establishes stability so that r, $\tilde{W}$ and $\tilde{W}$ are bounded. Further integrating and differentiating Eq. (4.85) yields

$$\int_0^\infty -\dot{V}dt < \infty$$

$$\ddot{V} = -2rK_v\dot{r}$$

and verifies the boundedness of $\dot{r}$ and $\ddot{V}$ implying that $\dot{V}$ is uniformly continuous. According to Barbalat's lemma, $\dot{V} \to 0$ as $t \to \infty$. similarly, based on Eq. 4.85,

$r \to 0$ as $t \to \infty$, thereby implying stable dynamics and the convergence of $e(t)$ to zero with time [Behera and Kar (2009); Kristic et al. (1995); Slotine and Li (1991)].

The combination of the FBL and NN enables the control design method to benefit from the strength of FBL in terms of decoupling and linearisation as well as function approximation of the NN. The system must however be guaranteed of asymptotic stability of the zero dynamics. □

4.5.4 DANN Controller Design

This section presents the performances of the DANN controller using time-domain response plots. The assessment of the controller performance based on its responses to constant reference inputs in the presence of either deterministic or random road excitations.

DANN-Controlled AVSS Responses to Deterministic Road Excitations

Tables 4.10 and 4.11 present the PID tuning parameters for the actuator feedback loops and values for the design parameters.

Table 4.10: PID Tuning Parameters - Deterministic Road Disturbance Input and Constant Reference Input

Sub-loop	PID Gains		
	K_p	K_i	K_d
spool-valve displacement	1×10^{-3}	1×10^{-6}	1×10^{-9}
Actuator force	1.3175	0.75	1×10^{-12}

Table 4.11: DANN Design Parameters - Deterministic Road Disturbance Input and Constant Reference Input

	Design Parameters		
	F	L	K_v
Values	0.01	400	910

Figure 4.23 presents the time history plot for the responses of the DANN controller to the constant reference input in the presence of deterministic road excitations. Table 4.5 presents the key to the abbreviations in Figure 4.23.

The peak values of the suspension travel range between $-3.7cm$ and $2.8cm$ which occurred at the first hump. The body acceleration ranged between $\approxeq \pm 1ms^{-2}$

similarly, the normalized wheel dynamic load ranged between $\approxeq \pm 1$. After each hump, the control input demand was at the maximum value. The control voltage was characterised by the presence of chattering at the locations of the humps.

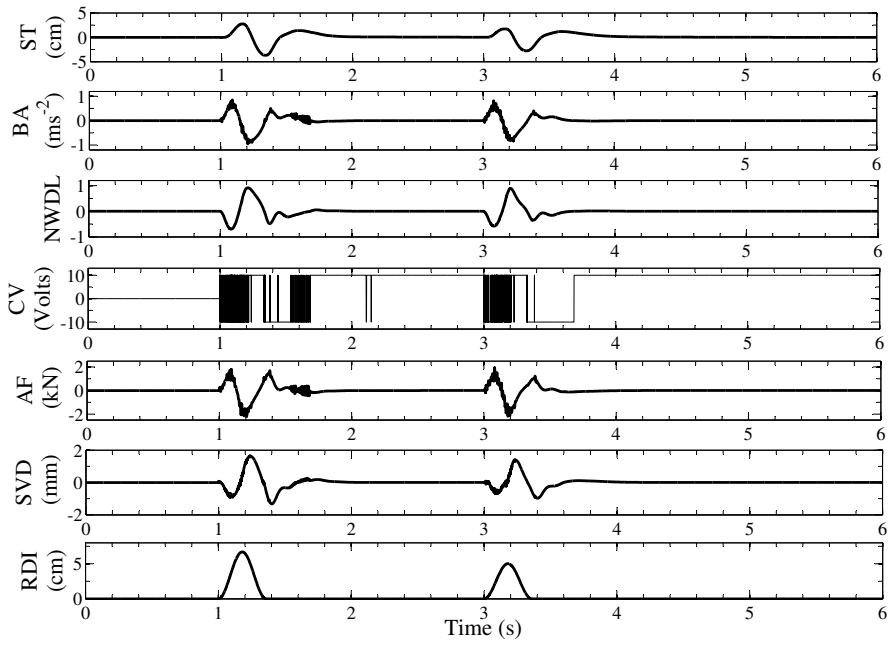

Figure 4.23: Time History of the AVSS Responses to Deterministic Road Excitations

The chattering was also visible on the body acceleration, actuator force and spool-valve displacement plots. The peak values for the actuator force and spool-valve displacement were within the allowable limits. All the signals returned to steady states after the humps within $0.6s$.

DANN-Controlled AVSS Responses to Random Road Excitations

This section presents the time domain responses of the DANN controller to constant reference and random road disturbance inputs. The PID tuning gains for the cascaded sub-loops and the DANN controller design parameters are presented in Tables 4.12 and 4.13.

Table 4.12: PID Tuning Parameters - Deterministic Road Disturbance Input

Sub-loop	PID Gains		
	K_p	K_i	K_d
spool-valve displacement	2×10^{-9}	1×10^{-10}	1×10^{-15}
Actuator force	3.7×10^{6}	1×10^{-6}	1×10^{-12}

Table 4.13: DANN Design Parameters - Deterministic Road Disturbance Input

	Design Parameters		
	F	L	K_v
Values	1×10^{-3}	1×10^{4}	1×10^{7}

Although the suspension travel did not exceed $4cm$, which is far lower than the allowable rattle space, it could not be regulated for a constant value. The suspension travel being influenced by the nature of the random road excitation oscillated about the zero reference input throughout.

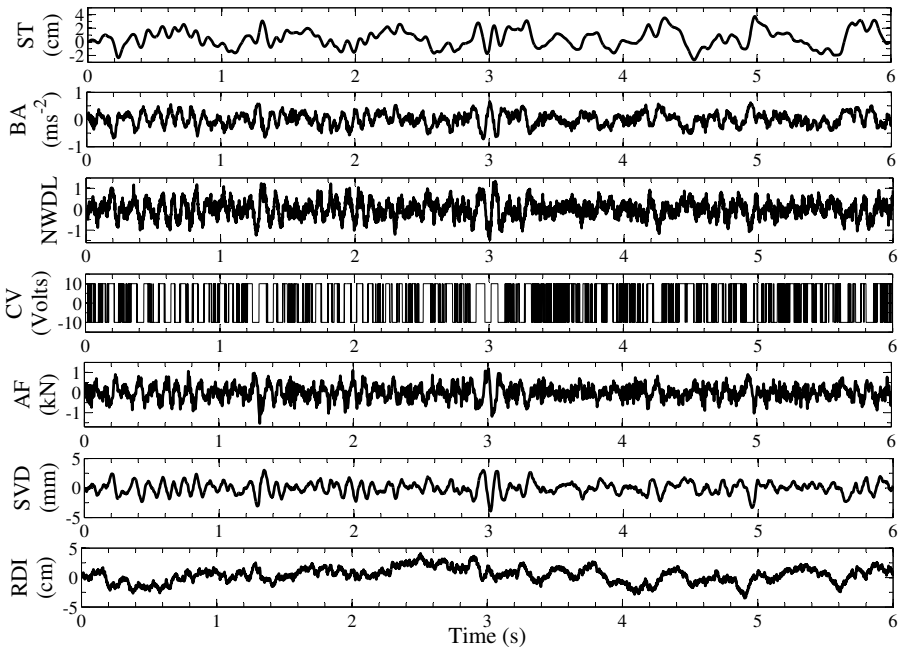

Figure 4.24: Time History of the AVSS Responses to Random Road Excitations

The control input plot was a series of combined sine-waves, oscillating between the voltage limits of the actuator. The control input also demonstrated chattering whose concentration is influenced by the amplitudes of road disturbance inputs at different points.

All the other signals were within the allowable limits. Peak values were marginally outside $\pm 1kN$. The spool-valve displacement peak values were also within $\pm 5mm$. The body acceleration was also within $\pm 1ms^{-2}$, and the normalized wheel dynamic load marginally exceeded 1 on a few occasions.

4.6 Performance Evaluation Based on Time Domain Results

This section presents comparison for the AVSS controllers in the time domain. The analysis in the first sub-section presents the comparisons of responses of the studied controllers under the influence of deterministic road disturbance input. The second subsection presents the comparisons for the cases involving random road disturbance input.

Suspension Responses to the Deterministic Road Disturbance

Studying Figures 4.25 through 4.30, a similar trend can be seen in all the graphs except in Figure 4.28 (that is the graph for control voltage). The plots for the two indirect adaptive neural network controllers (that is, NNFBL and NNMPC) are completely identical. Also, the difference between the direct and indirect adaptive neural network controllers is marginal.

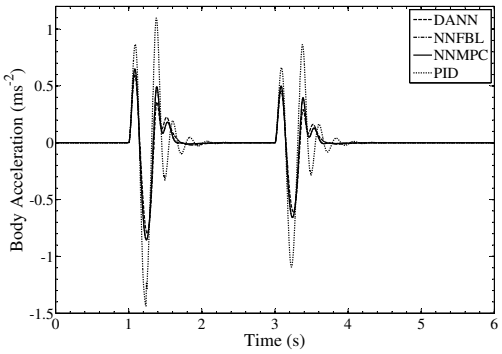

Figure 4.25: Comparison of the AVSS Body Acceleration Response for the Controllers

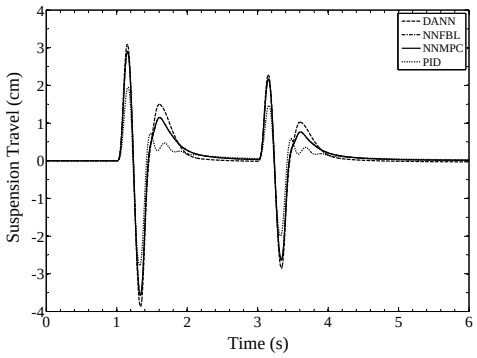

Figure 4.26: Comparison of the AVSS Suspension Travel Response for the Controllers

Figure 4.28 presents the plot for the control input to the controllers. The control input for the NNFBL was constant at the extreme value of $-10Volts$ throughout the plot. The control input for the DANN was $0Volts$ until the first hump. Afterwards, it follows a seemingly square wave pattern that is oscillating between the limit values of $\pm 10Volts$. The plot for NNMPC started from about $-1.2Volts$ and showed a cycle of oscillation each at the positions of the humps. The Control voltage plot for the PID controller maintained steady state at $0Volts$, except at the humps where there are oscillations.

Although Figure 4.30 shows that the spool-valve displacement in all the controllers is far below the maximum allowable value of $1cm$. The PID controller showed the least

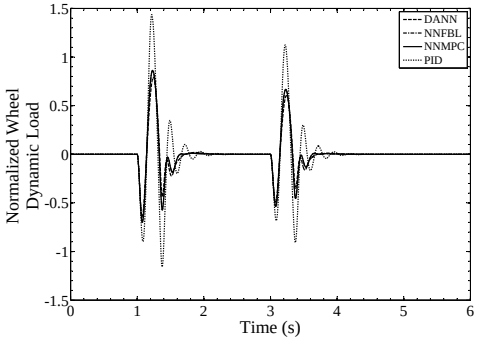

Figure 4.27: Comparison of the AVSS Normalized Wheel Dynamic Load Response for the Controllers

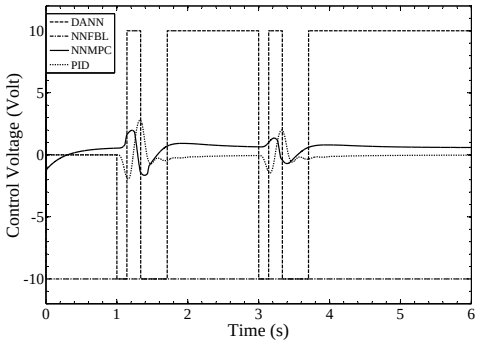

Figure 4.28: Comparison of the AVSS Control Input for the Controllers

peak values at the humps while the peak difference between the DANN, NNFBL and NNMPC spool-valve displacement demand was very marginal.

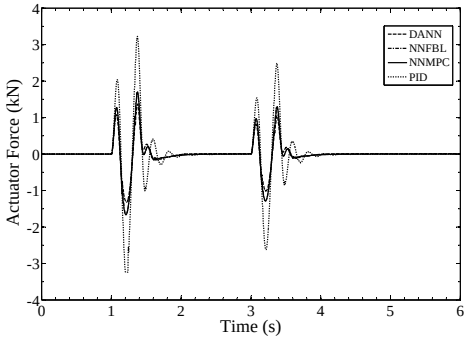

Figure 4.29: Comparison of the AVSS Actuator Force Response for the Controllers

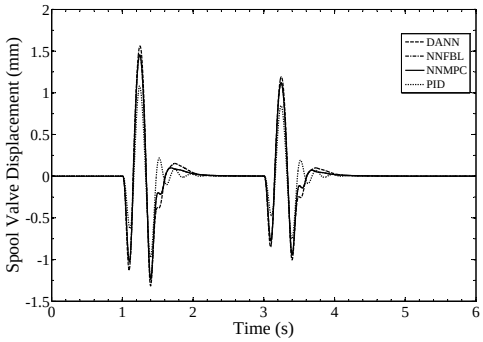

Figure 4.30: Comparison of the AVSS Spool-Valve Displacement Response to Random Road Disturbance

Suspension Responses to the Random Road Disturbance

This sub-section presents the comparisons of the responses for the controllers under the influence of random road disturbance input. The performance of the DANN controller was better for all the responses plotted except for the control input and the spool-valve displacement. The trend in DANN and NNFBL were similar in most cases, just as PID and NNMPC plots share similar trends in most cases.

The superior performance of the DANN controller, with regard to vehicle body acceleration is shown in Figure 4.31 with about half the order of magnitudes for NNMPC and PID controllers.

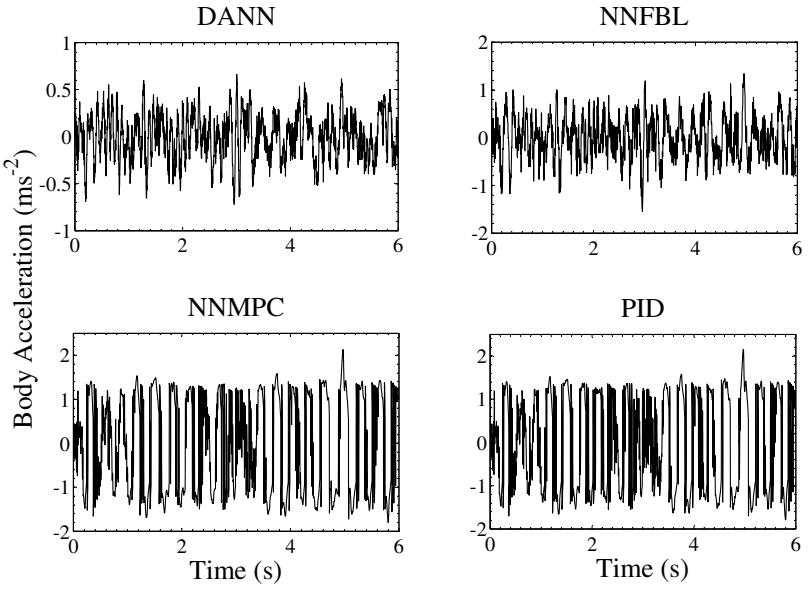

Figure 4.31: Comparison of the AVSS Body Acceleration Response for the Controllers

All the suspension controllers did not utilize the entire rattle space available, but Figure 4.32 shows that the two feedback linearisation based controllers required approximately half of the rattle space needed by the PID and NNMPC to give superior suspension performance.

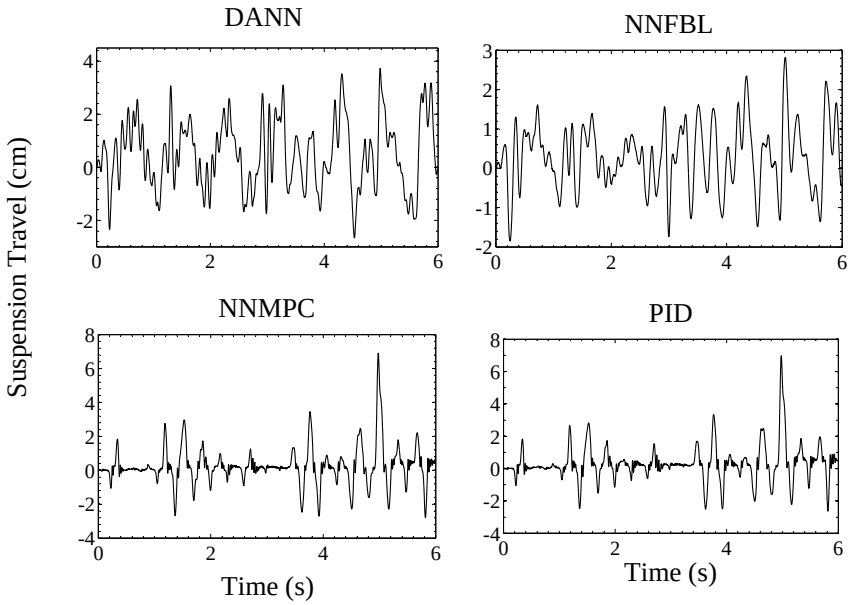

Figure 4.32: Comparison of the AVSS Suspension Travel Response for the Controllers

Figure 4.33 also shows a similar trend to the suspension travel and body acceleration

plots. The difference between the ranges of peak values for the NNFBL, NNMPC and PID plots, which is approximately $-2.5 \leq \text{NWDL} \leq 2.5$, is marginal.

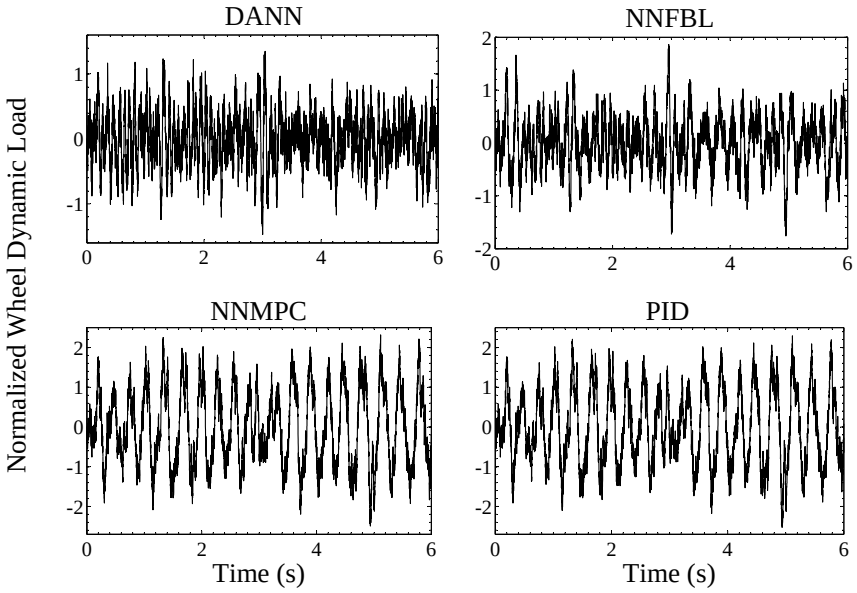

Figure 4.33: Comparison of the AVSS Normalized Wheel Dynamic Load Response for the Controllers

The control input plots for all the controllers are unique as shown in Figure 4.34. The figure also shows that the superior performances of the DANN and NNFBL controllers were achieved at the expense of their control inputs.

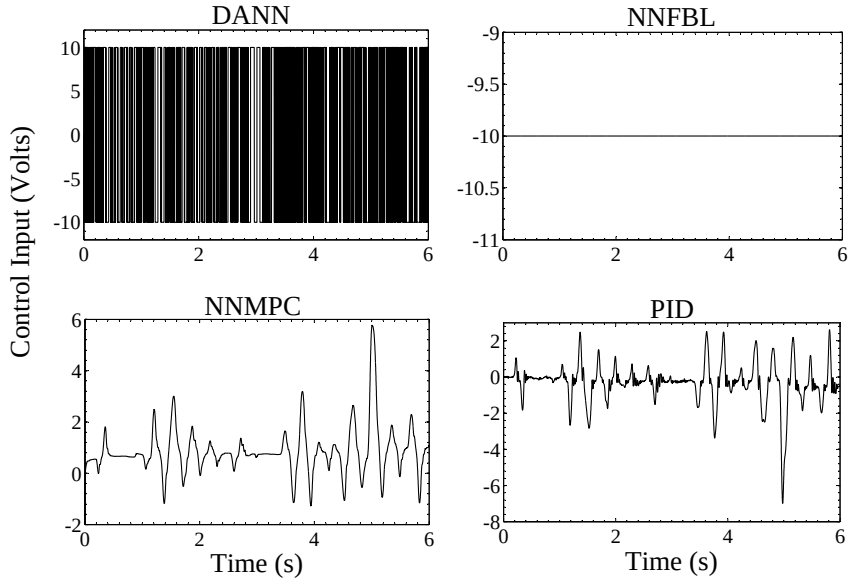

Figure 4.34: Comparison of the AVSS Control Input for the Controllers

The DANN control input consisted of continuous square wave signal oscillating between the maximum allowable values on the control input. The intensity of the oscillations directly proportional to the intensity of the waviness in the random road disturbance input.

The control input signal for the NNFBL was permanently on the $-10Volts$ mark. The control input signal for the NNMPC varied between approximately $-1.6Volts$ and $5.6Volts$. The PID controller showed similar trend but is characterised by the presence of intermittent chattering.

Figure 4.35 presents the plots for actuator force generated by the controllers. The plot for the NNMPC and PID are similar, being made up of square waves ranging between the maximum allowable values of the actuator forces. The plots for the DANN and NNFBL are within the allowable limits.

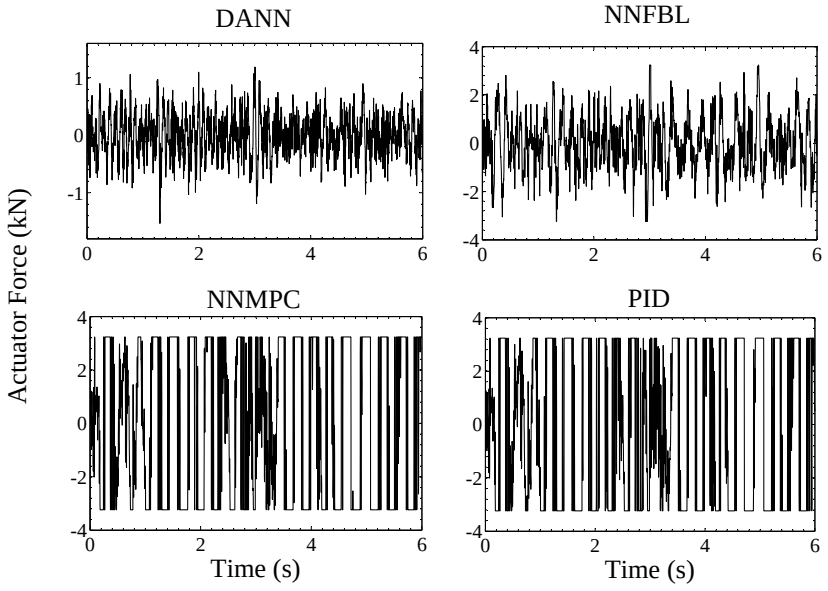

Figure 4.35: Comparison of the AVSS Actuator Force Dynamic Load Response for the Controllers

Figure 4.36 indicates the movement of the actuator spool-valve in the course of generation of the actuator forces. While the spool-valve motion in the DANN and NNFBL are in the order of millimeters, the motion in the NNMPC and PID are in the order of micrometers. This trend is similar to the pattern for the control input.

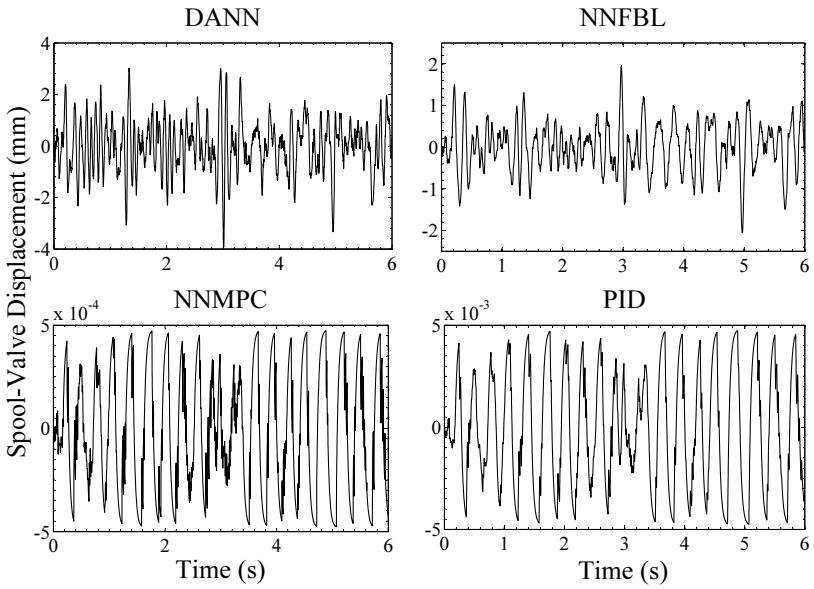

Figure 4.36: Comparison of the AVSS Spool-Valve Displacement Response for the Controllers

4.7 Performance Evaluation Based on Ride Comfort Analysis - Frequency Domain Results

Frequency domain analysis for vehicle ride comfort is important in vehicle suspension design because it provides a basis for characterising the dynamics of the system and evaluating passenger comfort. Frequency domain analysis also presents a better picture of the superior performance of fully active suspension system especially as disturbance rejection problems [ElMadany and Qarmoush (2011)].

Conventional frequency domain analysis can not be carried out on the system under study because of its nonlinear characteristics. Moreover, pseudo-frequency domain analysis can be carried out based on power spectral density (PSD) estimates using Welch algorithm in the $MATLAB/Simulink^{®}$ signal processing toolbox. Welch's method is an improvement on Bartlett's method where the signal undergoes partitioning into several overlapping segments, it is then windowed and the periodogram computed using the discrete Fourier transform. This process is shown schematically in Figure 4.37.

The following are the parameters used in computing the Welch's periodograms: the windowing function - Hanning window function; the number of points used in forming each fast Fourier transform, NFFT = 1024; length of the window, NWind = 256; and the sampling frequency of the windows was set at $85Hz$ to accommodate the

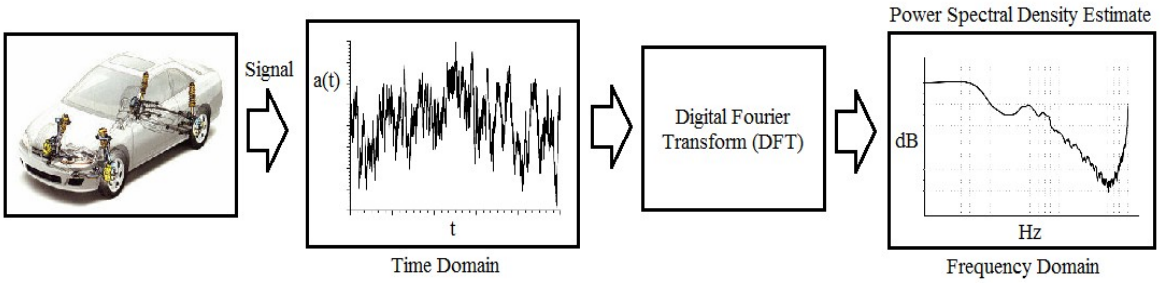

Figure 4.37: Power Spectral Density Estimate of Frequency Response

whole body vibration range.

The response gains in PSDs are measured in *Decibels (dB)* and they are estimated using Equation 4.86, where a is the measured acceleration level in m/s^2 and a_{ref} is the reference acceleration level (which is equivalent to 1 in $10^{-6}m/s^2$). Figure 4.38 shows the scale for conversion of response gains to the conventional unit of acceleration.

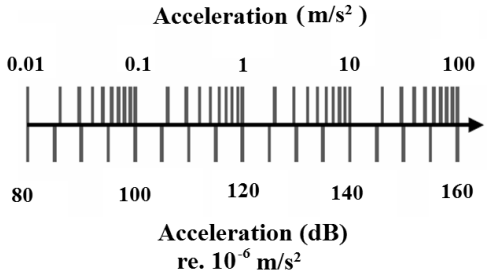

Figure 4.38: Decibel to m/s^2 Conversion

$$N(dB) = 10log_{10}\frac{a^2}{a_{ref}^2} = 20log_{10}\frac{a}{a_{ref}} \tag{4.86}$$

Figures 4.39 to 4.46 present the time and frequency domain plots of the frequency weighted RMS vertical acceleration magnitudes for deterministic and random road disturbance input to the vehicle. Similar frequency domain analysis conducted for actuator force, wheel dynamic load and suspension travel, showed similar trends to the ones for the vehicle body acceleration for all the controllers and will therefore not be reported.

4.7.1 Frequency Response Estimates for the DANN Controller

Figure 4.39 presents time and frequency domain plots for the frequency weighted RMS body acceleration of the vehicle in response to the twin humps road disturbances and DANN controller. The peak acceleration value was about $0.28ms^{-2}$ and

the response gain was on the decline from about $3.5dB$ at approximately $0.1Hz$ to about $-99.8dB$ at $63.1Hz$ where it started to climb.

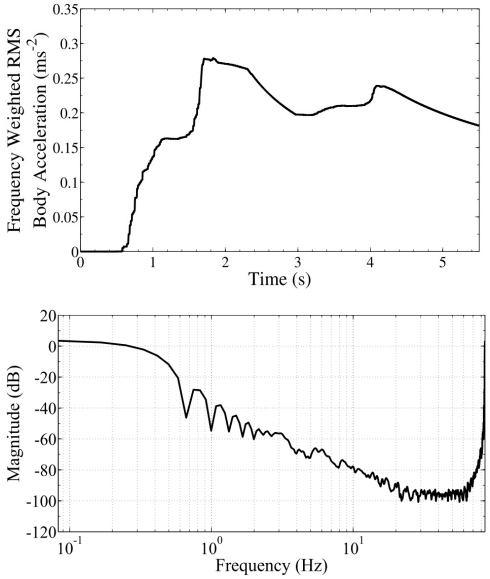

Figure 4.39: Frequency Weighted RMS Body Acceleration Response to Deterministic Road Disturbance for the DANN-Controlled AVSS

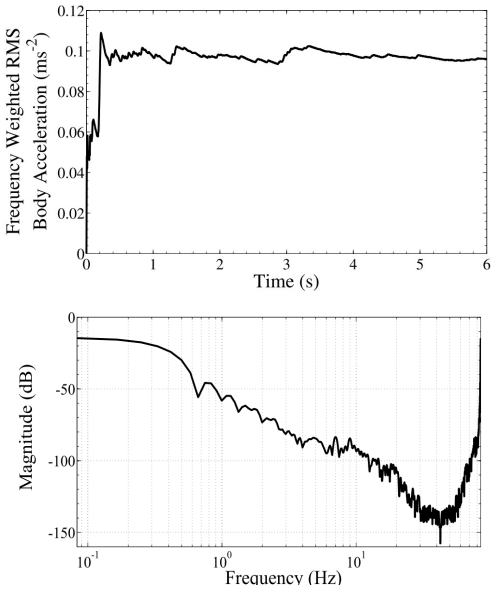

Figure 4.40: Frequency Weighted RMS Body Acceleration Response to Random Road Disturbance for the DANN-Controlled AVSS

The time and frequency domain plots in Figure 4.40 for random road disturbance input and DANN controller showed that, the peak frequency weighted RMS vertical acceleration value was about $0.11ms^{-2}$ and the response gain also declined from about $-14.67dB$ at approximately $0.1Hz$ to about $-157.7dB$ at $42.51Hz$ from where the response gain magnitude started to rise.

4.7.2 Frequency Response Estimates for the NNMPC Controller

Figure 4.41 presents the time and frequency domain plots for the frequency weighted RMS body acceleration of the vehicle in response to the deterministic road disturbances and NNMPC controller. The peak acceleration value reached was $0.3ms^{-2}$ and the response gain was on the declined from about $4.0dB$ at approximately $0.1Hz$ to about $-168.7dB$ at $41.7Hz$ where it started to rise.

Time and frequency domain plots in Figure 4.42 for random road disturbance input and NNMPC controller showed that, the peak frequency weighted RMS vertical acceleration value was about $0.44ms^{-2}$ and the response gain also declined from about $-2.37dB$ at approximately $0.1Hz$ to about $-130.10.2dB$ at $42.50Hz$ from where the response gain magnitude started to rise.

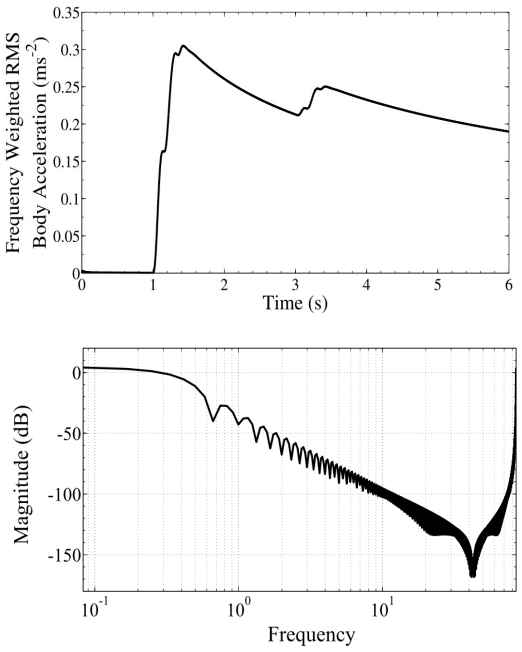

Figure 4.41: Frequency Weighted RMS Body Acceleration Response to Deterministic Road Disturbance for the NNMP- Controlled AVSS

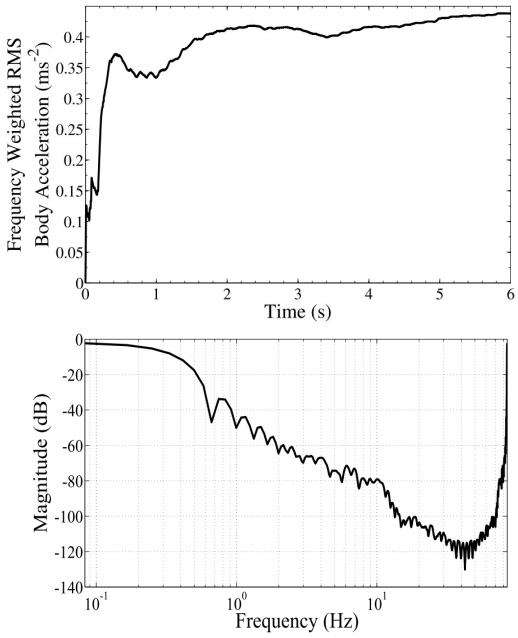

Figure 4.42: Frequency Weighted RMS Body Acceleration Response to Random Road Disturbance for the NNMPC-Controlled AVSS

4.7.3 Frequency Response Estimates for the NNFBL Controller

Figure 4.43 presents time and frequency domain plots for frequency weighted RMS body acceleration of the vehicle in response to the twin humps road disturbances and NNFBL controller. The peak acceleration value was about $0.28ms^{-2}$ and the response gain was on the declined from about $-8.6dB$ at approximately $0.1Hz$ to about $-174.4dB$ at $44.0Hz$ where it started to climb.

The time and frequency domain plots in Figure 4.44 for random road disturbance input and NNFBL controller showed that, the peak frequency weighted RMS vertical acceleration value was about $0.22ms^{-2}$ and the response gain also declined from about $-9.45dB$ at approximately $0.1Hz$ to about $-147.20dB$ at $42.51Hz$ from where the response gain magnitude started to rise.

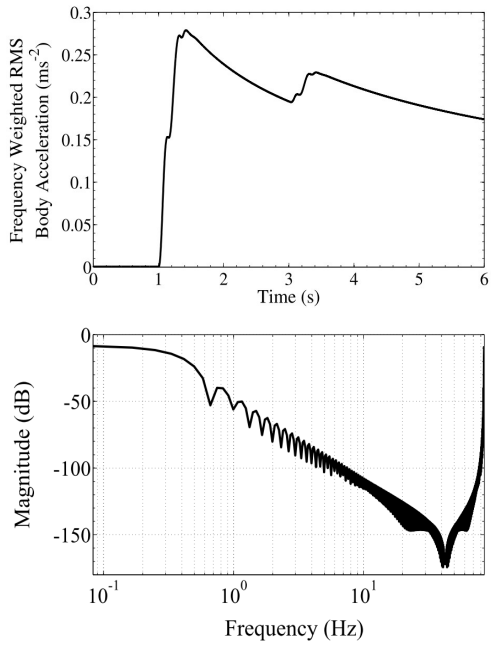

Figure 4.43: Frequency Weighted RMS Body Acceleration Response to Deterministic Road Disturbance for the NNFBL-Controlled AVSS

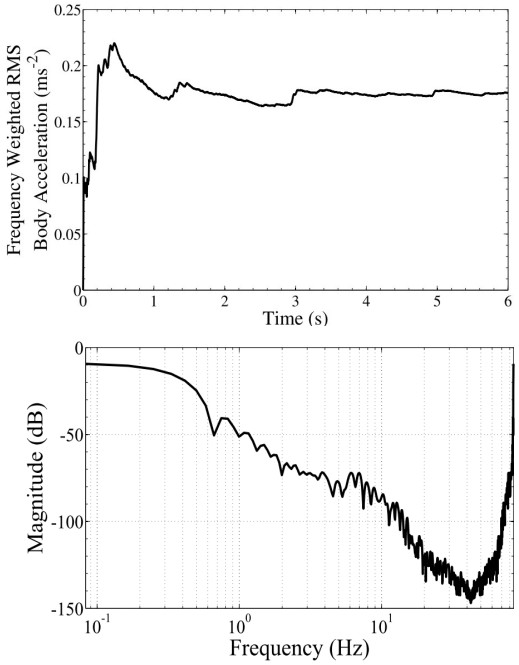

Figure 4.44: Frequency Weighted RMS Body Acceleration Response to Random Road Disturbance for the NNFBL-Controlled AVSS

4.7.4 Frequency Response Estimates for the PID Controller

Figure 4.45 presents the time and frequency domain plots for the frequency weighted RMS body acceleration of the vehicle in response to the deterministic road disturbances and PID controller. The peak acceleration value reached was $0.4ms^{-2}$ and the response gain was on the declined from about $-4.6dB$ at approximately $0.1Hz$ to about $-177.0dB$ at $42.5Hz$ where it started to rise.

The time and frequency domain plots in Figure 4.46 for random road disturbance input and PID controller showed that, the peak frequency weighted RMS vertical acceleration value was about $0.44ms^{-2}$ and the response gain also declined from about $-2.33dB$ at approximately $0.1Hz$ to about $-131.7dB$ at $42.50Hz$ from where the response gain magnitude started to rise.

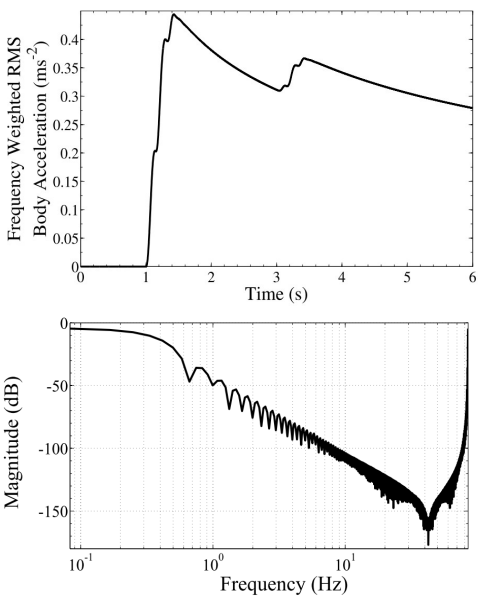

Figure 4.45: Frequency Weighted RMS Body Acceleration Response to Deterministic Road Disturbance for the PID-Controlled AVSS

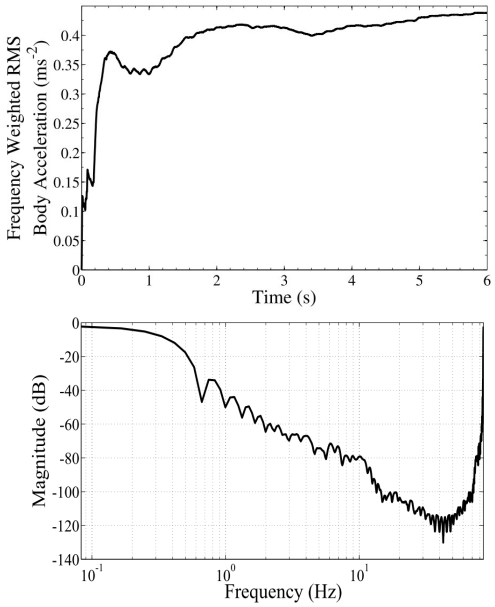

Figure 4.46: Frequency Weighted RMS Body Acceleration Response to Random Road Disturbance for the PID-Controlled AVSS

4.7.5 Vertical Vehicle Body Vibration and Human Comfort Evaluation

Frequency weighted RMS vehicle body vibration in the vertical direction has been presented in Figures 4.39 to 4.46 for all the controllers studied. These figures show that the risks associated with the low resonant frequencies vehicle motion modes listed in Section 1.2 have been eliminated.

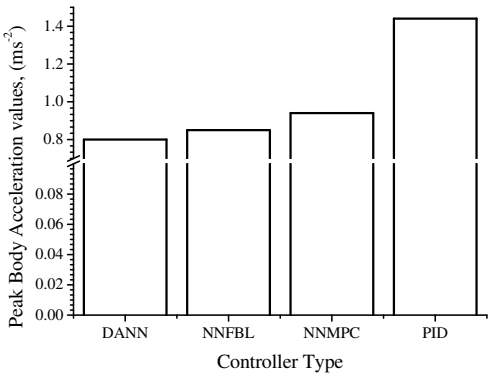

Figure 4.47: Peak Body Acceleration Values for Deterministic Road Input

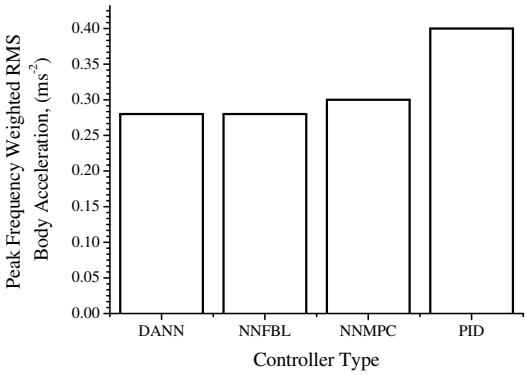

Figure 4.48: Peak Frequency Weighted RMS Body Acceleration Values for Deterministic Road Input

Figures 4.47 and 4.48 present comparisons of the peak body acceleration and frequency weighted body acceleration values for the deterministic road disturbance input. There is a marginal difference between the performances of the neural network-based controllers in this regard. The performance of the PID-controlled AVSS is however significantly poorer.

The trend shown by comparison of the peak body acceleration values and the peak frequency weighted acceleration values for random road disturbance input was different. Also, the performance of the neural network-based model predictive controller was at par with the PID controller. While the performance of the direct adaptive neuro-controller was more than twice better than the others.

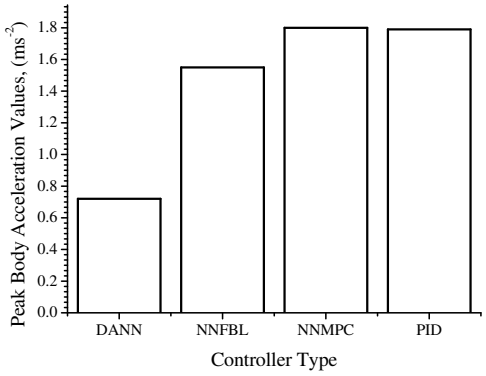

Figure 4.49: Peak Body Acceleration Values for Random Road Input

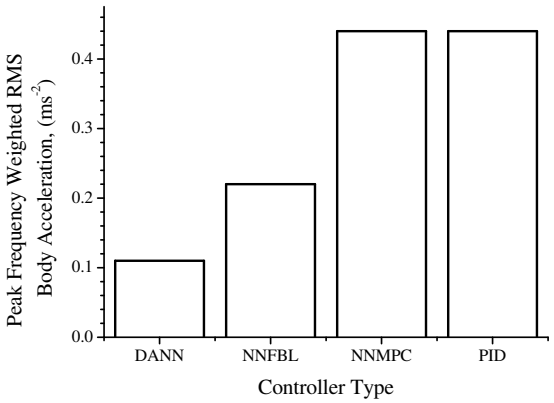

Figure 4.50: Peak Frequency Weighted RMS Body Acceleration Values for Random Road Input

Figures 4.48 and 4.50 shows that, the peak frequency weighted vertical acceleration values for all the controllers are below the European Commission stipulated exposure action value (EAV) of $0.5m/s^2$ [European Commission (2002)]. These performance are rated as shown in Table 4.14 using the International Organization for Standardization and the British Standards' rating for discomfort levels of passengers in a public vehicle [BS 6841 (1987); ISO 2631 (2003)].

The feedback linearisation based controllers (that is, DANN and NNFBL) outperformed the NNMPC and PID controllers in terms of ISO comfort level by being comfortable for both road situations. NNMPC is rated *little uncomfortable* for random road disturbance input. This result is corroborated by the tabular presentation of the performances of the controllers as percentages of the PID controller performances in Table 4.15.

Table 4.14: Comparison of the AVSS Controller Comfort Levels Based on International Standard Ratings [BS 6841 (1987); ISO 2631 (2003)]

	ISO Comfort Level (m/s^2)	
Controller Type	Deterministic Road Disturbance Input	Random Road Disturbance Input
DANN	not uncomfortable	not uncomfortable
NNFBL	not uncomfortable	not uncomfortable
NNMPC	not uncomfortable	a little uncomfortable
PID	a little uncomfortable	a little uncomfortable

Table 4.15: Peak Body Acceleration Values for the Designed Controllers as Percentages of the Benchmark Controller

Controller	Deterministic Road Disturbance		Random Road Disturbance	
	Actual Values	Weighted RMS Values	Actual Values	Weighted RMS Values
DANN	55.56%	70.0%	40.22%	25.0%
NNFBL	59.03%	70.0%	87.0%	50.0%
NNMPC	65.28%	75.0%	100.6%	100%

4.8 Performance Evaluation Based on Actuator Power Consumption

Power consumption level is a vital parameter in evaluating the performance and applicability of AVSS. It is also the major factor that makes semi-active suspension system more attractive for real life implementation [ElMadany et al. (2011)]. For the comparative analysis between the four controllers being studied, Equation 2.80 was used in estimating the power consumption for the actuator in each case [Crolla and Nour (1992); Marzbanrad et al. (2002); Williams (1997*b*)].

The suspension system under consideration combines a nonlinear passive suspension system with an electrohydraulic actuator. The damper and actuator in the suspension disrupts the continual oscillations of the suspension by dissipating the energy introduced to the system through the road input.

Figures 4.51 to 4.54 show that the actuator dissipated more energy with the random road disturbance input, however this difference in energy dissipated differ for the controllers. Table 4.16 shows the power consumption estimation of the controllers,

relative to that of benchmark PID controller.

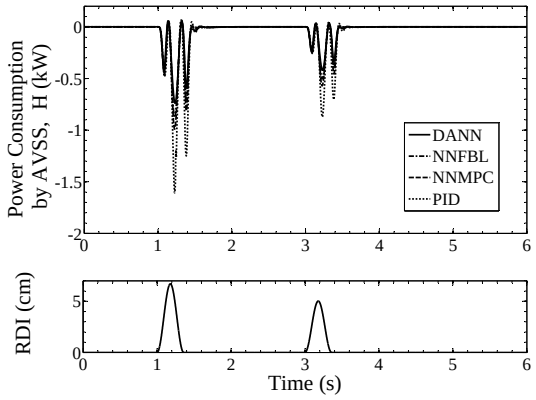

Figure 4.51: Actuator Power Consumption for the Deterministic Road Disturbance Input

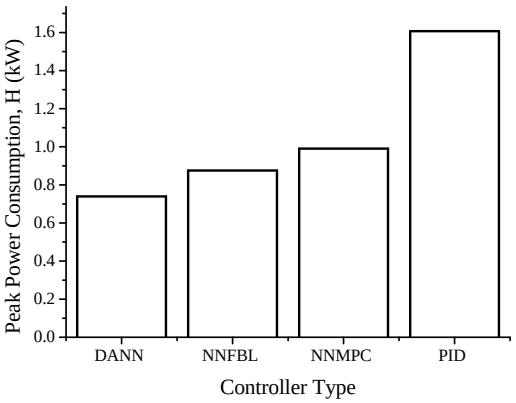

Figure 4.52: Distribution of the Peak Power Consumption by the Actuator for Deterministic Road Disturbance Input

The power dissipated by the actuator was insignificant except when the vehicle was going over the humps. There were oscillations within the period it went over the hump because of the restoring behaviour of the suspension spring. Except for the PID controller, the peak actuator power consumption for all the other controllers were less than $1kW$.

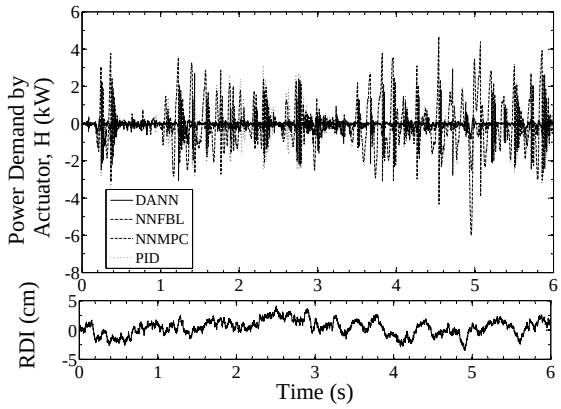

Figure 4.53: Actuator Power Consumption for the Random Road Disturbance Input

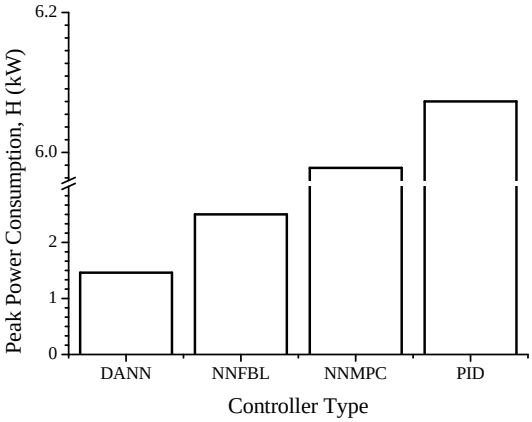

Figure 4.54: Distribution of the Peak Power Consumption by the Actuator for Random Road Disturbance Input

The direct adaptive neural network (DANN) controller outperformed the other controllers especially for the random road disturbance input case. The indirect adaptive neural network-based model predictive controller's performance was almost at par with the PID controller in the same situation.

Table 4.16: Peak Power Consumption for the Controllers as Percentages of PID

Road disturbance	DANN	NNFBL	NNMPC
Deterministic	46.0%	54.5%	61.6%
Random	24.0%	41.0%	98.5%

4.9 Performance Evaluation Based on Performance Index Evaluation

Aggregated values of the performance indices of the controllers was computed based on Equation 2.76. The results for the four controllers, using deterministic and random road disturbance inputs are shown in Figures 4.55 and 4.56. The controller with the optimal performance is the one with the least performance index.

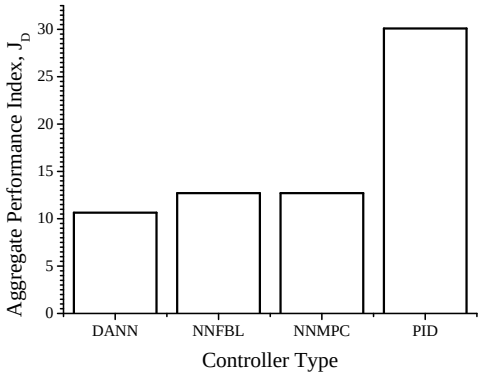

Figure 4.55: Aggregate Performance Index Computed for AVSS Response to Deterministic Road Disturbance

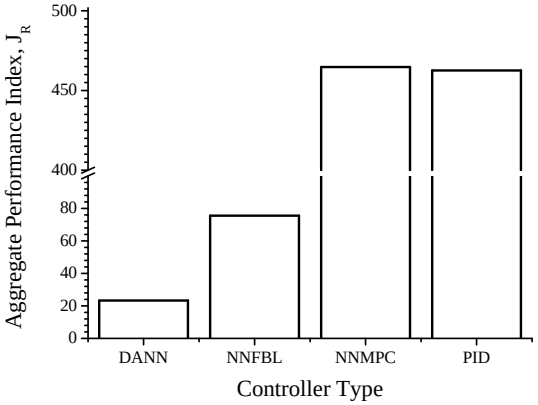

Figure 4.56: Aggregate Performance Index Computed for AVSS Response to Random Road Disturbance

The direct adaptive neural network (DANN) controller out performed the others in both cases. This is indicative of the inability of the predicted dynamic model in the indirect adaptive neural network controllers (that is, NNFBL and NNMPC) to capture the system dynamics as perfectly as the DANN controller. The difference is however marginal in the case for deterministic road disturbance input.

The performance of the neural network-based model predictive controller for random disturbance input case was at par with that of the PID controller. The percentage comparison of the other controllers to PID is presented in Table 4.17.

Table 4.17: Aggregate Performance Index Computation for the Controllers as Percentages of PID

Road disturbance	DANN	NNFBL	NNMPC
Deterministic	35.37%	42.22%	42.22%
Random	5.04%	16.33%	100.46%

4.10 Summary of Chapter Four - Selection of Best Performed Controller

On the whole, the performances of the three neuro-controllers were superior to the PID controller, though NNMPC's performance was at par with that of PID for random road disturbance input (see Figure 4.56). The performance of DANN was twice better than that of PID for most suspension parameters studied but this was achieved at the expense of poor control input characterised by chattering.

The NNFBL control was at par with the NNMPC's performance for the deterministic road disturbance input (see Figure 4.55) but the control input was also poor in both cases. While all the neuro-controllers designed required less than $1kW$ for roads with deterministic road disturbance, NNMPC required about 5 to 6 times of the same power for satisfactory performance on roads with random road disturbance inputs. Although, DANN and NNFBL controllers have better power consumption rates, their poor control input characteristics make them less practically implementable.

All the controllers designed showed good disturbance attenuation within the WBV frequency range. Their ride comfort levels based on the recommendations of BS6841, ISO2632 and the European commission were either acceptable or marginally unacceptable, as in the case of the PID control method (please see Table 4.14).

NNMPC was selected above the feedback linearisation control based NNFBL and DANN controller because its performance was achieved at a better cost for both deterministic and random road disturbance input cases (see, Figures 4.28 and 4.34). Implementation of NNMPC is slower (when compared to the FBL based control methods in DANN and NNFBL) because of its optimisation loop. It is the most employed industrial control method after PID and it is readily applicable to systems with time delays, multivariable interactions and constraints [Bequette (2007); Manenti (2011)].

5 Neural Network-Based Model Predictive Controller (NNMPC) Design for Full-Car AVSS

5.1 Introduction

Model predictive control (MPC) has found more application in the process industries because of its concept of prediction and online control [Jazayeri et al. (2008)]. In spite of its computational challenges, MPC combined with neural network holds good prospect for systems with hydraulic actuators [Bequette (2007); He (2009)].

Qin and Badgwell (2000) listed the following two cases where employment of nonlinear model predictive control is essential:

1. Highly nonlinear regulator control problem with high frequency disturbances.
2. Servo control problems associated with frequently changing operating points.

The theory of the NNMPC employed in this chapter has been discussed in Section 4.4. As shown in the previous chapter, the implementation of NNPMC method is done in two phases; system identification and control. All the numerical experimentations were carried out using the ordinary differential equation fixed step solver(ode45) at a sampling frequency of $1kHz$ in the MATLAB / SIMULINK® environment.

5.2 System Identification

The basic description of the system identification process is available in Section 4.2.1. While the process remain the same, the system being identified now is a multi-input-multi-output (MIMO) system. The four different processes that constitute system identification are: Experimentation, Model structure selection, Model estimation and Validation.

5.2.1 Experimentation

The system was excited using a non-saturating band-limited white noise excitation signal spanning the entire operation range of the system. A total set of $501,422$ input-output data samples were collected from the numerical experimentation of each vehicle suspension station in the form:

$$Z_{i,j}^{N} = f[u_{i,j}(k), y_{i,j}(k)]; \qquad k = 1, \ldots, N \tag{5.1}$$

where $Z_{i,j}^{N}$ is the input-output data set at each suspension wheel station, $u_{i,j}(k) \in [\pm 10V]$ is the input signal, $y_{i,j}(k)$ is the output signal k is the sampling instant and N is the total number of samples, $i \in [front, rear]$ and $j \in [left, right]$. The schematic arrangement for the numerical experimentation and data collection is shown in Figure 5.1.

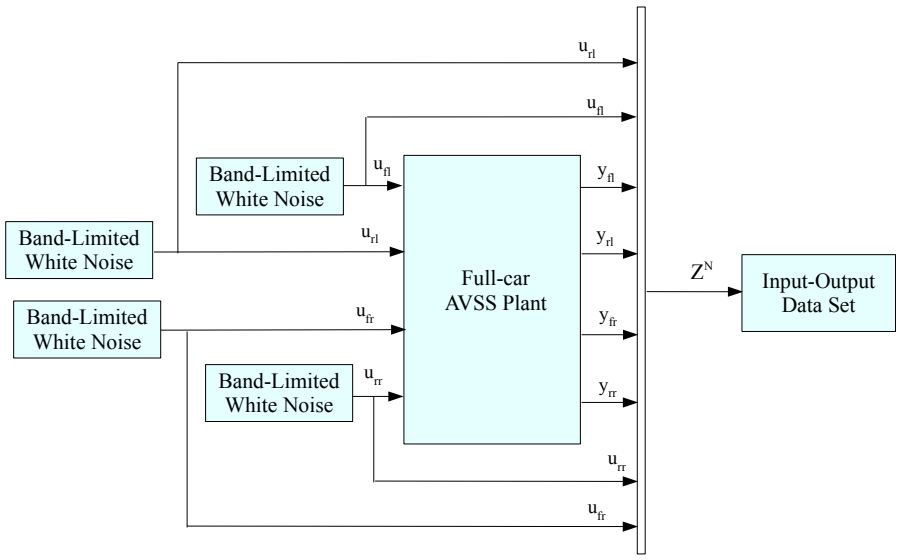

Figure 5.1: Input-Output Data Collection Structure

Figure 5.2 shows the $50,000$ input-output data set selected for each vehicle suspension station. The data set is subsequently divided into two for training and

validation purposes.

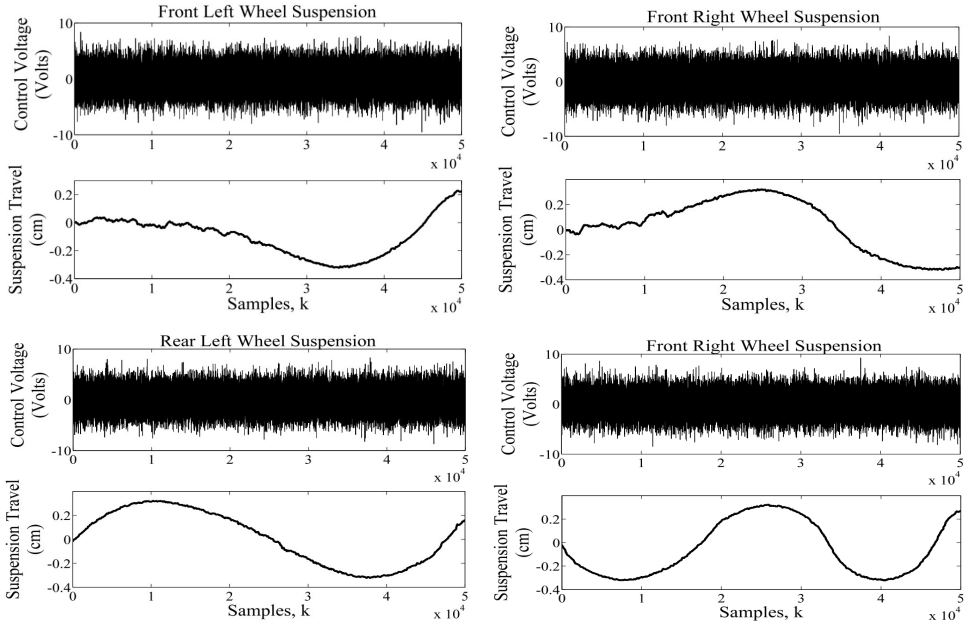

Figure 5.2: Input-Output Data Set for the Four Wheel Stations

The objective of system identification is to obtain a mapping based on the input-output training data to a set of possible weights $Z_{i,j}^{N}, \rightarrow \hat{\theta}$ thereby yielding $\hat{y}_{i,j}(k)$ predictions that are as close as possible to the true outputs, $y_{i,j}(k)$.

5.2.2 Model Structure Selection

The model structures listed in Tables 5.1 and 5.2 were tested to check for their suitability for the identification. The percentage fitness of output error model stood out among the linear models but the neural network models performed better.

Therefore the AVSS plant can be represented by the NNARX model, where the generalized NNARX model is given by

$$y_{i,j}(k) = f[\phi_{i,j}(k), \theta_{i,j}] + \varepsilon_{i,j}(k) \tag{5.2}$$

where f is the nonlinear function that is realized by the neural network model, $\phi_{i,j}(k)$ represents the regressors, vector $\theta_{i,j}$ contains the adjustable weights and $\varepsilon_{i,j}$ represents the model residual. As a result of the numerical experiment and training, the network implements an estimation of the non-linear transformation, $\hat{f}(*)$ which leads to the predicted output given by:

$$\hat{y}_{i,j}(k) = f[\phi_{i,j}(k), \theta_{i,j}] \tag{5.3}$$

Table 5.1: Percentage Fitness for Predicted Linear Models

Model Type	Description	Wheel Position			
		Front Left	Rear Left	Front Right	Rear Right
m2arx	Based on autoregressive exogenous inputs model	50.46	35.94	14.46	−3.70
m1pem	Based on prediction error estimate model	69.24	35.85	11.95	0.19
moe3	Based on output error model	85.29	35.10	62.96	83.11
bj5	Based on Box Jenkins polynomial model	72.65	37.15	16.96	−4.61
armax4	Based on autoregressive moving exogenous inputs model	69.32	35.89	17.76	−7.42

Table 5.2: Percentage Fitness for Predicted Neural Network-Based Nonlinear Models

Model Type	Description	Wheel Position			
		Front Left	Rear Left	Front Right	Rear Right
Sigmoidnet	Nonlinearity estimator for nonlinear ARX and Hammerstein-Wiener models	99.96	99.96	99.97	99.99
Wavenet	Nonlinearity estimator for nonlinear ARX	99.96	99.96	96.96	99.98
Neuralnet	Nonlinearity estimator for nonlinear ARX and Hammerstein-Wiener models	99.75	99.78	−47.55	99.94

and the regression vector is

$$\begin{aligned}\phi_{i,j}(k) &= [y_{i,j}(k-1), y_{i,j}(k-2), \ldots, y_{i,j}(k-n), u_{i,j}(k-d), u_{i,j}(k-d-1), \\ &\quad \ldots, u_{i,j}(k-d-m+1)] \end{aligned} \tag{5.4}$$

where d is the delay from input to the output in terms of number of samples, n and m are the number of past outputs and inputs respectively, while $i \in [front, rear]$ and $j \in [left, right]$.

It is customary to try a single hidden layer NN structure first, then the next step is the determination of the number of neurons in the hidden layer, this is achieved through the use of the lag space-order index plots. Figure 5.3 shows that the *knee-points* on the lag space-order index plots for all the vehicle suspension stations 2 indicating that the number of neurons in each hidden layer is five.

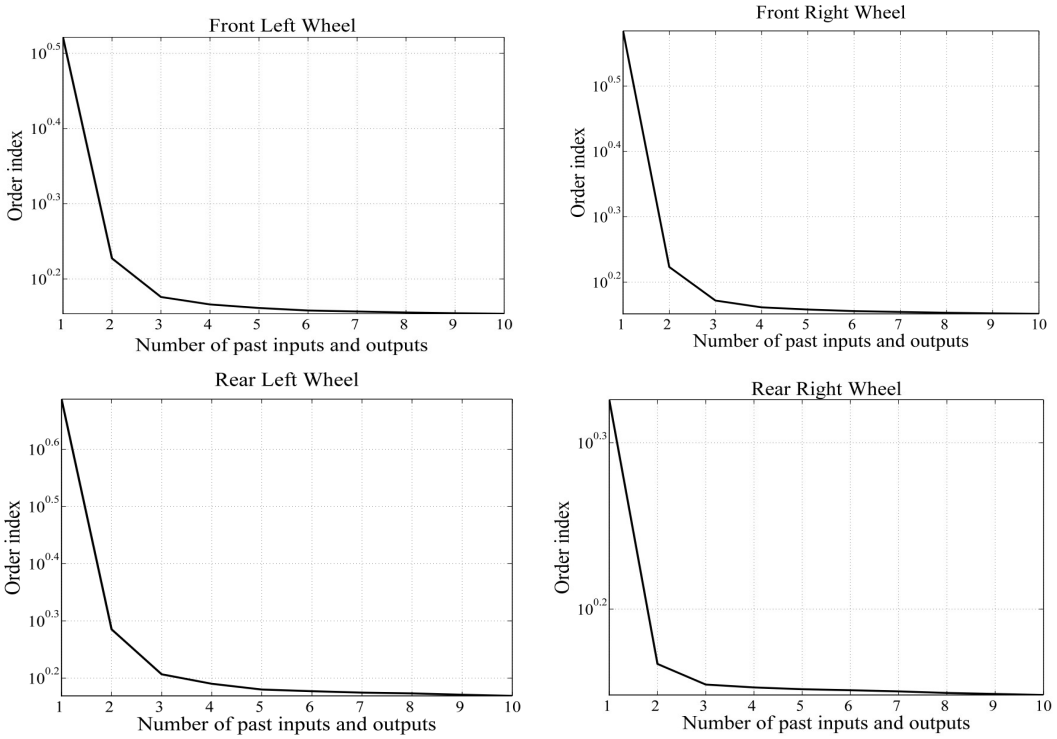

Figure 5.3: Order of Index versus Lag Space Plots for the Vehicle Suspension Stations

Therefore the appropriate multilayer feedforward neural network structure for each of the vehicle suspension station has two layers with five hidden layer neurons, this is illustrated by Figure 5.4

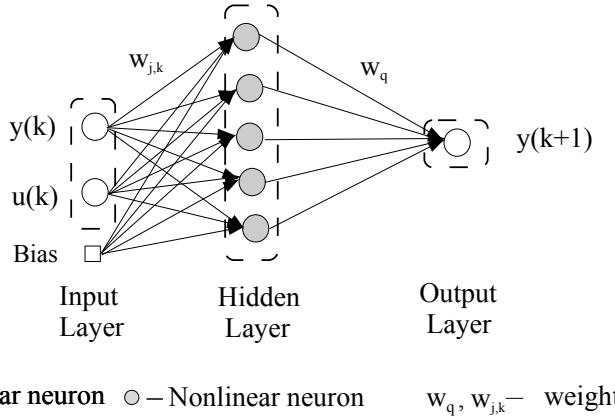

Figure 5.4: Multilayer Feedforward Neural Network Structure for Each Wheel Station

5.2.3 Model Estimation

Levenberg-Marquardt minimization is typically the first choice training algorithm for multi-layered perceptron neural networks and the hidden layer activation function adopted is the tangent hyperbolic function:

$$f(x) = tanh(x) = \frac{e^x - e^{-x}}{e^x + e^{-x}} \tag{5.5}$$

5.2.4 Model Validation

The system identification parameters for the AVSS is listed in Table 5.3. Model validation was achieved using one-step ahead prediction plots for the four neural network model types as well as, the plots for the residuals in Figures 5.5 to 5.8. Also the training performance plots are shown in Figures 5.9 to 5.12.

The plots for the residuals were of the order of 10^{-4} in magnitude except for the "front-right" wheel which has a order of 10^{-5}. Similarly, the one-step ahead predictions had approximately 100% fitness with the validation data acquired from the experiment except for the "front-right" wheel where it was -47.55%.

The training performance plots in Figures 5.9 to 5.12 shows that all the wheel stations utilized their maximum number of epochs (300) for the identification exercise. The mean-squared-error estimates for each exercise is presented in Table 5.4.

Table 5.3: Parameters for the Neural Network System Identification

Parameters for each suspension station suspension station	Value
Total number of training and validation samples	50000
Maximum number of epochs	300
Sampling frequency	1kHz
Time delay, n_k	1
Number of layers	2
Number of hidden layers neurons	5
Number of past outputs, n	2
Number of past inputs, n	2

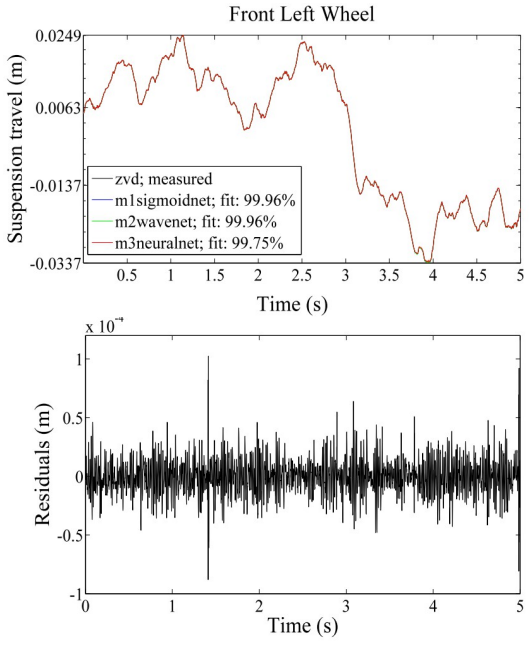

Figure 5.5: One Step Ahead Prediction and Residuals for Front Left Wheel Station

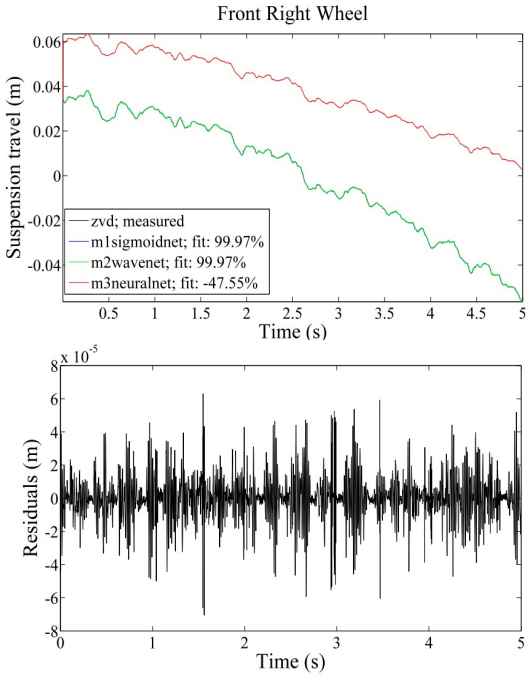

Figure 5.6: One Step Ahead Prediction and Residuals for Front Right Wheel Station

Table 5.4: Final Prediction Error Estimates

Wheel Station	MSE Value	Wheel Station	MSE Value
Front left	5.46×10^{-11}	Front right	6.53×10^{-11}
Rear left	6.04×10^{-11}	Rear right	3.32×10^{-10}

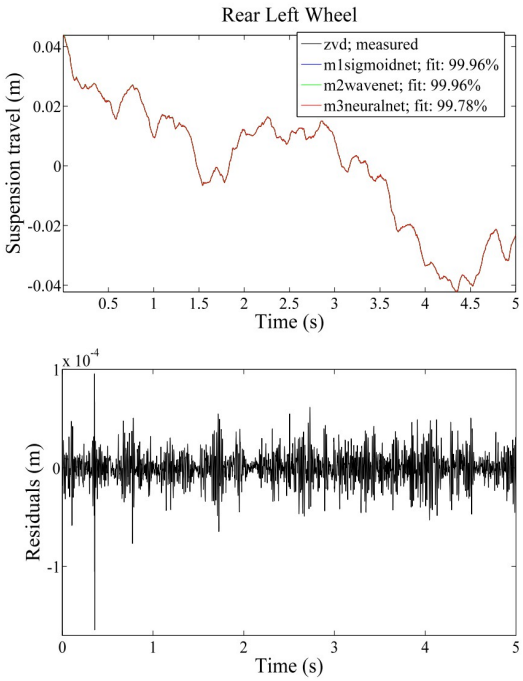

Figure 5.7: One Step Ahead Prediction and Residuals for Rear Left Wheel Station

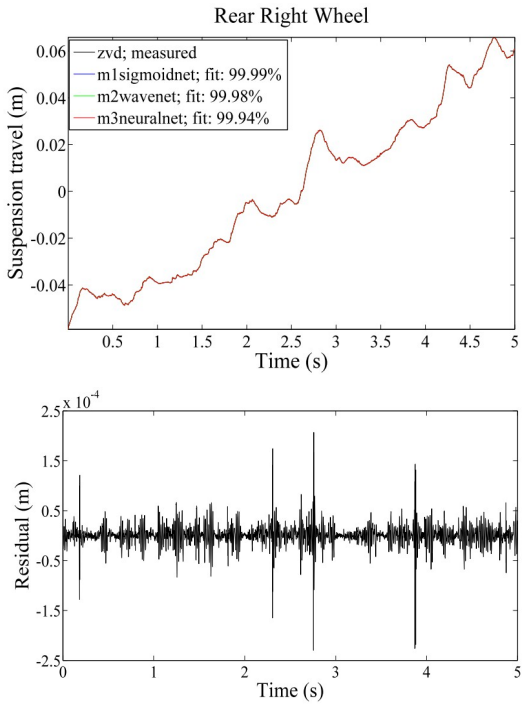

Figure 5.8: One Step Ahead Prediction and Residuals for Rear Right Wheel Station

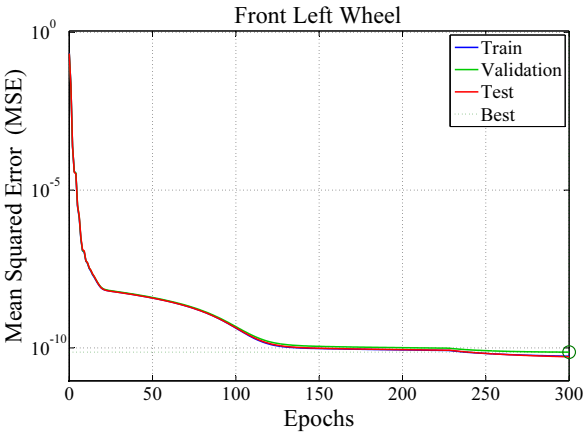

Figure 5.9: Neural Network Training Performance (Front Left Wheel)

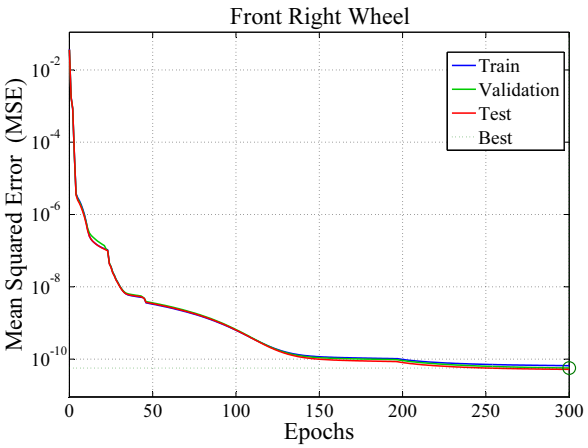

Figure 5.10: Neural Network Training Performance (Rear Left Wheel)

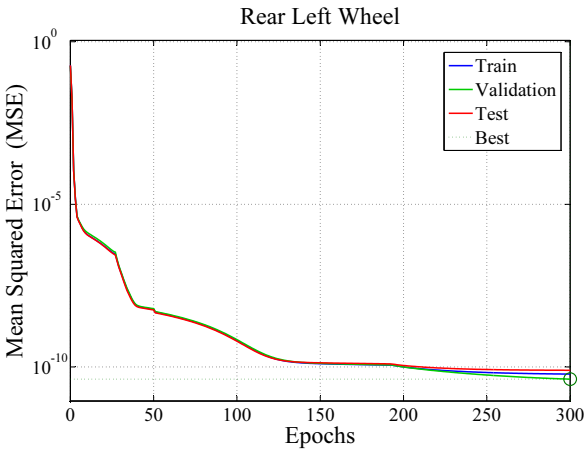

Figure 5.11: Neural Network Training Performance (Front Right Wheel)

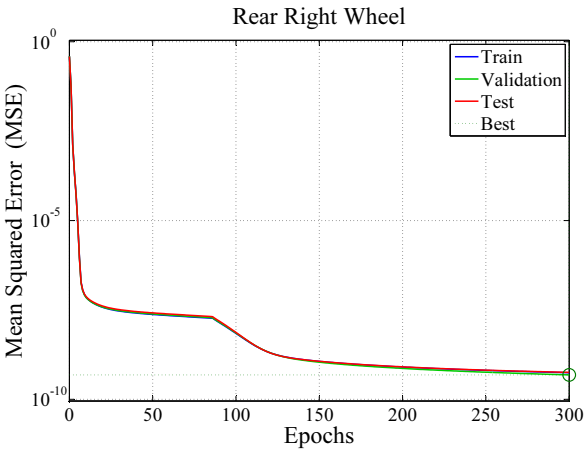

Figure 5.12: Neural Network Training Performance (Rear Right Wheel)

5.3 Controller Design

A block diagram illustrating the architecture of the full-car AVSS is presented in Figure 5.13. The neural network model predictive controllers are used in the outer control loops while the PID controllers are retained in the inner loops to assist in stabilising the actuator dynamics.

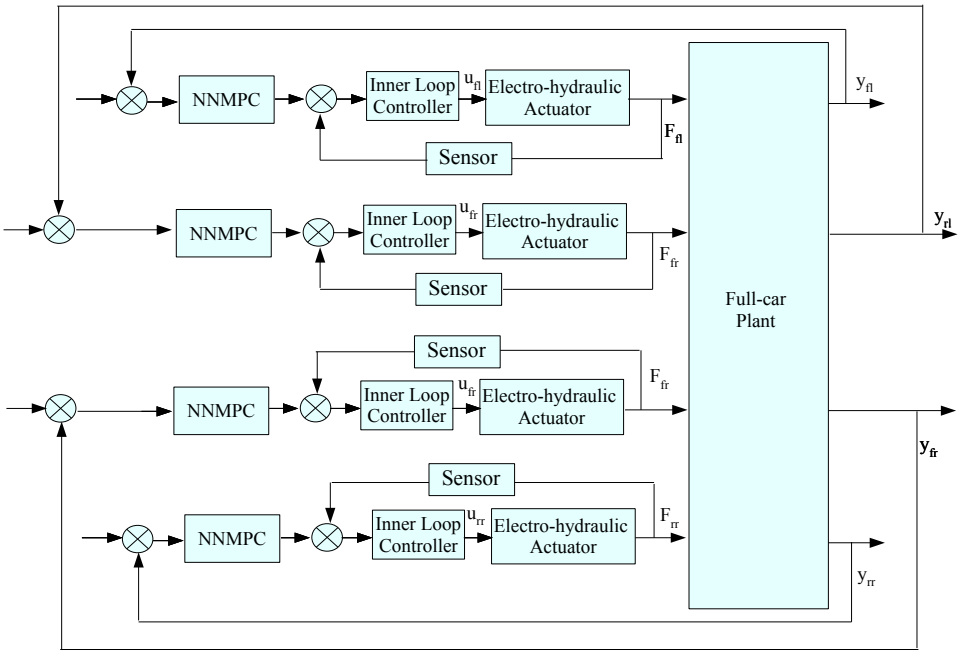

Figure 5.13: Full-Car NNMPC-Controlled AVSS Architecture

The arrangement of the controllers readily fits into a distributed network of controllers communicating over a *controller area network* (CAN) bus under the supervision of a *global controller*. It also introduces some degree of *active redundancy*

that is necessary for fault tolerant control and monitoring within a condition-based maintenance scheme [Jeppesen and Cebon (2004); Waldron et al. (2008)]. The parameters of the NNMPCs in the outer loops are given in Tables 5.5 and 5.8.

5.3.1 Responses of the NNMPC-Controlled Full-Car AVSS to Deterministic Road Disturbance Inputs

Tables 5.5 to 5.7 present the tuning parameters for the controllers and the key to acronyms used in time history plots for responses to the deterministic road excitation in this section. The plots for the responses are presented in Figures 5.14 to 5.19.

Table 5.5: Parameters for the Neural Network Model Predictive Controllers-Deterministic Road Disturbance Inputs

Parameters	Value	Parameters	Value
Control horizon, N_u	2	Cost horizon, N_2	9
Control weighting factor, ρ	0.01	Search parameter, α	0.001

Table 5.6: Tuning Parameters for the PID Controllers - Deterministic road Disturbance Inputs

Wheel Station	P	I	D
Front left	5×10^{-12}	1.34×10^{-6}	1×10^{-10}
Rear left	2×10^{-12}	1.74×10^{-6}	1×10^{-10}
Front right	5×10^{-13}	1.2×10^{-5}	1×10^{-10}
Rear right	7.5×10^{-12}	1×10^{-6}	1×10^{-10}

Table 5.7: Parameters Plotted in the Time Histories for NNMPC-Controlled Full-Car AVSS

Abbreviation	Full meaning	Abbreviation	Full meaning
ST	Suspension travel	BA	Body acceleration
PAA	Pitch angular acceleration	RAA	Roll angular acceleration
NWDL	Normalized wheel displacement	SVD	spool-valve displacement
RDI	Road disturbance input	AF	Actuator force
		CV	Control voltage

The performance of the NNMPC is superior to those of the PID controller and PVSS in terms of the plots for body heave acceleration and vehicle handling shown in Figure 5.14. The peak values are $2.8ms^{-2}$, $3.5rads^{-2}$ and $10.6rads^{-2}$ respectively.

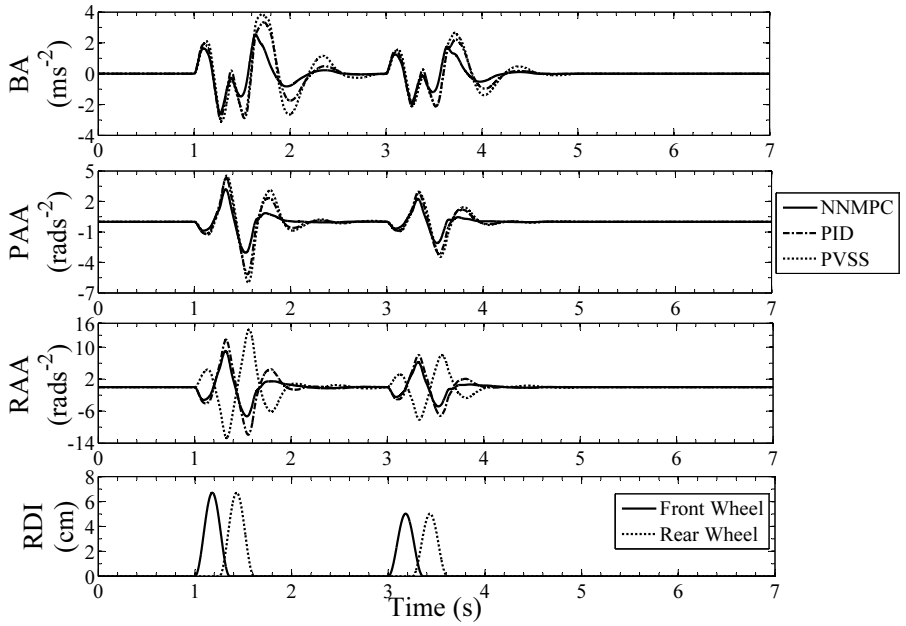

Figure 5.14: Body Heave Acceleration and Handling Responses to Deterministic Road Excitations

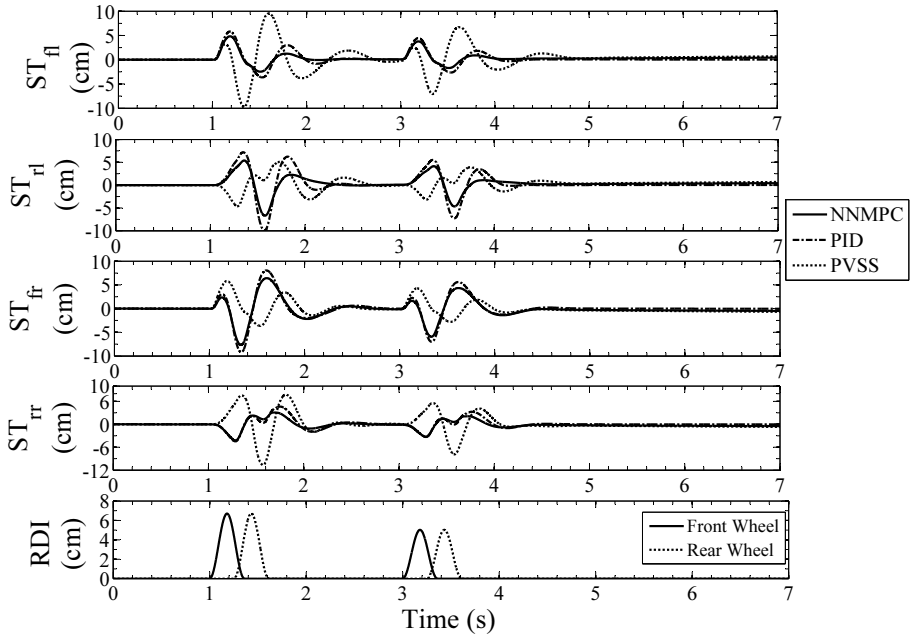

Figure 5.15: Time History of the NNMPC and PID-Controlled AVSS and PVSS Responses to Deterministic Road Excitations

Figure 5.15 shows the suspension travel time history for the four wheels. None

exceeded the $\pm 10cm$ allowable limits. The controlled suspension has better performance with regards to this parameter but when compared with each other, the difference is marginal. This showed that NNMPC has better body acceleration performance than the PID control though it used approximately the same suspension travel displacement.

For good road holding, the wheel dynamic load must be maximised. Figure 5.16 however shows that the penalty paid for better body acceleration, vehicle handling and suspension travel is poor wheel dynamic load, especially in the "front left" and the "rear right" wheels. This may also impact the efficiency of the brakes in these wheels.

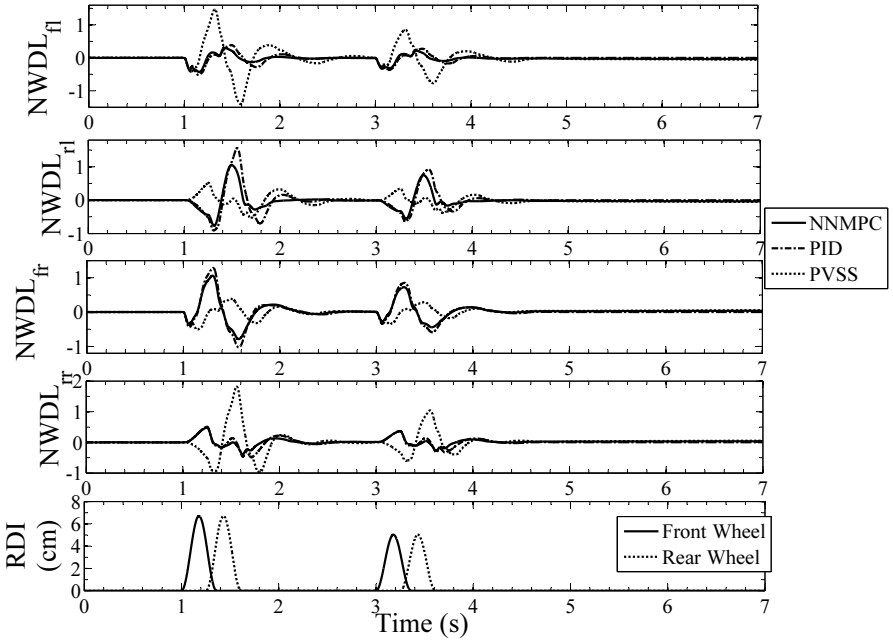

Figure 5.16: Normalized Wheel Dynamic Load Responses to Deterministic Road Excitations

Figure 5.17 shows that control voltage were within $\pm 3Volts$ at the wheel stations. The actuator forces were also much lower than the vehicle static load, Figure 5.18 shows that they are within $\pm 1.8kN$. While Figure 5.19 shows that the spool-valves were within $\pm 2.5mm$.

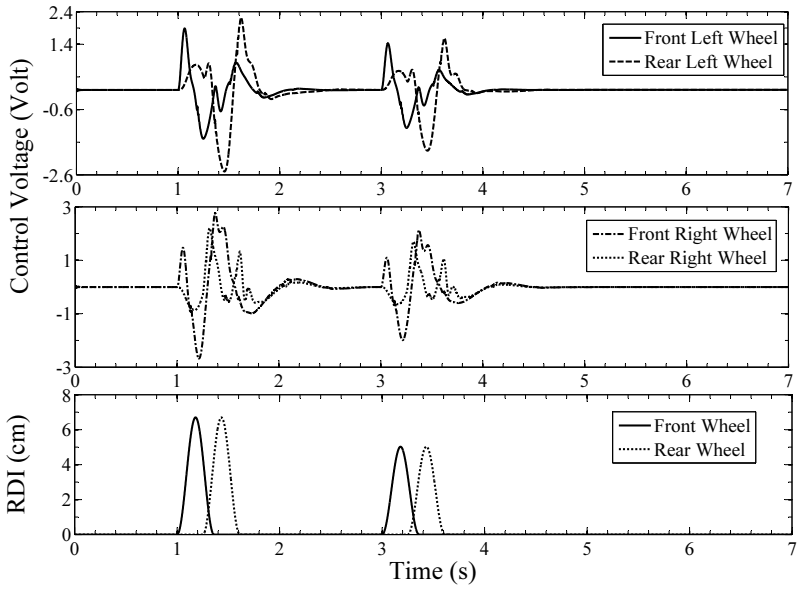

Figure 5.17: AVSS Control Voltage Responses in the Presence of Deterministic Road Excitations

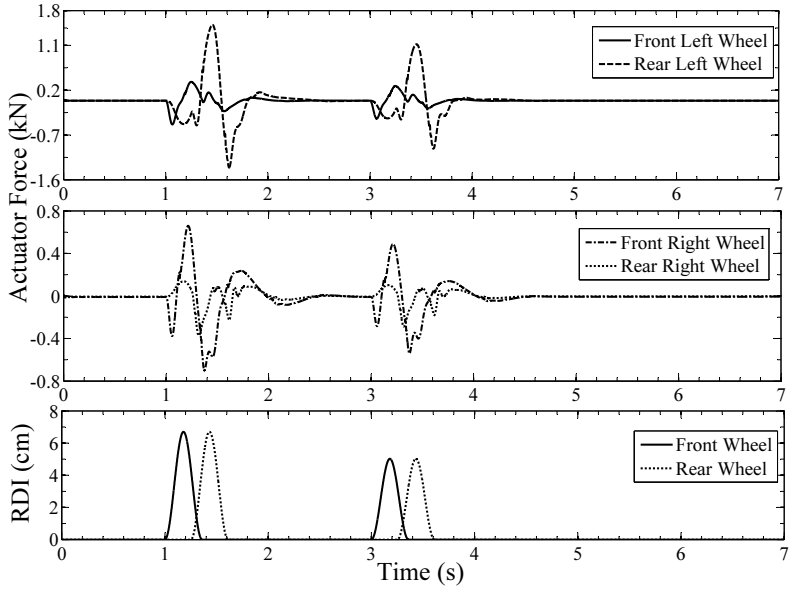

Figure 5.18: AVSS Actuator Force Responses in the Presence of Deterministic Road Excitations

5.3.2 Comparison Between the Controllers Using Peak and RMS Values for Deterministic Road Excitation

Figures 5.20 to 5.23 present the comparison of the performance of the NNMPC with that of the PID controller. Percentages of the peak values measured from the plots

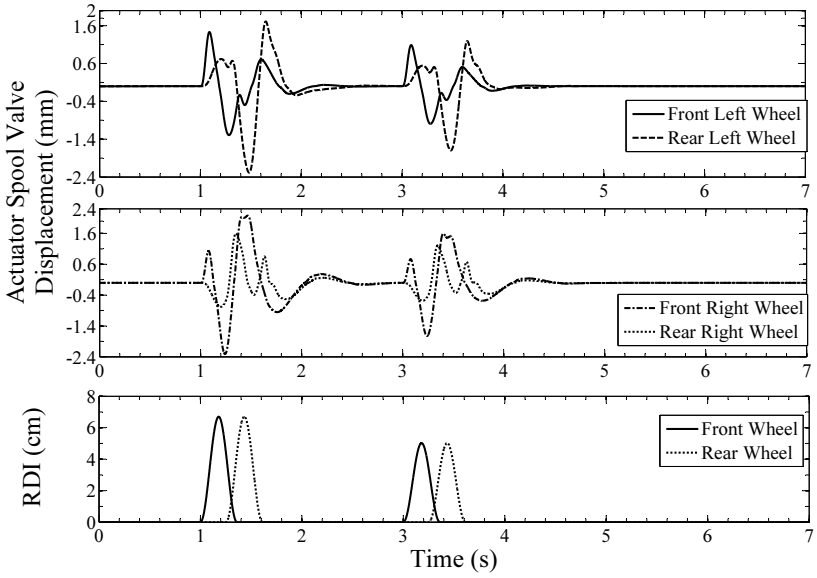

Figure 5.19: Time History of the NNMPC-Controlled, Full-Car AVSS Responses to Deterministic Road Excitations

and the RMS values estimated from the generated data are used in this case.

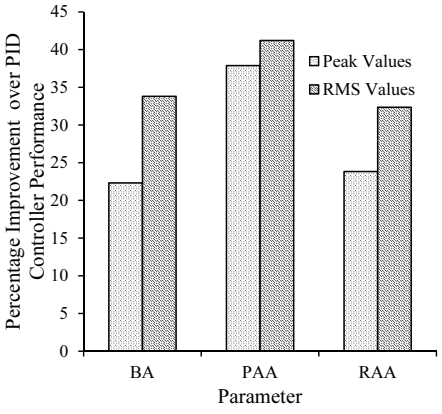

Figure 5.20: Evaluation of the Improved NNMPC Controller Performance Using Vertical Body Acceleration and Vehicle Handling Parameters-Deterministic Road Disturbance

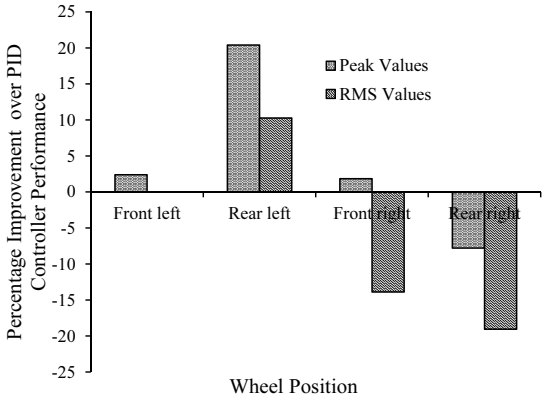

Figure 5.21: Evaluation of the Improved NNMPC Controller Performance Using Suspension Travel-Deterministic Road Disturbance

Figure 5.20 shows that there is at least a minimum improvement of 20% when considering the body heave acceleration and the angular acceleration modes. Similarly, Figure 5.23 shows that there is at least 16% reduction in energy utilisation.

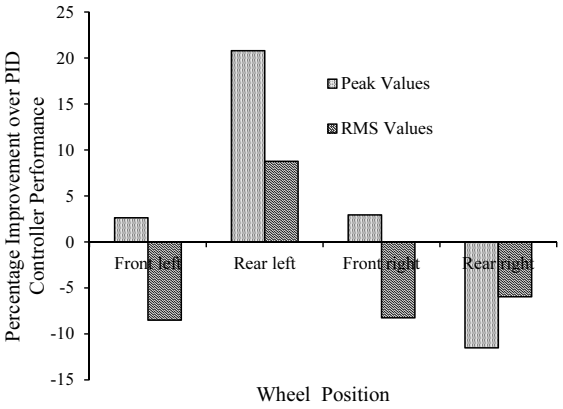

Figure 5.22: Evaluation of the Improved NNMPC Controller Performance Using Wheel Dynamic Load-Deterministic Road Disturbance

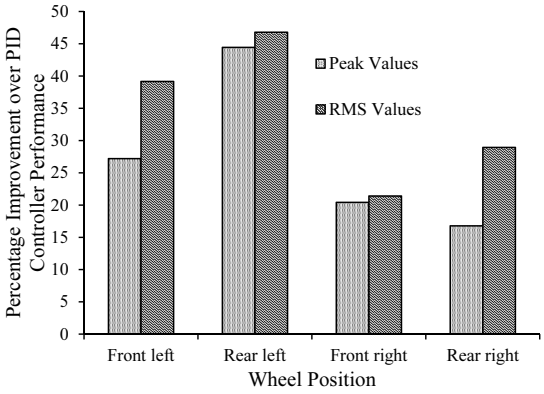

Figure 5.23: Evaluation of the Improved NNMPC Controller Performance Using Control Voltage

5.3.3 Responses of NNMPC-Controlled, Full-Car AVSS to Random Road Disturbance Inputs

Tables 5.8 and 5.9 present the tuning parameters for the NNMPC and PID controlled AVSS in the presence of random road excitations whose model is described in Section 2.6.2.

Table 5.8: Parameters for the Neural Network Model Predictive Controllers-Random Road Disturbance Inputs

Parameters	Value	Parameters	Value
Control horizon, N_u	5	Cost horizon, N_2	30
Control weighting factor, ρ	0.005	Search parameter, α	0.001

Table 5.9: Tuning Parameters for the PID Controllers-Random Road Disturbance inputs

Wheel Station	P	I	D
Front left	1.3×10^{-6}	5×10^{-10}	2×10^{-12}
Rear left	6.1×10^{-3}	6×10^{-9}	1×10^{-10}
Front right	5×10^{-6}	1.3×10^{-9}	1×10^{-10}
Rear right	7.5×10^{-3}	3.6×10^{-10}	1×10^{-12}

Figures 5.24 to 5.29 show the time history of responses of the AVSS to the random road excitation. The plots for the NNMPC and PID controlled AVSS have been separated and PVSS excluded for better clarity. The superior performance of the NNMPC to that of PID controller is demonstrated in Figure 5.24 for the body

acceleration and vehicle handling. The vertical body acceleration was improved by about $\pm 1 m/s^2$.

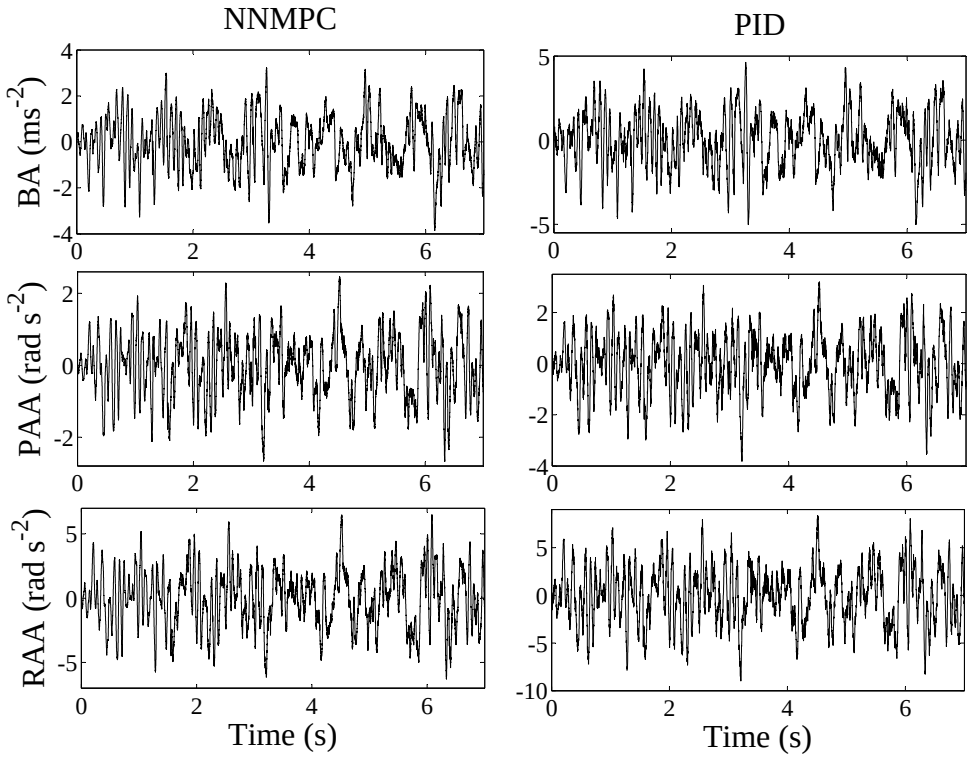

Figure 5.24: Body Heave Acceleration and Handling Responses to Random Road Excitations

Figures 5.25 and 5.26 show similar trends for the suspension travel and wheel dynamic load time history at the four wheel stations. Figure 5.27 shows that about three times more energy is demanded by the AVSS on a road with random excitation. This trend is however not followed by the "front right" wheel for both NNMPC and PID controllers.

the actuator force and control voltage demand by the AVSS controller was lower in the random disturbance case when compared to the deterministic case. The presence of the outliers in the signals however introduced difficulty in accurately establishing an appropriate scale for the estimating the real peak values of the signals (see Figure 5.28).

The NNMPC showed marginal improvement to the PID when considering the spool-valve displacement in Figure 5.29.

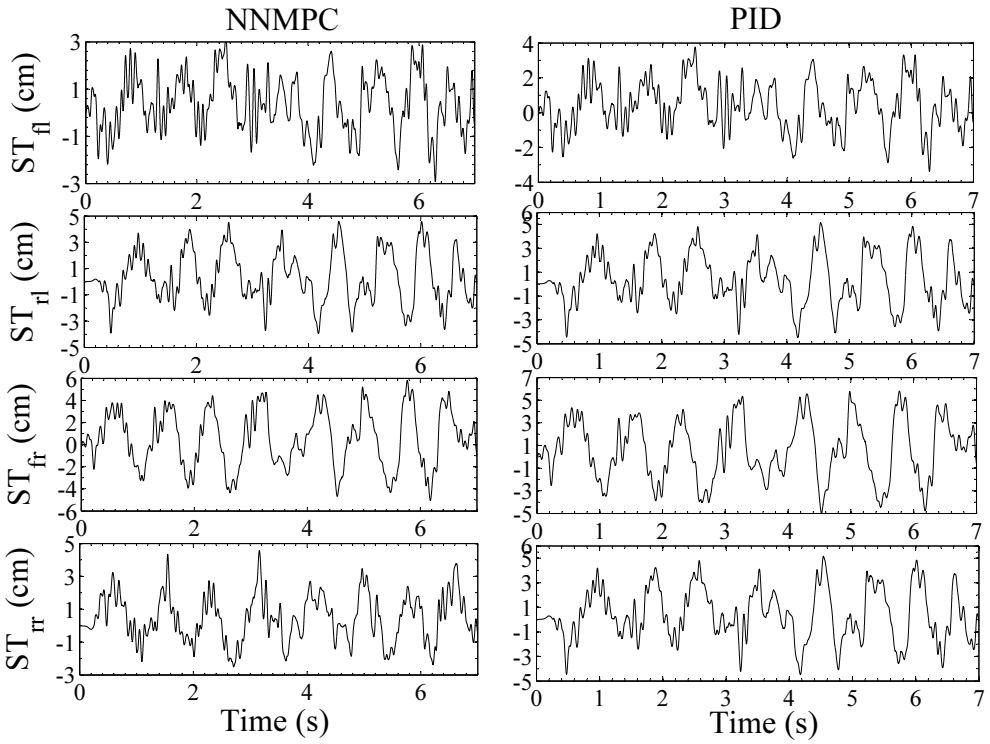

Figure 5.25: Suspension Travel Responses to Random Road Excitations

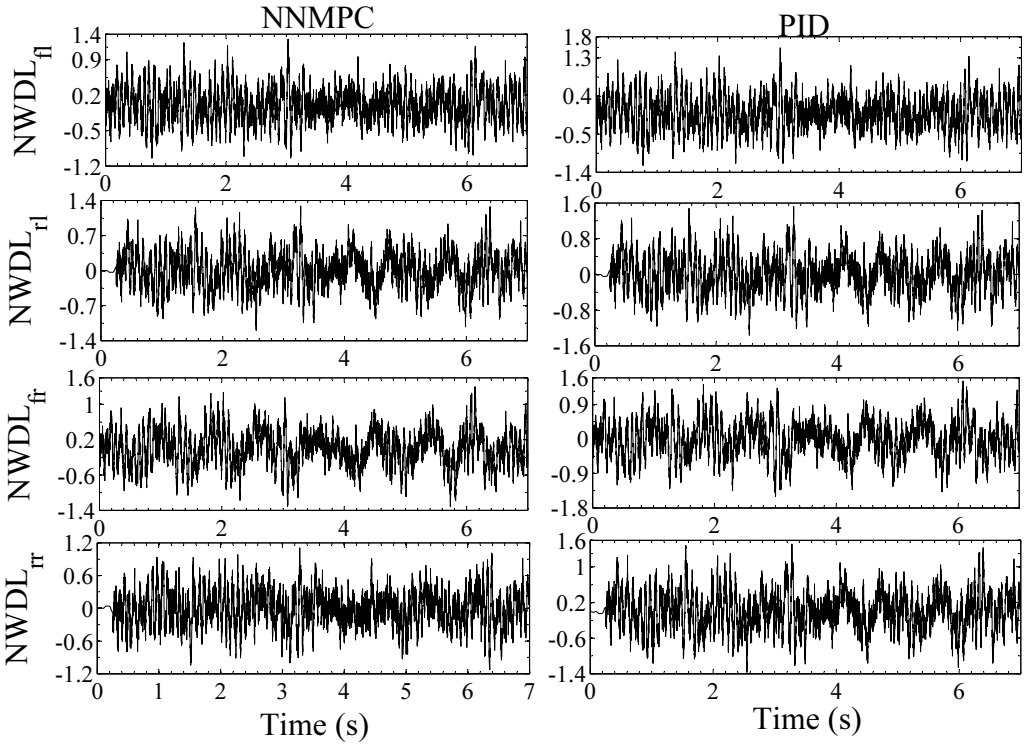

Figure 5.26: Normalized Wheel Dynamic Load Responses to Random Road Excitations

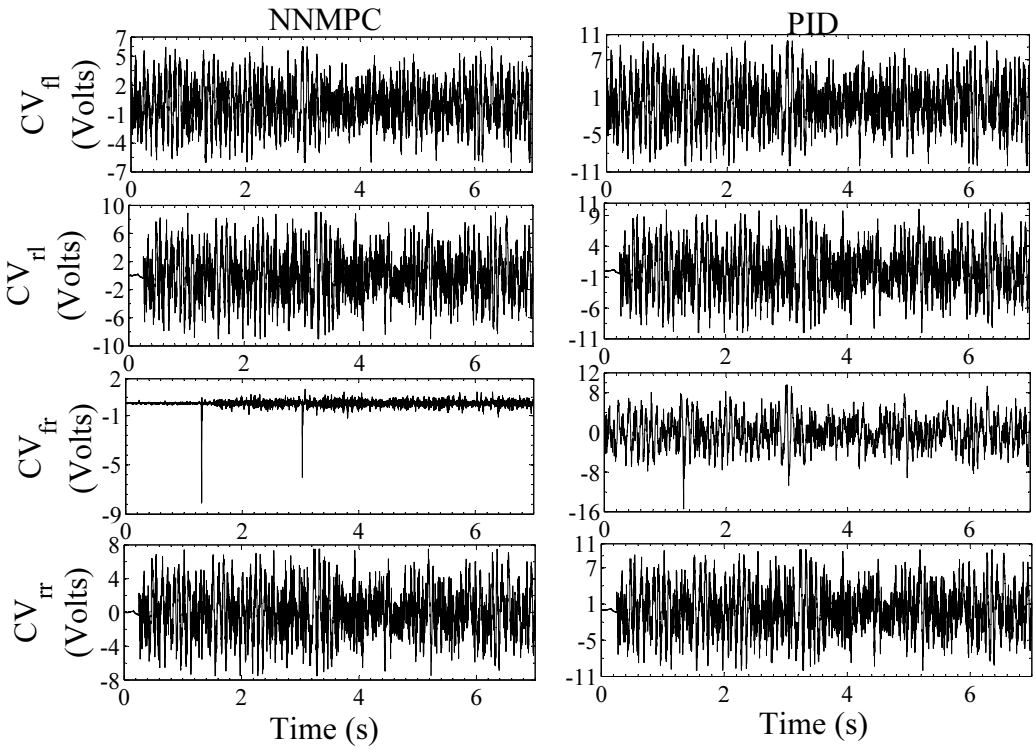

Figure 5.27: AVSS Control Voltages in the Presence of Random Road Excitations

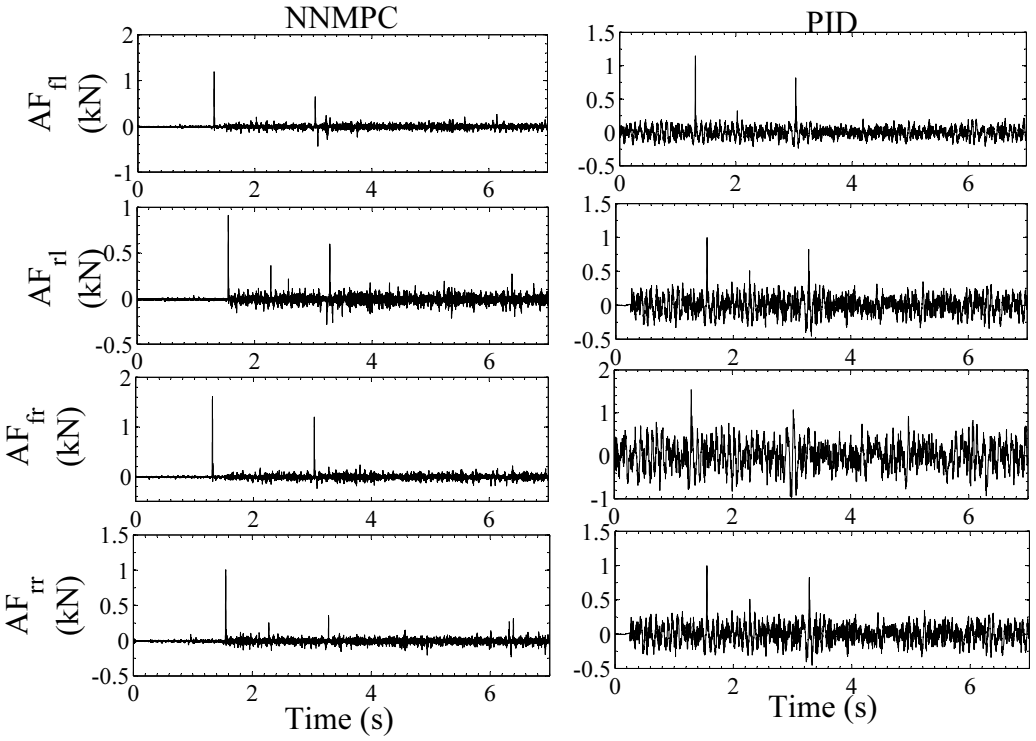

Figure 5.28: AVSS Actuator Force Responses to Random Road Excitations

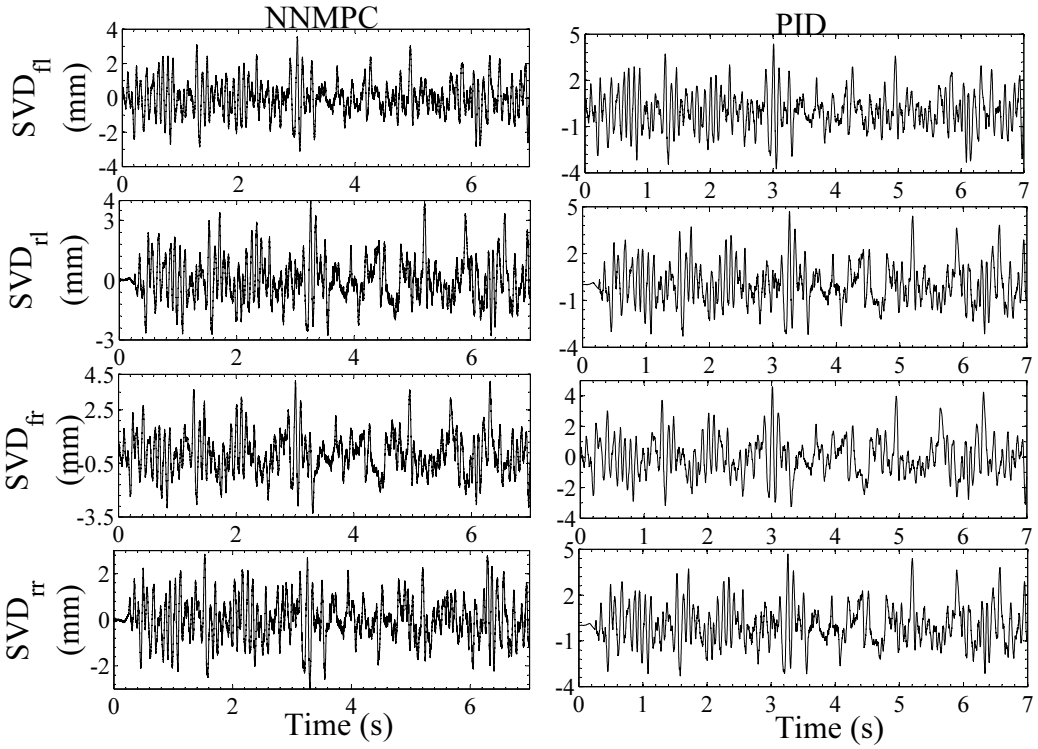

Figure 5.29: AVSS Actuator Spool-Valve Responses to Random Road Excitations

5.3.4 Comparison of the Designed Controllers Using Peak and RMS Values for Random Road Excitations

Figures 5.30 to 5.33 present the comparison of the performance of the NNMPC with that of the PID controller. Percentages of the peak values measured from the plots and the RMS values estimated from the generated data are used in this case.

Figure 5.30 shows an improvement of about 23% in the body heave acceleration, pitch and roll angular acceleration modes. Moreover, unlike the trend for the deterministic road disturbance case, all the plots for the random disturbance case show improvements for the NNMPC controller AVSS over the PID control.

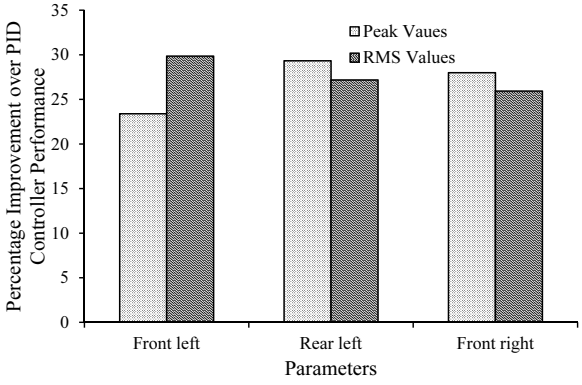

Figure 5.30: Evaluation of the Improved NNMPC Controller Performance Using Vertical Body Acceleration and Vehicle Handling Parameters-Random Road Disturbance

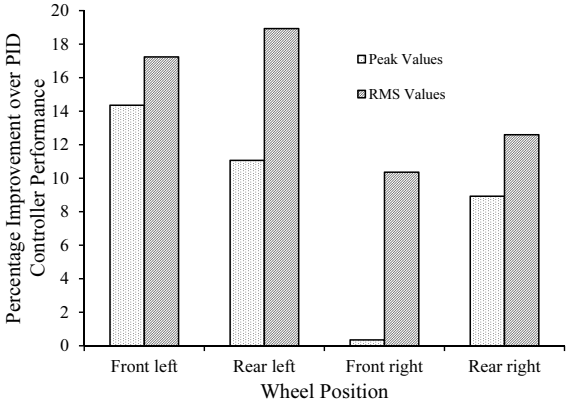

Figure 5.31: Evaluation of the Improved NNMPC Controller Performance Using Suspension Travel-Random Road Disturbance

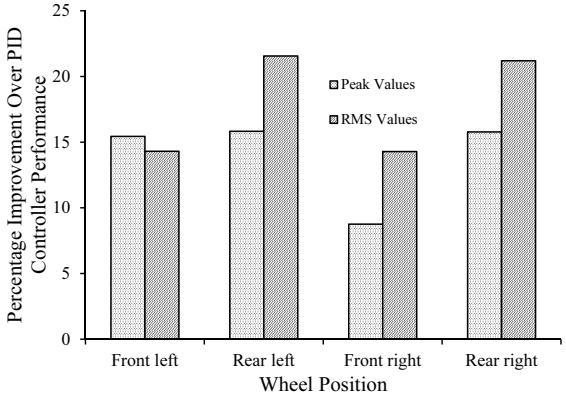

Figure 5.32: Evaluation of the Improved NNMPC Controller Performance Using Wheel Dynamic Load-Random Road Disturbance

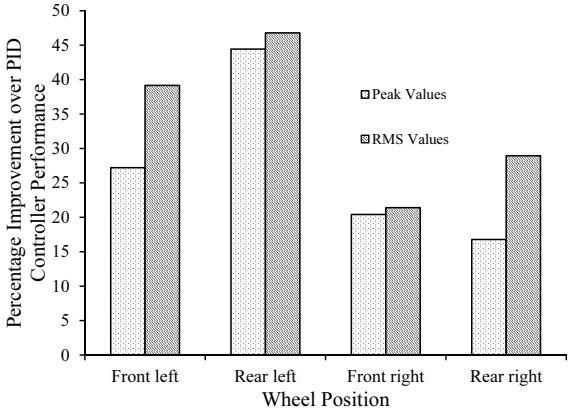

Figure 5.33: Evaluation of the Improved NNMPC Controller Performance Using Control Voltage-Random Road Disturbance

5.4 Frequency Domain Analysis

Frequency domain analysis will be limited to vertical body acceleration, pitch and roll angular accelerations in this work. They are able to give appropriate representation of the trend in frequency domain plots. Detail description of the pseudo-frequency domain analysis method used (that is PSD estimation) has been presented in Section 4.7.

Figures 5.34 to 5.37 show the frequency domain plots for the vertical acceleration, pitch and roll angular acceleration modes of the AVSS when exposed to deterministic and random road disturbance profiles. The figures present a comparison of the responses for NNMPC and PID controller as well as, the PVSS.

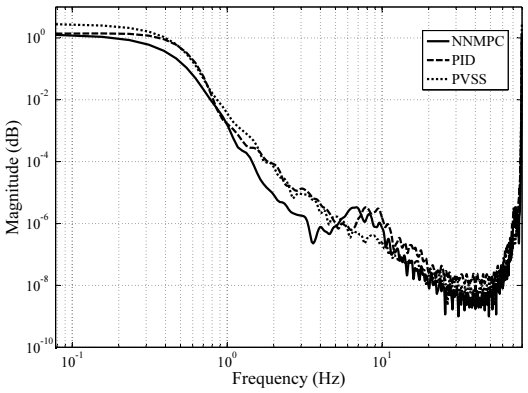

Figure 5.34: Frequency Response for Vertical Body Acceleration in the Presence of Deterministic Road Disturbance Inputs

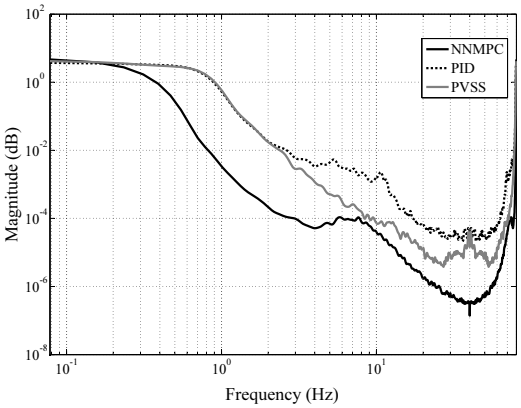

Figure 5.35: Frequency Response for Vertical Body Acceleration in the Presence of Random Road Disturbance Inputs

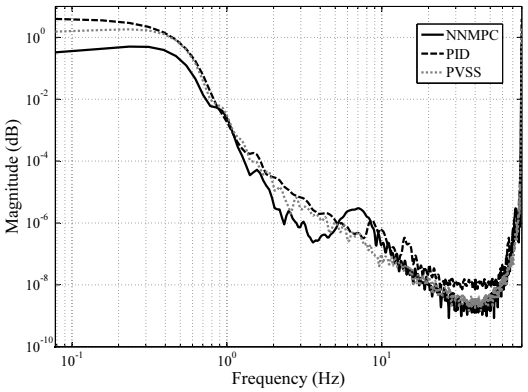

Figure 5.36: Frequency Response for Pitch Angular Acceleration in the Presence of Deterministic Road Disturbance Inputs

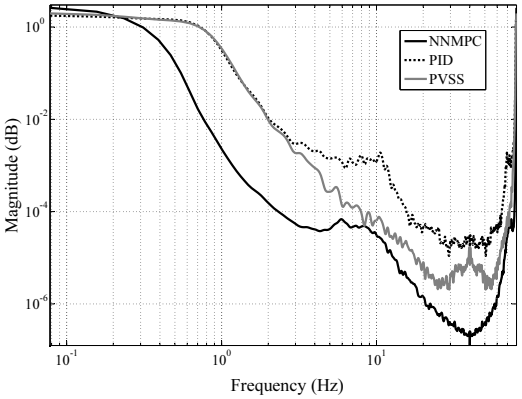

Figure 5.37: Frequency Response for Pitch Angular Acceleration in the Presence of Random Road Disturbance Inputs

All the figures showed good disturbance attenuation within the whole-body vibration frequency range of $0-80Hz$. Amplification, however started just after the $80Hz$ mark. This evidently demonstrates that the physical parameters of the suspension system have been optimally chosen; therefore, the passive suspension performs well in terms of disturbance rejection, but the active suspensions (especially with NNMPC) performs better.

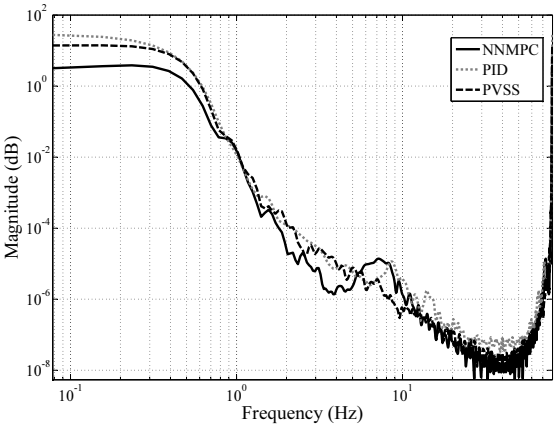

Figure 5.38: Frequency Response for Roll Angular Acceleration in the Presence of Deterministic Road Disturbance Inputs

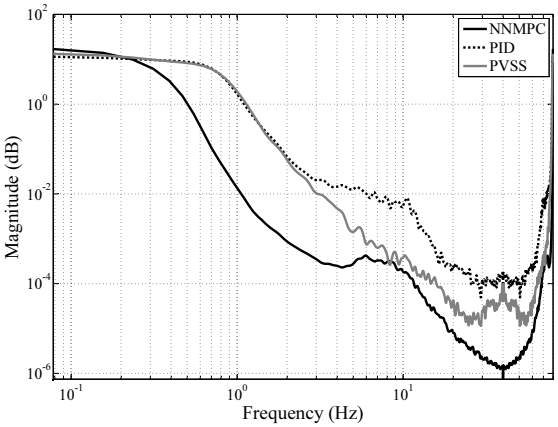

Figure 5.39: Frequency Response for Roll Angular Acceleration in the Presence of Random Road Disturbance Inputs

5.4.1 Frequency-Weighted RMS Acceleration - Ride Comfort

An evaluation of the vehicle ride comfort based on frequency-weighted RMS acceleration is presented in Table 5.10. The assessments were done based on international standards and specifications in BS 6841 (1987); ISO 2631 (2003) and European Commission (2002). The frequency-weighting used are based on the vibration perception filter design shown in Figure 2.44 in Subsection 2.9.3.

The ride comfort assessment for the two road excitations shows that the PID controlled suspension was outperformed by the NNMPC, corroborating the results in Figures 5.14 and 5.24. Handling the random road excitation was more challenging for both controllers but the PID controller had it about 1.5 times more challenging than the NNMPC. Therefore, ride by the occupants are safely in the *comfortable* region for both controller.

Table 5.10: Ride Comfort Assessments

Controller	Type of road disturbance input	Weighted Vibration Acceleration, a_v (ms^{-2})	Comfort Level	
			ISO (ms^{-2})	EU-EAV (ms^{-2})
NNMPC	Deterministic	0.2426	not uncomfortable	< EAV
	Random	0.6565	fairly uncomfortable	> EAV < ELV
PID	Deterministic	0.2445	not uncomfortable	< EAV
	Random	0.9078	fairly uncomfortable	> EAV < ELV

5.4.2 Sensitivity to Parameter Variation

In Figures 5.40 to 5.45, results of the analysis for the NNMPC controlled suspension to changes in the physical parameters related to the suspension is presented. Results for the body acceleration, pitch and roll angular accelerations were presented; because they are related to vibration and ride comfort assessment. Moreover, it is necessary to avoid repetition since similar trend will be expected in the plots for other parameters. All the plots showed disturbance attenuation within the WBV

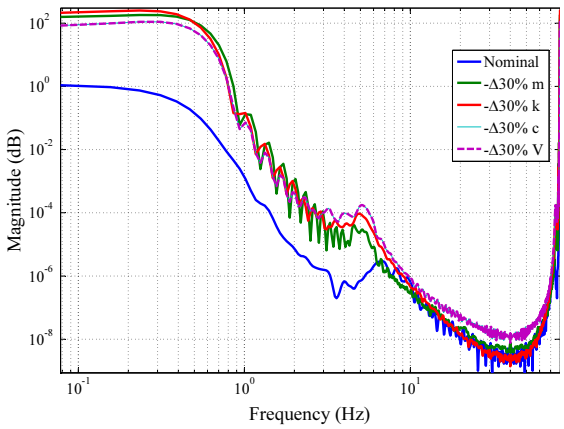

Figure 5.40: Effect of 30% Reduction Physical Parameters on Frequency Response for Vertical Body Acceleration

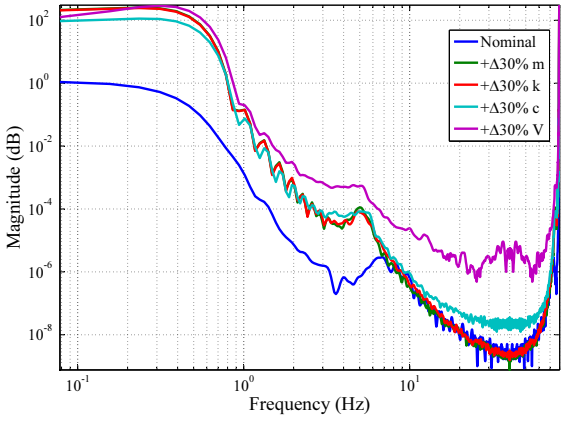

Figure 5.41: Effect of 30% Increase Physical Parameters Parameter Change on Frequency Response for Vertical Body Acceleration

frequency range. This range covers the resonance frequency ranges that are related to vehicle dynamics. It also covers the frequency ranges related to human comfort in moving vehicle (please see Subsections 1.2 and 2.9.3).

The response that is based on the *nominal* suspension parameter values can be seen to be separated from the others at frequencies that are approximately less than $7Hz$. Between 7 and $8Hz$ all the responses tend to cluster together. Therefore, within this range, it could be said that the suspension system tends to be insensitive to changes in the physical parameters.

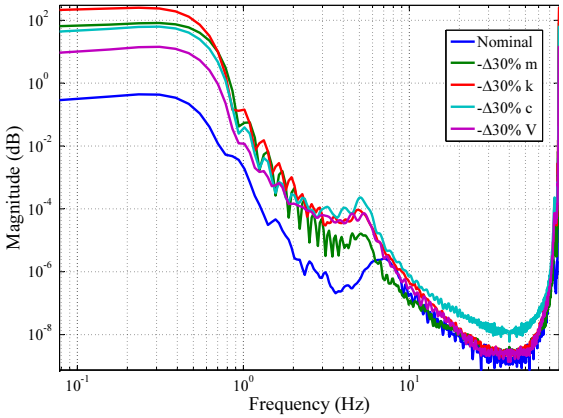

Figure 5.42: Effect of 30% Reduction Physical Parameters on Frequency Response for Pitch Angular Acceleration

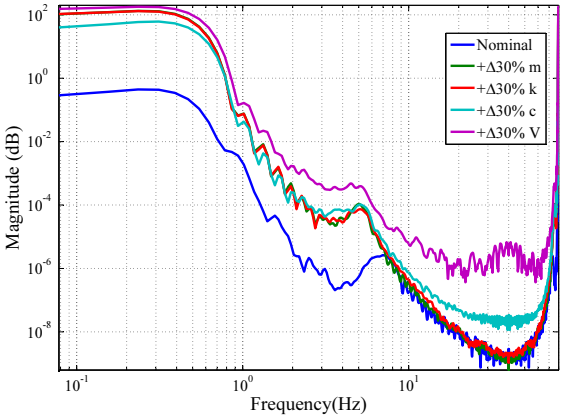

Figure 5.43: Effect of 30% Increase Physical Parameters on Frequency Response for Pitch Angular Acceleration

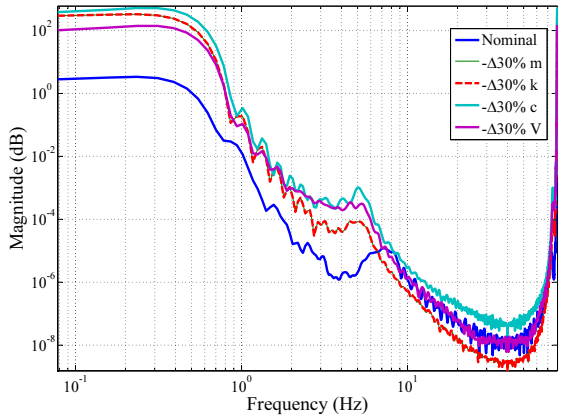

Figure 5.44: Effect of 30% Reduction Physical Parameters on Frequency Response for Roll Angular Acceleration

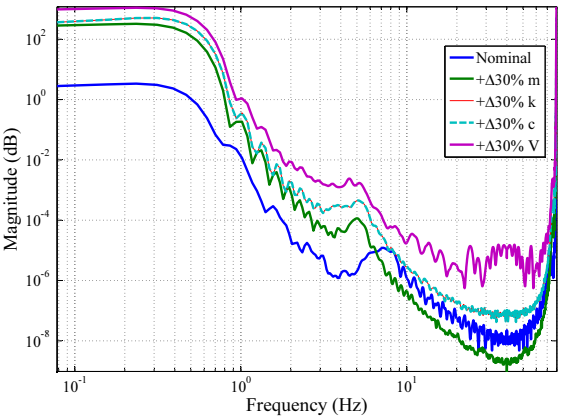

Figure 5.45: Effect of 30% Increase Physical Parameters Frequency Response for Roll Angular Acceleration

5.5 Summary of Chapter Five

The requisites for good model predictive control includes availability of dynamic model. Also, it is necessary for nonlinear models model to be affine. The 7DOF full vehicle suspension model under study meets this requirements, its dynamic model was obtained through neural network with a prediction fitness of about 99.9%.

In this chapter the superior performance of NNMPC-controlled AVSS over PID-Controlled AVSS and PVSS was demonstrated. Good ride comfort levels was also ascertained for these AVSSs according to international standards and specifications. Lastly, the NNMPC-controlled AVSS was observed to demonstrate robustness to parameter variations between frequencies $7 - 80Hz$.

6 Conclusion and Future Outlook

6.1 Introduction

This thesis has presented direct and indirect adaptive neuro-controllers that enhanced the potential performance of the AVSS. The neural network based model predictive controller was designed for a nonlinear, 7DOF full-car suspension system. The control results show that enhancements were achieved for ride comfort, vehicle handling and road holding without violating specified suspension travel limits.

The implemented architecture for the AVSS consist of inner PID feedback loops to stabilize the actuator dynamics, and outer NNMPC feedback loops to regulate the suspension travel in the presence of a twin-hump deterministic and a grade C (average) category of random road excitation.

The research work aimed at designing a suitable neuro-adaptive controller for a nonlinear full-car model. Neural network-based direct adaptive control (DANN), feedback linearization control (NNFBL) and model predictive control (NNMPC) methods were designed and their performances were evaluated for a simpler quarter-car case. Results presented in Chapter four showed that this three controllers had better performance when compared with the PID-controlled AVSS. However, NNMPC-controlled AVSS had the least performance of the three.

It is however noteworthy that, the superior performance of the DANN and NNFBL-controlled AVSSs were at the cost of poor control voltage (control input) whose signals were both characterised by chatterings. The control voltage values also switched intermittently between $\pm 10 Volts$ limit values. This problem makes their practical implementation more challenging and less attractive than the NNMPC-controlled AVSS inspite of their superior performances.

Evaluation of the NNMPC-controlled AVSS for the full-car model in Chapter five

shows that its performances were superior to those of the PID-controlled AVSS and the PVSS in terms of ride comfort, vehicle handling, road holding, suspension travel and control voltage. Disturbances were attenuated within the WBV range, which contains the resonance frequency ranges that are critical for the vehicle and human passengers. The superior wheel dynamic load performance assures better road holding and braking. This is well complemented by its better vehicle handling.

6.2 Neural Network-Based Model Predictive Control

Model predictive controllers has been successfully employed in the chemical and process plants, where the system dynamics is much slower than that of vehicle suspension. Its area of strength include; its suitability for online implementation, applicability for multivariable systems and the handling of state and input constraints. NNMPC overcomes the challenge of acquisition of accurate model by neural network-based system identification. This method of training is presently well developed and accurate as shown in Sections 4.2.1 and 5.2.

Another additional advantage of NNMPC is that the relatively simple to implement multi-layer perceptron neural network with one hidden layer is sufficient for its identification and control process. Therefore, the more complex and computationally demanding neural network structures are not needed. Moreover, the system identification process could be carried out offline, while control is done online. Implementing MPC with neural network is more attractive when compared to fuzzy logic because it requires less number of parameters, thereby becoming simpler.

Compared to the neural network-based feedback linearisation and PID controllers designed in this work, NNMPC was found to be relatively slower during implementation. This is expected because of the internal optimisation loop and computational challenges arising from the non-convex quadratic problem it solves. Implementation of the NNMPC will however come with hardware challenges in this regard.

6.3 Possible Future AVSS Controller Design Outlook

The current growth in vehicle suspension research has not influenced the choice of suspensions fitted to vehicles. Passive suspensions remain the manufacturers' choice because of its simplicity. It therefore becomes an economic decision to trade between

this simplicity and its performance limitations. The advances made in the areas of electronics, instrumentation and actuators are an indication that technological constraints will not continue to hinder the implementation of AVSS on commercial scale.

Linear actuators are already being used to replace the conventional electrohydraulic actuators in some AVSS research but its commercial viability is low [Xue et al. (2011)]. Therefore, it is still relevant to improve on the control performance of the electrohydraulic actuator systems with focus on reducing the size, increasing performance and capacity, and improving its control and stability.

Conventional control methods have proven inadequate in nonlinear control of vehicle suspensions, thus there is bound to be more focus on combining computational intelligence techniques with nonlinear control methods. Future AVSS controller design work can be expected to address the need for multiobjective optimisation of controlled parameters in AVSS or in intelligent tuning of the designed controllers.

Moreover, since controller designs are likely to lean more towards intelligent techniques, issues of fault tolerance and diagnosis will need to be considered in the design process. Computational challenges tend to increase with the complexity of the control method, thus simple conventional PID can be expected to play bigger roles in future AVSS control design.

6.3.1 Future PID-Based AVSS Controllers

PID-based controllers remain the most employed industrial controllers because of its simple structure, easy implementation, lower cost, relative effectiveness and more intuitive tuning procedures. Often, the economic benefits derivable from the PID outweighs its lack of robustness, especially when the vicinity of its operating region could be identified.

The popularity of PID controllers has resulted in progress being made in PID related research areas like: auto-tuning methods, implementation with evolutionary algorithms, pseudo-derivative feedback control algorithm, nonlinear PID controllers, robust PID controllers and fractional-order PID control methods. Unlike the advanced controllers, application of PID controllers are more universal and are easier to test.

These developments and the use of PID controllers for actuator dynamics stabilization show that the prospect for vehicle suspension control based on PID-based algorithm is high. The challenge lies in improving its robustness to parameter uncertainty and time-varying operating conditions. Recent works have shown that the robustness of PID controllers in AVSS can be improved by the addition of neural network-based controllers in the feedforward path.

In future, global optimisation techniques and evolutionary algorithms can be expected to play bigger roles in PID controller designs for AVSS but the challenge will lie in implementing this online because of the necessity for numerous iterations.

6.4 Recommendations for Future Works

Concluding this research work brings to the open following salient and interesting issues that should be pursued in further works:

1. There is a need to follow-up the analysis carried out with experimental validation. This could be done with the quarter-car hardware-in-the -loop laboratory setting or using an actual car.

2. The sensitivity analysis carried out showed that though a lot of works exists in the literature regarding optimal design of physical parameters for the PVSS, it should be the first step in AVSS design.

3. Controller design based on intelligently tuned PID control need to be studied more closely because of its prospects in terms of physical implementation and simplicity. Further development regarding hybrid-PID control methods is therefore recommended.

4. The scope of this work does not include investigation regarding induced roll motion modes and the effects of braking and cornering.

5. Inclusion of fault tolerance concept in the design analysis is also recommended for future works to enhance the quality and lifespan of the designed AVSS.

REFERENCES

Aghaie, Z. and Amirifar, R. (2007), H_2 and H_∞ controllers design for an active suspension system via Riccati equations and LMIs, *in* 'Proceedings of the 2nd International Conference on Innovative Computing, Information and Control, 2007 (ICICIC '07)', Kumamoto, Japan, pp. 341–341.

Ahlin, K. and Granlund, N. O. J. (2002), 'Relating road roughness and vehicle speeds to human whole body vibration and exposure limits', *International Journal of Pavement Engineering* **3**(4), 207–216.

Akbari, A., Geravand, M. and Lohmann, B. (2010), Output feedback constrained H_∞ control of active suspensions, *in* 'Proceedings of the 2nd IEEE International Conference on Advanced Computer Control (ICACC2010)', Shenyang, China, pp. 399–404.

Akcay, H. and Turkay, S. (2009), 'Influence of tire damping on mixed H_2/H_∞ synthesis of half-car active suspensions', *Journal of Sound and Vibration* **322**(1-2), 15–28.

Akesson, B. M. and Toivonen, H. T. (2006), 'A neural network model predictive controller', *Journal of Process Control* **16**(9), 937–946.

Al-Duwaish, H. N. and Rizvi, S. Z. (2011), 'A robust controller for non-linear MIMO systems using radial basis function neural network', *Proceedings of the Institute of Mechanical Engineers, Part I: Journal of Systems and Control Engineering* **225**(5), 667–682.

Al-Holou, N., Lahdhiri, T., Joo, D. S., Weaver, J. and Al-Abbas, F. (2002), 'Sliding mode neural network inference fuzzy logic control for active suspension system', *IEEE Transactions on Fuzzy System* **10**(2), 234–245.

Aldair, A. A. and Wang, W. J. (2010), 'Design of fractional order controller based on evolutionary algorithm for a full vehicle nonlinear active suspension system', *International Journal of Control and Automation* **3**(4), 33–46.

Alfi, A. and Fateh, M. M. (2011), 'Identification of nonlinear systems using modified particle swarm optimisation: A hydraulic suspension system', *Vehicle System Dynamics: International Journal of Vehicle Mechanics and Mobility* **49**(6), 871–887.

Alleyne, A. and Lui, R. (2000), 'Systematic control of a class of non-linear systems with application to electro-hydraulic cylinder pressure control', *IEEE Transactions on Control Systems Technology* **8**(4), 623–634.

Ang, K. H., Chong, G. and Li, Y. (2005), 'PID control system analysis, design, and technology', *IEEE Transactions on Control Systems Technology* **13**(4), 559–576.

Astrom, K. J. and Hagglund, T. (2001), 'The future of PID control', *Control Engineering Practice* **9**(11), 1163–1175.

Astrom, K. J. and Wittenmark, B. (1989), *Adaptive Control*, Addison-Wesley Publishing Company, Reading, Massachusetts, USA.

Awwad, A., Abu-Rub, H. and Toliyat, H. A. (2008), Nonlinear autoregressive moving average (NARMA-L2) controller for advanced AC motor control, *in* 'Proceedings of the 34th Annual IEEE Conference on Industrial Electronics (IECON 2008)', Orlando, FL, USA, pp. 1287–1292.

Ayalew, B. and Kulakowski, B. T. (2005), 'Modeling supply and return line dynamics for an electrohydraulic actuation system', *ISA Transactions* **44**(3), 329–343.

Azimi-Sadjadi, M. R. and Liou, R. J. (1992), 'Fast learning process of multilayer neural networks using recursive least squares method', *IEEE Transactions on Signal Processing* **40**(2), 446–450.

Bacciotti, A. and Rosier, L. (2005), *Liapunov Functions and Stability in Control Theory*, Springer Berlin Heidelberg, New York.

Bars, R., Colaneri, P., Dugard, L., Allgower, F., Kleimenov, A. and Scherer, C. (2008), Trends in theory of control system design, *in* 'Proceedings of the 17th World Congress, The International Federation of Automatic Control (IFAC)', Seoul, Korea, pp. 3392–3397.

Baslamisli, S. C. and Unlusoy, Y. S. (2009), 'Optimization of speed control hump profiles', *Journal of Transportation Engineering* **135**(5), 260–269.

Baumal, A. E., McPhee, J. J. and Calamai, P. H. (1998), 'Application of genetic algorithms to the design optimization of an active suspension system', *Computer Methods in Applied Mechanics and Engineering* **163**(1-4), 87–94.

Becker, M., Jaker, K. P., Fruhauf, F. and Rutz, R. (1996), Develeopment of an Active Suspension System for a Mercedes-Benz Coach (O404), *in* 'Proceedings of the IEEE International Symposium on Computer Aided Control System Design', Dearborn, MI, USA, pp. 146–151.

Behera, L. and Kar, I. (2009), *Intelligent Systems and Control: Principles and Application*, Oxford University Press, New Delhi, India.

Bequette, B. W. (2007), 'Non-linear model predictive control: A personal retrospective', *The Canadian Journal of Chemical Engineering* **85**(4), 408–15.

Biglarbegian, M., Melek, W. and Golnaraghi, F. (2008), 'A novel neuro-fuzzy controller to enhance the performance of vehicle semi-active suspension systems', *Vehicle System Dynamics: International Journal of Vehicle Mechanics and Mobility* **46**(8), 691–711.

Bogsjo, K., Podgorski, K. and Rychlik, I. (2012), 'Models for road surface roughness', *Vehicle System Dynamics: International Journal of Vehicle Mechanics and Mobility* **50**(5), 725–747.

Bomberger, J. D. and Seborg, D. E. (1998), 'Determination of model order for NARX models directly from input-output data', *Journal of Process Control* **8**(5-6), 459–468.

Bonin, G., Cantisani, G., Loprencipe, G. and Shrolli, M. (2007), Ride quality evaluation: 8 D. O. F vehicle model calibration, *in* 'Proceedings of the 4th International Societa Italiana Infrastrutture Viarie SIIV Congress', Palermo, Italy, pp. 1–12.

Breytenbach, B. and Els, P. S. (2011), 'Optimal vehicle suspension characteristics for increased structural fatigue life', *Journal of Terramechanics* **48**(6), 397–408.

BS 6841 (1987), *Measurement and Evaluation of Human Exposure to Whole-Body Mechanical Vibration and Repeated Shock*, British Standards Institution, London, U.K.

Buckner, G. D., Schuetze, K. T. and Beno, J. H. (2000), Active vehicle suspension control using intelligent feedback linearization, *in* 'Proceedings of the American Control Conference', Vol. 6, Chicago, IL USA, pp. 4014–4018.

Cao, D., Song, X. and Ahmadian, M. (2011), 'Editor's perspectives: Road vehicle suspension design, dynamics and control', *Vehicle System Dynamics: International Journal of Vehicle Mechanics and Mobility* **49**(1-2), 3–28.

Cao, J., Liu, H., Li, P. and Brown, D. (2008), 'State of the art in vehicle active suspension adaptive control systems based on intelligent methodologies', *IEEE Transactions of Intelligent Transportation Systems* **9**(3), 392–405.

Cao, J.-T., Li, P. and Liu, H. H. (2010), 'An extended fuzzy controller for a vehicle active suspension system', *Proceedings of the Institution of Mechanical Engineers, Part D: Journal of Automobile Engineering* **224**(6), 717–733.

Cao, J.-T., Liu, H. H., Li, P., Brown, D. J. and Dimirovski, G. (2007), 'A study of electric vehicle suspension control system based on an improved half-vehicle model', *International Journal of Automation and Computing* **4**(3), 236–242.

Castro, L. R., Agamennoni, O. E. and Alvarez, M. P. (2010), 'From linear to nonlinear identification: One step at a time', *Mathematical and Computer Modelling* **51**(5-6), 473–486.

Cetin, S. and Akkaya, A. V. (2010), 'Simulation and hybrid fuzzy-PID control for positioning of a hydraulic system', *Nonlinear Dynamics* **61**(3), 465–476.

Chai, L. and Sun, T. (2010), 'The design of LQG controller for active suspension based on analytic hierarchy process', *Mathematical problems in Engineering* **Vol. 2010**(Article id. 701951), 1–19.
URL: *http://www.hindawi.com/journals/mpe/2010/*

Chamseddine, A. and Noura, H. (2008), 'Control and sensor fault tolerance of vehicle active suspension', *IEEE Transactions on Control Systems Technology* **16**(3), 416–433.

Chantranuwathana, S. and Peng, H. (2004), 'Adaptive robust force control for vehicle active suspensions', *International Journal of Adaptive Control and Signal Processing* **18**(2), 83–102.

Chemachema, M. and Belarbi, K. (2011), 'Direct adaptive neural network controller for a class of nonlinear systems based on fuzzy estimator of the control error', *International Journal of Systems Science* **42**(7), 1165–1173.

Chen, H. and Guo, K. H. (2005), 'Constrained H_∞ control of active suspensions: An LMI approach', *IEEE Transactions on Control Systems Technology* **13**(3), 412–421.

Chen, J. and Yea, Y. (2002), 'Neural network-based predictive control for multivariable processes', *Chemical Engineering Communications* **189**(7), 865–894.

Chen, L. H. and Chiang, C. H. (2003), 'New approach to intelligent control systems with self-exploring process', *IEEE Transactions on Systems, Man and Cybernetics - Part B: Cybernetics* **33**(1), 56–66.

Chen, M. C., Wang, W. Y., Su, S. F. and Chien, Y. H. (2010), 'Robust T-S fuzzy-neural control of uncertain active suspension systems', *International Journal of Fuzzy Systems* **12**(4), 321–329.

Chen, S. and Xiao, X. (2011), *Optimal Design of Structure and Control Parameters of Active Suspension based on PID Control*, Vol. 227 of *Communications in Computer and Information Science (CCIS)*, pp. 204–210.

Chen, S., Zhou, H., Liu, H. and Yao, M. (2011), Optimal design of active suspension based on LQG control without road input signal, *in* 'Proceedings - 4th International Conference on Intelligent Computation Technology and Automation, ICICTA 2011', Vol. 1, pp. 456–459.

Chien, T. L., Chen, C. C., Tsai, M. C. and Chen, Y. C. (2009), 'Almost disturbance decoupling and tracking control for multi-input multi-output non-linear uncertain systems: Application to a half-car active suspension system', *Proceedings of the Institute of Mechanical Engineers, Part I: Journal of Systems and Control Engineering* **223**(2), 215–227.

Chiou, J. S. and Liu, M. T. (2009), 'Using fuzzy logic controller and evolutionary genetic algorithm for automotive active suspension system', *International Journal of Automotive Technology* **10**(6), 703–710.

Chiou, J.-S., Tsai, S.-H. and Liu, M.-T. (2012), 'A PSO-based adaptive fuzzy PID-controllers', *Simulation Modelling Practice and Theory* **26**(8), 49–59.

Cole, D. J. (2001), 'Fundamental issues in suspension design for heavy road vehicles', *Vehicle System Dynamics: International Journal of Vehicle Mechanics and Mobility* **35**(4-5), 319–360.

Cossalter, V., Doria, A., Garbin, S. and Lot, R. (2006), 'Frequency-domain method for evaluating the ride comfort of a motorcycle', *Vehicle System Dynamics: International Journal of Vehicle Mechanics and Mobility* **44**(4), 339–355.

Crivellaro, C. and Donha, D. C. (2011*a*), 'Fast experimental identification of suspension models for control design', *Proceedings of the Institute of Mechanical Engineers, Part D: Journal of Automobile Engineering* **225**(5), 609–626.

Crivellaro, C. and Donha, D. C. (2011*b*), Performance and stability barriers for robust control designs of SUV active suspensions, *in* 'Proceedings of the 17th World Congress, The International Federation of Automatic Control (IFAC)', Milano, Italy, pp. 2190–2195.

Crolla, D. A. and Nour, A. M. A. A. (1992), 'Power losses in active and passive suspensions of off-road vehicles', *Journal of Terramechanics* **29**(1), 83–93.

Dahunsi, O. A., Pedro, J. O. and Nyandoro, O. T. (2009), Neural network-based model predictive control of a servo-hydraulic vehicle suspension system, *in* 'Proceedings of the IEEE AFRICON', Nairobi, Kenya.

Dahunsi, O. A., Pedro, J. O. and Nyandoro, O. T. (2010), 'System identification and neural network based PID control of servo-hydraulic vehicle suspension systems',

Transactions of the South African Institute of Electrical Engineersion (SAIEE), Africa Research Journal (ARJ) **101**(3), 93–105.

Demuth, H. and Beale, M. (2006), *Neural Networks Toolbox Users Guide: For use with MATLAB*, The MathWorks, Inc., Natick, Massachusetts.

Dixon, J. C. (2007), *The Shock Absorber Handbook*, John Wiley and Sons, Ltd., West Sussex, England.

Do, A., Spelta, C., Savaresi, S., Sename, O., Dugard, L. and Delvecchio, D. (2006), An LPV control approach for comfort and suspension travel improvements of semi-active suspension systems, *in* 'Proceedings of the 49th IEEE Conference on Decision and Control (CDC)', Atlanta, GA, USA, pp. 5560–5565.

Dong, G. M., Zhang, N. and Du, H. P. (2011), 'Investigation into untripped rollover of light vehicles in the modified fishhook and the sine manoeuvres, Part II: Effects of vehicle inertia property, suspension and tyre characteristics', *Vehicle System Dynamics: International Journal of Vehicle Mechanics and Mobility* **49**(1-2), 949–968.

Dong, X. M., Yu, M., Li, Z., Liao, C. and Chen, W. (2009), 'A comparison of suitable control methods full vehicle with four MR dampers, Part I: Formulation of control schemes and numerical simulation', *Journal of Intelligent Material Systems and Structures* **20**(7), 771–786.

Du, H. and Zhang, N. (2007), 'H_∞ control of active vehicle suspensions with actuator time delay', *Journal of Sound and Vibration* **301**(1-2), 236–252.

Du, H. and Zhang, N. (2008*a*), 'Designing H_∞/GH_2 static - output feedback controller for vehicle suspensions using linear matrix inequalities and genetic algorithms', *Vehicle Systems Dynamics* **46**(5), 385–412.

Du, H. and Zhang, N. (2008*b*), 'Multiobjective static output feedback control design for vehicle suspensions', *Journal of System Design and Dynamics* **2**(1), 228–239.

Du, H. and Zhang, N. (2009), 'Static output feedback control for electrohydraulic active suspensions via T-S fuzzy model approach', *Journal of Dynamic Systems, Measurement and Control:Transactions of ASME* **131**(5), 051004–1–051004–11.

Du, H., Zhang, N. and Naghdy, F. (2011), 'Robust control of a vehicle electrorheological suspension subject to measurement noises', *Vehicle System Dynamics: International Journal of Vehicle Mechanics and Mobility* **49**(1-2), 257–275.

Duarte-Mermoud, M. A. and Prieto, R. A. (2004), 'Performance index for quality response of dynamical systems', *ISA Transactions* **43**(1), 133–151.

Dzielinski, A. (2002), 'Neural network-based NARX models in non-linear adaptive control', *International Journal of Applied Mathematics and Computer Science, AMCS* **12**(2), 235–240.

Ekoru, J. E. D., Dahunsi, O. A. and Pedro, J. O. (2011), PID control of a nonlinear half-car active suspension via force feedback, *in* 'Proceedings of the 2011 IEEE AFRICON', Livingstone, Zambia.

ElMadany, M. M. and Abduljabbar, Z. S. (1999), 'Linear quadratic gaussian control of a quarter-car suspension', *Vehicle System Dynamics: International Journal of Vehicle Mechanics and Mobility* **32**(6), 479–497.

ElMadany, M. M. and Al-Majed, M. I. (2001), 'Quadratic synthesis of active controls for a quarter-car model', *Journal of Vibration and Control* **7**(8), 1237–1252.

ElMadany, M. M., Bassam, B. A. and Fayed, A. (2011), 'Preview control of slow-active suspension systems', *Journal of Vibration and Control* **17**(2), 245–258.

ElMadany, M. M. and Qarmoush, A. O. (2011), 'Dynamic analysis of a slow-active suspension systems based on a full-car model', *Journal of Vibration and Control* **17**(1), 39–53.

Eski, I. and Yildrim, S. (2009), 'Vibration control of vehicle active suspension system using a new robust neural network control system', *Simulation Modelling Practice and Theory* **17**(5), 778–793.

European Commission (2002), *Directive 2002/44/EC of the European Parliament and the Council of 25 June 2002 on the minimum health and safety requirements regarding the exposure of workers to the risk arising from physical agents (vibration)*, Official Journal of the European Communities, Luxembourg.

Evers, W. J., Besselink, I., Teerhuis, A. and Nijimeijer, H. (2011), 'On the achievable performance using variable geometry active secondary suspension systems in commercial vehicles', *Vehicle System Dynamics: International Journal of Vehicle Mechanics and Mobility* **49**(10), 1553–1573.

Fallah, M. S., Bhat, R. and Xie, W. F. (2009), H_∞ robust control of active suspensions: A practical point of view, *in* 'Proceedings of the 2009 American Control Conference', St. Louis, MO USA, pp. 1385–1390.

Fateh, M. M. and Alavi, S. S. (2005), 'Impedance control of an active suspension system', *Mechatronics* **19**(1), 134–140.

Fateh, M. M. and Zirkohi, M. M. (2011), 'Adaptive impedance control of a hydraulic suspension system using particle swarm optimisation', *Vehicle System Dynamics: International Journal of Vehicle Mechanics and Mobility* **49**(12), 1951–1965.

Feng, J. Z., Li, J. and Yu, F. (2003), 'GA-based PID and fuzzy logic control for active vehicle suspension system', *International Journal of Automotive Technology* **4**(4), 181–191.

Fialho, I. and Balas, G. J. (2002), 'Road adaptive active suspension using linear parameter-varying gain-scheduling', *IEEE Transactions on Control Systems Technology* **10**(1), 43–54.

Fijalkowski, B. T. (2011), *Automotive Mechatronics: Operational and Practical Issues*, number 2 *in* 'Intelligent Systems, Control and Automation: Science and Engineering Vol. 52', Springer Netherlands, Netherlands.

Fischer, D. and Isermann, R. (2004), 'Mechatronic semi-active and active vehicle suspensions', *Control Engineering Practice* **12**(11), 1353–1367.

Gao, B., Tilley, D. G., Williams, R. A., Bean, A. and Donahue, J. (2006), 'Control of hydropneumatic active suspension based a non-linear quarter-car model', *Proceedings of the Institute of Mechanical Engineers, Part I: Journal of Systems and Control Engineering* **220**(1), 31–75.

Gao, Z. (2002), 'From linear to nonlinear control means: A practical progression', *ISA Transactions* **41**(2), 177–189.

Garces, F. R., Becerra, V. M., Kambhampti, C. and Warwick, K. (2003), *Strategies for Feedback Linearisation: A Dynamic Neural Network Approach*, Springer, London.

Gaspar, P., Szabo, Z. and Bokor, J. (2009), Active suspension in integrated vehicle control, *in* J. Kleban, ed., 'Switched Systems', Intech, Croatia, pp. 83–104.

Gaspar, P., Szabo, Z. and Bokor, J. (2011), LPV design of adaptive integrated control for road vehicles, *in* 'Proceedings of the 18th World Congress, The International Federation of Automatic Control (IFAC)', Milano, Italy, pp. 662–667.

Gaspar, P., Szaszi, I. and Bokor, J. (2003), 'Active suspension design using linear parameter varying control', *International Journal of Autonomous Systems (IJVAS)* **1**(2), 206–221.

Gavriloski, V., Danev, D. and Angushev, K. (2007), Mechatronic approach in vehicle suspension system design, *in* 'Proceedings of the 12th IFToMM World Congress', Besacon, France.

Ge, S. S. and Lee, T. H. (1997), 'Robust adaptive neural network control for a class of nonlinear system', *Proceedings of the Institute of Mechanical Engineers, Part I: Journal of Systems and Control Engineering* **224**(1), 41–53.

Ge, S. S., Lee, T. H. and Harris, C. J. (1998), *Adaptive Neural Network Control of Robotic Manipulators*, World Scientific Publishing Co. Pte. Ltd., Singapore.

Gillespie, T. D. (1992), *Fundamentals of Vehicle Dynamics*, Society of Automotive Engineers, Inc., Warendale, PA.

Giovanni, L. (2009), 'Predictive feedback control: An alternative to proportional-integral-derivative control', *Proceedings of the Institute of Mechanical Engineers, Part I: Journal of Systems and Control Engineering* **223**(7), 901–917.

Goncalves, E. N., Palhares, R. M. and Takahashi, R. H. C. (2008), 'A novel approach for H_2/H_∞ robust PID synthesis for uncertain systems', *Journal of Process Control* **18**(1), 19–26.

Goodwin, G. C., Dona, J. D., Rojas, O. J. and Perrier, M. (2001), A brief overview of nonlinear control, *in* 'Plenary Address: 3rd International Conference on Control Theory and Applications', Pretoria, South Africa.

Gopala Rao, L. V. V. and Narayanan, S. (2009), 'Sky-hook control of nonlinear quarter car model traversing rough road matching performance of LQR control', *Journal of Sound and Vibration* **323**(3-5), 515–529.

Griffin, M. J. (2007), 'Discomfort from feeling vehicle vibration', *Vehicle Systems Dynamics* **45**(7-8), 679–698.

Guan, C. and Pan, S. (2008), 'Adaptive sliding mode control of electro-hydraulic system with nonlinear unknown parameters', *Control Engineering Practice* **16**(11), 1275–1284.

Guclu, R. (2004), 'Active suspension control of eight degree of freedom vehicle model', *Mathematical and Computational Applications* **9**(1), 1–10.

Guglielmino, E. and Edge, K. A. (2004), 'A controlled friction damper for vehicle applications', *Control Engineering Practice* **12**(4), 431–443.

Guglielmino, E., Sireteanu, T., Stammers, C. W., Ghita, G. and Giuclea, M. (2008), *Semi-Active Suspension Control: Improved Vehicle Ride and Road Friendliness*, Springer-Verlag London Limited, London, U.K.

Guo, L. X. and Zhang, L. P. (2012), 'Robust H_∞ control of active vehicle suspensions under non-stationary running', *Journal of Sound and Vibration* **331**(26), 5824–5837.

Gysen, B. L. J., Paulides, J. J. H., Janssen, J. L. G. and Lomonova, E. A. (2010), 'Active electromagnetic suspension system for improved vehicle dynamics', *IEEE Transactions on Vehicular Technology* **59**(3), 1156–1163.

Hada, M. K., A.Menon and S.Y.Bhave (2007), 'Optimisation of an active suspension force controller using genetic algorithm for random input', *Defence Science Journal* **57**(5), 691–706.

Hagan, M. T., Demuth, H. B. and Jesus, O. (2002), 'An introduction to the use of neural networks in control systems', *International Journal of Robust and Non-Linear Control* **12**(11), 959–985.

Hayakawa, K., Matsumoto, K., Yamashita, M., Suzuki, Y., Fujimori, K. and Kimura, H. (1999), 'Robust H_∞ - output feedback control of decoupled automobile active suspension system', *IEEE Transactions on Automatic Control* **44**(2), 392–396.

Haykin, S. (2009), *Neural Networks and Learning Machines*, Pearson Education, Inc., New Jersey.

He, S. (2009), 'Neural predictive force control for a hydraulic actuator: Simulation and Experiment', *Applied Artificial Intelligence* **23**(2), 151–167.

He, X. and Asada, H. (1993), A new method for identifying orders of input-output models for nonlinear dynamic systems, *in* 'Proceedings of the American Control Conference', Vol. 6, San Fransisco, California, USA, pp. 2520–2523.

He, Y. and McPhee, J. (2005), 'A design methodology for mechatronic vehicles: Application of multidisciplinary optimization, multibody dynamics and genetic algorithms', *Vehicle Systems Dynamics* **43**(10), 697–733.

Herrnberger, M., Mader, D. and Lohmann, B. (2008), Linear robust control for a nonlinear active suspension model considering variable payload, *in* 'Proceedings of the 17th World Congress, The International Federation of Automatic Control (IFAC)', Seoul, Korea, pp. 6277–6281.

Hrovat, D. (1997), 'Survey of advanced suspension developments and related optimal control applications', *Automatica* **33**(10), 1781 – 1817.

Hu, J.-W. and Lin, J. S. (2008), Sliding mode controllers for active suspensions, *in* 'Proceedings of the 17th World Congress, The International Federation of Automatic Control (IFAC)', Seoul, Korea, pp. 3416–3421.

Huang, C.-J., Li, T.-H. S. and Chen, C.-C. (2009), 'Fuzzy feedback linearization control for MIMO nonlinear system and its application to full-vehicle suspension system', *Circuits, Systems, and Signal Processing* **28**(6), 959–991.

Huang, C. J., Lin, J. S. and Chen, C. C. (2010), 'Road-adaptive algorithm design of half-car active suspension system', *Expert Systems with Applications* **37**(6), 4392–4402.

Huang, S. J. and Chao, H. C. (2000), 'Fuzzy logic controller for a vehicle active suspension system', *Proceedings of the Institute of Mechanical Engineers, Part D: Journal of Automobile Engineering* **214**(1), 609–626.

Huang, S. J. and Lin, W. C. (2002), 'A neural network based sliding mode controller for active vehicle suspension', *Proceedings of the Institute of Mechanical Engineers, Part D: Journal of Automobile Engineering* **211**(11), 1381–1397.

Hunt, K. J., Sbarbaro, D., Zbikowski, R. and Gawthrop, P. J. (1992), 'Neural Networks for Control Systems - A Survey', *Automatica* **28**(6), 1083–1111.

Hyvarinen, J. K. (2004), The Improvement of Full Vehicle Semi-Active Suspension Through Kinematic Model, PhD thesis, University of Oulu, Oulu, Finland.

Ikenaga, S., Lewis, F. L., Davis, L., Campos, J., Evans, M. and Scully, S. (1999), Active suspension control using a novel strut and active filtered feedback: Design and implementation, *in* 'Proceedings of the IEEE International Confrence on Control Applications', Kohala Coast-Island of Hawai'i, Hawai'i, USA, pp. 1502–1508.

Ioannou, P. A. and Sun, J. (1995), *Robust Adaptive Control*, Prentice hall, Ltd., New Jersey.

Isidori, A. (1995), *Nonlinear Control Systems*, Springer-Verlag New York, Inc., Secaucus, NJ, USA.

ISO 2631 (2003), *Mechanical Vibration and Shock - Evaluation of Human Exposure to Whole-Body Vibration - Part 1: General Requirements*, International Organization for Standardization, Geneva, Switzerland.

ISO 8608 (1995), *Mechanical Vibration - Road Surface Profiles - Reporting of Measured Data*, International Organization for Standardization, Geneva, Switzerland.

ITE Technical Council Task Force on Speed Humps (1993), 'Guidelines for the design and application of speed humps-summary of a proposed recommended practice', *Institute of Transport Engineers (ITE) Journal* **63**(5), 11–15.

James, D. J. G., Burnham, K. J., Richardson, M. J. and Williams, R. A. (1999), 'Improving vehicle performance using adaptive control techniques', *Artificial Life and Robotics* **3**(4), 236–241.

Jazayeri, A., Fatehi, A., Sadjadian, H. and Khaki-Sedigh, A. (2008), Disturbance rejection in neural network model predictive control, *in* 'Proceedings of the 17th World Congress, The International Federation of Automatic Control (IFAC)', Seoul, Korea, pp. 6–11.

Jelali, M. and Kroll, A. (2003), *Hydraulic Servo-Systems:Modelling, Identification and Control*, Springer-Verlag, London.

Jeppesen, B. P. and Cebon, D. (2004), 'Analytical redundancy techniques for fault detection in an active heavy vehicle suspension', *Vehicle System Dynamics: International Journal of Vehicle Mechanics and Mobility* **42**(1-2), 75–88.

Jha, R. and He, C. (2004), 'A comparative study of neural and conventional adaptive predictive controllers for vibration suppression', *Smart Materials and Structures* **13**(4), 811–818.

Joo, D. S., Al-Holou, N., Weaver, J. M., Lahdhiri, T. and Al-Abbas, F. (2000), Nonlinear modeling of vehicle suspension system, *in* 'Proceedings of the American Control Conference', Chicago, Illinois, USA, pp. 115–119.

Junyi, C. and Binggang, C. (2011), 'Fractional-order control of pneumatic position servosystems', *Mathematical Problems in Engineering* **2011**(Article id. 287565), 1–14.
URL: *http://www.hindawi.com/journals/mpe/2011/*

Juuso, E. K. (2004), 'Integration of intelligent systems in development of smart adaptive systems', *International Journal of Approximate Reasoning* **35**(3), 307–337.

Kaddissi, C., Saad, M. and Kenne, J. P. (2009), 'Interlaced backstepping and integrator forwarding for nonlinear control of an electrohydraulic active suspension', *Journal of Vibration and Control* **15**(1), 101–131.

Kar, I. and Behera, L. (2009), 'Direct adaptive neural control for affine nonlinear systems', *Applied Soft Computing* **9**(3), 756–764.

Karen, I., Kaya, N., Ozturk, F., Korkmaz, I., Yildizhan, M. and Yurttas, A. (2012), 'A design tool to evaluate the vehicle ride comfort characteristics: Modeling, physical testing and analysis', *International Journal of Advanced Manufacturing Technology* **60**(5-8), 755–763.

Karpenko, M. and Sepehri, N. (2012), 'Electrohydraulic force control design of a hardware-in-the-loop load emulator using a nonlinear QFT technique', *Control Engineering Practice* **20**(6), 598–609.

Kawaji, S., Matsunaga, N. and Arao, M. (1999), 'Toward an information-integrated control system - the control - theoretic view of intelligent control technology', *Artificial Life and Robotics* **3**(4), 203–208.

Kaynak, O., Erbatur, K. and Ertugrul, M. (2001), 'The fusion of computationally intelligent methodologies and sliding-mode control - A Survey', *IEEE Transactions on Industrial Electronics* **48**(1), 4–21.

Khorshid, E., Alkalby, F. and Kamal, H. (2007), 'Measurement of whole-body vibration exposure from speed control humps', *Journal of Sound and Vibration* **304**(3-5), 640–659.

Kim, C. and Ro, P. I. (1998), 'A sliding mode controller for vehicle active suspesion systems with nonlineariies', *Proceedings of the Institute of Mechanical Engineers, Part D: Journal of Automobile Engineering* **212**(2), 79–92.

Kim, G., Kang, S., Lee, Y., Park, S. and Jung, W. (2012), 'Study on durability and reliability of strut type suspension noise based on experimental methods', *Journal of Mechanical Science and Technology* **26**(1), 21–29.

Kim, M. S., Kim, K. W. and Yoo, W. S. (2011), 'Method to objectively evaluate subjective ratings of ride comfort', *International Journal of Automotive Technology* **12**(6), 831–837.

Kim, Y. G., Kwon, H. B., Kim, S. W., Park, C. K. and Park, T. W. (2003), 'Correlation of ride comfort evaluation methods for railway vehicles', *Proceedings of the Institute of Mechanical Engineers, Part F: Journal of Rail and Rapid Transit* **217**(2), 73–88.

Koch, G., Fritsch, O. and Lohmann, B. (2008), Potential of low bandwidth active suspension control with continuously variable damper, *in* 'Proceedings of the 17th World Congress, The International Federation of Automatic Control (IFAC)', Seoul, South Korea, pp. 3392–3397.

Koch, G. P. A. (2011), Adaptive Control of Mechatronic Vehicle Suspension Systems, PhD thesis, Technische Universitat Munchen, Munich, Germany.

Koshkouei, A. J. and Burnham, K. J. (2008), Sliding mode controllers for active suspensions, *in* 'Proceedings of the 17th World Congress, The International Federation of Automatic Control (IFAC)', Seoul, Korea, pp. 3416–3421.

Kristic, M., Kanellakopoulos, I. and Kokotovic, P. (1995), *Nonlinear and Adaptive Control Design*, John Wiley and Sons, Inc, New York, USA.

Kropac, O. and Mucka, P. (2008), 'Effect of obstacles in the road profile on the dynamic response of a vehicle', *Proceedings of the Institute of Mechanical Engineers, Part D: Journal of Automobile Engineering* **222**(3), 353–370.

Kumar, M. S. (2008), Development of active suspension system for automobiles using PID controller, *in* 'Proceedings of the World Congress on Engineering 2008 (WCE2008)', London, U. K., pp. 1–6.

Kumar, M. S. and Vijayarangan, S. (2006), 'Linear quadratic regulator controller design for active suspension system subjected to random road surfaces', *Journal of Scientific and Industrial Research (JSIR)* **65**(3), 213–226.

Kuo, Y. and Li, T. S. (1999), 'GA-based fuzzy PI/PD controller for automotive active suspension system', *IEEE Transactions on Industrial Electronics* **46**(6), 1051–1056.

La Salle, J. and Lefschetz, S. (1991), *Stability Theory by Liapunov's Direct Method*, Academic Press, New York.

Lawrynczuk, M. (2007), 'A family of model predictive control algorithms with artificial neural networks', *International Journal of Applied Mathematics and Computer Science, AMCS* **17**(2), 217–232.

Lawrynczuk, M. (2009), 'Efficient nonlinear predictive control based on structured neural models', *International Journal of Applied Mathematics and Computer Science, AMCS* **19**(2), 233–246.

Lazar, M. and Pastravanu, O. (2002), 'A neural predictive controller for non-linear systems', *Mathematics and Computers in Simulation* **60**(3-5), 315–324.

Lee, A. Y. and Salman, M. A. (1989), 'On the design of active suspension incorporating human sensitivity to vibration', *Optimal Control Application and Methods* **10**(2), 189–195.

Lee, S. and Kim, W. J. (2010), 'Active suspension control with direct-drive tubular linear brushless permanent-magnet motor', *IEEE Transactions on Control Systems Technology* **18**(4), 859–870.

Leighton, N. J. and Pullen, J. (1994), 'A novel active suspension system for automotive application', *Proceedings of the Institute of Mechanical Engineers, Part D: Journal of Automobile Engineering* **208**(4), 243–250.

Lennox, B., Montague, G. A., Frith, A. M., Gent, C. and Bevan, V. (2001), 'Industrial application of neural networks - An Investigation', *Journal of Processing Control* **11**(5), 497–507.

Li, H., Gao, H., Liu, H. and Liu, M. (2012), 'Fault-tolerant H_∞ control for active suspension vehicle systems with actuator faults', *Proceedings of the Institute*

of Mechanical Engineers, Part I: Journal of Systems and Control Engineering **226**(3), 348–363.

Li, H., Tang, C. Y. and Zhang, T. X. (2008), Controller of vehicle active suspension systems using LQG method, *in* 'Proceedings of the IEEE International Conference on Automation and Logistics', Qindao, China, pp. 401–404.

Li, P. Y. and Yuan, Q. (2005), Flux observer for spool displacement sensing in self-sensing push-pull solenoids, *in* 'Proceedings of the 6th International Conference on Fluid Power Transmission and Control (ICFP 2005)', Hanzhou, China, pp. 1–5.

Liang, C.-C. and Chiang, C.-F. (2006), 'A study on biodynamic models of seated human subjects exposed to vertical vibration', *Interntional Journal of Industrial Ergonomics* **36**(10), 869–890.

Lin, J. and Lian, R.-J. (2011), 'Intelligent control of active suspension systems', *IEEE Transactions on Industrial Electronics* **58**(2), 618–628.

Lin, J.-S. and Huang, C.-J. (2004), 'Nonlinear backstepping active suspension design applied to a half-car model', *Vehicle System Dynamics: International Journal of Vehicle Mechanics and Mobility* **42**(6), 373–393.

Ljung, L. (2006), Identification of nonlinear systems, *in* 'Proceedings of the 9th International Conference on Control, Automation, Robotics and Vision (ICARCV 2006)', Singapore, pp. 1–9.

Loyer, B., Jezequel, L. and Arnoux, E. (2008), Robust multi-objective optimization of an active vehicle suspension system using simplified models and evolutionary techniques, *in* 'Proceedings of the International Conference on Engineering Optimization (EngOpt 2008)', Rio de Janeiro, Brazil, pp. 1–10.

Lu, J. and DePoyster, M. (2002), 'Multiobjective optimal suspension control to achieve integrated ride and handling performance', *IEEE Transactions on Control Systems Technology* **10**(6), 807–821.

Lufty, O. F., Noor, S. B. M., Marhaban, M. H. and Abbas, K. A. (2009), 'A geneticatlly trained adaptive neuro-fuzzy inference system network utilized as a PID-like feedback controller for non-linear systems', *Proceedings of the Institute of Mechanical Engineers, Part I: Journal of Systems and Control Engineering* **223**(3), 289–429.

Maher, D. and Young, P. (2011), 'An insight into linear quarter-car model accuracy', *Vehicle System Dynamics: International Journal of Vehicle Mechanics and Mobility* **49**(3), 463–480.

Mailah, M. and Priyandoko, G. (2007), 'Simulation of suspension system with adaptive fuzzy active force control', *International Journal on Simulation Modelling* **6**(1), 25–36.

Manenti, F. (2011), 'Considerations on nonlinear model predictive control techniques', *Computers and Chemical Engineering* **35**(11), 2491–2509.

Marzbanrad, J., Ahmadi, G., Hojjat, Y. and Zohoor, H. (2002), 'Optimal active control of vehicle suspension system including time delay and preview for rough roads', *Journal of Vibration and Control* **8**(7), 967–991.

Miaomiao, M. and Chen, H. (2006), Constrained H_2 control of active suspensions using LMI optimization, *in* 'Proceedings of the 25th Chinese Control Conference4th International Symposium on Advanced Vehicle Control', Harbin, Heilongjiang, pp. 623–628.

Milosavljevic, S., McBride, D. I., Bagheri, N., Vasilev, R. M., Mani, R., Carman, A. B. and Rehn, B. (2011), 'Exposure to whole-body vibration and mechanical shock: A field study of quad bike use in agriculture', *The Annals of Occupational Hygiene* **55**(3), 286–295.

Mirza, N., Hussain, K., Day, A. J. and Klaps, J. (2005), 'Investigation of the dynamic characteristics of suspension parameters on a vehicle experiencing steering drift during braking', *Proceedings of the Institute of Mechanical Engineers, Part D: Journal of Automobile Engineering* **219**(12), 1429–1441.

Mokri, S. S., Husain, H., Martono, S. S. and Shafie, A. (2008), 'Real time implementation of NARMA-L2 control of a single link manipulator', *American Journal of Applied Sciences* **5**(Dec.), 1642–1649.

Montazeri-GH, M. and Soleymani, M. (2008), 'Genetic optimization of a fuzzy active suspension system based on human sensitivity to the transmitted vibrations', *Proceedings of the Institute of Mechanical Engineers, Part D: Journal of Automobile Engineering* **222**(10), 1769–1780.

Nagai, M., Moran, A., Tamura, Y. and Koizumi, S. (1997), 'Identification and control of nonlinear active pneumatic suspension for railway vehicles, using neural network', *Control Engineering Practice* **5**(8), 1137–1144.

Nakata, N. and Zhao, X. (2011), Numerical simulation of model-based control strategy for hydraulic actuators, *in* 'The 6th International Workshop on Advanced Smart Materials and Smart Structures Technology (ANCRiSST2011)', Dalian, China, pp. 1–9.

Nardi, F. (2000), Neural Network based Adaptive Algorithm for Nonlinear Control, PhD thesis, School of Aerospace Engineering, Georgia Institute of Technology, Atlanta.

Ng, A. Y. and Kim, H. J. (2004), Stable adaptive control with online learning, *in* Y. W. L. Saul and L. Bottou, eds, 'Advances in Neural Information Processing Systems 17', MIT Press, Cambridge MA, USA, pp. 977–984.

Nguyen, Q. H., Choi, S. B. and Park, Y. G. (2012), 'An analytical approach to optimally design of electrorheological fluid damper for vehicle suspension system', *Meccanica* **47**(7), 1–15.

Ngwangwa, H. M., Heyns, P. S., Labuchagne, F. J. J. and Kululanga, G. K. (2010), 'Reconstruction of road defects and road roughness classification using vehicle responses with artificial neural networks simulations', *Journal of Terramechanics* **47**(2), 97–111.

Ni, X., Verhaegen, M., Krijgsman, A. J. and Verbruggen, H. B. (1996), 'A new method for identification and control of nonlinear diynamic systems', *Engineering Applications of Artificial Intelligence* **9**(3), 231–243.

Norgaard, M., Ravn, O., Hansen, L. K. and Poulsen, N. K. (1996), The NNSYSID toolbox - a MATLAB® toolbox for system identification with neural networks, *in* 'Proceedings of the IEEE International Symposium on Computer-Aided Control System Design', Dearborn, MI, pp. 374–379.

Norgaard, M., Ravn, O., Poulsen, N. K. and Hansen, L. K. (2000), *Neural Networks for Modelling and Control of Dynamic Systems: A Practitioner's Handbook*, Springer, Boston, MA.

Nusantoro, G. D. and Priyandoko, G. (2011), 'PID state feedback controller of a quarter car active suspension system', *Journal of Basic and Applied Scientific Research* **1**(11), 2304–2309.

O'Dwyer, A. (2006), *Handbook of PI and PID Controller Tuning Rules*, Imperial College Press, London.

Okumura, K., Oya, M. and Wada, H. (2010), 'Robust ride comfort control of vehicles without measurements of tire deflection', *Artificial Life Robotics* **15**(2), 133–137.

Onat, C., Kucukdemiral, I. B., Sivrioglu, S. and Yuksek, I. (2007), 'LPV model based gain-scheduling controller for a full vehicle active suspension system', *Journal of Vibration and Control* **13**(11), 1629–1666.

Orvnaas, A., Stichel, S. and Persson, R. (2011), 'Active lateral secondary suspension with H_∞ control to improve ride comfort: Simulations on a full-scale model', *Vehicle System Dynamics: International Journal of Vehicle Mechanics and Mobility* **49**(9), 1409–1422.

Palkovics, L., Gaspar, P. and Bokor, J. (1993), Design and performance of an active vehicle suspension system, *in* 'Proceedings of the American Control Conference', San Francisco, California, pp. 696–700.

Park, J. H., Kim, S. H. and Moon, C. J. (2009), 'Adaptive neural control for strict-feedback nonlinear systems without backstepping', *IEEE Transactions on Neural Networks* **20**(7), 1204–1209.

Parlos, A. G., Parthasarathy, S. and Atiya, A. F. (2001), 'Neuro-predictive process control using on-line controller adaptation', *IEEE Transactions on Control Systems Technology* **9**(5), 741–755.

Pedro, J. O. (2007), 'H_2 - LQG/LTR controller design for active suspension systems', *R and D Journal of the South African Institution of Mechanical Engineering* **23**(2), 32–41.

Pedro, J. O. and Dahunsi, O. A. (2011), 'Neural network based feedback linearization control of a servo-hydraulic vehicle suspension system', *International Journal of Applied Mathematics and Computer Science, AMCS* **21**(1), 137–147.

Pedro, J. O., Dahunsi, O. A. and Baloyi, N. (2011), Direct adaptive neural control of a quarter-car active suspension susytem, *in* 'Proceedings of the 2011 IEEE AFRICON', Livingstone, Zambia.

Pedro, J. O. and Mgwenya, T. R. (2004), LQR control of a full - car active suspension with actuator dynamics, *in* 'Proceedings of the 4th South African Conference on Applied Mechanics, SACAM '04', Johannesburg, South Africa, pp. 203–207.

Poussot-Vassal, C., Sename, O., Dugard, L., Gaspar, P., Szabo, Z. and Bokor, J. (2006), Multi-objective qLPV H_∞/H_2 control of a half vehicle, *in* 'Proceedings of the 10th MINI Conference on Vehicle System Dynamics, Identification and Anomalies', Budapest, Hungary.

Poussot-Vassal, C., Sename, O., Dugard, L., Gaspar, P., Szabo, Z. and Bokor, J. (2008), 'A controlled friction damper for vehicle applications', *Control Engineering Practice* **16**(12), 1519–1534.

Priyandoko, G., Mailah, M. and Jamaluddin, H. (2009), 'Vehicle active suspension system using skyhook adaptive neuro active force control', *Mechanical Systems and Signal Processing* **23**(3), 855–868.

Qin, S. J. and Badgwell, T. A. (2000), An overview of nonlinear model predictive control applications, *in* F. Allgower and A. Zheng, eds, 'Nonlinear Predictive Control', Birkhäuser Verlag, Basel; Switzerland, pp. 369–392.

Rahmat, M. F., Zulfatman, Z., Husain, A. R., Ishaque, K., Y. M. Sam, R. G. and Rozali, S. M. (2011), 'Modeling and controller design of an industrial hydraulic actuator system in the presence of friction and internal leakage', *International Journal of Physical Sciences* **6**(14), 3505–3517.

Raj, A. H. K. and Padmanabhan, C. (2009), 'A new passive non-linear damper for automobiles', *Proceedings of the Institute of Mechanical Engineers, Part D: Journal of Automobile Engineering* **223**(11), 1435–1443.

Renn, J. and Wu, T. (2007), 'Modelling and control of a new $\frac{1}{4}t$ servo-hydraulic vehicle active suspension system', *Journal of Marine Science and Technology* **15**(3), 265–272.

Richer, E. and Hurmuzlu, Y. (2000), 'A high performance pneumatic force actuator system: Part 1 - Nonlinear mathematical model', *Journal of Dynamic Systems, Measurement and Control:Transactions of ASME* **122**(3), 416–425.

Rouss, V., Charon, W. and Cirrincione, G. (2009), 'Neural model of the dynamic behaviour of a non-linear mechanical system', *Mechanical Systems and Signal Processing* **21**(4), 1145–1159.

Ryu, S., Kim, Y. and Park, Y. (2008), 'Robust H_∞ preview control of an active suspension system with norm-bounded uncertainties', *International Journal of Automotive Technology* **9**(5), 585–592.

Sam, Y. M., Osman, J. H. S., Ruddin, M. and Ghani, A. (2004), 'A class of proportional-integral sliding mode control with application to active suspensions system', *Systems and Control Letters* **51**(3-4), 217–223.

Sam, Y. M. and S.Osman, J. H. (2005), 'Modelling and control of the active suspensions system using proportional integral sliding mode approach', *Asian Journal of Control* **7**(2), 91–98.

Savaresi, S. M., Poussot-Vassal, C., Spelta, C., Sename, O. and Dugard, L. (2010), *Semi-Active Suspension Control Design for Vehicles*, Elsevier Ltd, Oxford, U. K.

Sekulic, D. and Dedovic, V. (2011), 'The effect of stiffness and damping of the suspension system elements on the optimisation of the vibrational behaviour of a bus', *International Journal for Traffic and Transport Engineering* **1**(4), 231–244.

Seo, J., Venogopal, R. and Kenne, J. P. (2007), 'Feedback linearization based control of a rotational hydraulic drive', *Control Engineering Practice* **15**(12), 1495–1507.

Shahian, B. and Hassul, M. (1993), *Control System Design Using MATLAB*, Prentice Hall, Inc, New Jersey, USA.

Sharkawy, A. B. (2005), 'Fuzzy and adaptive fuzzy control for the automobiles active suspension system', *Vehicle Systems Dynamics* **43**(10), 795–806.

Sharp, R. S. and Peng, H. (2011), 'Vehicle dynamics applications of optimal control theory', *Vehicle Systems Dynamics* **49**(7), 1073–1111.

Shen, D. K., Ling, X. Q., Liu, J. and Wang, H. (2010), Modelling and simulation of a fuzzy PID controller for active suspension system, *in* 'Proceedings of the 7th International Conference on Fuzzy Systems and Knowledge Discovery (FSKD 2010)', Yantai, China, pp. 701–705.

Shi, J. W., Li, X. W. and Zhang, J. W. (2010), 'Feedback linearization and sliding mode control for active hydropneumatic suspension of a special-purpose vehicle', *Proceedings of the Institute of Mechanical Engineers, Part D: Journal of Automobile Engineering* **224**(1), 41–53.

Shirahatt, A., Prasad, P. S. S., Panzade, P. and Kulkarni, M. M. (2008), 'Optimal design of passenger car suspension for ride and road holding', *Journal of the Brazillian Society of Mechanical Science and Engineering* **30**(1), 66–76.

Shivakumara, B. S. (2010), 'Study of vibration and its effect on health of the motorcycle driver.', *Online Journal of Health and Allied Sciences* **9**(2), 1–4.

Slaski, G. (2011), The influence of adaptive damping level on vehicle vibration comfort - passenger car experimental tests results, *in* 'Proceedings of the 7th International Conference, TRANSBALTICA 2011', Vilnus, Lithuania, pp. 206–210.

Slotine, J. J. and Li, W. (1991), *Applied Nonlinear Control*, Prentice Hall, Englewood Cliffs, New Jersey.

Smith, W. A., Zhang, N. and Hu, W. (2011), 'Hydraulically interconnected vehicle suspension: Handling performance', *Vehicle System Dynamics: International Journal of Vehicle Mechanics and Mobility* **49**(6), 87–106.

Smoker, J., Baz, A. and Zheng, L. (2009), 'Virtual reality simulation of active car suspension system', *The International Journal of Virtual Reality* **8**(2), 75–82.

Spentzas, K. N. and Kanarachos, S. A. (2002), 'A neural network approach to the design of a vehicle's non-linear hybrid suspension system', *Proceedings of the*

Institute of Mechanical Engineers, Part B: Journal of Engineering Manufacture **216**(5), 833–838.

Spooner, J. T., Maggiore, M., Ordonnez, R. and Passino, K. M. (2002), *Stable Adaptive Control and Estimation for Nonlinear Systems: Neural and Fuzzy Approximator Techniques*, John Wiley and Sons, Inc, New York, USA.

Sun, F. and Cui, Y. (2011), Influence of parameter variations on system identification of full car model, *in* 'Proceedings of the International MultiConference of Engineers and Scientists 2011 Volume II', Hong Kong.

Tatjewski, P. and Lawrynczuk, M. (2006), 'Soft computing in model-based predictive control', *International Journal of Applied Mathematics and Computer Science, AMCS* **16**(1), 7–26.

Tavazoei, M. S. (2010), 'Notes on integral performance indices in fractional-order control systems', *Journal of Process Control* **20**(3), 285–291.

Thoresson, M., Uys, P., Els, P. and Snyman, J. (2009), 'Efficient optimisation of a vehicle suspension system, using a gradient-based approximation method, part 2: Optimisation results', *Mathematical and Computer Modelling* **50**(9-10), 1437–1447.

Turkay, S. and Akcay, H. (2008), 'Aspects of achievable performance for quarter-car active suspensions', *Journal of Sound and Vibration* **311**(1-2), 440–460.

Turkay, S. and Akcay, H. (2011), Multi-objective control of full-vehicle suspensions: A case study, *in* 'Proceedings of the 17th World Congress, The International Federation of Automatic Control (IFAC)', Milano, Italy, pp. 2190–2195.

Turnip, A., Park, S. and Hong, K. S. (2010), 'Sensitivity control of a MR-damper semi-active suspension', *International Journal of Precision Engineering and Manufacturing* **11**(2), 209–218.

Verros, G., Natsiavas, S. and Papadimitriou, C. (2005), 'Design optimization of quarter-car models with passive and semi-active suspensions under random road excitation', *Journal of Vibration and Control* **11**(5), 581–606.

Waldron, K. J., Hung, T. T. and Madadnia, J. (2008), Configuration design of a robotic vehicle for rough terrain mobility, *in* 'Proceedings of the 15th International Conference on Mechatronics and Machine Vision in Practice (M2VIP08)', Auckland, New-Zealand.

Wang, D., Huang, J., Lan, W. and Li, X. (2009), 'Neural network-based robust adaptive control of nonlinear systems with unmodelled dynamics', *Mathematics and Computers in Simulation* **79**(5), 1745–1753.

Wang, J., Wilson, D. A. and Halikias, G. D. (2001), H_∞ robust-performance control of decoupled active suspension systems based on LMI method, *in* 'Proceedings of the 2001 American Control Conference', Arlington, VA USA, pp. 2658–2663.

Wang, J., Wilson, D. A., Xu, W. and Crolla, D. A. (2005), Active suspesion control to improve vehicle ride and steady-state handling, *in* 'Proceedings of the 44th IEEE Conference on Decision and Control, and European Control Conference 2005', Seville, Spain, pp. 1982–1987.

Wang, J., Xu, W. and Chen, W. (2006), 'Optimal Hankel-norm reduction of active suspension model with application in suspension multiobjective control', *International Journal of Vehicle Design* **40**(1-3), 175–195.

Wang, Y. H. and Shih, M. C. (2011), 'Design of a genetic-algorithm-based self-tuning sliding fuzzy controller for an active suspension system', *Proceedings of the Institute of Mechanical Engineers, Part I: Journal of Systems and Control Engineering* **225**(3), 367–383.

Williams, R. A. (1997*a*), 'Automotive active suspensions part 1: Basic principles', *Proceedings of the Institute of Mechanical Engineers, Part D: Journal of Automobile Engineering* **211**(6), 415–426.

Williams, R. A. (1997*b*), 'Automotive active suspensions, Part 2: Practical Considerations', *Proceedings of the Institute of Mechanical Engineers, Part D: Journal of Automobile Engineering* **211**(6), 427–444.

Xinjie, J. and Shengjin, L. (2009), Design of the fuzzy-PID controller for new vehicle active suspension with electro-hydrostatic actuator, *in* 'Proceedings of the 4th IEEE Conference on Industrial Electronics and Applications (ICIEA 2009)', Xian, China, pp. 3724–3727.

Xue, X. D., Cheng, K. W. E., Zhang, Z., Lin, J. K., Wang, D. H., Bao, Y. J., Wong, M. K. and Cheung, N. (2011), Study of art of automotive active suspensions, *in* 'Proceedings of the 4th International Conference on Power Electronics Systems and Applications (PESA)', Hong Kong, China, pp. 1–6.

Yagiz, N. and Sakman, L. E. (2005), 'Robust sliding mode control of a full vehicle without suspension gap loss', *Journal of Vibration and Control* **11**(11), 1357–1374.

Yamashita, M., Fujimori, K., Hayakawa, K. and Kimura, H. (1994), 'Applications of H_∞ control to active suspension systems', *Automatica* **30**(11), 1717–1729.

Yan, Z. and Wang, J. (2011), A neural network approach to nonlinear model predictive control, *in* 'Proceedings of the 37th Annual Conference on (IEEE) Industrial Electronics Society (IECON2011)', Melbourne, Australia, pp. 2305–2310.

Yesildirek, A. and Lewis, F. L. (1995), 'Feedback linearization using neural netwoks', *Automatica* **31**(11), 1659–1664.

Yesildirek, A. and Lewis, F. L. (2001), 'Adaptive feedback linearization using efficient neural networks', *Journal of Intelligent and Robotic Systems* **31**(1-3), 253–281.

Yoshimura, T. and Teramura, I. (2005), 'Active suspension control of a one-wheel car model using single input rule modules fuzzy reasoning and a disturbance observer', *Journal of Zhejiang University Science* **6A**(4), 251–256.

Yoshizawa, T. (1996), *Stability Theory by Liapunov's second Method*, The Mathematical Society of Japan, Tokyo, Japan.

Younesian, D. and Nankali, A. (2009), 'Spectral optimization of the suspension system of high-speed trains', *International Journal of Vehicle Structures and Systems* **1**(4), 98–103.

Yu, C., Zhu, J., Che, J. and Sun, Z. (2005), Input-output data modelling using fully tuned RBF networks for a four degree-of-freedom tilt rotor aircraft platform, *in* A. Gelbukh, A. de Albornoz and H. Terashima, eds, 'Proceedings of the 4th Mexican International Conference on Advances in Artificial Intelligence', Springer-Verlag, Berlin, pp. 1145–1154.

Yu, H., Feng, Z. J. and Wang, X. Y. (2004), 'Nonlinear control for a class of hydraulic servo system', *Journal of Zhejiang University Science* **5**(11), 1413–1417.

Zaidel, D., Hakkert, A. S. and Pistiner, A. H. (1992), 'The use of road humps for moderating speeds on urban streets', *Accident Analysis and Prevention* **24**(1), 45–56.

Zhang, L. J., Lee, C. M. and Wang, Y. S. (2002), 'A study on nonstationary random vibration of a vehicle in time and frequency domains', *International Journal of Automotive Technology* **3**(3), 101–109.

Zhao, Q., Yin, J. and Li, D. (2011), Intelligent compound control of vehicle active suspension based on RBF neural network, *in* 'Proceedings of the Third International Conference on Measuring Technology and Mechatronics Automation (ICMTMA)', Harbin, China, pp. 441–444.

Zhong, X., Ichchou, M., Gillot, F. and Saidi, A. (2010), 'A dynamic-reliable multiple model adaptive controller for active vehicle suspension under uncertainties', *Smart Materials and Structures* **19**(4), 1673–1678.

Zhou, J., Goodall, R., Ren, L. and Zhang, H. (2009), 'Influences of car body vertical flexibilty on ride quality of passenger railway vehicles', *Proceedings of the Institute*

of Mechanical Engineers, Part F: Journal of Rail and Rapid Transit **223**(5), 461–471.

Zuo, L. and Nayfeh, S. A. (2003*a*), 'Low order continuous-time filters for approximation of the ISO 2631-1 human vibration sensitivity weightings', *Journal of Sound and Vibration* **265**(2), 459–465.

Zuo, L. and Nayfeh, S. A. (2003*b*), 'Structured H_2 optimization of vehicle suspensions based on multi-wheel models', *Vehicle System Dynamics: International Journal of Vehicle Mechanics and Mobility* **40**(5), 351–371.

Zuscikova, M. and Belavy, C. (2011), H_∞ controller design for active suspension system, *in* M. Fikar and M. Kvasnica, eds, 'Proceedings of the 18th International Conference on Process Control', Tatraska Lomnica, Slovakia, pp. 394–399.

APPENDIX A - AVSS Parameters

The description and values of the physical parameters used in modelling the quarter-car are provided in Table A.1

Table A.1: Parameters for the Quarter - Car Model

Parameter	Symbol	Value
Sprung mass	m_s	$290kg$
Unsprung mass	m_u	$40kg$
Suspension linear stiffness	k_s^l	$2.35 \times 10^4 N/m$
Suspension nonlinear stiffness	k_s^{nl}	$2.35 \times 10^4 N/m$
Suspension linear damping coefficient	b_s^l	700
Suspension nonlinear damping coefficient	b_s^{nl}	400
Suspension asymmetric damping coefficient	b_s^{nl}	400
tyre stiffness	k_t	$1.9 \times 10^5 N/m$
tyre damping coefficient	b_t	130
Piston area	A_{hyd}	$3.35 \times 10^{-4} m^2$
Supply pressure	P_s	$10.34MPa$
Actuator parameter	α	4.515×10^{13}
Actuator parameter	β	1
Actuator parameter	γ	1.545×10^9
Servo valve gain	K	$0.001m/V$
Time constant	τ	$0.033s$
First hump amplitude	a_1	$6.7cm$
Second hump amplitude	a_2	$5cm$
Input disturbance wavelength	λ	$4m$
Vehicle forward velocity	V_1	$40km/h$
(Deterministic road excitation)		
Vehicle forward velocity	V_2	$72km/h$
(Deterministic road excitation)		

Table A.2: Parameters for the Full - Car Model

Parameter	Symbol	Value
Sprung mass	m_s	$1160kg$
Unsprung masses	m_{ufl}, m_{ufr}	$40kg$
	m_{url}, m_{urr}	
Pitch axis moment of inertia	I_θ	$2200kgm^2$
Roll axis moment of inertia	I_ϕ	$460kgm^2$
Suspension linear stiffness	k_s^l	$2.35 \times 10^4 N/m$
Suspension nonlinear stiffness	k_s^{nl}	$2.35 \times 10^4 N/m$
Suspension linear damping coefficient	b_s^l	$700Ns/m$
Suspension nonlinear damping coefficient	b_s^{nl}	$400Ns/m$
Suspension asymmetric damping coefficient	b_s^{nl}	$400Ns/m$
tyre stiffness	k_t	$1.9 \times 10^5 N/m$
tyre damping coefficient	b_t	$130Ns/m$
Piston area	A_{hyd}	$3.35 \times 10^{-4} m^2$
Supply pressure	P_s	$10.34MPa$
Actuator parameter	α	4.515×10^{13}
Actuator parameter	β	1
Actuator parameter	γ	1.545×10^9
Servo valve gain	K	$0.001m/V$
Time constant	τ	$0.033s$
First hump amplitude	a_1	$6.7cm$
Second hump amplitude	a_2	$5cm$
Input disturbance wavelength	λ	$4m$
Vehicle forward velocity	V_1	$40km/h$
(Deterministic road excitation)		
Vehicle forward velocity	V_2	$72km/h$
(Deterministic road excitation)		

APPENDIX B - Glossary of Terms

- Ride Comfort: This is the subjective feeling experienced by the driver or other vehicle occupants. It is made up of several factors like;
  - Chassis vibration, noise, temperature, etc.
  - Driver's feelings, age, health, etc.

  Vehicle suspension is mainly concerned about the filtering or attenuating of the chassis vibration.

- Whole Body Vibration (WBV): $0.5 \leq LFV \leq 80Hz$ [BS 6841 (1987); ISO 2631 (2003); Milosavljevic et al. (2011)]

- Low Frequency Vibration (LFV) range: $0 \leq LFV \leq 10Hz$ [Poussot-Vassal et al. (2008)]

- High Frequency Vibration (LFV) range: $HFV > 10Hz$ [Poussot-Vassal et al. (2008)]

- Windowing: This is the multiplying of the time domain data block values by a mathematical function before FFT computation is carried out on the data block. Windowing compensates for some FFT algorithm limitations which causes leakage.

- Hanning Window: This is a window function given by

$$Hanning\ \ window = \frac{1}{2}(1 - cos\theta) \quad for \quad 0 \leq \theta \leq 2\pi$$

  A data block multiplied by Hanning window appears like a complete wave thereby limiting signal leakage associated with FFT.